Prediction Formulae for Processes on and in Porous Bonded Revetments
– An Experimental and Numerical Study –

Von der
Fakultät Architektur, Bauingenieurwesen und Umweltwissenschaften
der Technischen Universität Carolo-Wilhelmina
zu Braunschweig

zur Erlangung des Grades einer
Doktoringenieurin (Dr.-Ing.)
genehmigte

Dissertation

von
Gisa Foyer
geboren am 07.05.1985
aus Rostock

Eingereicht am: 12. April 2013
Disputation am: 19. Juli 2013

Berichterstatter: Prof. Hocine Oumeraci
Prof. Holger Schüttrumpf

2013

Vorwort

Diese Arbeit ist im Rahmen eines Promotionsstipendiums entstanden. Daher möchte ich auch zunächst der Deutschen Bundesstiftung Umwelt (dbu) und ihren Mitarbeitern für die finanzielle Unterstützung danken. Vielmehr geholfen hat mir aber das Vertrauen, dass ihrerseits in meine Arbeit gesetzt wurde. Außerdem war der Austausch mit anderen Stipendiaten außerhalb der eigenen Disziplin immer eine Bereicherung, insbesondere um alltägliche Probleme des Doktorandendaseins zu bewältigen aber auch um sich nicht in Details der eigenen Arbeit zu verrennen.

Die Mühen meines Doktorvaters Prof. Oumeraci möchte ich auch besonders hervorheben. Von der Beantragung des Stipendiums über das Verfassen der Zwischenberichte bis zur Vervollständigung der Arbeit hat er sich immer Zeit genommen, Hilfestellungen zu geben oder Probleme zu diskutieren. Ohne seine Unterstützung und die des Leichtweiß-Instituts für Wasserbau wären meine Besuche von internationalen Konferenzen auch schon zu Beginn meiner Arbeit nicht möglich gewesen.

Natürlich möchte ich mich auch bei allen meinen Kollegen und Mitstipendiaten in der Abteilung Hydromechanik und Küsteningenieurwesen bedanken: für das nette Miteinander, für entspannende Runden bei Geburtstagskuchen und anderen Events, für gemeinsame Mittagspausen in der Mensa oder in unserer Kochrunde, für abendliche Ausflüge, für gemeinsame sportliche Aktivitäten, für die fachliche und praktische Hilfe und natürlich besonders fürs Zuhören. Ich hatte eine schöne Zeit mit euch und habe einiges von euch gelernt, fachlich und menschlich, was mir in meinem weiteren Arbeitsleben hoffentlich helfen wird.

Zu allerletzt aber dafür umso mehr möchte ich mich bei meinem Mann bedanken, dafür dass er diese gut 3 Jahre mit mir durchgestanden hat, ohne verrückt zu werden, auch wenn das wahrscheinlich nicht immer einfach war. Danke für den Versuch alle meine Probleme mit mir zu lösen und dafür, dass du mir immer den Rücken freigehalten hast.

Braunschweig, April 2013 Gisa Foyer

Kurzfassung

Klimaveränderungen innerhalb des letzten Jahrhunderts führten und führen zu einem steigenden Meeresspiegel. Dies hat direkte Konsequenzen für Küstenschutzbauwerke weltweit und auch in Deutschland. Anpassungen der bestehenden Deichbauwerke an die neuen Bedingungen sind daher unumgänglich, aber die meisten Verfahren führen zu zusätzlichen Problemen. Die zwei Standardverfahren und ihre Nachteile sind: (i) Aufbringen eines dichten Deckwerks zur äußeren Stärkung des Deiches führt zur großflächigen Versiegelung der Oberfläche und (ii) Erhöhung des Deiches geht einher mit einem großen Platzbedarf und einem dementsprechend großen Eingriff in die Umwelt. Ein alternatives Verfahren zum Schutz von Ufereinfassungen und Deichen gegen Seegang ist die Verwendung von porösen, gebundenen Deckwerken. Diese Konstruktion vereint die Vorteile der geschlossenen Deckwerke (gute Stabilität) mit denen der geschütteten Deckwerke (hohe Durchlässigkeit und Dissipation der Energie). Außerdem ermöglicht die hohe Porosität eine zügige Wiederansiedlung der marinen Flora und Fauna. Ungeachtet dieser Vorteile sind die Prozesse in der Interaktion zwischen Seegang, durchlässigen Deckwerken und ihrer Gründung bisher kaum erforscht, was eine Anwendung dieser neuartigen Deckwerke erschwert. Die vorliegende Dissertationsschrift soll daher einen genaueren Einblick in die Prozesse dieser Interaktion geben.

Zur Identifikation aller involvierten Prozesse und etwaiger Wissenslücken in der Forschung wurde zunächst eine systematische Literaturanalyse durchgeführt. Weiterhin wurden im Vorfeld gewonnene, experimentelle Daten aus dem großen Wellenkanal (GWK) in Hannover aus großmaßstäblichen Versuchen detailliert untersucht, um Prozesse eingehend zu beschreiben und so die zusätzlichen numerischen Simulationen zu planen. Diese numerischen Simulationen mit dem CFD-Modell COBRAS-UC (VARANS – Volume averaged Reynolds averaged Navier-Stokes) dienten zur Erweiterung der Versuchsbedingungen aus den GWK-Versuchen, um weitere Deckwerksneigungen und Wellenbedingungen abzudecken. Basierend auf der erweiterten Datenbasis konnten Berechnungsformeln für die einzelnen hydrodynamischen Prozesse entwickelt werden.

Bei den Untersuchungen konnten mehrere allgemeine und spezifische Besonderheiten der porösen, gebundenen Deckwerke auf die Prozesse festgestellt werden. Zunächst ist die Bedeutung des Brandungsstaus in früheren Untersuchungen häufig unterschätzt worden. Dieser Parameter ist meist nur für Strände und Bauwerke mit sehr flachen Neigungen untersucht worden, aber auch für die eher steilen Deckwerke, die hier untersucht worden sind, ist ein immenser Einfluss, insbesondere auf den Wellenauflauf und –ablauf, nachgewiesen worden. Weiterhin konnte der Einfluss des Deckwerks und seiner Schichtdicke auf die Wellenreflexion und den Wellenauflauf und –ablauf sowie die zugehörigen Geschwindigkeiten beschrieben werden. Der Einfluss des Brandungsstaus ist auch im Sandfundament nachweisbar, wobei insbesondere die Lage des maximalen internen Brandungsstaus in der Nähe des Deckwerkes auffällig war.

Abstract

Climate changes within the last century caused and are still causing rising sea water levels. This has imminent consequences for the coastal protection systems worldwide and also in Germany. Adaptations of the dike structures to the new situation are needed, but the standard methods often entail environmental problems. The two mostly used methods and their drawbacks are: (i) closed revetments to enforce the dike structure which leads to sealing of the soil and (ii) heightening of dikes which has a high space requirement and, therefore, a high impact on the environment. An improved approach for the protection of embankments and dikes against sea waves is the use of porous and bonded revetments. This type of structure combines the advantages of bonded revetments (high stability) and of rubble layers (high permeability). Especially the high porosity allows for a quick resettlement of marine flora and fauna. Despite their relevance, highly porous revetments are poorly understood in terms of the processes associated with the interaction of waves, structure and foundation, thus hindering a wider application of this type of structure. The present thesis should, therefore, give a more detailed overview of the effects of a porous, bonded revetment on said processes.

A systematic analysis of the literature was performed to identify all processes involved in the interaction as well as possible knowledge gaps in former research studies. Furthermore, the data from large-scale tests which were performed prior to the dissertation in the Large Wave Flume (GWK) in Hannover were analysed further to describe the processes precisely and to carefully plan the additional numerical simulations. The numerical simulations with the CFD-model COBRAS-UC (VARANS – Volume averaged Reynolds averaged Navier-Stokes) were used to extend the range of the tested conditions of the GWK-tests including different slope steepnesses and wave conditions. Based on the extended data set, prediction formulae for the hydrodynamic processes were developed.

The analyses showed several general and specific findings for the porous, bonded revetments. First of all, the importance of the wave set-up on the structure is often underestimated. This parameter is mostly considered for beaches and structures with flatter slopes. But for steeper structures like the porous bonded revetment considered in this study, a distinct effect of the wave set-up especially on the wave run-up and run-down was also determined. Furthermore, the effect of the porous bonded revetment and its thickness on the hydrodynamic processes such as wave reflection, wave run-up/run-down and the corresponding velocities is described. Moreover, the effect of the wave set-up is present in the sand foundation, where especially the location of the maximum set-up in the sand is noteworthy.

Contents

List of Notations

Parameter	Dimension	Description
a, b	-	Random parameter for curve fitting
a, b, c		Forchheimer coefficients
a_1, a_2, a_3, a_4	-	Empirical coefficients
b_L	m	Water table length
c'	-	Correction factor in Franzius' formula for run-up velocity
C_d	-	Dissipation coefficient
C_m	-	Virtual mass coefficient
C_r	-	Reflection coefficient $= H_r/H_i$
C_t	-	Transition coefficient
D	mm	Grain diameter
D_{15}, D_{50}, D_{85}	mm	Grain diameter which is not exceeded by 15, 50 or 85%
D_{eq}	mm	Equivalent grain diameter
d_r	mm	Residual displacement normal to slope
d_{rev}	m	Revetment thickness
E_d	J	Dissipated energy
E_i	J	Incident energy
E_r	J	Reflected energy
E_t	J	Transmitted energy
g	m/s²	Gravitational acceleration
H	m	Wave height
h	m	Water depth
h_0	m	Initial water depth
H_b	m	Wave height at breaking point
h_b	m	Water depth at breaking point
H_i	m	Incident wave height
H_{loc}	m	Wave height at foot of structure (local wave height)
H_m, H_0	m	Mean deep water wave height
H_{m0}	m	Zero moment wave height in deep water
H_r	m	Reflected wave height
H_S	m	Significant wave height
H_{S0}	m	Deep water, significant wave height
H_t	m	Transmitted wave height
h_t	m	Water depth at toe of structure
i	-	Hydraulic gradient
k	-	Wave number
K_S	-	Specific permeability
L	m	Wave length
L_0	m	Deep water wave length
L_b	m	Wave length at point of breaking
n	-	Porosity
$p_{2,max}$	kPa	Maximum pressure on bottom of the revetment
p_{max}	kPa	Maximum pressure on the revetment
R	-	Non-dimensional reflection parameter
R	m	Wave run-up or run-down height
R_d	m	Wave run-down height
$R_{d,int}$	m	Internal wave run-down height
$R_{d2\%}$	m	Wave run-down height only exceeded by 2%
Re	-	Reynolds number

Re_i	-	Reynolds number based on wave period
R_u	m	Wave run-up height
$R_{u,int}$	m	Internal wave run-up height
$R_{u2\%}$	m	Wave run-up height exceeded by 2%
S'	m	Horizontal distance from occurrence of maximum run-up velocity
T	s	Wave period
t	s	Time
T_m	s	Mean wave period
$T_{m-1,0}$	s	Period from the 0^{th} and minus first moment
T_P	s	Peak period
u	kPa	Pore pressure
u_0	kPa	Pressure on the sand foundation
u_f	m/s	Filter velocity
u_r	kPa	Residual pore pressure
u_t	kPa	Transient pore pressure
v_{int}	m/s	Local velocity on bottom of the revetment
$v_{int,max}$	m/s	Max. upwards directed internal local flow velocity (parallel to revetment)
$v_{int,min}$	m/s	Max. downwards directed internal local flow velocity (parallel to revetment)
$v_{int,Rd}$	m/s	Max. internal wave run-down velocity
$v_{int,Ru}$	m/s	Max. internal wave run-up velocity
v_{max}	m/s	Max. upwards directed external local flow (parallel to revetment)
v_{min}	m/s	Max. downwards directed external local flow velocity (parallel to revetment)
v_R	m/s	Velocity resulting from the differentiation of the wave run-up signal
v_{Rd}	m/s	Max. external wave run-down velocity
v_{Ru}	m/s	Max. external wave run-up velocity
v_u	m/s	Run-up velocity
$v_{u,max}$	m/s	Maximum run-up velocity
$v_{u2\%}$, $v_{u50\%}$	m/s	Maximum run-up velocity exceeded by 2% resp. 50%
x_A	m	Horizontal distance from SWL
α	°	Slope angle
α_f, β_f	-	Dimensionless Forchheimer coefficients
γ_b, γ_f, $\gamma_{f,surging}$, γ_β	-	Correction factor for a berm; surface layout (& surging breaking); attack angle
Δx	m	Horizontal cell size
Δy	m	Vertical cell size
η	m	Distance from SWL to MWL
η_{int}	m	Wave set-up on core surface within revetment
η_{max}	m	Wave set-up on slope surface
η_{min}	m	Wave set-down at wave gauge
η_{Sand}	m	Set-up in the sand foundation
λ	m	Penetration length
μ	Ns/m²	Dynamic viscosity
ν	m²/s	Kinematic viscosity
ξ	-	Surf similarity parameter/ Iribarren number $= \frac{\tan\alpha}{\sqrt{H/L}}$
ξ_{0P}	-	Surf similarity parameter based on H_{S0} and L_0 (T_P)
ξ_b	-	Surf similarity parameter based on H_b and L_0
ξ_m	-	Surf similarity parameter based on mean values in deep water

$\xi_{m-1,0}$	-	Surf similarity parameter based on H_{m0} and L_0 ($T_{m-1,0}$)
ξ_{mod}	-	Modified surf similarity parameter $= \frac{\tan\alpha}{\sqrt{H/L \cdot \left(1+\frac{d_{rev}}{H}\right)}}$
ξ_P	-	Surf similarity parameter based on H_S and L_P
ξ_{S0}	-	Surf similarity parameter based on H_S and L_0 (T_m)
ρ_W	m³/s	Density of water
σ	N/m²	Normal stress
σ'	-	Coefficient of variation
σ'	N/m²	Effective stress

COBRAS-UC	Cornell Breaking Wave and Structures (University of Cantabria)
EMWL	External mean water level
FZK	Forschungszentrum Küste (Coastal research centre)
GWK	Großer Wellenkanal (Large wave flume)
IMWL	Internal mean water level
LWI	Leichtweiß-Institute for hydraulic engineering and water resources
MRA	Multiple regression analysis
MWL	Mean water level
PBA	Polyurethane bonded aggregate
PT	Pressure transducer
RA	Regression analysis
RANS	Reynolds averaged Navier Stokes
RUG	Run-up gauge
SWL	Still water level
VOF	Volume of fluid
WG	Wave gauge
WP	Work package

1 Introduction

Climate changes within the last century lead to rising sea water levels of about 25 cm at the German North Sea Coastline (NLWKN, 2012). This has imminent consequences for the coastal protections worldwide. Adaptations to the new situation are also needed for dike structures, but the standard methods often entail environmental problems. The two mostly used methods and their drawbacks are: (i) revetments to enforce the dike structure which leads to sealing of the soil and (ii) heightening of dikes which has a great place requirement. An improved approach for the protection of embankments and other slopes against sea waves is the use of porous and bonded revetments. This type of structure combines the advantages of stability of bonded revetments and permeability of rubble layers. Especially the permeability allows for a resettlement of marine flora and fauna (Fig. 1.1a). Despite their relevance, permeable revetments are poorly understood in terms of the processes associated with the interaction of wave, structure and foundation.

a) Elastomeric revetment covered with algae (Arcadis, 2008)

b) Permeable, bonded revetment in wave flume (Oumeraci et al., 2010)

Fig. 1.1 Permeable, elastically bonded revetments

A series of systematic model tests was conducted using a polyurethane bonded aggregate (PBA) revetment in the Large Wave Flume (GWK), Hannover (Fig. 1.1b). The PBA-material consists of a stone aggregate that is coated with a polyurethane bonding agent leaving the pore volume completely open thus providing a higher porosity than obtained using asphalt as a bonding agent. The test included three different revetment constructions with a slope steepness of 1:3 positioned on a sand foundation separated by either a geotextile alone or a geotextile and a filter layer. The experimental set-up contained two cameras and over 80 measuring devices which allows for an investigation of almost all present processes. The report “Hydraulic Performance, Wave Loading and Response of Elastocoast Revetments and their Foundation” (Oumeraci et al., 2010) proposed the first results of these tests. It includes empirical approaches to describe wave loads on and beneath the revetment, reflection performance and pore pressure development in the soil for regular waves and for wave spectra but it could not cover all processes.

1.1 Objectives

Although the advantages of PBA revetments are obvious, they and revetments similar to them are often not used because of missing dimensioning formulae and insufficient knowledge about the construction and maintenance. The main objective of this thesis is to thoroughly investigate the interaction between waves, a porous bonded revetment and its foundation to provide the first insight and eventually determine dimensioning formulae for highly porous, bonded revetments. This investigation includes all processes in front, on, in and below the revetment. Most of all a comparison between smooth, impermeable revetments and porous, rough revetments is needed to describe the effect of a porous revetment on all processes. A focus should be laid on physical plausibility so that, finally, more generic prediction formulae to describe the processes involved in this interaction are developed. To describe complex processes with formulae, parameters such as summarised in Fig. 1.2 are required.

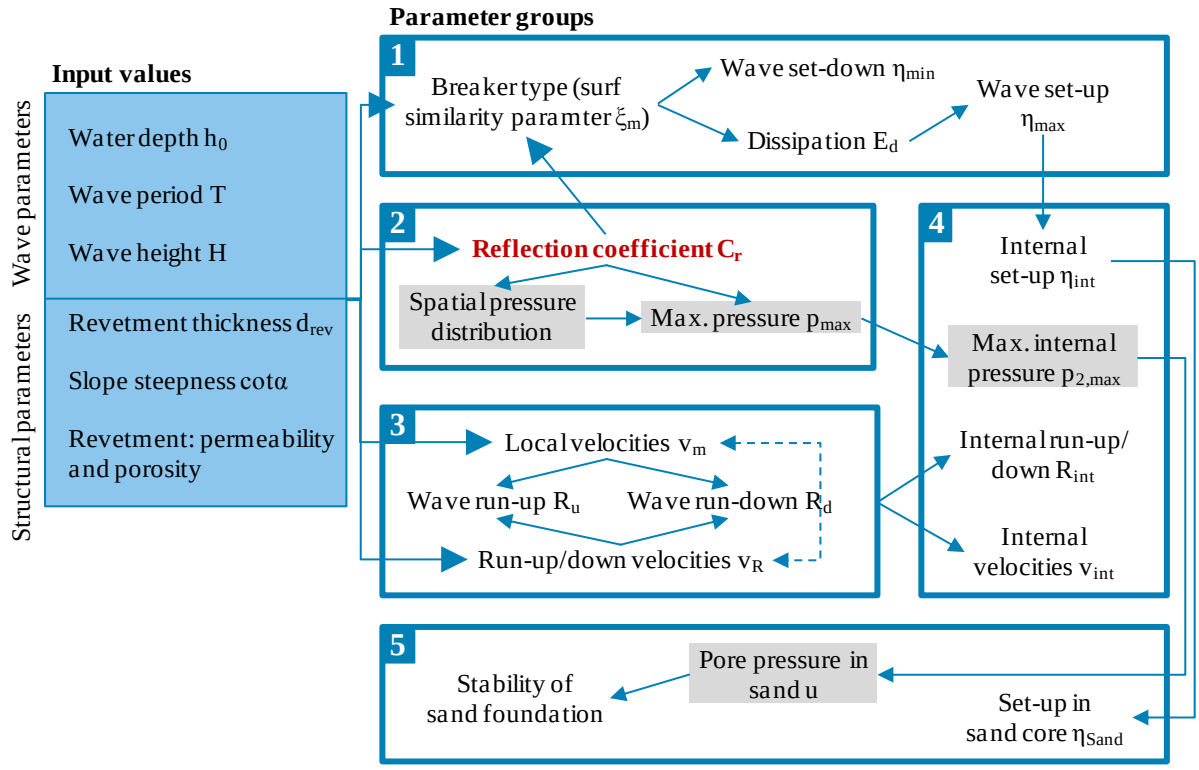

Fig. 1.2 Overview of parameters and their interrelation as analysed in this study

The highlighted parameter "reflection coefficient C_r" in Fig. 1.2 represents the most important parameter of all, because it can be used to describe the basic wave conditions in front of the structure. On the other hand, the highlighted pressure parameters had to be eliminated from the data pool because they have been thoroughly analysed in Oumeraci et al. (2010) and Ludwigs (2009). This elimination will also be discussed briefly in Chapter 5. One process is particularly difficult to describe: the stability of the sand foundation. In this case, a more complex analysis is performed based on several parameters.

1.2 Methodology

To achieve the above described objectives, the following substeps were determined:

1. State of the art review to determine knowledge gaps as well as prediction approaches that can be used and/or improved
2. Further analysis of the experiments described in Oumeraci et al. (2010) focussing on all processes neglected up to now
3. Preparation, execution and analysis of numerical simulations to enlarge the data set of Oumeraci et al. (2010)
4. Development of prediction equations for the parameters in Fig. 1.2

All these steps have been performed and are documented in several progress reports (Ludwigs & Oumeraci, 2011a; Ludwigs & Oumeraci, 2011b; Foyer & Oumeraci, 2012; Foyer & Oumeraci, 2013). The overall results will be presented in this thesis. For the presentation of the results, the parameter groups from Fig. 1.2 are adapted into Chapters 4 - 7 according to their location of occurrence (Fig. 1.3) preceded only by a summary of the state of the art review (Chapter 2) and the description of the model set-ups (GWK and numerical simulations) in Chapter 3. In Chapter 4, parameter groups 1 and 2 are joined together, because of the strong interrelation between wave breaking and wave reflection.

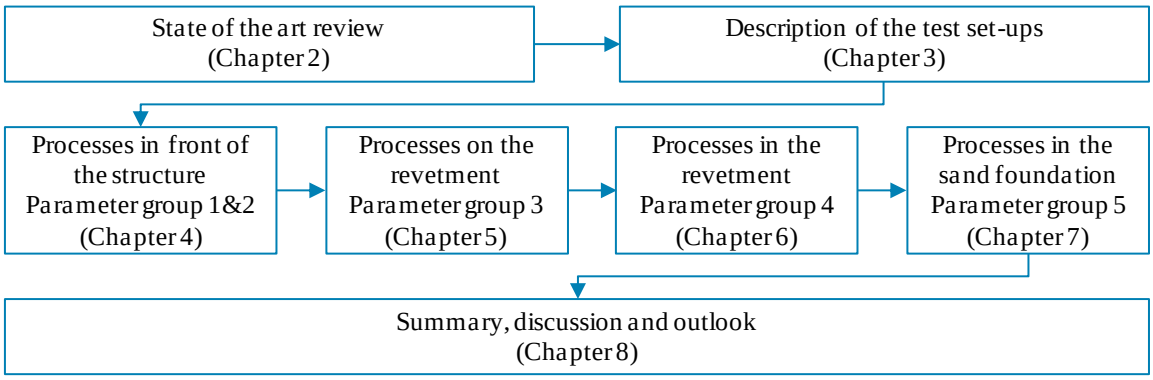

Fig. 1.3 Structure of the present study

In all chapters, a brief description of the parameter group is given at the beginning before analysing all parameters separately. For all parameters, prediction formulae are proposed. An evaluation of the uncertainty of the developed formulae is needed. Several statistical values were considered for this purpose, but during the analysis the coefficient of variation σ' as it is defined in eq. (1.1) was chosen, because it is the most reliable (see Foyer & Oumeraci, 2013). With the coefficient of variation σ' it is for example possible to enable a comparison of the statistical results of parameters that differ greatly in their range. A few other advantages and disadvantages of different standard deviations and coefficient of variations are also stated in Kortenhaus (2003).

$$\sigma' = \frac{\sqrt{\frac{1}{n-1} \cdot \sum\left(\mathrm{y} - f(x)\right)^2}}{\bar{y}} \tag{1.1}$$

This thesis is completed with a summary of all important findings and all proposed prediction formulae in Chapter 8. Moreover, a discussion of the findings is presented and an outlook to further required research and experiments is given.

2 State of the Art Review

The objective of this chapter is to review and analyse the knowledge on the hydrodynamic processes which are involved in the interaction between waves, a porous revetment and its sand foundation. To achieve this aim, existing theories and formulae which describe the processes are presented in the following starting with the wave reflection (Section 2.1) which is the most important hydrodynamic process because it governs the entire energy balance in the wave-structure interaction. The reflection coefficient C_r describes the input and output energy of the system and thus the main boundary conditions of all other processes.

Another group of parameters describes the swash processes on a revetment. These are presented in Section 2.2 and this includes not only the wave run-up and run-down heights and the corresponding velocities but also the wave set-up and set-down (even though the latter one is not directly involved in the swash). The pressures on the revetment caused by wave loading are, however, not considered because the results of the large-scale investigations in the GWK are thoroughly analysed in Oumeraci et al. (2010) and Ludwigs (2009). Moreover, the numerical simulations were not able to provide reliable data for a more detailed analysis (see Foyer & Oumeraci, 2012).

In Section 2.3 the flow in porous media is reviewed. The presented studies focus on theoretical and semi-empirical approaches to describe the flow in a porous medium. All of them use the approach to non-stationary flow based on the improved theories of Darcy-Forchheimer. However, the objective of this thesis is also to describe the swash processes inside the porous revetment. So, later on results on the internal wave set-up and the internal swash processes (wave run-up and run-down heights and corresponding velocities) are presented (Chapter 6).

The last group of processes involved in the interaction between waves, a porous revetment and a sand foundation are the processes beneath the revetment inside the sand foundation. These are reviewed in Section 2.4 focusing on the set-up in the foundation and thus on the pore pressures in the revetment.

An overview of the processes and the parameters involved is also given in Fig. 2.1. Each group shown in Fig. 2.1 represents one of Sections 2.1 - 2.4. To complete the knowledge base for the present thesis, Section 2.5 comprises the basics of numerical modelling with Reynolds-Averaged-Navier-Stokes (RANS) equations and also gives a brief introduction to the numerical model that is used for the thesis: COBRAS-UC. In this last part, the focus is laid on the incorporation of flow in porous media into the RANS-model using the theories described in Section 2.3.

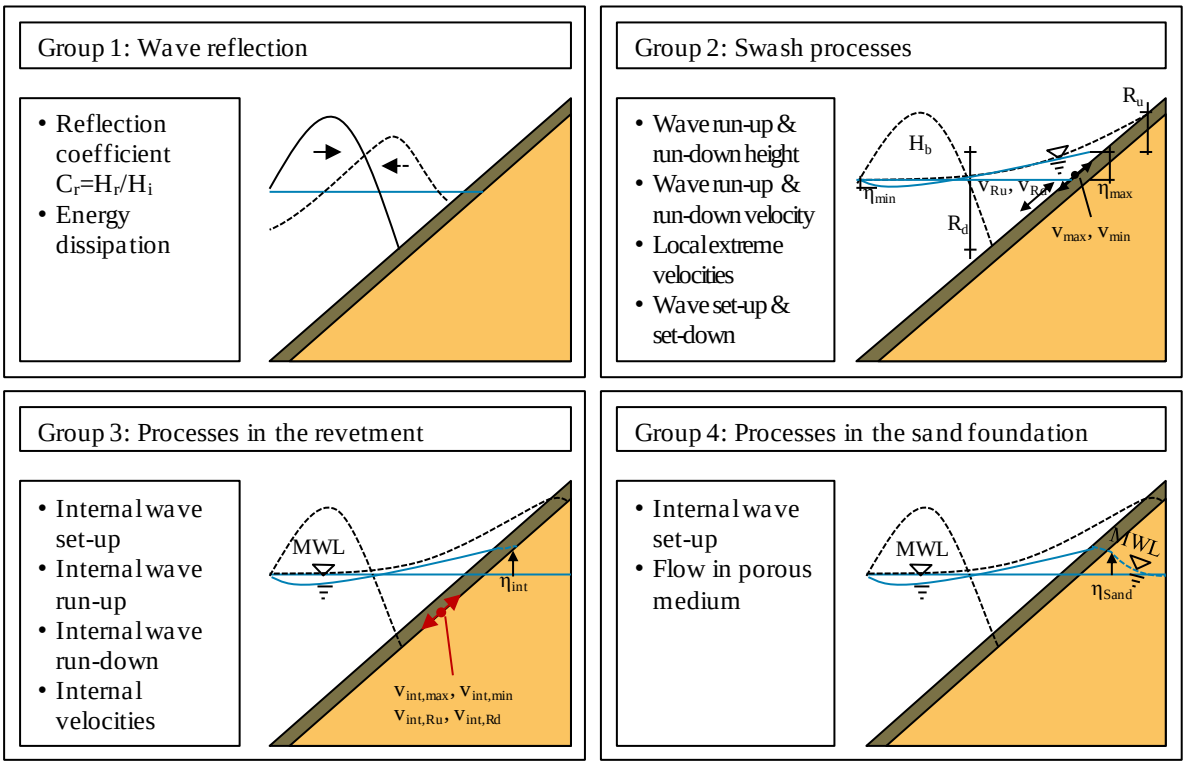

Fig. 2.1 Processes involved in the interaction between waves, porous revetments and a sand foundation

2.1 Wave reflection

Wave reflection is one of the most important hydrodynamic processes, because it is related to almost every other process. For wave damping structures the following relationship between wave reflection, energy dissipation and wave transmission based on energy conservation is commonly used (e.g. Seelig, 1983):

$$1 = C_r^2 + C_t^2 + C_d^2 \tag{2.1}$$

$$C_r = \sqrt{\frac{E_r}{E_i}};\ C_t = \sqrt{\frac{E_t}{E_i}};\ C_d = \sqrt{\frac{E_d}{E_i}} \tag{2.2}$$

The C-values in eqs. (2.1) and (2.2) signify the square root of the energy coefficients E/E_i and their indices indicate the specific energy types: reflected (r), transmitted (t) and dissipated (d). Equation (2.1) gives the energy conservation law based on eq. (2.2). With the help of equations (2.1) and (2.2), one energy part can be calculated if the other two energy contributions are known. However, these values are all difficult to measure and simplifications are often needed. The energy ratio is, therefore, often assumed to be proportional to the wave height (e.g. Seelig & Ahrens, 1981; Seelig, 1983; van der Meer, 1993):

$$\sqrt{\frac{E_r}{E_i}} = \frac{H_r}{H_i}; \sqrt{\frac{E_t}{E_i}} = \frac{H_t}{H_i}; \sqrt{\frac{E_d}{E_i}} = \frac{H_d}{H_i} \tag{2.3}$$

Equation (2.3) is often found in literature and is almost always used as definition for the reflection coefficient C_r. Even though some studies were made on the transmission coefficient C_t, for the here investigated structure this factor can generally be neglected. Thus, in case of a revetment with no transmitted wave energy behind the structure, the knowledge on the reflected energy will directly provide the dissipated energy and likewise the knowledge on the dissipated energy provides the reflected energy:

$$1 = C_r^2 + C_d^2 \tag{2.4}$$

Wave energy dissipation at or in embankements is mainly affected by the layout of the structure. Smooth, impermeable vertical walls have a negligible small dissipation coefficient C_d of about $C_d = 0$. For smooth, impermeable slopes investigations on the reflection coefficient are available; one of the first was made by Battjes in 1975, resulting in an empirical formula (eq. (2.5)) using the surf similarity parameter ξ.

$$C_r = 0.1 \cdot \xi^2 \tag{2.5}$$

This equation overestimates the reflection coefficient especially for high surf similarity parameters ξ (see e.g. Seelig & Ahrens, 1981) and it only considers the wave height H, the deep water wave length L_0 and the slope α of the structure ($\xi = \tan\alpha/\sqrt{H/L}$) to affect the reflection coefficient. This is insufficient for porous and rough surfaces. Therefore, several studies are presented in the following which focus on the effect of porosity, friction, etc. on the reflection coefficient C_r.

Generally, different approaches can be used to account for effects of porosity in empirical and numerical studies: either implementing the grain diameter D in some sort or including the porosity n in the equation. A representative study for the first group is the one performed by Seelig & Ahrens (1981) who investigated the reflection performance of revetments and rubble mound breakwaters. The laboratory tests included smooth slopes (1:2.5; 1:15) and 1:2.5 rubble mound breakwaters with 1 to 4 armour layers. Furthermore, comparisons with other studies were made. The analyses resulted in a general formula (eq. (2.6)) for the reflection coefficient and several additional equations to account for the structural and wave characteristics (e.g. breaking in front or on the structure), surface roughness (eq. (2.7)), multiple armour layers, breakwaters or sandy beaches and spectral effects. To account for the roughness, the equivalent grain diameter D_{eq} is used.

$$C_r = \frac{a_1 \cdot \xi^2}{\xi^2 + a_2} \tag{2.6}$$

$$a_1 = \exp\left[-1.7\sqrt{\frac{D_{eq}}{L}}\cot\alpha - 0.5\left(\frac{H_i}{H_b}\right)^{1.3}\right] \tag{2.7}$$

Equation (2.6) describes the reflection at smooth slopes with the surf similarity parameter ξ and the two empirical parameters a_1 and a_2 with $a_1 = 1.0$ and $a_2 = 5.5$ for $\cot\alpha \leq 6$ and waves breaking on the slope. The parameters a_1 and a_2 can be altered to account for changes of the slope surface and for changes in the breaking point. Eq. (2.7) shows this for parameter a_1. The value for parameter a_2 is, however, purely empirical. The approach of Seelig & Ahrens (1981) as described in eq. (2.6) is the most widely used one to describe the wave reflection at any coastal structure. Other studies in that direction are not specifically addressed here, because mostly they only give empirical values for the parameters a_1 and a_2. A partial overview of these can for example be found in USACE (2002) in Chapter VI.

The most obvious problem with the applicability of the results of Seelig & Ahrens (1981) on the present study are the relative grain diameters tested which ranged from $D_{eq}/H_i = 2.4 - 71.9$. For a revetment made out of bonded rock material with a diameter of $D_{50} \approx 3$ cm and incident wave heights $H_i = 0.2 - 1.3$ m these are in an order of ~O(100) too large and an adjustment might be needed for the structure in focus of this thesis.

A second study using the grain diameter to predict wave reflection was made by Davidson et al. (1996). The objective of this investigation was to develop a new non-dimensional parameter that would account for more wave and material characteristics than the surf similarity parameter ξ. For this investigation, data from two full-scale breakwaters was analysed. Tab. 2.1 gives an overview of the two considered structures as well as the analysed wave conditions. The reflection parameter C_r was calculated with an energy based approach ($C_r = \sqrt{(E_r/E_i)}$) according to linear wave theory. This approach made it necessary to exclude wave conditions leading to plunging or spilling breakers. As in Seelig & Ahrens (1981) the stone diameter in Davidson et al. (1996) is much larger than in the structure in focus of this thesis.

The analysed data was used to perform a multiple regression analysis (MRA) resulting in a new non-dimensional parameter R (eq. (2.8)). Afterwards the formula for the reflection coefficient C_r proposed by Seelig & Ahrens (1981) (eq. (2.6)) was altered using this new parameter R (eq. (2.9)).

Tab. 2.1 Wave conditions and structure parameters Davidson et al., 1996

Parameter	tan α =1.23	tan α =0.64
h_t (m)	0.99-4.62	1.15-4.56
H_i (m)	0.06-1.64	0.15-1.47
T_P (s)	3-19	4-15
ξ	6.4-70.7	4.4-23.1
D_{eq} (m)	1.38	1.44

$$R = \frac{h_t L_0^2 \tan\alpha}{H_i D_{eq}^2} \tag{2.8}$$

$$C_r = \frac{a_3\sqrt{R}}{a_4 + \sqrt{R}} \tag{2.9}$$

The advantage of this method is that not only the stone diameter D is accounted for but also the water depth h_t at the toe of the structure. The main disadvantage is the empirical nature of a_3 and a_4. However, formulae (2.8) and (2.9) present the most complex calculation for the reflection coefficient C_r for non-plunging waves at this time.

To complete the review of results on the reflection coefficient, the results of Oumeraci et al. (2010) are presented in Fig. 2.2. This approach is based on Seelig & Ahrens (1981) and shows also two formulae as determined in Allsop & McConnell (1999) which is also based on Seelig & Ahrens (1981). The results of the polyurethane bonded aggregate (PBA) revetment are located between the prediction curves for smooth impermeable slopes and a two layer rock amour.

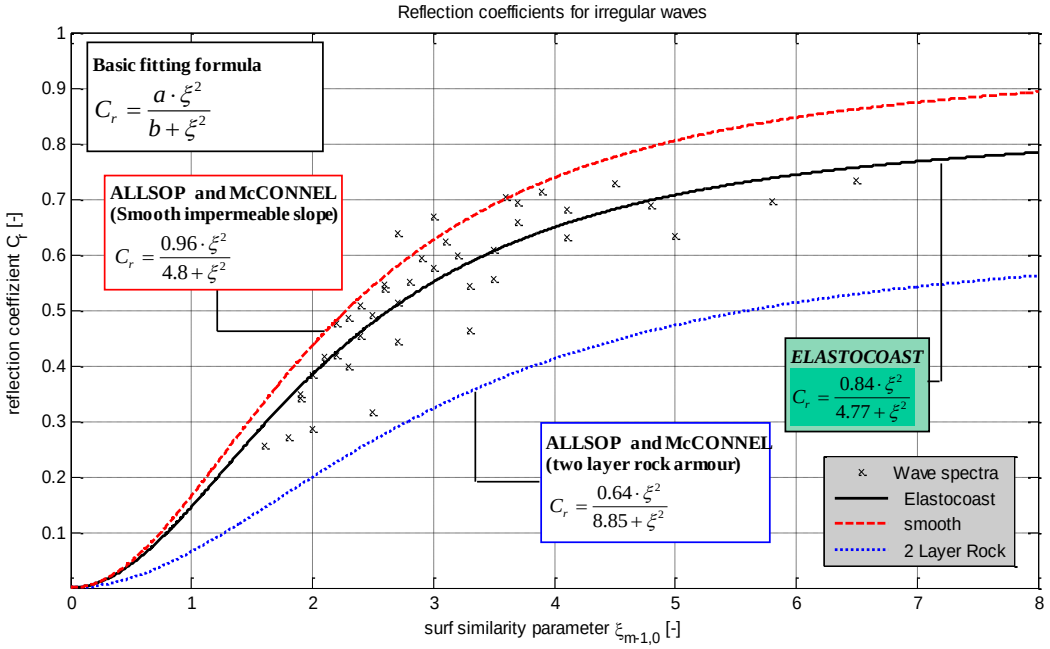

Fig. 2.2 Reflection coefficient for a PBA revetment (Oumeraci et al., 2010)

Generally, the reviewed studies on the reflection coefficient, show dependencies on wave length L_0, incident wave height H_i, equivalent grain size D_{eq}, slope angle α and also water depth at the toe of the structure h_t. The type of dependency as well as the composition of the parameters varies considerably. Furthermore, almost all formulae show one common problem: for very high surf similarity parameter ξ the reflection coefficient does not tend to 1 as they should under ideal conditions. This is only the case for smooth revetments according to Seelig & Ahrens (1981) (with $a_1 = 1$). For a better and physically sound approach, this issue has to be approached more appropriately. Therefore, a parameter study is required to verify the dependencies of the dissipation on the structure properties and wave parameters.

2.2 Swash processes

The swash region defines the most important zone of interaction between waves and any coastal protection system. Therefore, it is important to precisely define the location of this zone with the wave run-up height and the wave run-down height. Furthermore, the loads in this area have to be analysed. In this thesis, these are the velocities on the revetment. Studies on these parameters are reviewed in the present section with the wave run-up and run-down height in Subsection 2.2.2 and the corresponding velocities presented in Subsection 2.2.3. Even though most studies only consider the wave run-up and run-down heights with respect to still water level (SWL), the actual line around which the swash oscillates is by definition the mean water level (MWL). The difference between both lines is indicated by the wave set-up and wave set-down. These parameters are, therefore, necessary for any further investigation and they are reviewed in the first part of this section (Subsection 2.2.1).

2.2.1 Wave set-up and set-down

A process that is highly entangled with the wave run-up and run-down is the wave set-up. This process is described in detail in Gourlay (1992). Wave set-up and also set-down are caused by wave shoaling and breaking (Longuet-Higgins & Stewart, 1964) and mark the difference between SWL and MWL. Thus, they also affect the wave run-up and run-down heights as shown in Fig. 2.3. For regular waves the MWL is constant over time but for irregular waves it changes. In Fig. 2.3 the static wave set-up is depicted. The dashed line shows the SWL and the solid line represents the MWL with wave set-up and wave set-down. Additionally, the upper and lower envelopes of the water level elevation are shown which result in the wave run-up and run-down height on the revetment surface.

Wave set-down and wave set-up can be explained and described using the theory of Longuet-Higgins & Stewart (1964). Many approaches to the change in MWL are based on this theory, for example the one used in Goda (1975) or in USACE (2002), and all, more or less, result in the same equation (eq. (2.10), taken from Goda (1975)). It describes the change in MWL over the distance x.

$$\frac{d\eta}{dx} = -\frac{1}{\eta + h} \cdot \frac{d}{dx}\left(\frac{1}{8} \cdot H^2 \cdot \left(\frac{1}{2} + \frac{2kh}{\sinh 2kh}\right)\right) \tag{2.10}$$

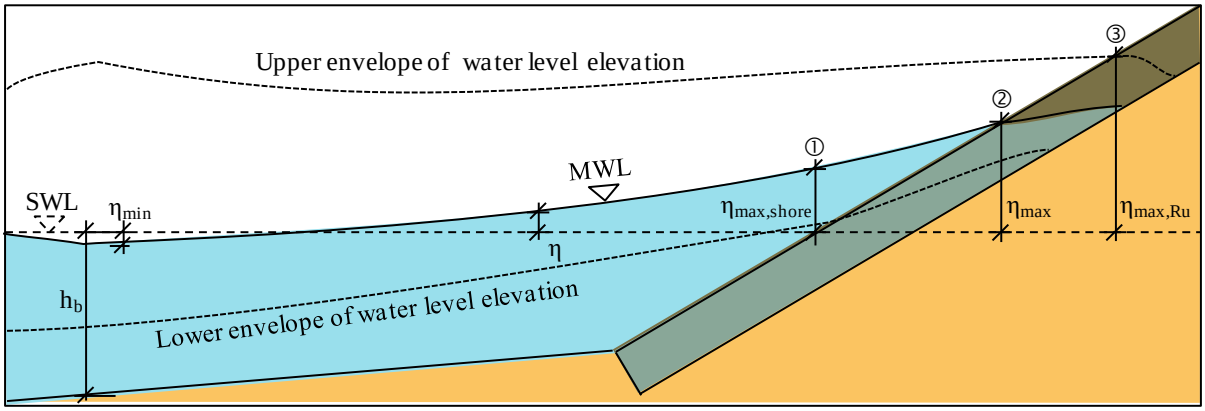

Fig. 2.3 Wave set-up and set-down – definition sketch

Generally, the definition of the wave set-up is not one hundred per cent clear throughout former studies. For positions seaside of the lowest run-down, the wave set-up (set-down) is the difference between the mean value of the measured time series and SWL. Determining the wave set-up landside of the intersection between beach/revetment and SWL is more difficult. Therefore, different definitions are used. Some theories, for example, do not include the landside area as e.g. eq. (2.10) which is not defined for non-positive h. The maximum wave set-up is, therefore, often defined at the intersection between SWL and the surface of the beach (see position ① in Fig. 2.3) and not at the actual coastline (see position ② in Fig. 2.3). Other studies define the maximum wave set-up as the wave run-up (see Nielsen, 1989 and position ③ in Fig. 2.3). The latter definition is, however, not very plausible and is, therefore, not supported here.

Overall, most studies define the development of the wave set-up in the swash zone as being linearly rising from the maximum wave set-down to the maximum wave set-up and also with an asymptotic increase directly at the shoreline (van Dorn, 1976, Battjes et al., 1978). A general problem is that all studies focus on beaches with mostly very flat slopes. This decreases the applicability to standard revetments. However, a general effect of the slope steepness was found. While for very smooth beaches a prediction formula of the type of eq. (2.11) (see Hanslow & Nielsen, 1993) is proposed, for steeper beaches, the surf similarity parameter is often included (eq. (2.12) – see Hanslow & Nielsen, 1993; Gourlay, 1992; Stockdon et al., 2006). Generally, the empirical approaches show large scatter in their results for the wave set-up (Fig. 2.4). A better approach should, therefore, be developed.

$$\frac{\eta_{max} \; or \; \eta_{max,Ru} \; or \; \eta_{max,shore}}{H} = \frac{constant}{\sqrt{H/L}} \tag{2.11}$$

$$\frac{\eta_{max} \; or \; \eta_{max,Ru} \; or \; \eta_{max,shore}}{H} = constant \cdot \xi \tag{2.12}$$

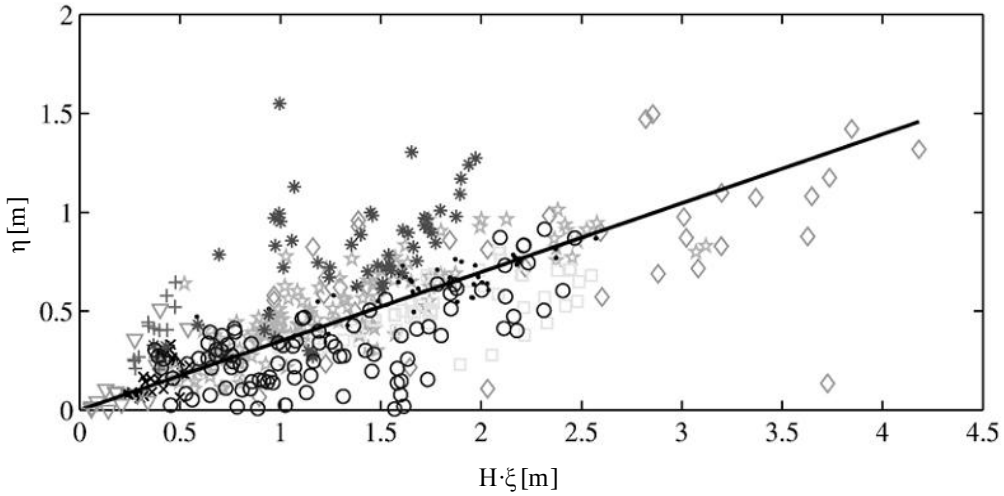

Fig. 2.4 Wave set-up at the revetment from different sites (Stockdon et al., 2006)

Calculation approaches on the wave set-down are less frequently found, because the parameter is less important for the loading on structures. Two descriptions can be found in (Oumeraci, 2007) (eq. (2.13)) and USACE (2002) (eq. (2.14)). Both are based on wave parameters at the point of breaking which is the point of the maximum wave set-down.

$$\eta_{min} = -\frac{1}{16} \cdot \frac{H_b^2}{h_b} \tag{2.13}$$

$$\eta_{min} = -\frac{1}{8} \cdot \frac{H_b^2 \cdot \frac{2 \cdot \pi}{L_b}}{\sinh\left(\frac{4 \cdot \pi}{L_b} \cdot h_b\right)} \tag{2.14}$$

Due to this very close link between the wave set-down and the breaking process, it is also possible to describe the location of the maximum wave set-down using a breaking criterion as for example given in Goda (2000) (eq. (2.15)).

$$\frac{H_b}{L_0} = 0.17 \cdot \left(1 - e^{-1.5 \cdot \frac{\pi h}{L_0}\left(1 + 15 \cdot \tan^{\frac{4}{3}} \alpha\right)}\right) \tag{2.15}$$

Overall, it can be concluded that wave set-up is more important than wave set-down because it is directly linked to the loading area on the surface of a coastal protection structure. Furthermore, a better and more consistent definition of the wave set-up has to be formulated.

2.2.2 Wave run-up and run-down

For an overall analysis of the loads on a revetment the upper and lower limit of the water movement are indispensable, mainly, because they determine the outer boundaries for many other processes. Especially, for the wave run-up height on smooth slopes as the upper boundary, many investigations have been performed in the last decades which are presented here first. The effects e.g. of a rough surface and permeability have, however, often only been considered for special cases like concrete block revetments. A short review on this topic is presented in the following, too. Regarding the wave run-down, the lower boundary, the results are scarcer than for the wave run-up. The available experimental results on the wave run-down height are presented together with the respective wave run-up studies. Because the available theoretical approaches all lack a certain amount of applicability to real data, no theoretical approaches to the wave run-up and run-down heights are presented here.

Wave run-up and run-down on smooth slopes is affected mainly by the slope steepness tanα and the wave parameters wave height H and wave period T. This dependency leads to the frequent usage of the surf similarity parameter ξ for many wave run-up analyses. One of them was performed by Schüttrumpf (2001). The main focus of this study was the overflow on sea dikes. Experiments on smooth slopes (cotα = 3, 4, 6) were carried out considering also the different processes on the dike. Contrary to other studies (see e.g. EurOtop, 2007), continuous formulae for the wave run-up height (eq. (2.16)) and wave run-down height (eq. (2.17)) were developed. Both, the wave run-up height $R_{u2\%}$ and the wave run-down height $R_{d2\%}$, are 2%-exceeding values and are related to the significant wave height H_S. An additional parameter was used in the formulae which is the surf similarity parameter ξ_{S0} based on the slope angle tanα, the significant wave height H_S and the deep water wave length L_0 (based on T_m).

$$\frac{R_{u2\%}}{H_S} = 3.0 \cdot \tanh(0.65 \cdot \xi_{S0}) \tag{2.16}$$

$$\frac{R_{d2\%}}{H_S} = -0.7 - 0.7 \cdot \tanh(\xi_{S0} - 2.1) \tag{2.17}$$

The hyperbolic tangent function resulted clearly in a better fit for the experimental data. However, a generally large scatter was observable which might indicate a problem with the chosen parameters (significant wave height H_S, surf similarity parameter ξ_{S0}) or other issues with the test set-up or –programme. Similar results as for the wave run-up height were obtained for the wave run-down height analysis.

A very detailed investigation focussing on the effects of rough and permeable surfaces on the wave run-up and run-down processes was made by van der Meer & Stam (1991) based on the one hand on a series of tests including permeable and impermeable rock slopes and on the other hand on comparisons with past laboratory tests and empirical formulae. During the analysis of existing formulae, a dependency on the surf similarity parameter ξ_P (based on peak period T_P and significant wave height H_S) was stated by the authors. Especially for $\xi_P < 2$, a linear function was found to be valid. This applies to both smooth, impermeable slopes and

permeable rock slopes as shown in Fig. 2.5. For surf similarity parameter $\xi_P < 2$ the following equations were proposed:

$$\text{smooth, impermeable slopes:} \quad \frac{R_{u2\%}}{H_S} = 1.5 \cdot \xi_P \tag{2.18}$$

$$\text{permeable rock slopes:} \quad \frac{R_{u2\%}}{H_S} = 0.83 \cdot \xi_P \tag{2.19}$$

These formulae underline the difference in wave run-up heights between smooth and rock slopes for small surf similarity parameters ($\xi_P < 2$). For values around $\xi_P = 2 - 4$ a maximum in the distribution of $R_{u2\%}/H_S$ for smooth slopes is observable. Contrariwise, a continuous rise up to $\xi_P \approx 6$ can be stated for the rock slope. This discrepancy between the two curves is getting smaller with higher ξ_P and from about $\xi_P = 6 - 7$ no difference in relative wave run-up height remains.

The second part of the study contains the analyses of effects of a rock slope on the wave run-up. Therefore the conditions were varied:

- slope steepness: cotα = 1.5 – 6
- rock grading D_{85}/D_{15} = 1.25; 2.25
- core permeability: impermeable, permeable, homogeneous (same diameter)
- surf similarity parameter $\xi_{S0} \approx 1 - 8$

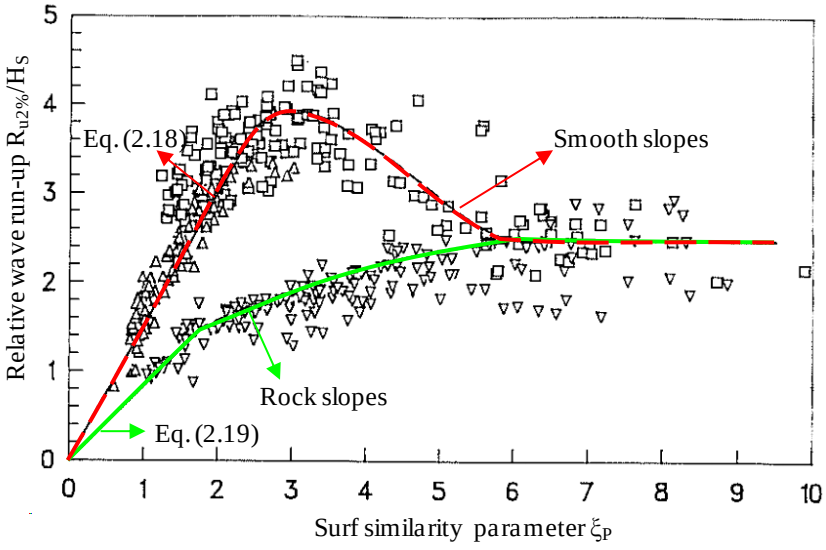

Fig. 2.5 Comparison of wave run-up height on smooth and rock slopes (van der Meer & Stam, 1991)

To determine final equations the influences of wave height, wave period, slope angle, permeability, spectral shape and water depth were investigated.

The first step of the study was the comparison of existing tests on a riprap slope to the performed ones (Fig. 2.6a). Thus, the grain grading was found to have no influence. In Fig. 2.6b the performance of the varying core permeability modes is depicted. For $\xi_{S0} < 3$ no distinct difference is present but for higher ξ_{S0} the permeable and homogenous curves remain constant while the wave run-up height for impermeable cores still rises continuously. A tentative explanation was given for this development. It stated the more significant effect of dissipation as well as high flow velocities for smaller ξ_{S0} (plunging and collapsing breakers). For surging breakers ($\xi_{S0} > 3$) the permeability is the more dominant parameter affecting the wave up-rush and down-rush which leads to smaller wave run-up heights for permeable cores. The final results are two equations which describe the wave run-up height on impermeable slopes (eqs. (2.20) and (2.21); Fig. 2.6b).

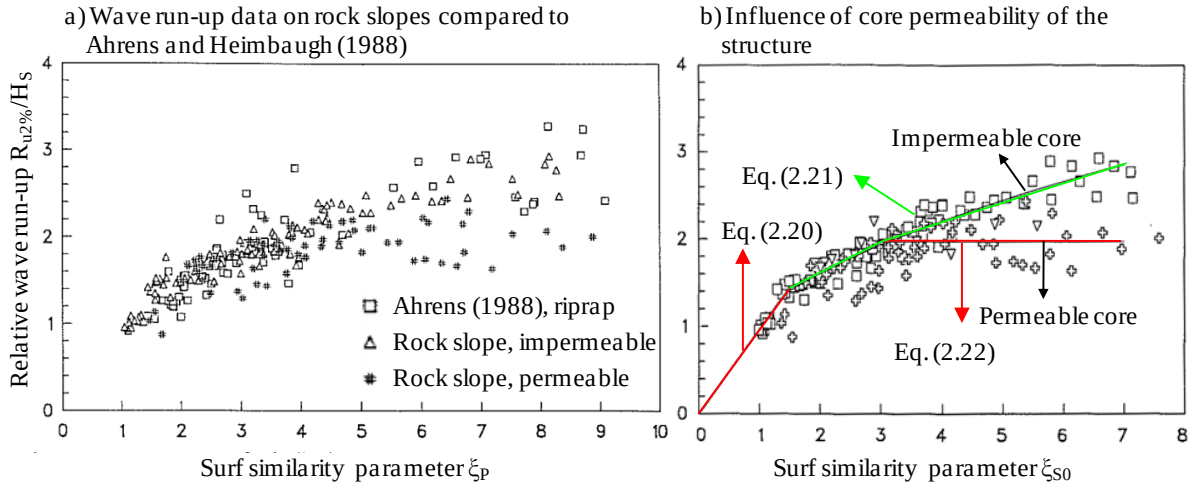

Fig. 2.6 Comparison of wave run-up on permeable and impermeable slopes (van der Meer & Stam, 1991)

$$\frac{R_{u2\%}}{H_S} = 0.96 \cdot \xi_{S0} \qquad \text{for } \xi_m < 1.5 \tag{2.20}$$

$$\frac{R_{u2\%}}{H_S} = 1.17 \cdot \xi_{S0}^{0.46} \qquad \text{for } \xi_m > 1.5 \tag{2.21}$$

With a maximum value for a permeable core:

$$\frac{R_{u2\%}}{H_S} = 1.97 \tag{2.22}$$

Other studies on rough and/or permeable structures lead to the same conclusions but used e.g. exponential approaches only (Losada & Giménez-Curto, 1981) or a notional permeability (van der Meer, 1993). The applicability of these concepts on other structures is somewhat difficult if not impossible and they are, therefore, not considered here. Furthermore, some theoretical and semi-empirical approaches and studies were reviewed. This included the

approach of Hughes (2004) that used the momentum flux parameter which is based on the theory of radiation stress established in Longuet-Higgins & Stewart (1964) to describe the wave run-up height. A similar approach was also used by Madsen & Fuhrman (2007). Both approaches show no improvements compared to purely empirical formulae and they give no more insight into the processes. The same applies for the theoretical approach of Kirkgöz (1981) using the Chézy coefficient to describe the friction of a surface. Therefore, none of these studies is presented here in detail.

The most frequently used formulae for wave run-up and run-down heights are documented in general guidelines. These recommended formulae are generally based on former studies as they are also presented above. The recommendations of two important guidelines can be summarised as follows:

(i) The "Coastal Engineering Manual" - CEM - (USACE, 2002) gives a broad overview of approaches to calculate wave run-up and run-down heights. Hereafter, the proposed equations for smooth, impermeable slopes are presented. Equation (2.23) shows the wave run-up formula which is divided into two parts and equation (2.24) gives the wave run-down formula which also consists of two parts. Both are based on deep water parameters and are valid for wave spectra. Surprisingly, the point of separation for the two parts is not the same for the wave run-up and run-down height (ξ_{0P} = 2.5 and 4.0).

$$\frac{R_{u2\%}}{H_S} = \begin{cases} 1.6 \cdot \xi_{0P} & for\ 0 < \xi_{0P} \leq 2.5 \\ -0.2 \cdot \xi_{0P} + 4.5 & for\ \xi_{0P} > 2.5 \end{cases} \tag{2.23}$$

$$\frac{R_{d2\%}}{H_S} = \begin{cases} -0.33 \cdot \xi_{0P} & for\ 0 < \xi_{0P} \leq 4.0 \\ -1.5 & for\ \xi_{0P} > 4.0 \end{cases} \tag{2.24}$$

(ii) EurOtop (2007) covers wave overtopping and the related processes and therefore, does not cover the wave run-down height. A complex version for the wave run-up height estimation is proposed by applying a split function as well as coefficients for roughness (γ_f), wave attack angle (γ_β) and a berm (γ_b). It can, thus, be used for impermeable slopes with varying surface layouts.

$$\frac{R_{u2\%}}{H_{m0}} = \max \begin{Bmatrix} 1.65 \cdot \gamma_b \cdot \gamma_f \cdot \gamma_\beta \cdot \xi_{m-1,0} \\ 1.00 \cdot \gamma_b \cdot \gamma_{f,surging} \cdot \gamma_\beta \left(4.0 - \frac{1.5}{\sqrt{\xi_{m-1,0}}} \right) \end{Bmatrix}$$

$$\gamma_{f,surging} = \begin{cases} \gamma_f & \xi_{m-1,0} < 1.8 \\ \gamma_f + \left(\xi_{m-1,0} - 1.8 \right) \cdot \frac{1 - \gamma_f}{8.2} & 1.8 \leq \xi_{m-1,0} \leq 10 \\ 1 & \xi_{m-1,0} > 10 \end{cases} \tag{2.25}$$

Overall, the strong dependency of the wave run-up height R_u and run-down height R_d on the surf similarity parameter ξ is confirmed. A generic formula is, however, not available mainly due to differing input parameters (local or deep water values, different statistical values).

Fig. 2.7 and Fig. 2.8 show the results of Oumeraci et al. (2010). Fig. 2.7 presents the results of the wave run-up height for irregular waves. The functions were determined using the EurOtop (2007) (eq. (2.25)) approach for impermeable slopes. Only a general coefficient accounting for both permeability and roughness was introduced. Therefore, an additional approach using separated coefficients for permeability and roughness is suggested. A dependency on the reflection parameter should be checked as well, especially, for higher surf similarity parameters $\xi_{m-1,0} > 2.7$. Next to these modifications, additional parameters to the surf similarity parameter $\xi_{m-1,0}$ have to be considered because the scatter within the data is still very high.

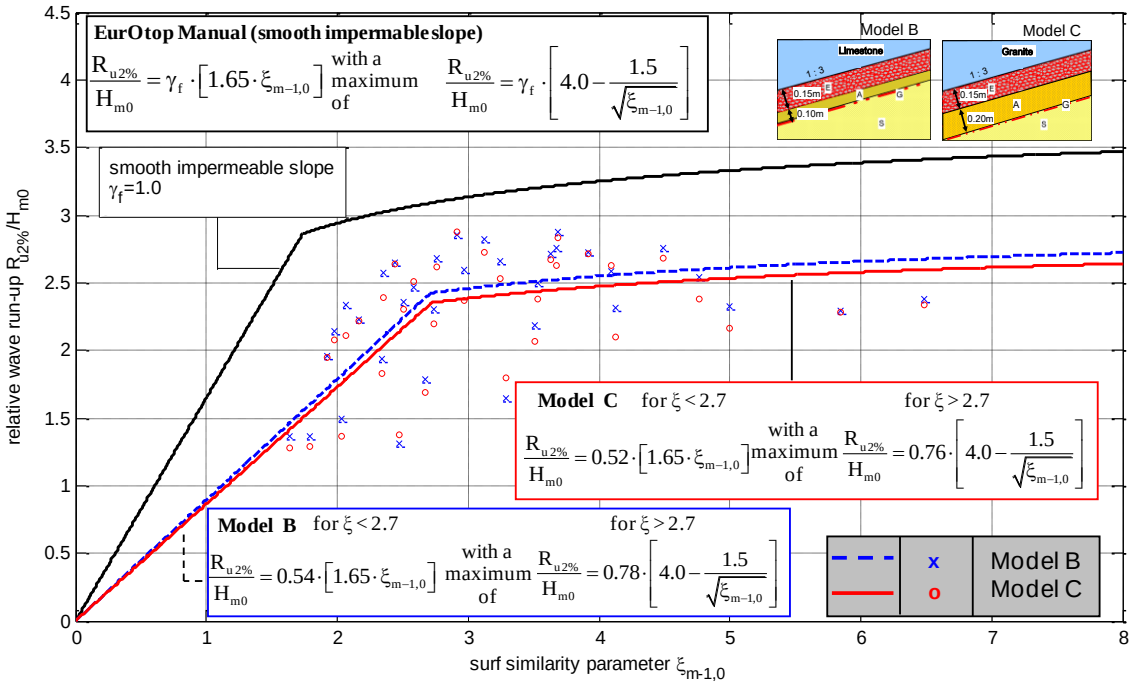

Fig. 2.7 Wave run-up height on a PBA revetment (Oumeraci et al., 2010)

The second figure (Fig. 2.8) from Oumeraci et al. (2010) shows the corresponding wave run-down heights for irregular waves. A simple approach was used again (Pilarczyk et al., 1995 resp. USACE, 2002 – eq. (2.24)). The distribution of the data points is more in line than for the wave run-up height (Fig. 2.8). This indicates a smaller dependency on other parameters than the surf similarity parameter. A modification of the approach similarly to the wave run-up height is, however, reasonable.

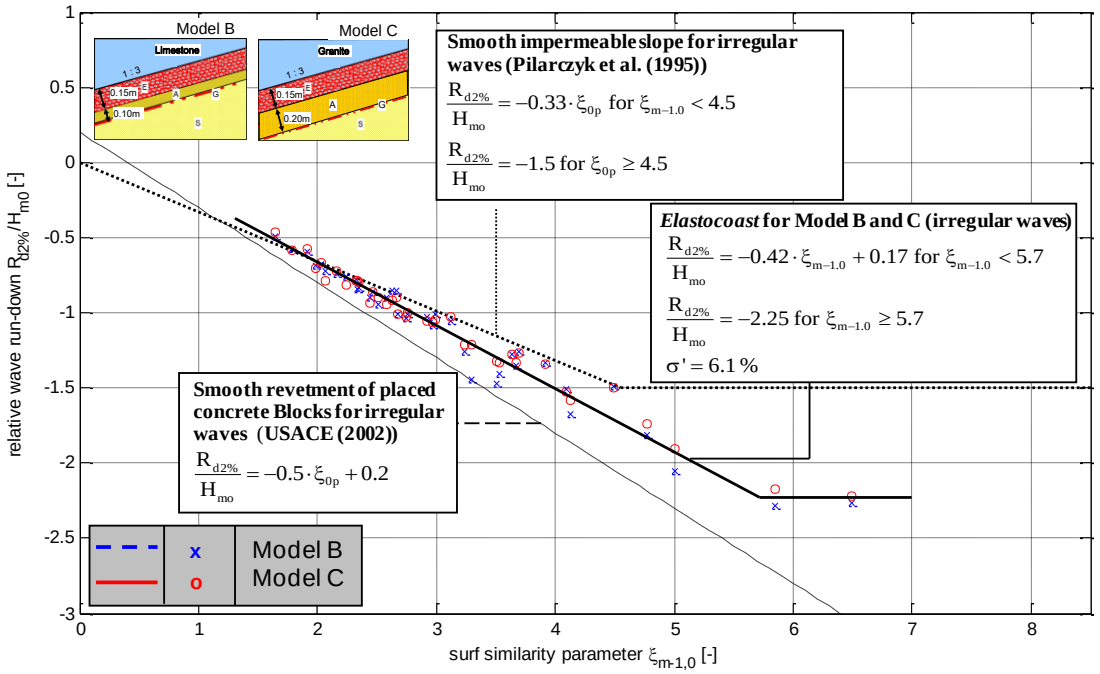

Fig. 2.8 Wave run-down height on a PBA revetment (Oumeraci et al., 2010)

2.2.3 Wave run-up and run-down velocities

Next to the wave run-up and run-down heights the swash velocities play an important role. Franzius (1965) investigated the velocity distribution during wave run-up for different slope steepnesses (1:2.27 – 1:6) and wave steepnesses (H_m/L_m = 0.041, 0.058, 0.080). Using a simple relation between potential and kinetic energy, a formula is given for the wave run-up velocity v_u on a water-free slope:

$$v_u = \sqrt{v_{u,max}^2 - 2 \cdot g \cdot S' \cdot \sin\alpha} \tag{2.26}$$

The maximum wave run-up velocity v_{max} signifies the last local maximum of the velocity distribution before the highest run-up height is obtained. S' is the distance on the slope surface from SWL (Fig. 2.9).

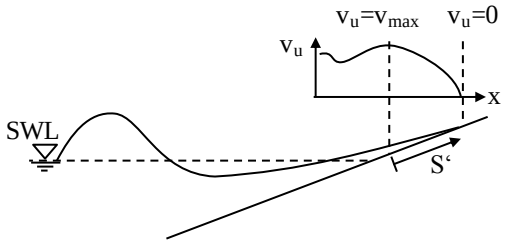

Fig. 2.9 Definition sketch for S'

Laboratory experiments (scale 1:10) were carried out to validate this equation on smooth slopes with varying steepnesses. For surging breakers ($H_m/L_m = 0.041$ and $\cot\alpha = 2.27 – 4$), the maximum velocity always occurred around 0.35 m landwards of the shoreline. Overall, the difference between the measured and approximated data using eq. (2.26) was found to be rather large especially for steep slopes.

For steeper waves ($H_m/L_m = 0.08$ and $\cot\alpha = 2.3 – 5.4$), the influence of backwash water was documented to result in a more complex velocity distribution. Through the interaction of up- and down-rush the velocity is decreased before increasing again when leaving the backwash water zone. One exception from the standard velocity distribution was determined for the steepest slope (1:2.27), where the backwash process seems to be completed, before the next wave arrives. This leads to the assumption that not the wave steepness alone determines whether an interaction with the backwash occurs but also the slope steepness. Therefore, the surf similarity number ξ might be a better parameter for this evaluation.

Finally, Franzius (1965) proposed a correction factor c' to handle the problem of the deviation between approximation (eq. (2.26)) and the measurements:

$$v_u = \sqrt{v_{u,max}^2 - 2 \cdot c' \cdot g \cdot S' \cdot \sin\alpha} \tag{2.27}$$

Given that c' is a constant coefficient for each wave climate its value can be determined at $v_u = 0$. The results of this approach are shown in the following figure (Fig. 2.10) and they are quite inconclusive in respect to similarity of the distribution. This suggests again a further need for investigations of the effects on the wave run-up velocity.

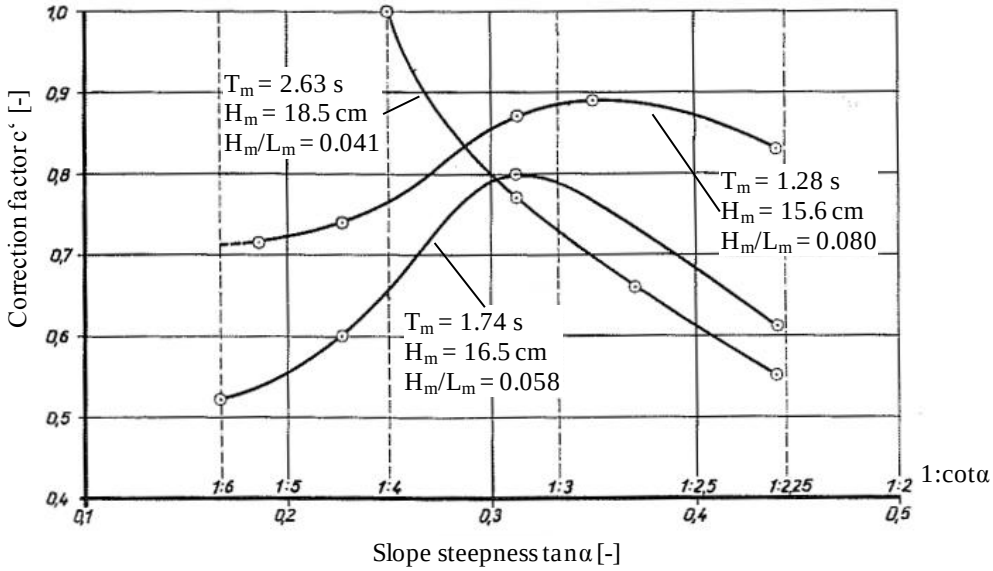

Fig. 2.10 Coefficient c' for the calculation of run-up velocity v_u (Franzius, 1965)

The wave run-up and run-down velocities were also analysed in Schüttrumpf (2001). These analyses resulted in a formula to describe the distribution of the mean maximum wave run-up velocity $v_{u50\%}$ over the slope (eq. (2.28)).

$$v_{u50\%}(S') = 0.53 \cdot \sqrt{\pi \cdot g \cdot (R_{u2\%} - S' \cdot \sin\alpha)} \tag{2.28}$$

According to Schüttrumpf (2001), the wave run-up velocity $v_{u50\%}$ depends only on the wave run-up $R_{u2\%}$ and the slope angle. For a better comparison, the formula was reformulated slightly without changing the results.

Based on Schüttrumpf (2001), a formula for the wave run-up velocity $v_{u2\%}$ (eq. (2.29)) is given in EurOtop (2007):

$$v_{u2\%} = 1.55 \cdot \sqrt{g \cdot (R_{u2\%} - x_A \cdot \tan\alpha)} \tag{2.29}$$

The equation differs from the original one (eq. (2.28)). This could be a result of the approaches to calculate the wave run-up height $R_{u2\%}$, which is used in the formulae. Totally different approaches are used: tangent hyperbolic (eq. (2.16)) and linear respectively square-root (eq. (2.25)); but also the surf similarity parameters ξ_{S0} and ξ_{0P} are different. Furthermore, the exceedance value is changed (from 50% in eq. (2.28) to 2% in eq. (2.29)). This might also explain the change in the factor from $0.53\sqrt{\pi} = 0.94$ (eq. (2.28)) to 1.55 (eq. (2.29)).

The review of different approaches to describe the swash processes reveals one general problem: the definitions of the parameters used in the approaches differ extremely. This results in several different surf similarity parameters which cannot be compared easily. However, a few findings apply overall: (i) the wave set-up is necessary to ensure a good analysis of the wave run-up and run-down heights, though it is often not used and a consistent definition is needed; (ii) the wave run-up and run-down heights mostly depend on the surf similarity parameter and are affected by both roughness and porosity and (iii) the swash velocities have not yet been analysed sufficiently.

2.3 Flow in porous media

The flow of any fluid is mainly determined by its regime, either it is laminar or turbulent. Especially turbulent flow is difficult to handle mathematically. This problem gets even more serious for flow in media with a complex porous structure as commonly used for revetments made of rock material. The present section focuses on solutions or simplifications of this problem as well as on the search for an applicable theory/approach to the specific conditions of a bonded porous revetment under non-stationary flow.

Generally, several models are available to describe the flow in porous media depending on the prevailing flow regime. The simplest and well-known model is the linear equation which was developed by Darcy in 1856 (eq. (2.30)) for laminar and stationary flow. Basically, the linear dependency between the hydraulic gradient i and the filter velocity u_f is described using a

coefficient normally named a. This coefficient is inversely proportional to the hydraulic permeability of the medium.

$$i = a \cdot u_f \tag{2.30}$$

Due to the restriction to laminar flow, the Darcy approach is in principle not applicable to highly turbulent flow processes as they occur in porous revetments made of gravel. Therefore, several alternatives were developed to serve the purpose of treating turbulent and unsteady flows. Phillip Forchheimer proposed an extended version of the Darcy equation in 1901 (eq. (2.31)). It contains an additional term $b \cdot u_f|u_f|$ to account for losses caused by convection and turbulence. The parameter b is chosen similarly to the parameter a of Darcy as a representation of the material characteristics.

$$i = a \cdot u_f + b \cdot |u_f| \cdot u_f \tag{2.31}$$

Several studies, empirical and theoretical, have been performed to determine the parameters a and b. An overview of the most important results is presented in Tab. 2.2.

Most of the approaches use geometrically based, analytical methods to determine the parameters either with a pipe (Ergun, 1952; Engelund, 1953) or a sphere analogy (Kozeny, 1927/Carman, 1937). Contrariwise, the coefficients α_f and β_f are the results of empirical investigations and can have either a very complex form (Shih, 1990), be simple mean values, as applied by Ergun, or depict a range of values (Engelund, 1953). Ward (1964) even determined the parameters a and b fully based on empirical approaches. Generally, a dependency on either both a simple grain size D (or D_{15} or D_{eq}) and the porosity n (Kozeny /Carman , Ergun , Engelund , Shih) or the specific permeability K_S (Ward, 1964) was found.

Tab. 2.2 Formulae for coefficients a and b (based on Burcharth & Andersen, 1995 and van Gent, 1993)

Author	a	α_f	b	β_f
Kozeny (1927)/ Carman (1937)	$180 \cdot \frac{(1-n)^2}{n^3} \frac{\nu}{gD^2}$	-	-	-
Ergun (1952)	$\alpha_f \cdot \frac{(1-n)^2}{n^3} \frac{\nu}{gD^2}$	150	$\beta_f \cdot \frac{1-n}{n^3} \frac{1}{gD}$	1.75
Engelund (1953)	$\alpha_f \cdot \frac{(1-n)^2}{n^3} \frac{\nu}{gD_{eq}^2}$	780	$\beta_f \cdot \frac{1-n}{n^3} \frac{1}{gD_{eq}}$	1.8 -3.6
Ward (1964)	$\frac{\nu}{gK_s}$	-	$\frac{\beta_f}{g\sqrt{K_S}}$	0.55
Shih (1990)	$\alpha_f \cdot \frac{(1-n)^2}{n^3} \frac{\nu}{gD_{15}^2}$	$1684 + 3.12 \cdot 10^{-3} \left(\frac{g}{\nu^2}\right)^{\frac{2}{3}} D_{15}^2$	$\beta_f \cdot \frac{1-n}{n^3} \frac{1}{gD_{15}}$	$1.72 + 1.57 \cdot \exp[-5.1 \cdot 10^{-3} \left(\frac{g}{\nu^2}\right)^{\frac{1}{3}} D_{15}]$

Polubarinova-Kochina extended the Darcy-Forchheimer formula by a third term in 1952 (called hereafter extended Forchheimer equation), which additionally accounts for the effect of flow acceleration:

$$i = a \cdot u_f + b \cdot |u_f| \cdot u_f + c \cdot \frac{\partial u_f}{\partial t} \tag{2.32}$$

The new parameter c is normally determined with a virtual mass concept. It is determined semi-empirically. Different approaches are available for the determination of parameter c and equations (2.33) and (2.34) present the most common results (cf. Sollitt & Cross, 1972; Gu & Wang, 1991; van Gent, 1993; Burcharth & Andersen, 1995).

$$c = \frac{1 + C_m \frac{1-n}{n}}{g} \tag{2.33}$$

$$c = \frac{1 + C_m \frac{1-n}{n}}{ng} \tag{2.34}$$

In both equations, (2.33) and (2.34), C_m is a virtual mass coefficient and n the porosity. The only difference between eq. (2.33) and (2.34) is the porosity n in the denominator. It is, however, still not clear which version is the more appropriate one. van Gent (1993) and Gu & Wang (1991) derived an equation of the same form as eq. (2.34) and Sollitt & Cross (1972) as well as Burcharth & Andersen (1995) determined a result of the form of eq. (2.33). The difference lies in the considered area for the derivation of c. The velocity u_f itself is a fictional quantity because it stands for the mean velocity averaged over the cross-sectional flow area which includes both pores and grains. If this assumption is also made for the derivation of C_m, eq. (2.33) would be obtained (Burcharth & Andersen, 1995).

This brief overview of the equations available for porous flow leaves the question of applicability open. It is not always stated clearly which formulae and parameters are applicable for which flow regime and whether non-stationary flow is also considered. Therefore, this aspect is treated in the following.

The effect of waves on flow in porous media was investigated by Gu & Wang (1991) for a plane bottom (no slope angle). The relative importance of the single terms of the flow equation (2.32) is shown as a function of two differently defined Reynolds numbers. Both numbers are based on the grain size D, but Re is the Reynolds number related to filter velocity u_f (eq. (2.35)) and Re_i is the Reynolds number based on wave period T (eq. (2.36)).

$$Re = \frac{u_f D}{\nu} \tag{2.35}$$

$$Re_i = \frac{2\pi D^2}{\nu T} \tag{2.36}$$

Using this approach has the advantage of showing the effect of wave action on the porous flow, which was not considered by the authors mentioned before. The filter velocity u_f is rarely known beforehand, but a pre-estimation of the flow regime can be made by using the wave period based Reynolds number Re_i. An overview of the resulting classification is shown in Tab. 2.3. The classification was confirmed by a laboratory study with standing waves over varying gravel sizes (Gu & Wang, 1991).

Tab. 2.3 Dominant forces for coastal wave conditions (Gu & Wang, 1991)

Description	D	u_f	Re	Re_i	Dominant force
Coarse sand or finer	<2mm	$<O(10^{-3})$	$<O(1)$	$<O(1)$	Laminar
Pebble, or small gravel	**1cm**	**$O(10^{-2})$**	**$O(10^2)$**	**$O(10^2)$**	**Laminar Turbulence Inertia**
Large gravel crusted stone	10cm	$O(10^{-1})$	$O(10^4)$	$O(10^4)$	Turbulence Inertia
Boulder crusted stone	0.3-1.0m	$O(10^0)$	$O(10^6)$	$O(10^5)$	Turbulence Inertia
Artificial blocks, large rocks	>1.0m	$>O(10^0)$	$>O(10^6)$	$>O(10^6)$	Turbulence Inertia

The second material group in Tab. 2.3, with a grain size of about 1cm, is important for the gravel material of the revetment and the flow regime considered in this study. According to Gu & Wang (1991), the flow regime for standard wave climates is in a range that is affected by all three factors: laminar, turbulence and inertia.

van Gent (1993) analysed the amount of the contribution of the laminar, turbulent and inertia term based on an oscillating flow through different materials. For the material group nearest to the subject of the study (D_{50} = 0.02 m; n = 45%), the turbulent term is dominant while the inertia term is negligibly small.

Three different formulae are available to describe flow in porous media. All three models are semi-empirical and several attempts to determine the empirical components have led to very different outcomes. A dependency on the properties of the porous medium is expected including grain size, shape and porosity. Additionally, the flow regime affects the parameters, thus making the treatment of oscillating flows extremely difficult. For the porous medium and the flow regimes considered in this study, the laminar, turbulent and inertia terms should be considered in the flow model to be selected, but the latter is assumed to be quite small.

2.4 Processes in the sand foundation

In this section, processes in the sand foundation which are mainly caused by hydrodynamic processes on the slope surface are reviewed. This means that the geotechnical processes and related stability issues are not described (overview see Ludwigs & Oumeraci, 2011a). This is because the data base of this thesis does not cover geotechnical parameters except for pore pressures in the soil and therefore no extensive analysis is possible here. Moreover, most of the pore pressures from the GWK-data have already been investigated intensively in Oumeraci et al. (2010) and this thesis should, therefore, only focus on the internal water level and some basic stability issues. For this objective, it is important to describe the internal wave set-up. The wave set-up depends mostly on a time frame of minutes up to very long durations. Therefore, this section will first review the set-up in the foundation and possible causes for its occurrence (Subsection 2.4.1) and then also review another process which occurs in a similar time frame: the residual pore pressure build-up (Subsection 2.4.2). This review is particularly needed in order to identify a clear distinction between set-up in the foundation and residual pore pressure.

2.4.1 Internal wave set-up

Internal wave set-up or the set-up in the foundation is the change of the water level inside a structure under wave attack. Internal water table changes are generally caused by a higher inflow rate than outflow rate. How this situation of a positive inflow balance into a structure can be reached is, however, different for varying structures and wave conditions. Different descriptions are found in the literature: in Barends (1993) the internal water table set-up is contributed to some kind of storing of the water in the structure; in Losada et al. (1998) it is suggested that internal breaking is causing the set-up and in Hall & Foster (1990), which is based on experiments, a rising water level in front of the structure is determined as the cause for internal rise of the water table. In the following, these studies and their findings are presented.

From Barends (1993) and Barends & van Hoven (2007) a theoretical approach to describe internal wave set-up in a dam which is impermeable at the rear end can be combined to:

$$\frac{\eta_{Sand,max}}{h_0} = \sqrt{1 + \frac{0.1 \cdot c' \cdot H_i^2}{n \cdot \lambda \cdot h_0 \cdot \tan\alpha} \cdot \left(1 - e^{-\frac{b_L}{\lambda}} \cdot \left(1 + \frac{b_L}{\lambda}\right)\right)} \tag{2.37}$$

where c’ is a constant accounting for effects like aeration with c’ > 1. λ is the infiltration depth and b_L is the width of the structure respectively the water table length. Furthermore, according to Barends (1993), the maximum internal wave set-up in a dam which is closed at the rear end is located at the closed end meaning the water level rises from the shore side of the structure to its impermeable other side.

Losada et al. (1998) came to a similar conclusion concerning the spatial layout of the internal set-up using a different theoretical approach than Barends (1993). This investigation used a

shallow water model to simulate the wave propagation through a vertical porous structure under wave attack with different angles. The results for a semi-finite breakwater are shown in Fig. 2.11. As predicted by Barends (1993), the maximum set-up within the structure is found at the closed end. Furthermore, the set-down in front of the structure shows two local extremes. This is rather unusual and points to two locations of wave breaking: one in front of the structure and one at the outer boundary of the breakwater.

Both investigations, Barends (1993) and Losada et al. (1998), basically focus on long waves because the theoretical description of breaking waves is rather complex. This simplification does not represent the typical sea state during storms and, thus, might lead to wrong conclusions (meaning the internal breaking described in Losada et al., 1998 cannot be transferred to plunging breakers). Therefore, an experimental study using a different wave climate is presented in the following.

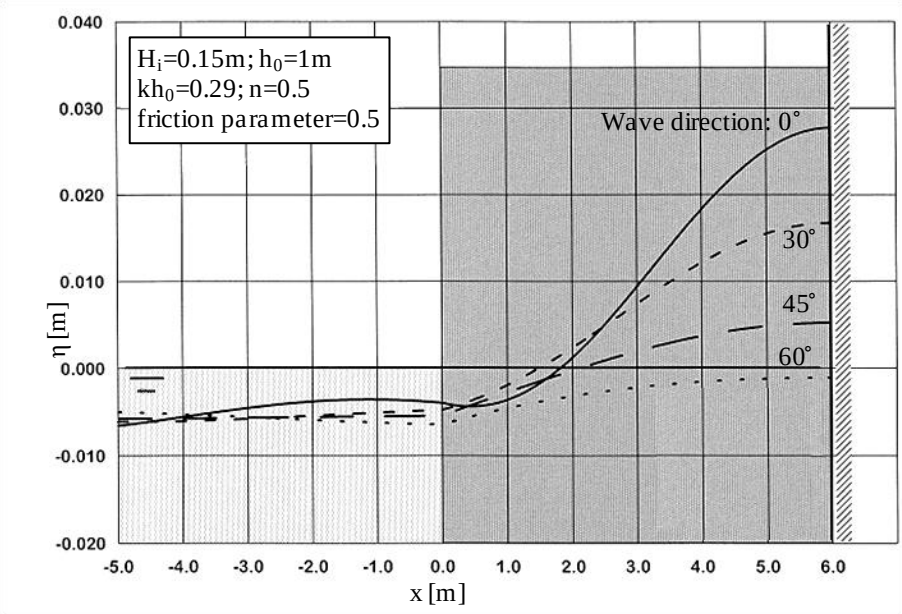

Fig. 2.11 Set-up in a semi-finite breakwater for different angles of wave incidence (based on Losada et al., 1998)

Hall & Foster (1990) focuses on the difference between newly installed breakwaters and reshaped ones meaning breakwaters with an outer slope that was put into a more stable shape. The objective of the study was to show the effect of both shapes on the internal mean water level and pore pressures. The associated tests were performed in a wave flume (0.9 m x 1.75 m x 50 m). For the breakwater the following materials were used: armour with D_{50} = 40 mm, filter layer with D_{50} = 16 mm and core material with D_{50} = 3.5 mm. Wave climates with surf similarity parameters ξ = 1.47 – 7.21 were used to test the 1:2 slope. The results for ξ = 2.7 and 3.82 are presented in Fig. 2.12. For this study only the results from the conventional breakwaters are of interest. These show a maximum internal set-up near or at the outer slope of the core for both tests. This stands in contradiction to the results of Barends (1993) and Losada et al. (1998). Two reasons for this discrepancy are possible: (i) the testing

time was too short for the internal build-up or (ii) the spatial layout of the set-up also depends on the breaker type. Therefore, further research is needed on this topic.

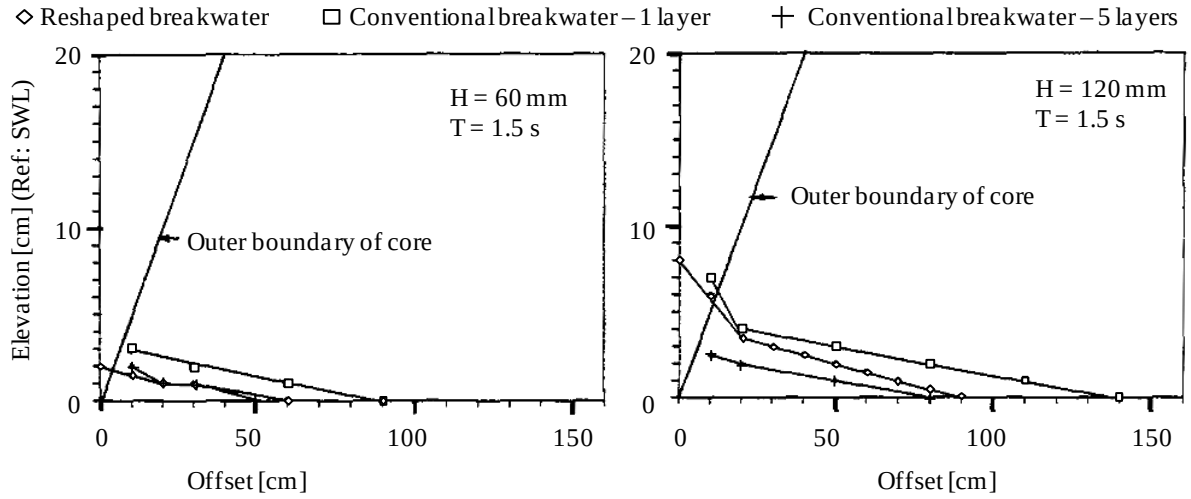

Fig. 2.12 Internal phreatic set-up (Hall & Foster, 1990)

2.4.2 Residual pore pressure

Due to the oscillatory motions of both waves and structure, the pore pressures in the soil may vary greatly. The pressure variations caused by oscillatory motions are often called excess pore pressures in relation to the hydrostatic pore pressures. This excess pore pressure u can be separated into two main parts; the transient pore pressure u_t and the residual pore pressure u_r (Fig. 2.13).

The transient pore pressure u_t depends mostly on wave properties while the development of the residual component is characterised mainly by soil properties. If the drainage conditions are favourable and the frequency of the load cycles are high enough, the pore pressure that is built up during one load cycle will fully dissipate before the occurrence of the next load cycle. Especially under impermeable structures such as caisson breakwaters, this process has not enough time to reach the pressure value from the preceding cycle and over time an additional pore pressure, namely the residual pore pressure, develops. For permeable structures, the residual pore pressure is not as important as the transient pore pressure due to the good drainage provided by the highly porous revetment. Nevertheless, residual pore pressures might still be induced. Studies on this process are rarer than studies on transient pressures. Even the parameterization of the process is difficult. One part of the process that was investigated by Kudella & Oumeraci (2004) is the decrease of residual pore pressure without new generation of pressure i.e. waves. Based on four tests this relation can be expressed by eq. (2.38).

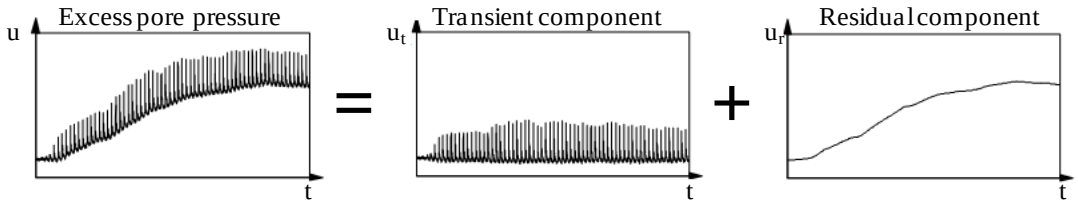

Fig. 2.13 Excess pore pressure with transient and residual component (based on Kudella & Oumeraci, 2004)

$$u_r = u_{r,0} \cdot e^{\frac{t-t_0}{T_{Drain}}} \tag{2.38}$$

A definition for the single coefficients and parameters as for example the start time t_0 and initial residual pore pressure $u_{r,0}$ are all depicted exemplarily in Fig. 2.14. The relation gives information on the drainage of a soil after a wave attack. It might also be used to describe the build-up of the residual pore pressure.

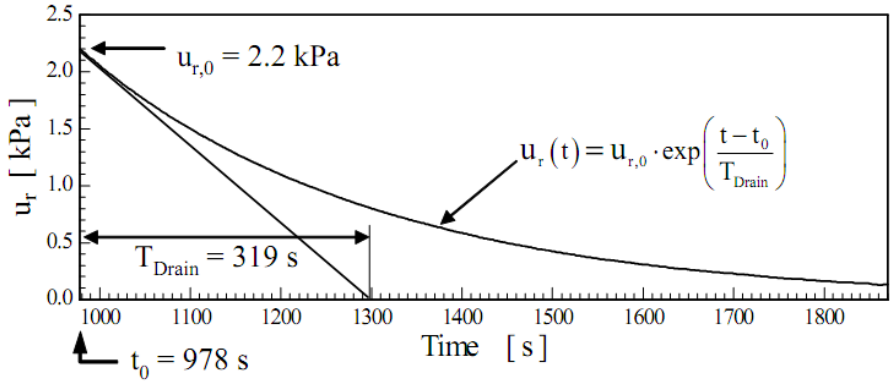

Fig. 2.14 Dissipation of residual pore pressure (Kudella & Oumeraci, 2004)

One important effect of residual pore pressures is their influence on the stability of a soil. A build-up of residual pore pressure might for example cause liquefaction in the soil (Groot et al., 2006). This is in general also the most important difference between residual pore pressures and a set-up of the water table.

Two contradictory versions for the spatial layout of the internal wave set-up are found and have, therefore, to be checked. Furthermore, it has to be determined whether a build-up of residual pore pressure is likely to occur beneath a highly permeable revetment.

2.5 Numerical modelling

The theory of fluid mechanics is a subtheory of continuous mechanics focusing on fluids. In the following paragraphs the most important equations and models are described. For a better readability the Einstein notation is used. This also simplifies a comparison to other works. The consequence is that an index actually stands for the sum over all possible index-values. A more detailed overview can be found in Oertel & Laurien (2003).

2.5.1 Navier-Stokes and RANS

Generally, for the solution of a physical problem not only one axiom is sufficient. Therefore, several equation sets have been developed which take into account varying aspects of the issue. An often used one was determined by Navier and Stokes and is written in Sigloch (2009) as follows:

$$\rho \cdot \left(\frac{\partial u_i}{\partial t} + \frac{\partial u_i}{\partial x_j} \cdot u_j \right) = \rho \cdot f_i - \rho \cdot \frac{\partial p}{\partial x_i} + \mu \frac{\partial^2 u_i}{\partial x_j^2} \tag{2.39}$$

It basically consists of the conservation of momentum and includes also the dynamic viscosity μ. However, it still only applies for laminar flows and this approach is insufficient for this study.

A possible form of modification is the consideration of turbulence. This can be done for example with the Reynolds approach: The varying components are separated into their temporal mean value ($\bar{u}$) and their fluctuation (u'), e.g.

$$u = \bar{u} + u' \tag{2.40}$$

An equation set based on this separation is called Reynolds-Averaged-Navier-Stokes (RANS) and the presented formula (2.39) changes into the following - see Sigloch (2009):

$$\rho \cdot \left(\frac{\partial \bar{u}_i}{\partial t} + \frac{\partial \bar{u}_i}{\partial x_j} \cdot \bar{u}_j \right) = \rho \cdot f_i - \rho \cdot \frac{\partial \bar{p}}{\partial x_i} + \frac{\partial}{\partial x_j} \left(\mu \cdot \frac{\partial \bar{u}_i}{\partial x_j} - \rho \cdot \overline{u_i' \cdot u_j'} \right) \tag{2.41}$$

In this notation $\rho \cdot \overline{u_i' \cdot u_j'}$ can be assembled in a tensor matrix which then includes the so called Reynolds stresses. Therefore, taking the turbulence into account makes it also necessary to find an approach to calculate or obtain these additional components. A few possibilities to undertake this task are presented in the next section.

2.5.2 Turbulence models

For most real life problems, turbulence models are required. In the previous subsection, a basis for the implementation of turbulence is given for RANS-equations. However, additional formula and models are needed to account for the solution of the additional terms. These equations or system of equations are often called closure models. This name is derived from their purpose of making the RANS-equations solvable for numerical codes by completing the system of formulae. Due to the high number of variables, which are necessary for turbulent processes more equations have to be determined (through boundary conditions or additional relations) to ensure solvability.

Most of the turbulence models use the concept of eddy viscosity others treat every Reynolds stress separately. Generally the complexity of the different approaches equals their exactitude

but it also relates to their computing time. Here only the k-ε-model is presented because it is the one used for the numerical simulations of this thesis (see Subsection 2.5.3).

The models depending on k and ε belong to the Two-equation-models because they consist of two differential equations. Additionally to this fact, these model introduce two new variables namely k the turbulent energy and ε the dissipation rate. These are normally described by formulae using semi-empirical approaches for example using the turbulent viscosity:

$$\mu_t = C_\eta \cdot \rho \cdot \frac{k^2}{\varepsilon} \tag{2.42}$$

$$\nu_t = \frac{\eta_t}{\rho} = C_\eta \cdot \frac{k^2}{\varepsilon} \tag{2.43}$$

This procedure leads on the one hand to the necessity of obtaining additional material values for the specific problems and also to high computing times. On the other hand the documented results are much better than for the Zero-Equation-Models. In the following the formulae for a common two-dimensional, inviscid and incompressible approach are shown.

$$\frac{\partial k}{\partial t} + \frac{\partial (k \cdot u_j)}{\partial x_j} = \frac{\nu_t}{\sigma_k} \cdot \frac{\partial^2 k}{\partial x_j^2} + \nu_t \cdot 2 \cdot \frac{\partial \bar{u}_i}{\partial x_j} \cdot \left(\frac{\partial \bar{u}_i}{\partial x_j} + \frac{\partial \bar{u}_j}{\partial x_i} \right) - \varepsilon \tag{2.44}$$

$$\frac{\partial \varepsilon}{\partial t} + \frac{\partial (\varepsilon \cdot u_j)}{\partial x_j} = \frac{\nu_t}{\sigma_\varepsilon} \cdot \frac{\partial^2 \varepsilon}{\partial x_j^2} + C_{\varepsilon 1} \cdot \nu \cdot \frac{\varepsilon}{k} \cdot \frac{\partial \bar{u}_i}{\partial x_j} \cdot \left(\frac{\partial \bar{u}_i}{\partial x_j} + \frac{\partial \bar{u}_j}{\partial x_i} \right) - C_{\varepsilon 2} \cdot \frac{\varepsilon^2}{k} \tag{2.45}$$

Due to the number of approaches using k and ε several varying definitions and formulae can be found. These all apply for certain boundary conditions. Therefore, depending on the specific problem modifications might be needed.

2.5.3 COBRAS-UC

There are several numerical models using the RANS-equations to solve especially fluid related problems. One that is specialised in water wave related question is the two-dimensional model COBRAS (or the graphically developed COBRAS-UC, COBRAS = Cornell Breaking Wave and Structures; UC = University of Cantabria). It was developed from the NASA model RIPPLE and uses the Volume of Fluid (VOF) method, thus, allowing the simulation of proper wave breaking. The description of the used equations and other properties can be found in a User's manual (COBRAS, 2005) as well as several papers (for example Losada et al., 2008; Lara et al., 2008). COBRAS and COBRAS-UC can simulate tests with and without turbulence models as they are described in Section 2.5.2. Furthermore, the numerical model can implement porous as well as impermeable, smooth

bodies into a wave-subjected flume. Lara et al. (2008) and Losada et al. (2008) deal with porous media and found reasonably good results of the simulations compared to physical tests. The results for the Forchheimer coefficients α_f and β_f and the inertia coefficient C_m (see Section 2.3, Tab. 2.2 and equations (2.32) - (2.34)) obtained in Lara et al. (2008) and Losada et al. (2008) are shown in Tab. 2.4. The results seem rather random because only the value for β_f is changed but shows no correspondence to the mean grain diameter D_{50}. Comparing the numerical model to the theory presented in Section 2.3, it can be summarised that COBRAS-UC uses the approaches shown in Tab. 2.2 (Engelund, 1953) and additionally eq. (2.33). Even though the latter one is not the favoured approach, it can be accepted as long as only one porosity n is used. Moreover, both, Lara et al. (2008) and Losada et al. (2008), used a k-ε model for their tests.

Tab. 2.4 Forchheimer and inertia coefficients for differing materials from COBRAS-UC

D_{50} [m]	α_f [-]	β_f [-]	C_m [-]	Paper
0.0035	200	0.8	0.34	Lara et al. (2008)
0.0100	200	0.8	0.34	Losada et al. (2008)
0.0350	200	1.1	0.34	Lara et al. (2008), Losada et al. (2008)
0.1350	200	0.7	0.34	Losada et al. (2008)

A RANS-VOF-model with an extended Darcy-Forchheimer model for flow in porous media can be applied to the problem and type of structure considered in this study. The values for the Forchheimer and inertia coefficients determined by Lara et al. (2008) and Losada et al. (2008) can provide proper reference values for the prospective investigations.

2.6 Summary and implications for the investigations

Several implications for this thesis might be drawn from the results of this state of the art review: (i) the reflection analysis should be based on the approach proposed by Seelig & Ahrens (1981); (ii) the wave set-up should be included in the analysis especially for the investigations on the wave run-up and run-down and (iii) more research on the velocities on the revetment is necessary.

The processes inside the porous revetment are mostly unknown and need to be analysed extensively. One other focus will be the residual pressures in the sand core beneath the revetment and the changes in the internal water table. Especially, the question which of both is actually present beneath a porous revetment needs to be answered.

A general problem with most of the formulae reviewed above is the incorrectness of the results for the extreme values of the surf similarity parameter ($\xi \rightarrow 0$ and $\xi \rightarrow \infty$) which affects most of the processes on, in and beneath the revetment. An example is the reflection coefficient that does not tend to $C_r = 1$ for very high surf similarity parameter ξ as it should do under ideal and frictionless conditions. It is therefore proposed, that the boundary conditions listed in Tab. 2.5 are fulfilled for any prediction approach that will be made.

Tab. 2.5 Boundary conditions for several hydraulic parameters at extreme values of surf similarity parameters $\xi \rightarrow 0$ and $\xi \rightarrow \infty$ under ideal conditions

$\xi = \frac{\tan \alpha}{\sqrt{H/L}}$ H_{loc} = wave height at the structure	$\xi \rightarrow 0$ 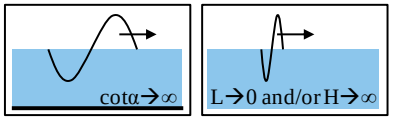	$\xi \rightarrow \infty$ 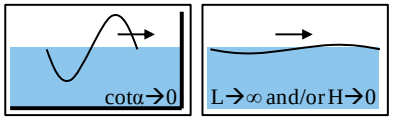
Wave set-down $\eta_{S,WG}$	0	0
Wave set-up $\eta_{S,RUG}$	0	0
Dissipation E_{diss}	1	0
Reflection coefficient C_r	0	1
Local velocities v_m	0	$2 \pi H_{loc}/T$
Wave run-up R_u	0	H_{loc}
Wave run-down R_d	0	H_{loc}
Run-up/down velocities v_R	0	$2 \pi H_{loc}/T$
Internal velocities v_{int}	0	$2 \pi H_{loc}/T$
Internal wave run-up/down R_{int}	0	H_{loc}
Internal set-up η_{int}	0	0

Even though the numerical model COBRAS-UC shows some shortcomings, it is still appropriate enough to perform the planned simulations. A k-ε-turbulence model and the description of the flow in porous media based on the extended Darcy-Forchheimer equation (eq. (2.32)) should be used.

3 Experimental and Numerical Test Set-Ups and Programmes

The data for the analyses in this thesis is obtained from two different test series: large-scale tests in the large wave flume (GWK) in Hannover and numerical simulations with COBRAS-UC. In the following, both set-ups and the related test programmes are presented. For the GWK-tests, Section 3.1 summarises briefly the detailed description of the report by Oumeraci et al. (2010). For the numerical simulations, the development of the mesh and the test set-up are presented as well as the test programme (Section 3.2).

3.1 Large scale tests in the GWK

Large scale model tests were performed in 2009 in the GWK of the Coastal Research Centre (FZK) in Hannover, Germany (see Fig. 3.1a). The objective of the tests was to investigate the interaction between waves and an innovative porous, bonded revetment on a sand foundation. For these tests, the Elastocoast® material was used to construct the polyurethane bonded aggregate (PBA) revetment. This material is constructed using a rubble aggregate that is coated with a polyurethane bonding agent. During the hardening of the bonding agent, the contact points of the rubble are, thus, connected without filling the pore volume. The material used in the GWK had a porosity of about n = 0.4.

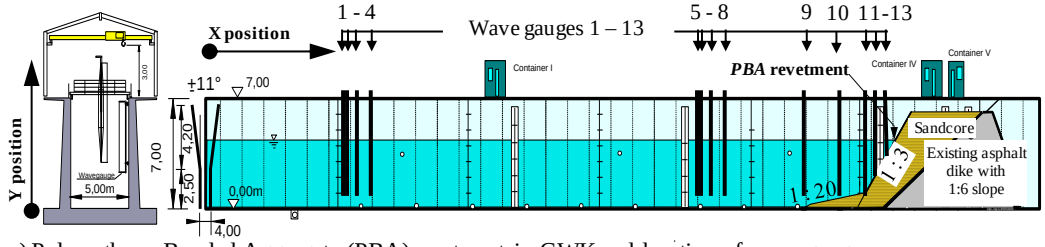

a) Polyurethane Bonded Aggregate (PBA) revetment in GWK and location of wave gauges

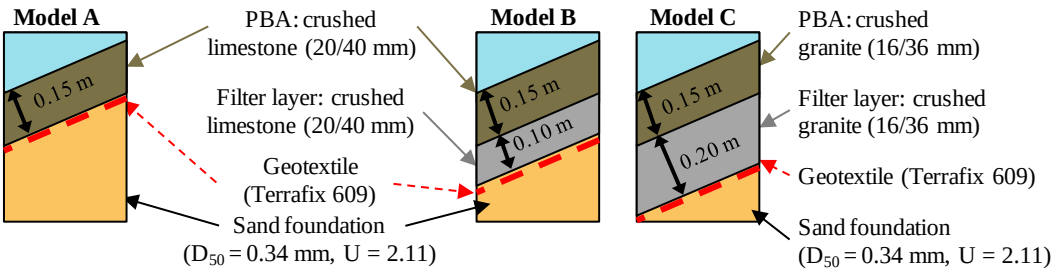

b) Tested PBA revetment models in GWK

Fig. 3.1 Test set-up of the PBA revetment (based on Oumeraci et al., 2010)

The GWK is more than 300 m long, 5 m wide and 7 m deep. The PBA revetment was installed upon a sand foundation with a slope steepness of 1:3 at the end of the flume. Furthermore a 1:20 sand foreshore was installed in front of the structure. The test set-up is depicted in Fig. 3.1a. To test different revetment layouts simultaneously, two model alternatives were installed side by side over the 5m-wide flume: first, model alternatives A

and B and then model alternatives B and C (cf. Fig. 3.1b). The models were separated by a thin wooden wall (see Fig. 3.2). For more information on the test set-up see Oumeraci et al. (2010).

More than 80 measuring devices were installed in the GWK. An overview is given in Fig. 3.2. For this thesis, only some of the devices are important which are briefly described in the following:

(i) Wave run-up gauges (RUG): Two wire resistance gauges were fixed to each model alternative behind each other. They measured the vertical distance of the water surface from SWL (Fig. 3.2).

(ii) Pressure transducers (PT) on and in the revetment: Several PTs were installed on and just beneath the bonded revetment as well as just beneath the filter layer (Fig. 3.2).

(iii) Pressure transducers in the sand foundation: Several PTs were installed beneath the expected impact area in the sand foundation of each model alternative (Fig. 3.2). Furthermore, three additional PTs were installed between the two model alternatives further into the sand to record the water table within the sand foundation.

(iv) Wave gauges (WG): 13 wave gauges were installed along the flume wall (Fig. 3.1a). Two gauge arrays to perform reflection analyses for a location directly in front of the foreshore and also near to the wave generator. Moreover, five wave gauges were installed above the foreshore and the revetment.

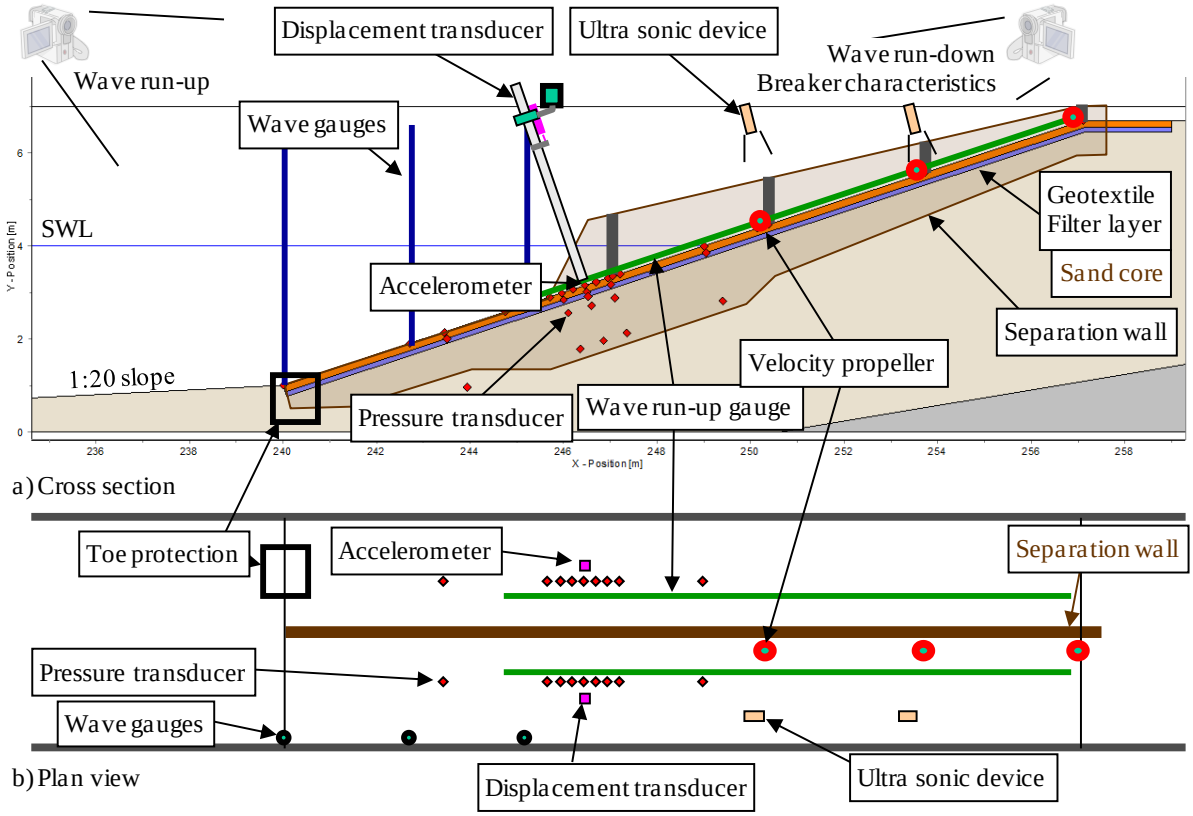

Fig. 3.2 Deployed measuring and observation devices in the GWK-tests (Oumeraci et al., 2010)

More detailed information on the positioning, the type of measurements and the data acquisition can be found in Oumeraci et al. (2010) and all information needed for this thesis is provided at the respective places. Furthermore, an overview of all important devices is given in Appendix A.1 (Tab. A.1 and Tab. A.2).

For the tests in the GWK, different types of waves were used. First of all, tests with regular waves were performed. Each test of this kind contained between 50 and 100 waves. Furthermore, tests with irregular waves were carried out with Jonswap-spectra (300 - 1000 waves). A few tests with focused waves and solitary waves were also performed, but these are not considered here. An overview of the range of wave conditions that were used in the GWK is given in Tab. 3.1 and a list of all performed tests with regular waves can be found in Appendix A.1 in Tab. A.3 and Tab. A.4.

Tab. 3.1 Wave conditions considered in the GWK-tests

	H_m/H_{m0}	$T_m/T_{m-1,0}$	$\xi_m/\xi_{m-1,0}$	h_0
Regular waves	0.17- 1.40 m	2.99 – 8.05 s	1.2 – 8.1	3.4 – 4.2 m
Irregular waves	0.19 – 1.17 m	2.66 – 7.11 s	1.6 – 6.6	3.4 – 4.2 m

3.2 Numerical simulations

The main objective of performing numerical simulations was to extend the data basis for this thesis. This applies most of all to the extension of model alternatives. The GWK-tests only included three slightly different revetment structures all with the same slope angle. Therefore, one focus was laid on using different slope angles. But also the revetment thickness was varied also including a smooth revetment (d_{rev} = 0 m). Moreover, a broader range of surf similarity parameter was obtained by using different slope steepnesses and wave parameters. Furthermore, the numerical simulations made it possible to analyse the processes in the revetment itself, which are normally hidden.

To achieve this objective, the 2D numerical model COBRAS-UC described in Subsection 2.5.3 was used. Before performing numerical tests, several preparatory steps had to be made: (i) a suitable numerical mesh for the simulations had to be developed (Subsection 3.2.1); (ii) pre-tests to validate the model set-up using the GWK-data and to set the Forchheimer coefficients (Subsection 3.2.2); (iii) the final test set-up had to be developed based on the described objectives and on the limitations of COBRAS-UC (Subsection 3.2.3) and (iv) the test programme had to be finalised (Subsection 3.2.4).

3.2.1 Development of the mesh

As the precision of the model is mainly determined by the cell size, the development of the numerical mesh (also called grid) is an important step for the numerical simulations. First, a very coarse mesh was chosen (Fig. 3.3a): with 10 cm x 10 cm to 20 cm x 10 cm the cells are rather large and the mesh was, therefore, only used to perform basic tests. One of these aimed at determining the possibility of simulating the processes in the sand foundation, which was found to be very time consuming even with such a coarse mesh. The same result was found

for the next finer mesh size (Fig. 3.3b). Therefore, the possibility of simulating the processes in the sand foundation had to be excluded from the test set-up.

Generally, a larger space in front of the revetment than in the first two meshes is necessary for two reasons: (i) the waves generated at the left end of the flume need more space to fully develop into shallow water waves and (ii) a better comparability to the original physical tests is ensured by the longer flat part (e.g. in a reflection analysis). An attempt to incorporate this space resulted in similar cell sizes (see Fig. 3.3c) as before (Fig. 3.3b), but due to a longer flume a larger number of cells was necessary. Tests with Stokes II and V waves were performed with the mesh shown in Fig. 3.3c instead of using sine waves. However, these measurements were not sufficiently accurate compared to the original GWK-data, so the mesh was altered again. It resulted in a three-part mesh with cell sizes from 2 cm x 4 cm to 5 cm x 4 cm which was eventually used for validation (Fig. 3.3d).

The main problem when performing longer tests with the mesh shown in Fig. 3.3c is the occurrence of re-reflection at the left side of the flume, where the waves are generated. This problem could only be solved by creating waves externally and using them as an input for the model. This was then done for the validation tests using a MATLAB routine generating Stokes V waves with the theory of Fenton (1985) for the mesh in Fig. 3.3d. The results of this approach are presented in Subsection 3.2.2. Even though, this solved the problems with the re-reflection on the left side, there were still problems with the generation of the waves. The externally generated Stokes V waves tend to break during generation which causes them to lose a considerable amount of energy towards the revetment. A better solution had, therefore, to be found for the final simulations.

It was then decided to split the simulations into two parts using two numerical flumes (see Fig. 3.3e-1 and e-2). On the left side of the empty flume (Fig. 3.3e-1) Stokes II and Stokes V waves (depending on the wave climate of the respective test) are generated using the routine implemented in COBRAS-UC. The reflection problem is then solved by making the right side of the empty flume permeable to the waves, so no reflection on the right side occurs. At the same time the water elevation and orbital velocities are measured at the right side. These are then used as input data for the second part of the numerical flume which could, thus, also be made shorter and with an even finer mesh (Fig. 3.3e-2).

For the final numerical flume including the revetment, a non-uniform Δy distribution was chosen for two reasons: (i) a maximum number of 50,000 cells can be simulated in COBRAS-UC, which would have been reached for very flat slope steepnesses with a fine, uniform Δy and (ii) a faster performance of the tests with steep slopes is possible with fewer cells. This configuration made it necessary to use the same cell distribution in y-direction in the empty numerical flume, too, so a better transfer from the first to the second part is possible. This could be achieved for the two differently deep flumes by adding a subzone also in y-direction for the upper 2 m of the second part of the flume (which is not implemented in the empty flume).

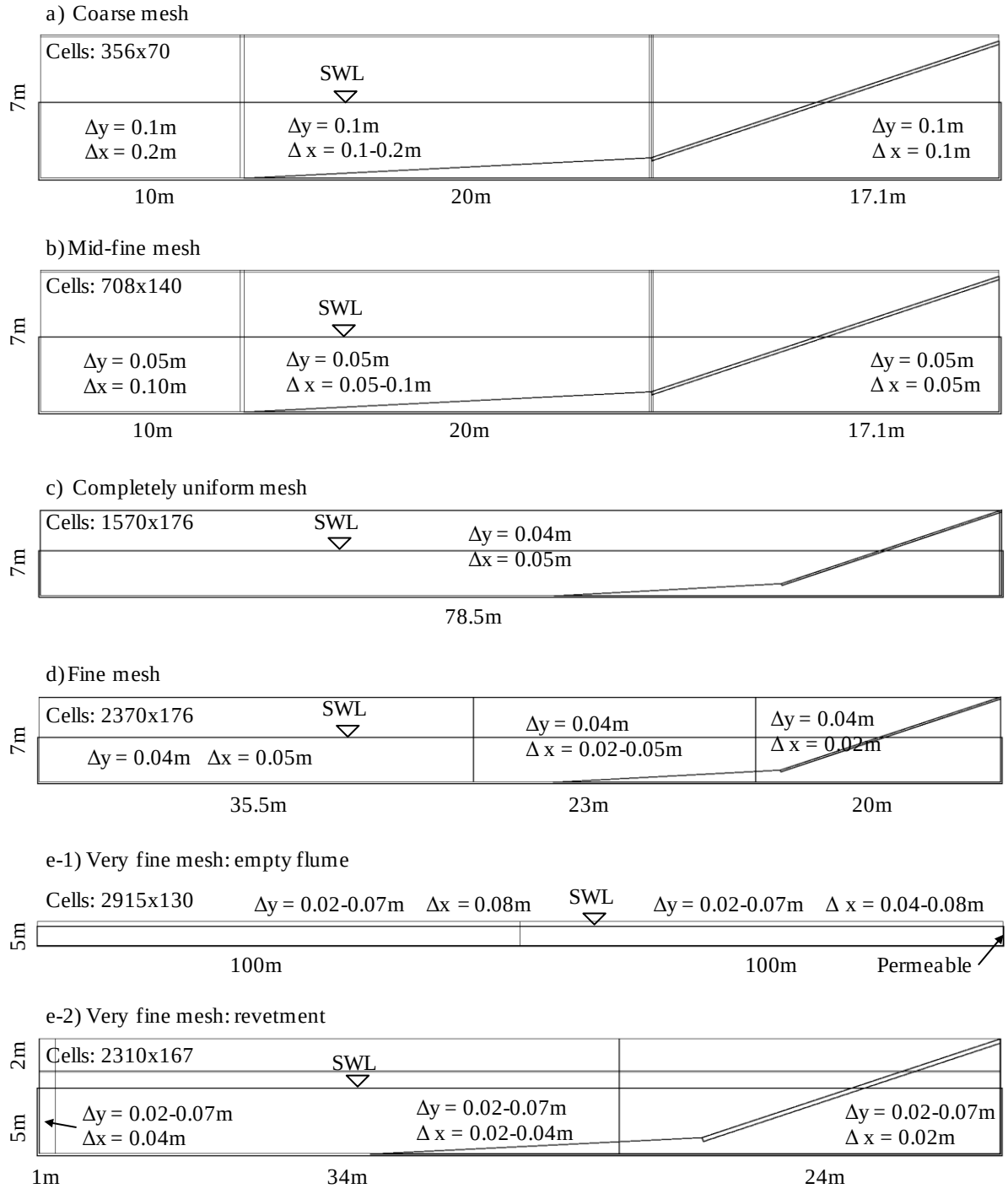

Fig. 3.3 Chronological development of mesh characteristics

3.2.2 Pre-tests

Several parameters can be varied in COBRAS-UC. Thus, the results from the numerical simulations can be fit to the experimental results. A few of these are already determined by the experimental set-up, these are: the porosity (n = 0.4) and the grain size of the material used for the revetment (D_{50} = 0.03 m). Other parameters have to be calibrated. For porous

media, these are especially the coefficients from the extended Forchheimer equation a, b and c or the associated dimensionless parameters α_f, β_f and C_m respectively (see also eq. (2.32)).

From former studies that used COBRAS-UC with porous media, the coefficients shown in Tab. 2.4 are found and are used as initial values for the calibration of the numerical model. These were altered in a series of tests to determine their effect on hydraulic parameters such as wave run-up height R_u and the wave reflection coefficient C_r. Based on all boundary conditions, two different sets of calibration tests were performed: (i) 11 tests using externally generated Stokes V waves with a wave height H = 0.581 m and T = 4.95 s as in one of the original tests from the GWK-tests (test number 09051501), these are all listed as "Stokes V (external)" under wave generation in Tab. 3.2 and (ii) 3 tests with waves from an empty wave flume (Fig. 3.3e-1) using wave conditions from three different original tests (09051501, 09051403, 09051503) which are listed as "empty flume" under wave generation in Tab. 3.2. Additionally to these pre-tests, four original GWK-tests are listed in Tab. 3.2

Tab. 3.2 Pre-tests with two different ways of wave generation and reference results from GWK-tests

Test number	h_0 [m]	R_u [m]	C_r [-]	H [m]	T [s]	R_u/H [-]	ξ [-]	α_f [-]	β_f [-]	C_m [-]	Wave generation
090515 01	3.7	1.07	0.49	0.58	4.95	1.85	2.71				GWK
11112501	3.7	1.09	0.52	0.54	4.95	2.00	2.80				Stokes V (external)
11112502	3.7	0.70	0.46	0.56	4.95	1.26	2.77	200.0	1.1	0.34	Stokes V (external)
11112504	3.7	0.83	0.39	0.56	4.95	1.49	2.76	200.0	0.1	0.10	Stokes V (external)
11112506	3.7	0.83	0.39	0.56	4.95	1.49	2.76	0.1	0.1	0.10	Stokes V (external)
11112901	3.7	0.82	**0.46**	0.56	4.95	1.47	2.77	1000.0	1.1	0.34	Stokes V (external)
11112902	3.7	0.85	**0.46**	0.56	4.95	**1.53**	2.77	200.0	0.8	0.34	Stokes V (external)
11112903	3.7	0.86	0.45	0.56	4.95	**1.55**	2.77	200.0	0.5	0.34	Stokes V (external)
11112904	3.7	0.82	**0.46**	0.56	4.95	1.48	2.77	1000.0	0.8	0.34	Stokes V (external)
11112905	3.7	0.85	0.41	0.56	4.95	**1.53**	2.77	1000.0	0.1	0.10	Stokes V (external)
11120205	3.7	0.83	0.36	0.56	4.95	1.49	2.77	100.0	0.5	0.10	Stokes V (external)
11120206	3.7	0.84	0.36	0.56	4.96	1.51	2.77	500.0	0.5	0.34	Stokes V (external)
11120903	3.8	0.78	0.47	0.55	5.01	1.41	2.80	200.0	0.8	0.34	Empty flume
090514 03	3.4	0.34	0.86	0.18	7.90	1.85	7.66				GWK
11120902	3.4	0.18	0.80	0.10	7.87	1.79	10.47	200.0	0.8	0.34	Empty flume
090515 03	3.7	1.56	0.14	1.24	3.92	1.26	1.47				GWK
11120901	3.8	0.97	0.19	1.29	3.99	0.75	1.46	200.0	0.8	0.34	Empty flume
090518 01	3.9	1.28	0.70	0.57	7.98	2.22	4.39				GWK

Performing a reflection analysis and calculating the wave run-up height R_u lead to the parameters shown in Tab. 3.2. The three best fits for each parameter are highlighted in bold red numbers. To enable a better comparison, the main results are also shown in Fig. 3.4 and Fig. 3.5 as dimensionless parameters against the surf similarity parameter ξ.

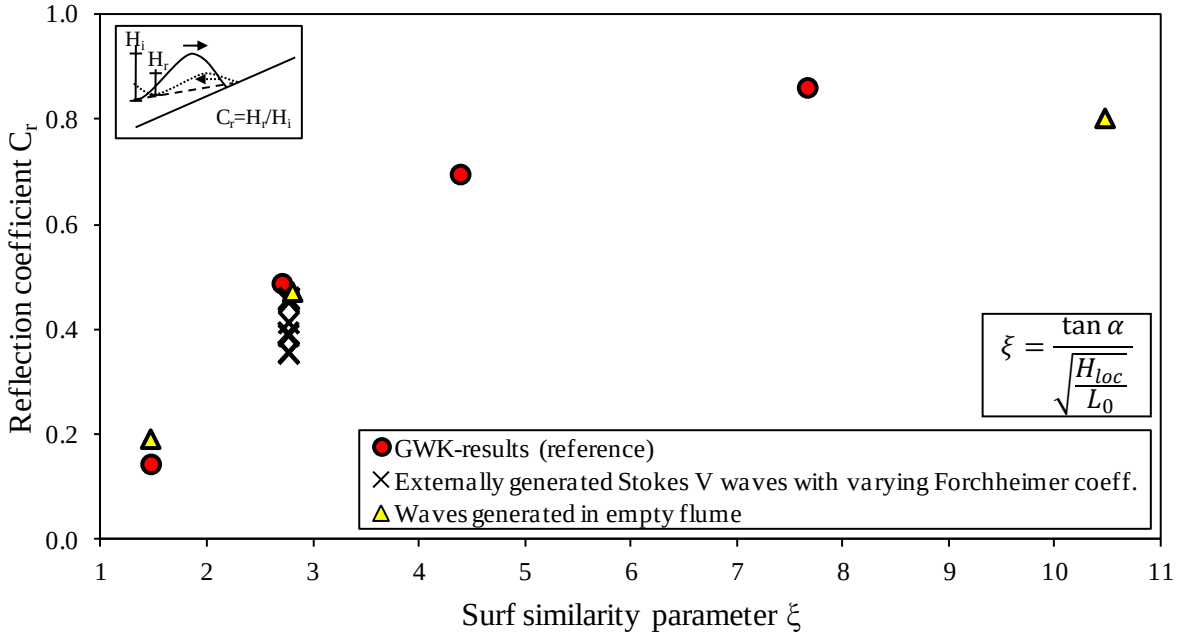

Fig. 3.4 Reflection coefficient C_r versus surf similarity parameter ξ for numerical and laboratory data

For the reflection coefficient C_r (Fig. 3.4), generally, a good correlation between the reference tests from the GWK (red circle) and the waves generated in an empty numerical flume (yellow triangle) is found. A slight overprediction of the reflection coefficient is present for the test with the smallest surf similarity parameter and a small underprediction for the test with the highest surf similarity parameter. The reflection coefficients of the tests with varying Forchheimer coefficients range from $C_r = 0.36 – 0.46$ whereas the GWK-reference test led to a reflection coefficient of $C_r = 0.49$. Generally, the tests with small C_m-values (0.1 in Tab. 3.2) and small α_f-values (0.1 and 100 in Tab. 3.2) result in very small reflection coefficients and thus do not represent the original tests very well. The sensitivity to β_f seems to be smaller, than to the other Forchheimer parameters (see Tab. 3.2).

For the wave run-up height R_u (Fig. 3.5), the correlation between laboratory tests and the numerical results is lower than for the reflection coefficient but it is still acceptable. Furthermore, the scatter in the original GWK-data was also particularly large for the wave run-up height. For these reasons, the accuracy of the results is considered to be sufficient. In Tab. 3.2 the three highest R_u-values of the validation test are highlighted bold red, because they present the best fit to the GWK-data. These three differ greatly in the values of the extended Forchheimer coefficients and no clear conclusion of the effect of α_f, β_f and C_m on the wave run-up height can be drawn.

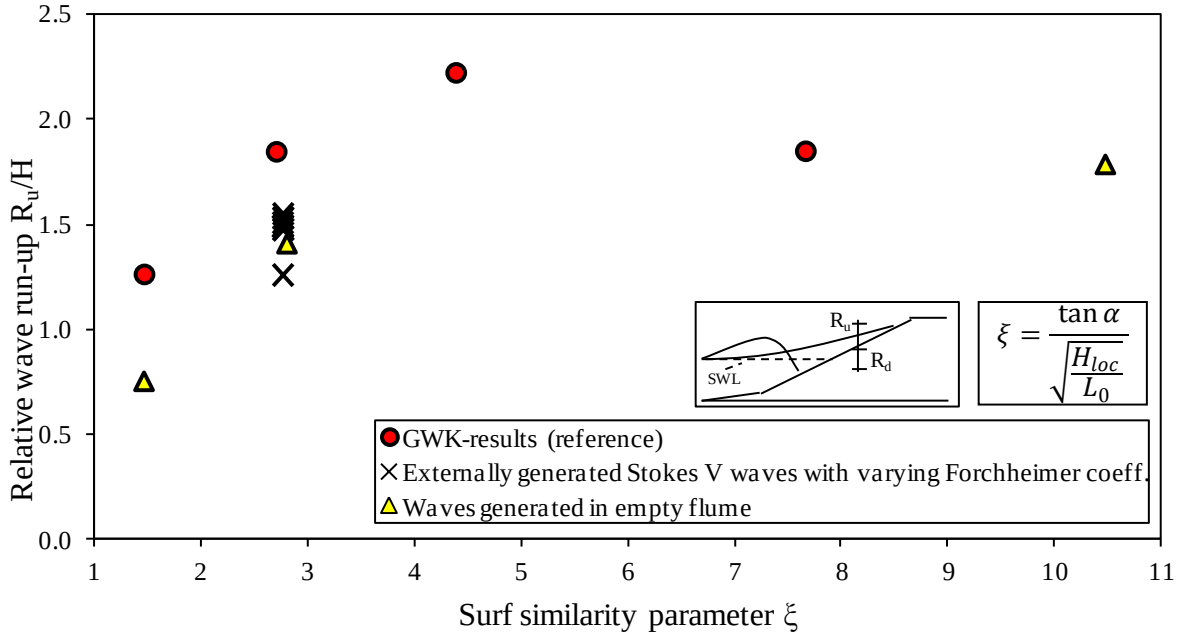

Fig. 3.5 Wave run-up R_u/H versus surf similarity parameter ξ for numerical and laboratory data

The third parameter, that should have been investigated, is the wave run-down height. During the investigation, very high (positive) wave run-downs directly on the revetment were found. By comparing this finding with the video recordings, it was found that the water layer on the revetment was not correctly measured in the GWK-tests. Fig. 3.6 shows the point where the wave run-up gauge measured the wave run-down due to its location a few centimetres above the revetment. This point does not represent the actual point of lowest wave run-down and, therefore, a comparison is impossible.

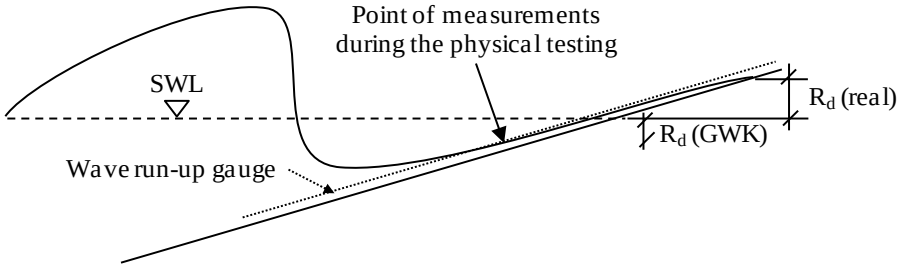

Fig. 3.6 Definition sketch for wave run-down

Considering the two analysed hydraulic parameters R_u and C_r, only one test shows good fits for both parameters (test number 11112902 with $\alpha_f = 200$, $\beta_f = 0.8$ and $C_m = 0.34$ for the extended Forchheimer flow described by eq. (2.32)). These values fit to the values proposed by Lara et al. (2008) and Losada et al. (2008) (Tab. 2.4) and are, therefore, chosen for all further numerical simulations. Furthermore, a large effect of coefficient β_f was found, while changing C_m had almost no consequences for the simulations. The effect of α_f is smaller than that of β_f but still observable. These findings comply with the study of van Gent (1993) that is mentioned in Section 2.3.

3.2.3 Final test set-up

Based on the state of the art review (Chapter 2), the GWK-tests and the pre-tests, a final test set-up was developed. The extended Forchheimer coefficients for the revetments have already been determined in the previous subsection with $\alpha_f = 200$, $\beta_f = 0.8$ and $C_m = 0.34$. These parameters are used for all revetment thicknesses in the simulations ($d_{rev} = 0.25$ m and 0.5 m) but clearly not for the absence of a revetment ($d_{rev} = 0$ m). An overview of the resulting model configurations is given in Fig. 3.7. The COBRAS-UC k-ε-turbulence model was used. Furthermore, an initial water depth $h_0 = 4$ m was used in all tests and the numerical set-up as shown in Fig. 3.3e-1 and e-2 is the basis for all further details of the set-up and for the test programme. Finally, the sand foundation and the 1:20 foreshore were assumed to be impermeable and smooth.

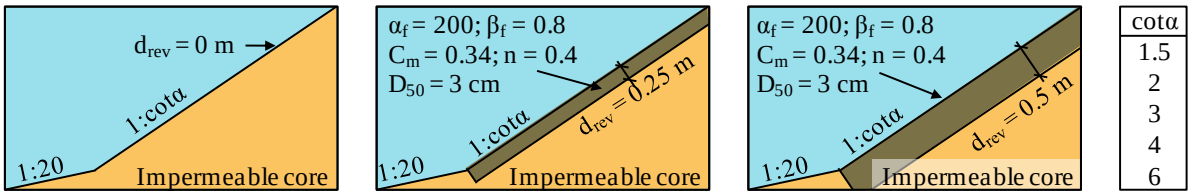

Fig. 3.7 Revetment configurations for the numerical simulations

To record all processes, nine wave gauges (WG) are located in front of the structure and on the foreshore (Fig. 3.8). For the processes on the revetment, a rectangular area was chosen in which the filling of the cells, the pressure, the horizontal and the vertical velocities are saved into files for each cell in the area. This area starts at the left upper end of the revetment ($x = 40$ m; $y = 1$ m) and ends in the right upper corner of the numerical flume ($x = 40$ m + cotα · 6 m; $y = 7$ m). From the saved values, several time series were extracted which are listed in Appendix A.1 Tab. A.5. Only for the tests with the slope steepness cotα = 6 a different solution had to be found, because otherwise it would have exceeded the maximum cell number in x-direction of about 3200. A slightly shorter flume (x = 75.8 m instead of 76 m) was chosen for this case. This cut has no effect on the tests, because it only affects the very top of the revetment.

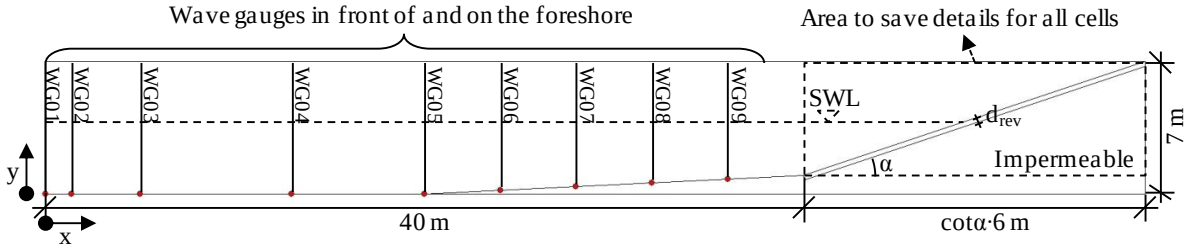

Fig. 3.8 Elements to save numerical results

3.2.4 Test programme

A test programme covering a wide range of surf similarity parameter was performed. An overview of the tests is given in Tab. 3.3. A range of $\xi = 0.6 – 13.7$ based on the input values

is thus obtained. All listed tests were performed for d_{rev} = 0; 0.25 and 0.5 m. Due to problems with the wave generation that arose during the mesh development (see Section 3.2.1), it was decided to check for the correct wave theories to ensure the best wave generation possible. In Fig. 3.9 the tests, which are planned for each slope steepness, are marked. Five of these tests are located in the range of the Stokes II theory and three are more or less in the range of the Stokes V wave theory. Consequently, it was decided to generate the waves according to the theory that was determined (see Tab. 3.3).

Tab. 3.3 Revised test programme with separation into Stokes II and Stokes V generated waves (ξ = 0.6 – 13.7)

cotα		1.5					2					3					4					6				
T [s]		3	5	6	8	9	3	5	6	8	9	3	5	6	8	9	3	5	6	8	9	3	5	6	8	9
H [m]	0.3	4.6	-	9.1	-	13.7	3.4	-	6.8	-	10.3	2.3	-	4.6	-	6.8	1.7	-	3.4	-	5.1	1.1	-	2.3	-	3.4
	0.6	3.2	-	6.5	8.6	-	2.4	-	4.8	6.5	-	1.6	-	3.2	4.3	-	1.2	-	2.4	3.2	-	0.8	-	1.6	2.2	-
	1.0	2.5	4.2	-	-	-	1.9	3.1	-	-	-	1.2	2.1	-	-	-	0.9	1.6	-	-	-	0.6	1.0	-	-	-

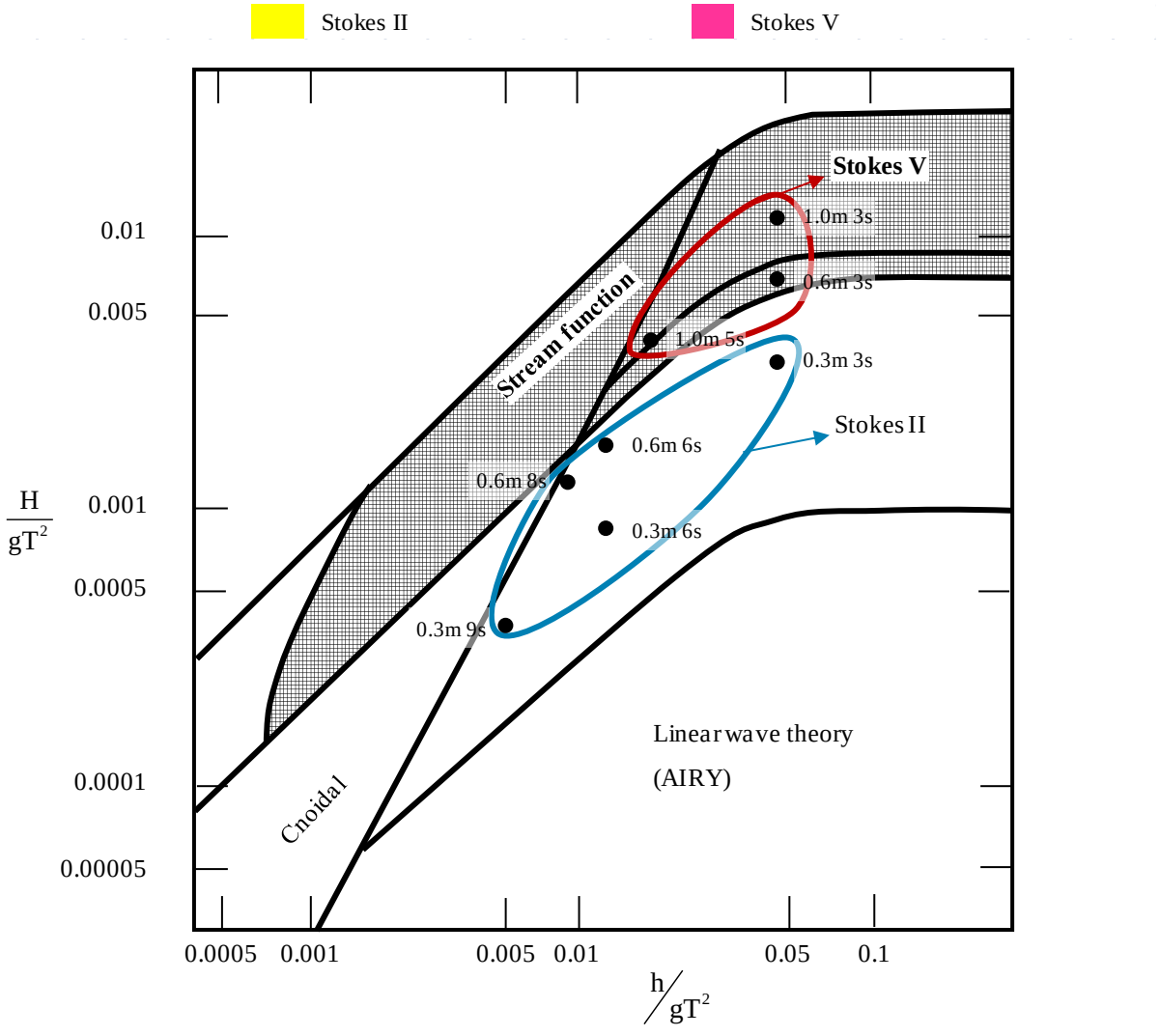

Fig. 3.9 Wave theories for all proposed wave parameters (based on Oumeraci, 2007)

Based on the presented test programme, a series of tests was conducted. All tests were performed with around 10 – 20 waves. A protocol of this series is shown in Appendix A.1 Tab. A.6. Several problems were encountered which included mostly premature test disruptions especially for several tests with the wave parameters H = 1.0 m and T = 3 s. Often, an analysis of these tests was still possible with a shorter test duration than planned, but after some disruption, the tests with H = 1 m and T = 3 s were cut out of the test programme.

Overall, tests with a much wider range of surf similarity parameter ξ were performed with the numerical model (ξ = 0.6 – 13.7) compared to the GWK-tests (ξ = 1.2 – 8.1). This difference is caused by the variation of slope steepnesses in the numerical simulations ($\cot\alpha$ = 1.5; 2; 3; 4; 6 compared to $\cot\alpha$ = 3 in GWK).

The model COBRAS-UC was successfully validated using the data from the GWK-tests. Forchheimer coefficients to describe the flow in the revetment were determined as: α_f = 200, β_f = 0.8 and C_m =0.34. A test programme with over 100 tests with a much wider range of structure conditions than in the GWK-tests was performed.

4 Processes in Front of the Structure

Although the focus of this study is the interaction between waves and a porous revetment, some processes in front of the structure are also affected by the revetment or their analysis is necessary as a basis for other processes, as for example the breaker type which is influenced by the reflected waves, the latter also being affected by the porous revetment. An example for a process that is rarely included in the analysis is the change in water level which is mostly described by the maximum wave set-up η_{max} and set-down η_{min}. Furthermore, the wave set-up on the slope describes an important point of the mean water level (MWL) which is very relevant for the wave run-up and run-down heights. Even though the reflection itself occurs directly at the structure, it mostly depends on the wave breaking which occurs in front of the structure. Therefore, the wave reflection and dissipation are also included in this chapter.

The processes will be handled here in the order they occur from the classification of the breaker type (Section 4.1), via wave set-down (Subsection 4.2.3) and wave set-up (Subsection 4.2.4) to wave reflection and energy dissipation (Section 4.3). Each section is introduced by a brief description on how the parameters were obtained or how the analysis was performed.

4.1 Breaker type classification

The classification of the breaker type was performed using three different approaches: (i) video analysis of the GWK-tests (Subsection 4.1.1); (ii) analysis of the numerical "videos" (Subsection 4.1.2) and (iii) classification based on hydrodynamic parameters (Subsection 4.1.3). As a result a set of proposed limits is defined between the four basic breaker types (spilling, plunging, collapsing, surging) which are shown in Fig. 4.1 and discussed below.

The characteristics of the four main breaker types illustrated in Fig. 4.1 can be summarised as follows:

(i) *Spilling breakers* dissipate a large amount of their energy in the breaking process. Instead of forming a breaking line, a breaking zone in which the wave height continuously decreases can be observed.
(ii) *Plunging breakers* are mostly characterised by a wave roll that forms at the breaking line.
(iii) *Collapsing breakers* start to form similarly to the plunging breaker. However, the wave roll does not fully form and collapses. Furthermore, this breaker type results in significant air entrainment which can be observed as foam on the water surface.
(iv) *Surging breakers* only show a slight shoaling before hitting the structure. The interaction with the structure is associated with negligibly small energy dissipation and without any observable foam.

A description of the breaker type as a function of the surf similarity parameter can also be found in numerous former studies (e.g. in Battjes (1974)).

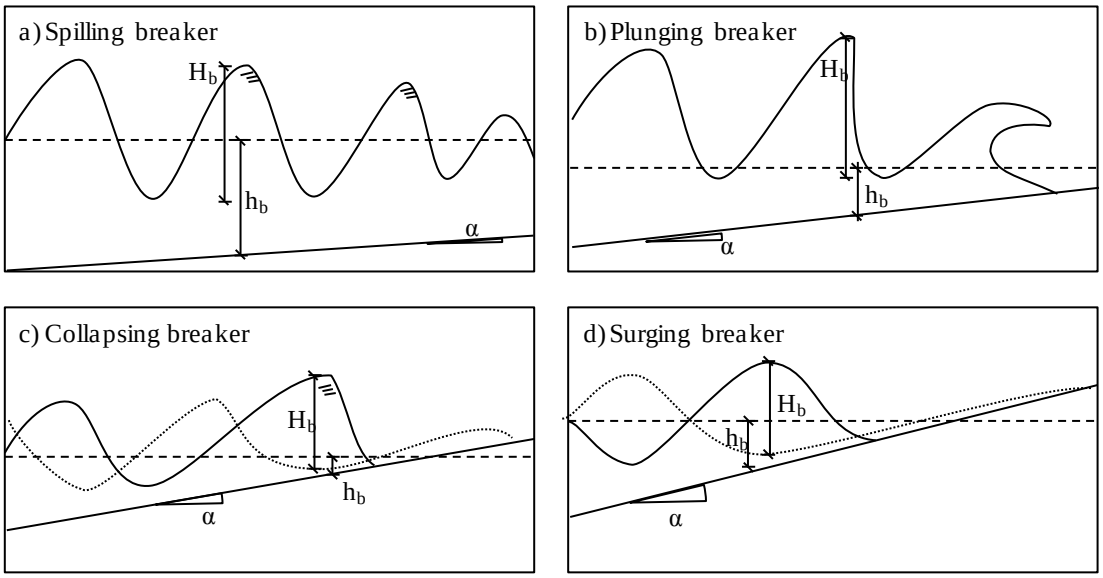

Fig. 4.1 Definition sketch for breaker type classification

Besides the main breaker types shown in Fig. 4.1 diverse transition forms have also to be considered because a clear and distinct classification is often not possible. These transition forms are spilling-plunging, plunging-collapsing and collapsing-surging breakers. The spilling-plunging type is associated with a decreasing wave height in front of the structure but also results in a plunge. The plunging-collapsing breaker type is characterised by a wave roll together with some kind of collapsing. The collapsing-surging type is associated with a high turbulence rate during the wave run-up, like collapsing breakers, while there is no sign of a wave roll, as for surging breakers.

4.1.1 Breaker types from video analysis of GWK-tests

A video analysis was performed to identify the breaker type for all GWK-tests with regular waves. The tests with wave spectra were not considered, because the analysis is more difficult and thus associated with more uncertainties. As indicated in Fig. 3.2, two cameras were permanently deployed for the model set-up in GWK. The camera located on the structure directed into the flume is used for the identification of the breaker type. Fig. 4.2 exemplarily shows a single video frame of this camera. The labelling at the back wall was also used to determine the breaker height and the location of incipient breaking.

Based on the video analysis, all tests with regular waves were classified into one of the above defined breaker types. Due to the limitations of the wave generator in the GWK and the relatively steep slope steepness 1:3 tested, no spilling breaker occurred. Overall, five of the seven (including intermediate types) possible breaker types could be observed in the GWK-tests. Several overlaps of the surf similarity parameter ranges are found for those five types. This could be caused by the different revetment alternatives. However, the differences between the combined model alternatives A and B in the first test phase and the combined model alternatives B and C in the second test phase are not very distinct and a noticeable effect on the breaker type is not expected. Therefore, the overlaps are either caused by

difficulties in the exact identification of the breaker types or by a dependency on another parameter than already accounted for in the surf similarity parameter ξ_m, e.g. revetment properties. Despite the overlaps for the five groups, ξ_m -thresholds for the three observed main breaker types are proposed in Fig. 4.3.

Fig. 4.2 Example video frame

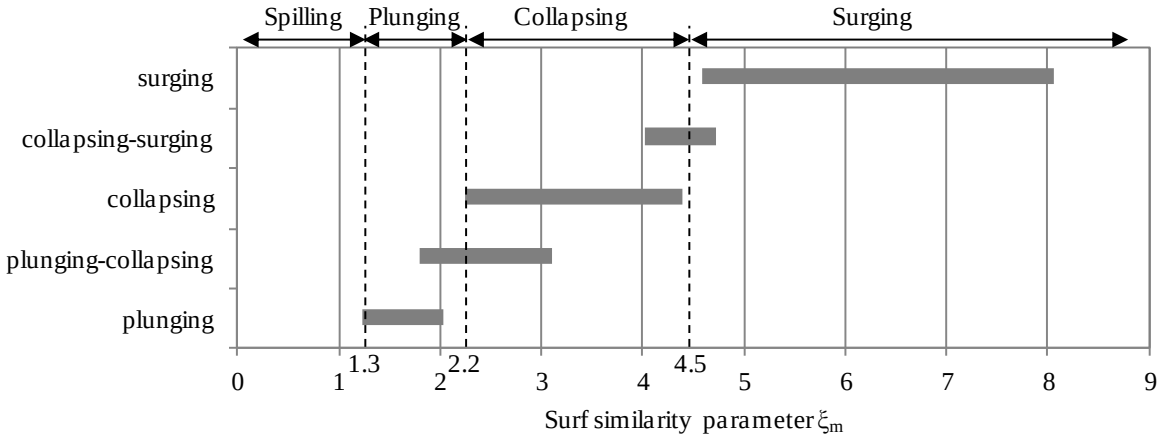

Fig. 4.3 Breaker types versus surf similarity parameter based on video analysis of all GWK-tests with regular waves

4.1.2 Breaker type analysis for the numerical simulations

The classification of the tests from the numerical simulations into the breaker types is made using the graphic depiction for COBRAS-UC data in L~Davis. The same main breaker types as defined in Fig. 4.1 and the same transition forms as described in Section 4.1.1 are also used here. Due to the apparent effects of the revetment thickness d_{rev}, the classification is plotted separately for the three values d_{rev} = 0.00 m; 0.25m and 0.5 m (Fig. 4.4).

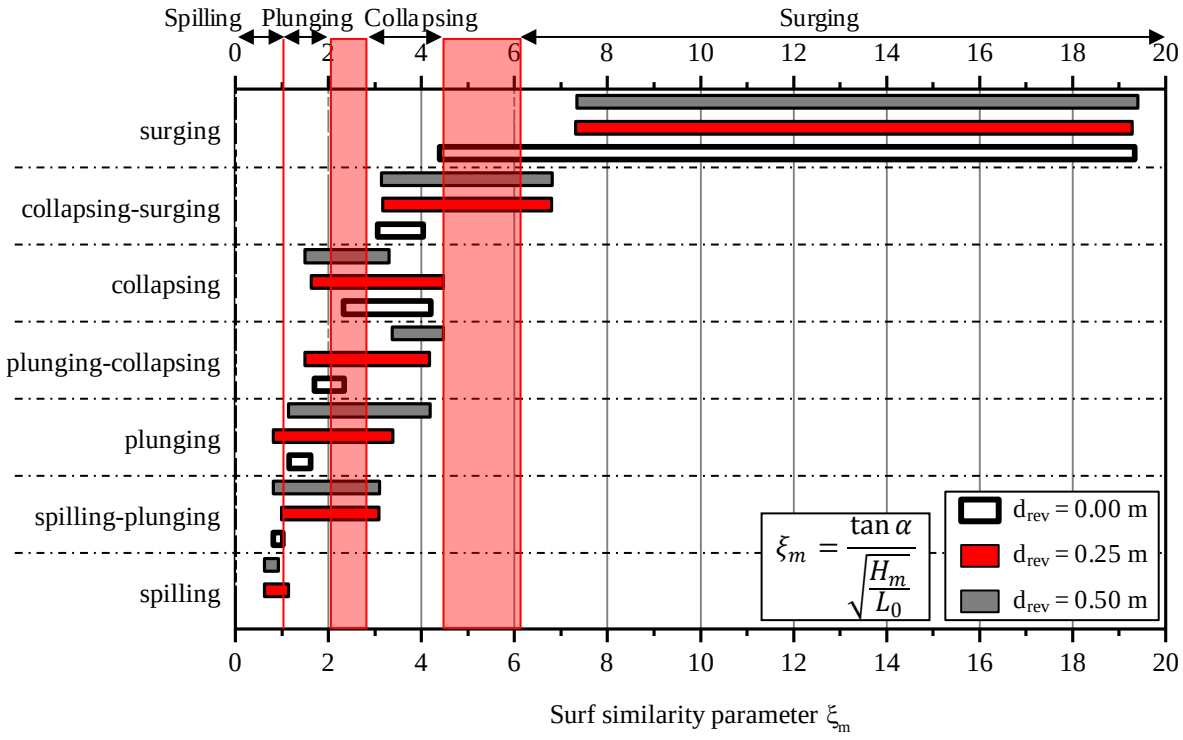

Fig. 4.4 Breaker type classification for numerically simulated tests

Analysing Fig. 4.4, several findings can be documented. The most obvious finding is the absence of spilling breakers for the experimental set-ups with d_{rev} = 0 m (impermeable smooth slope) which is caused by the already mentioned issues in the numerical modelling for the wave conditions H = 1.0 m and T = 3 s. This wave condition was not tested for d_{rev} = 0 m due to the numerical issues. In case of d_{rev} = 0.25 & 0.5 m some tests have been performed and led to the spilling breakers shown in Fig. 4.4. Furthermore, issues with a clear distinction between several breaker types are observable. For almost all neighbouring breaker types, overlaps of the corresponding surf similarity parameter ξ_m are present. Especially for small surf similarity parameter $\xi_m < 4$, all breaker types (spilling-plunging, plunging, plunging-collapsing and collapsing) exist almost simultaneously. One reason for this is the complex determination of the breaker type. However, the starting point of each category (the smallest surf similarity parameter ξ_m for which it was found) is quite similar for all revetment thicknesses d_{rev} for the categories spilling-plunging, plunging, collapsing and collapsing surging. For the ending point of each category (the largest surf similarity parameter ξ_m for which it was found) similar values are only found for the surging breaker type which is a result of the test programme. In general, Fig. 4.4 shows an effect of the revetment thickness on the breaker type. However, this effect seems to depend on more parameters than the surf similarity parameter ξ_m and has, therefore, to be investigated further.

For a better comparability, a tentative classification into the four basic breaker types; spilling, plunging, collapsing and surging; with steady limits is made for all configurations considered here. The results are shown later on in Tab. 4.1. The mean value between each maximum and minimum of the standard breaker types is chosen, e.g. the limit between spilling and plunging

breaking waves is the mean value of the maximum ξ_m for spilling breaking and the minimum ξ_m for plunging breaking.

The limits between the breaker types as listed in Tab. 4.1 are quite similar for all configurations. Both porous revetments from the numerical simulations result in a wider range of surf similarity parameter ξ_m for the plunging breaker type and the range of the surf similarity parameter for the collapsing breaker type for those two configurations is not necessarily wider but found for larger absolute surf similarity parameter values than for d_{rev} = 0 m. This finally leads to a later start of the surging breaker range for those two configurations at ξ_m = 6.1 and 5.3 instead of ξ_m = 4.5 (GWK) and ξ_m = 4.3 (d_{rev} = 0 m). The differences in the limits between the breaker types are caused by several issues but the most important is that the video material from the numerical simulations does not explicitly show details like foam on the water and splashing which makes a classification very difficult.

4.1.3 Parameter based analysis of breaker types

In this section, several main hydrodynamic parameters are analysed for different behaviours within certain ranges of surf similarity parameters ξ_m. The range of surf similarity parameter ξ_m is split into several stages which are similar to the breaker types used in Sections 4.1.1 and 4.1.2 but are not exactly the same. The first and most important parameter is the reflection coefficient and the resulting four stages I-IV are presented in Fig. 4.5, showing the reflection coefficient C_r for the three revetment thicknesses from the numerical simulations (Section 3.2.4) as well as for the two test phases from the model experiments in the GWK (Oumeraci et al., 2010; Model A: d_{rev} = 0.15 m, Model B: d_{rev} = 0.25 m and Model C: d_{rev} = 0.35 m). The four stages are characterised by similar trends of the data sets: stage I is an accumulation of data points; in stage II, a linear trend is observable; stage III is characterised by a scattering of the data sets and stage IV shows a linear trend again. Even though these stages do not fully correspond to the breaker types as defined visually, they indicate a change in the hydrodynamic processes and are thus, primarily an indicator for changes in the breaking process. Because these different behaviours do not exactly show the same limits for all data sets, Fig. 4.5 shows the limits for each of the five data sets. These differ slightly, as expected. Especially for the limit between stages III and IV, a larger scatter is found. This is mostly due to the smaller range of surf similarity parameter ξ_m in the GWK-experiments which, from this definition, is fully outside this last stage (IV).

The results of this classification based on the reflection coefficient are listed together with the limits from the two former approaches (see Fig. 4.3 and Fig. 4.4) in Tab. 4.1. The results from Fig. 4.5 do not fit very well with those from the other two approaches even though it can be assumed that changes in the reflection behaviour are mostly caused by different breaker types.

A similar procedure was also performed for the wave run-up and run-down (based on the data sets shown in Fig. 5.2 and Fig. 5.3) as well as the corresponding wave run-up and run-down velocities (based on the data sets shown in Fig. 5.9 and Fig. 5.11, details in Foyer & Oumeraci, 2013). The resulting limits vary greatly and especially for the GWK-results not all

stages I – IV are present for all parameters. Moreover, the differences between the different revetment thicknesses are only partly present.

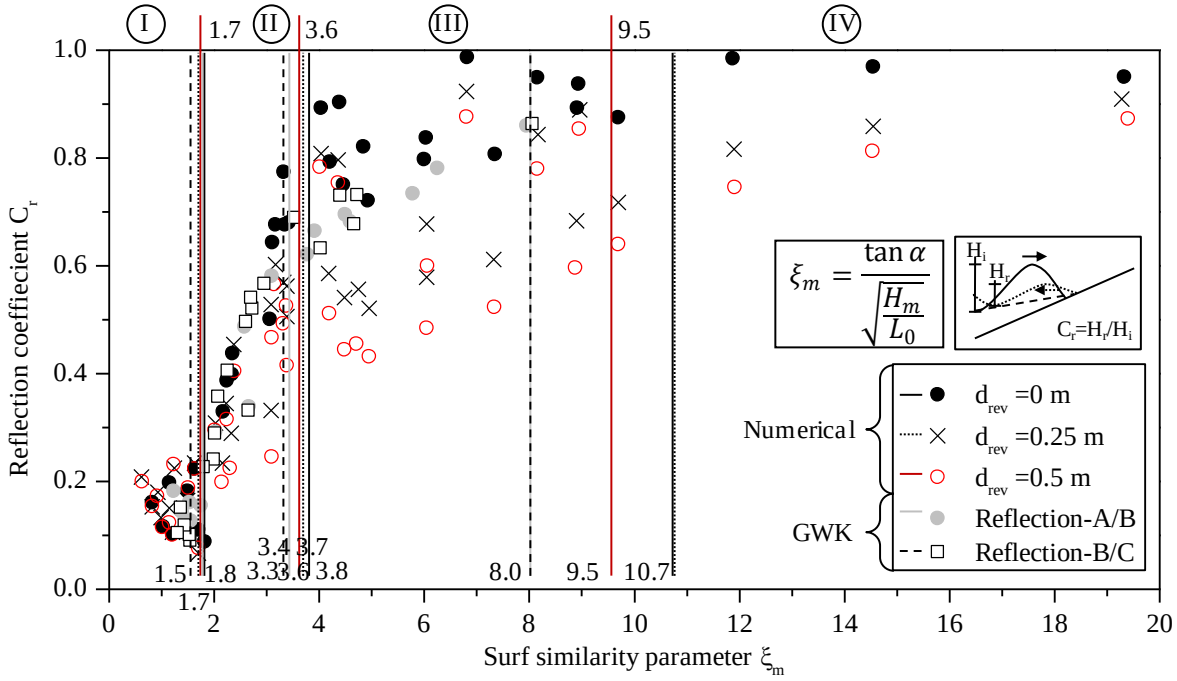

Fig. 4.5 Limits of stages I - IV according to the trend seen in the reflection behaviour

Tab. 4.1 Overview of surf similarity parameter limits between the four main breaker types and stages I-IV

Parameter	Model/ d_{rev} [m]	Spilling breaker/ Stage I	Plunging breaker/ Stage II	Collapsing breaker/ Stage III	Surging breaker/ Stage IV
Breaker type (video analysis)	A/B/C (GWK)	-	1.3 – 2.2	2.2 – 4.5	> 4.5
	d_{rev} = 0	-	1.1 – 2.0	2.0 – 4.3	> 4.3
	d_{rev} = 0.25	< 1.0	1.0 – 2.4	2.4 – 6.1	> 6.1
	d_{rev} = 0.5	< 1.0	1.0 – 2.8	2.8 – 5.3	> 5.3
Wave reflection	A/B (GWK)	< 1.8	1.8 – 3.4	3.4 – 8.0	> 8.0
	B/C (GWK)	< 1.5	1.5 – 3.3	3.3. – 8.0	> 8.0
	d_{rev} = 0	< 1.8	1.8 – 3.8	3.8 – 10.7	> 10.7
	d_{rev} = 0.25	< 1.7	1.8 – 3.7	3.7 – 10.7	> 10.7
	d_{rev} = 0.5	< 1.7	1.8 – 3.6	3.6 – 9.5	> 9.5
Swash height	A/B/C (GWK)	-	-	2.3 – 5.1	> 5.1
	d_{rev} = 0/0.25/0.5	< 1.4	1.4 – 2.8	2.8 – 10.7	> 10.7
Swash velo-cities	A/B/C (GWK)	< 1.7	1.7 – 3.3	3.3 – 5.2	> 5.2
	d_{rev} = 0/0.25/0.5	< 2.0	2.0 – 5.0	5.0 – 11.9	>11.9

The overall results are presented in Tab. 4.1. The obtained ξ_m -limits between the four main breaker types and those between stages I-IV of the reflection behaviour differ greatly. Unexpectedly, the limits determined for the swash heights (wave run-up and run-down) are most similar to those from the video analysis while the results from the reflection coefficient are quite different. Overall, it can be concluded that a precise determination of the limits of

the breaker types solely based on the surf similarity parameter ξ_m might be problematic. Furthermore, the effect of the revetment thickness d_{rev} is partly found (e.g. video analysis and reflection coefficient) but also sometimes not present (swash height and velocities). Because the primary determination of the breaker type should be made according to the outer appearance of the wave during breaker, the results of the video analysis are favoured. Consequently, a modified surf similarity parameter has to be developed, which also accounts for effects of the properties of the revetment (roughness, permeability, etc.). Therefore, further research and tests are needed for a better prediction of the breaker type and it is, therefore, advised to perform more model tests with this focus.

Based on an extensive analysis of breaker types, the following ξ_m–thresholds are proposed for the revetment thicknesses d_{rev} = 0.00 m; 0.25 m and 0.5 m:

- Spilling to plunging breaker: ξ_m = 1.5 (for all considered thicknesses)
- Plunging to collapsing breaker: ξ_m = 2.0 (d_{rev} = 0 m)/ 2.4 (0.25 m)/ 2.8 (0.5 m)
- Collapsing to surging breaker: ξ_m = 4.0 (d_{rev} = 0 m)/ 5.5 (0.25 m & 0.5 m)

Several conclusions can be drawn from the results and directly from the video analysis: (i) the permeable and rough revetment causes more turbulence thus leading to collapsing and collapsing-surging breaker types (instead of surging breakers) at higher surf similarity parameter ξ_m compared to a smooth and impermeable slope and (ii) the effect of the revetment on the breaker type also depends on other wave parameters (e.g. wave height), which leads to overlaps of the range of surf similarity parameters ξ_m for each breaker type and each revetment thickness.

A good option to account for the effect of the permeable and rough revetment on the breaker type would be to include d_{rev} in a modified surf similarity parameter. However, this has to be done using comparative data.

4.2 Wave set-down & set-up

Wave set-up and set-down are closely linked to the breaker type and the wave height. Both, wave set-up and set-down represent changes in the mean water level at and seawards of the structure as shown in Fig. 2.3. The wave set-down is more linked to the process of shoaling in front of the structure and the wave set-up that occurs from the maximum wave set-down to the surface of the structure, is an indicator for the rate of wave energy dissipation induced by the breaking process. Furthermore, the location of the maximum wave set-down is at the same time the location of the wave breaking.

In the following, the procedure to obtain the maximum wave set-up η_{max} and set-down η_{min} (as defined in Fig. 2.3) from the GWK-test series and from the numerical test series are described first (Subsection 4.2.1) before comparing the results of both test series (Subsection 4.2.2). Finally, the two parameters η_{min} and η_{max} are analysed in Subsection 4.2.3 (wave set-down) and Subsection 4.2.4 (wave set-up).

4.2.1 Determination of wave set-down and wave set-up

As mentioned in Section 2.2.1, the definition of the maximum wave set-up η_{max} is not clear throughout former studies. The definition of the maximum wave set-up as the maximum wave run-up (e.g. Nielsen, 1989) does not make sense especially when considering that the swash should vary around the MWL described by the wave set-up.

The deployment of wave run-up gauges (RUG) in the GWK-tests and the layout of the numerical simulations make a measurement of the water layer directly on the revetment possible. Therefore, the maximum wave set-up η_{max} will be defined thereafter as the mean value directly on the slope surface and not as the mean value of the vertical water elevation at the initial shore line (cf. Fig. 2.3). For the tests series considered in this thesis, this is the temporal mean value of the measurements of the RUG. This also corresponds to the determination of the maximum wave set-down η_{min} which is the temporal mean value of the water elevation measurements in front of the structure and from this the minimum values (maximum wave set-down).

4.2.1.1 GWK experiments

Before starting with the analysis, the recordings of the two wave run-up gauges (see Fig. 3.2 and Tab. A.1) deployed on each model alternative in the GWK had to be merged together. This was achieved by using a MATLAB® routine (Appendix B.1) which added the recordings of the upper gauge to that of the lower one, in the time steps where the lower gauge was fully under water. Generally, it has to be kept in mind that this method comes with the advantage of a better presentation of the data but also with the disadvantage of only patched data, e.g. not always a continuous transitions between both parts (see Fig. 4.6 upper right corner).

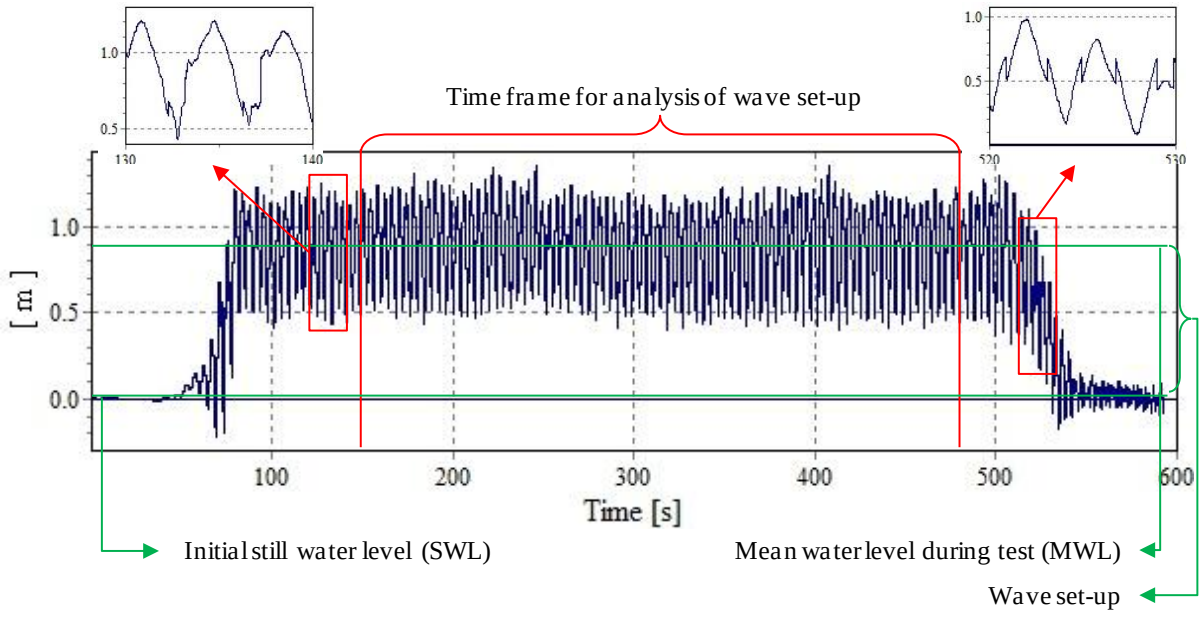

Fig. 4.6 Definition sketch of the approach to determine wave set-up

To finally obtain the wave set-up and set-down, the time series recorded by the wave gauges WG10 - 13 and the merged run-up gauges RUG1(3) and RUG2(4) were analysed as follows:

- Definition of the time frame in which the wave set-up/set-down occurred
- Definition of the initial still water level
- Determination of the water level within the chosen time frame of the entire time series
- Determination of wave set-up and set-down

An example for this analysis procedure is given in Fig. 4.6 for wave set-up. Both, the initial still water level (SWL) and the mean water level during the test (MWL), are shown in Fig. 4.6. The difference between both water levels is the wave set-up at the observed RUG. For wave set-down, the same routine was used on the data of the WG in front of the structure.

Using the procedure described in Fig. 4.6 the wave set-down at wave gauge WG 11, 12 and 13 as well as the wave set-up on the slope were determined. For the wave set-down, the maximum overall wave set-down at the respective WG was chosen for the further analysis.

4.2.1.2 Numerical simulations

Wave set-up and set-down from the numerical simulations were basically determined in the same way as for the GWK-tests: determining the mean water elevation within a certain time frame at the wave run-up gauge and the wave gauges in front of the structure. Unlike for the experiments in the GWK, the time series for the RUGs had first to be calculated from the saved data of the numerical simulations. Thus, a RUG on the surface of the revetment and one within the revetment (RUG-int) are positioned in the numerical set-up. These instruments and their location on the slope are listed in Tab. A.5. The time series were obtained using a MATLAB routine (Appendix B.2).

For wave set-down, a second routine was used to determine the maximum wave set-down in front of the structure and its location (Appendix B.3). This routine used the same time frame as the reflection analysis and determines the wave set-down at each column of cells in front of the structure and then determines the overall maximum wave set-down (minimum value) and its location.

4.2.2 Comparison of GWK-tests and numerical results

Before starting with the analysis, a comparison of data from the numerical simulations and the experiments in the GWK is performed to further validate the numerical simulations. Fig. 4.7 shows the relative wave set-up η_{max}/L_0 versus the surf similarity parameter ξ_m. The three different revetment configurations in the GWK experiments (Model A – d_{rev} = 0.15 m, Model B – d_{rev} = 0.25 m, Model A – d_{rev} = 0.35 m) resulted in wave set-ups, that are all located along one line. The absence of any deviation between the three data sets from the GWK-tests suggests a large effect of the breaker type and no effect of the revetment alternative. The results from the numerical simulations (only $\cot\alpha = 3$) are positioned almost along the GWK-data. This indicates a good agreement between the data sets. The numerical results are slightly larger than the GWK-results. This is caused by difference in location of the measuring. In the

GWK, the water level elevation was measured some centimetres above the surface of the revetment leading to smaller readings.

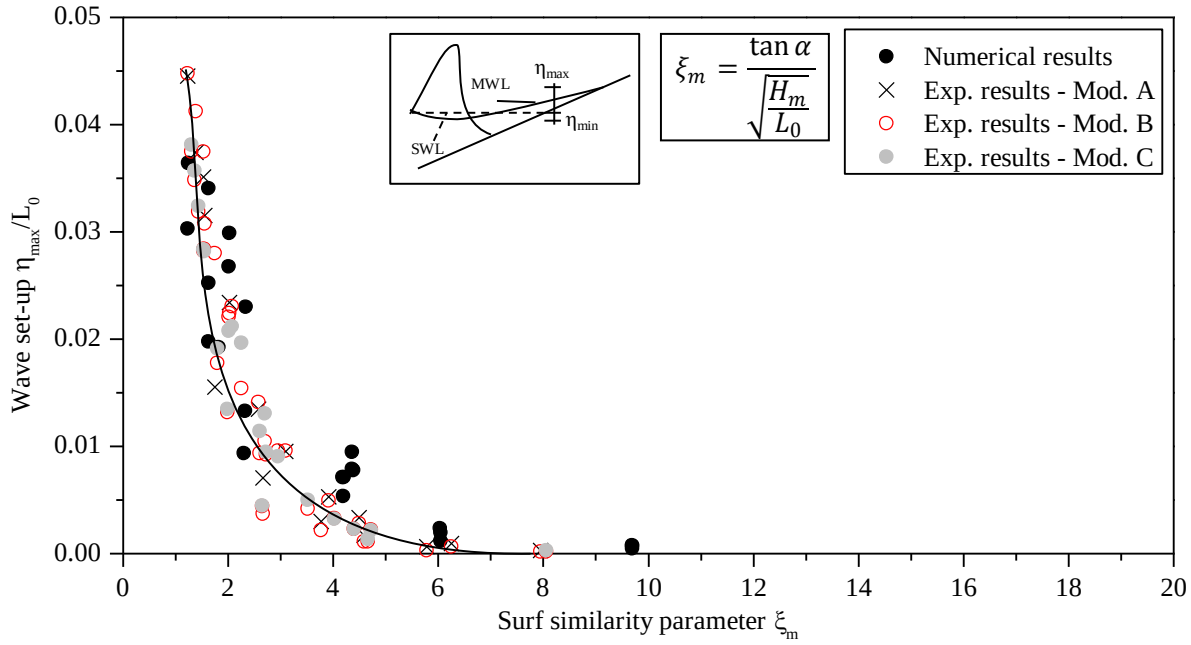

Fig. 4.7 Comparison of relative wave set-up in GWK experiments and numerical simulations (cotα = 3)

Wave set-up is an indication for the energy dissipation due to wave breaking whereas wave set-down is an indication for the increase of the wave height due to shoaling (Longuet-Higgins & Stewart, 1964). It is particularly found for plunging breakers due to the relatively large increase in wave height before breaking as documented in the data from the GWK tests as well as from the numerical simulations (only cotα = 3) as shown in Fig. 4.8. The GWK-data sets were not grouped according to the three model alternatives because (i) the wave set-down is always obtained for the combination of the two installed alternatives and (ii) the wave set-down occurs in an area that is not separated by the wooden wall (Fig. 3.2). Both data sets in Fig. 4.8 exhibit the same features with very small to zero relative wave set-down η_{min}/L_0 for surf similarity parameters $\xi_m > 6$ and with the highest absolute relative wave set-down η_{min}/L_0 for surf similarity parameters $\xi_m = 1.5 – 4.5$. This similarity suggests also a good agreement between the GWK-data and the results of the numerical simulations. However, the higher spatial resolution in the numerical simulations generally provides larger absolute values, which is very plausible.

For the further investigations, only the results from the numerical simulations are used. This is on the one hand caused by the problems with the wave run-up gauges associated with the patching of two recorded time series (Fig. 4.6) and the slightly elevated location of the gauge above the slope surface (Fig. 3.6) and on the other hand, the spatial resolution in the GWK-tests is by far not high enough to provide acceptable results (Fig. 4.8).

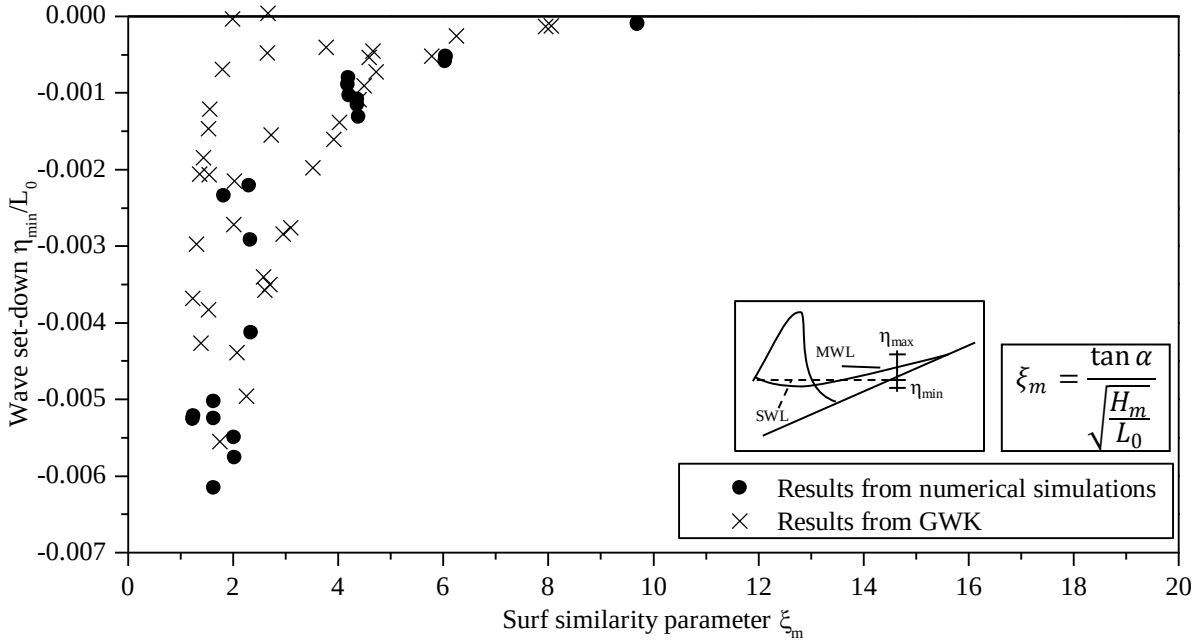

Fig. 4.8 Comparison of relative wave set-down in GWK experiments and numerical simulations (cotα = 3)

4.2.3 Wave Set-Down

To develop appropriate prediction formulae, the wave set-down is first compared to predicted wave set-downs as they are obtained using equations given by (Oumeraci, 2007) and USACE (2002) (eqs. (2.13) and (2.14)). The results are shown in Fig. 4.9. The two formulae show a similar tendency but both do not match the data from the numerical simulations. Especially larger wave set-downs are underestimated by the two equations. This indicates that the simplifications and the assumptions underlying eqs. (2.13) and (2.14) are not fully justified and at least one important factor was not considered. Because the theoretical approaches to the wave set-up are normally based on the simplification of the breaking process, especially for plunging and collapsing breakers a deviation from the actual wave set-down is expected.

The effect of the surf similarity parameter ξ_m on the relative wave set-down η_{min}/L_0 is shown in Fig. 4.10 for the five different slope steepnesses tested in the numerical simulations. A distinct effect of the slope steepness can be stated from Fig. 4.10 (additionally to ξ_m). All data sets for the five numerically tested slope steepnesses line up almost perfectly next to each other. The largest (absolute) values are obtained for the steeper slopes (here cotα = 1.5 and 2) while smaller values are present for flatter slopes. Moreover, the difference between the data sets gets smaller for flatter slopes. Therefore, it can be concluded that the effect of the slope steepness is more pronounced for steeper slopes while for flatter slopes similar results are obtained. This finding is in line with the conclusions of former studies on the wave set-up (e.g. Stockdon et al., 2006; cf. Section 2.2.1).

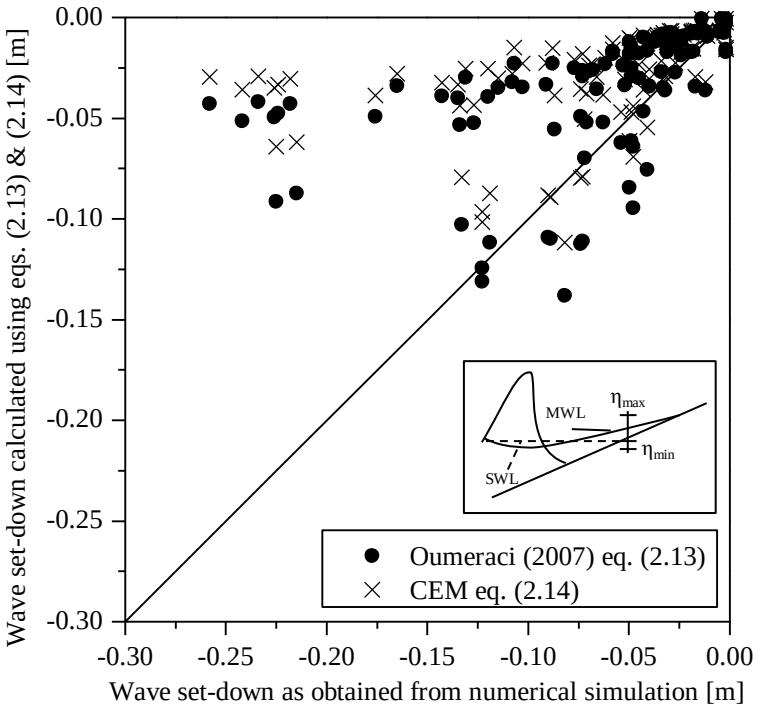

Fig. 4.9 Predicted wave set-down η_{min} using eqs. (2.13) & (2.14) versus η_{min} from the numerical simulations (cotα = 1.5 – 6)

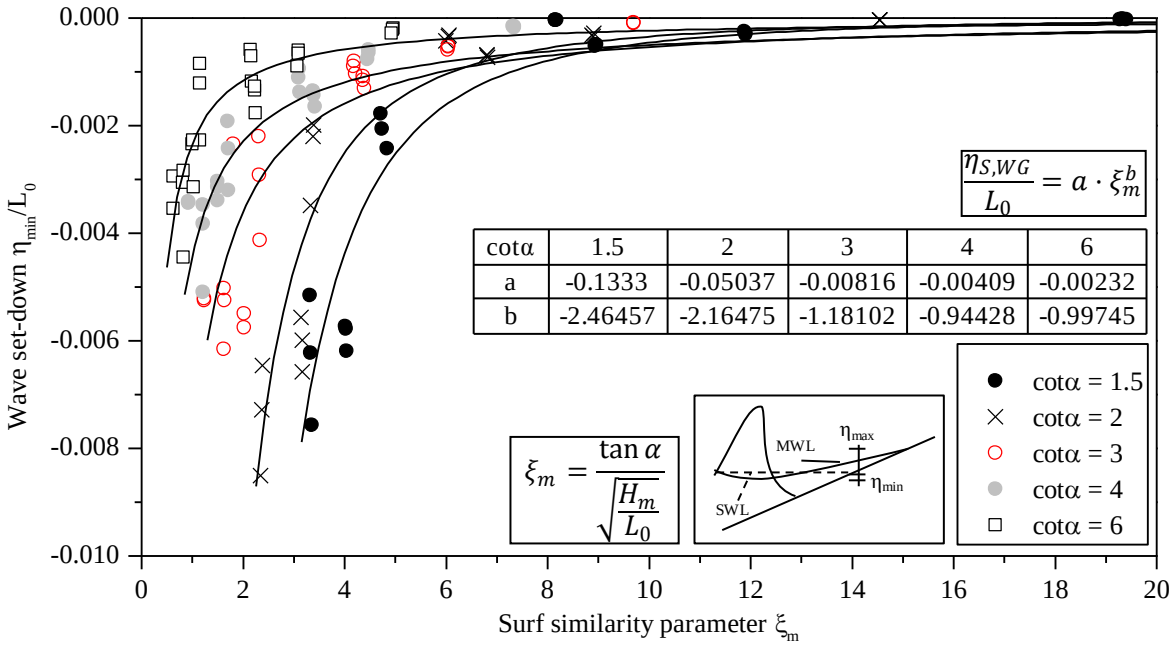

Fig. 4.10 Relative wave set-down vs. surf similarity parameter for different slope steepnesses cotα = 1.5 to 6 (only numerical simulations)

The effect of the revetment thickness on the wave set-down is less pronounced than that of the slope steepness and is therefore not presented here in detail (see Foyer & Oumeraci, 2012). Only very large absolute values of the wave set-down are affected by the revetment thickness.

This is most likely a direct consequence of the changes of the breaker type that are caused by the revetment thickness as described in Section 4.1.

In order to particularly account for the effect of the slope steepness, several approaches to develop a prediction equation for the wave set-down were examined. First of all, an exponential approach of the type of eq. (4.1) was adopted with different values for a and b which depend on the slope steepness using a regression analysis (RA). This approach fulfils the two extreme boundary conditions determined for the wave set-down in Tab. 2.5. For $\xi_m \rightarrow \infty$, a wave set-down of $\eta_{min}/L_0 = 0$ is obtained. For $\xi_m = 0$, the situation is slightly more complicated. The relative wave set-down tends to $\eta_{min}/L_0 = -\infty$ instead of 0. Nevertheless, this behaviour is most likely correct because of the wave length that tends to $L_0 \rightarrow 0$ for $\xi_m \rightarrow 0$ thus leading to $\eta_{min}/L_0 = -\infty$.

$$\frac{\eta_{min}}{L_0} = a \cdot \xi_m^b \tag{4.1}$$

The result of this RA was not satisfying because it led to large over- and underestimation for large absolute values $|\eta_{min}/L_0|$ and only for small absolute values $|\eta_{min}/L_0|$ a relatively good prediction is obtained (see Fig. 4.10). Therefore, an additional multiple regression analysis (MRA) was performed with the relative wave set-down η_{min}/L_0, the surf similarity parameter ξ_m and the slope steepness $\cot\alpha$. However, the results were still not acceptable (Foyer & Oumeraci, 2013). Therefore, it was decided to treat wave set-down together with wave set-up to include effects that might influence both parameters (see Section 4.2.4).

For a complete overview of the mean water level (MWL), the location of the wave set-down is needed. In general, it is possible to use the horizontal distance between the shoreline and the maximum wave set-down, but a more common approach to analyse the location of wave set-down or incipient wave breaking is to divide the wave height at breaking H_b by the corresponding water depth at the maximum wave set-down h_b (breaking depth as defined in Fig. 2.3). As a result, the breaking criterion H_b/h_b is obtained. For a better comparability, the surf similarity parameter was modified by also using the wave height at incipient breaking H_b. The water depth at maximum wave set-down h_b is here defined as the water depth in the initial conditions meaning with respect to SWL. The wave height at breaking H_b is not measured but calculated based on linear wave theory from the deep water wave height H_0 using the shoaling coefficient. Even though this procedure is not exact for very steep waves as they are found for the spilling and plunging breakers, the results are still satisfying. The data points for all tested values of slope steepness line up quite well (Fig. 4.11). Therefore, the breaking criterion H_b/h_b is used for a RA later on. A few outliers, which were caused by problems in the determination of h_b, had to be removed.

Fig. 4.11 shows that the breaking criterion H_b/h_b increases with increasing surf similarity parameter ξ_b for $\xi_b < 1$. After reaching a maximum of $H_b/h_b \approx 1.6$, the breaking criterion decreases first rapidly and then stagnates at around $H_b/h_b \approx 0.5$. The data points in Fig. 4.11 generally describe the threshold between breaking and non breaking for given wave

conditions. No effect of the revetment could be identified even though the breaker type is affected by the revetment thickness for plunging and surging breakers.

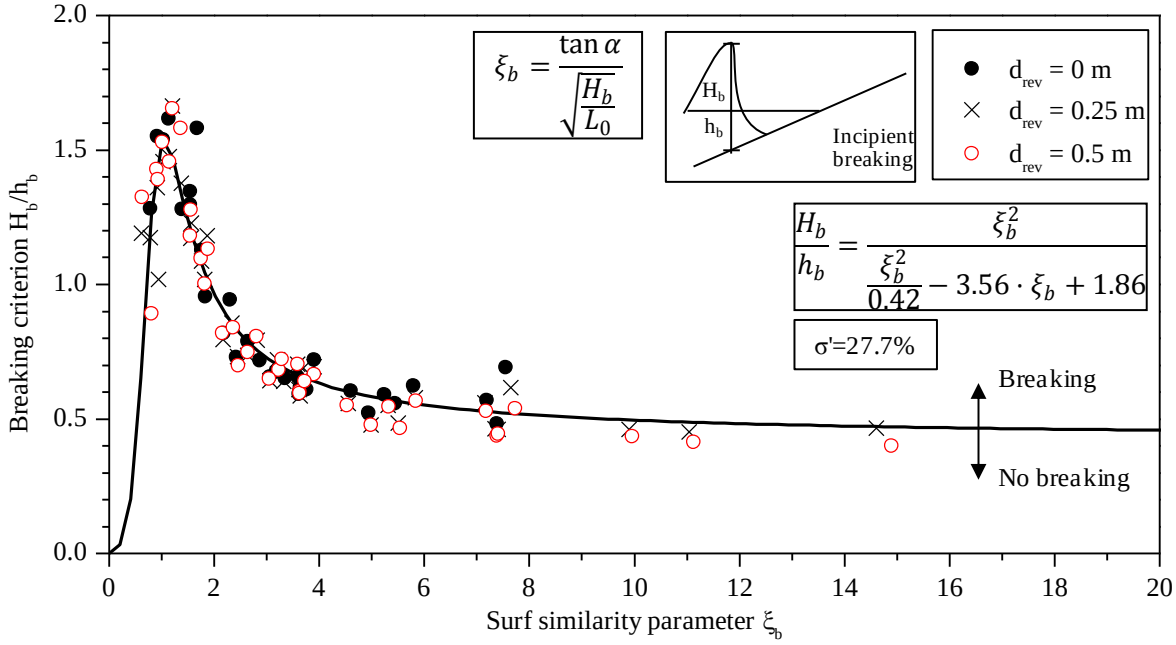

Fig. 4.11 Breaking criterion H_b/h_b versus surf similarity parameter ξ_b (excluding four outliers, only numerical simulations)

To represent the trend of the data set in Fig. 4.11 well, a non-linear fractioned function with three parameters was chosen. The fitted equation is presented in eq. (4.2). In general, the obtained curve is a relatively good fit for the data set and also fulfils the following boundary conditions: (i) $\xi_b \rightarrow 0 \hookrightarrow H_b/h_b \rightarrow 0$ and (ii) $\xi_b \rightarrow \infty \hookrightarrow H_b/h_b \rightarrow$ positive non-zero value. The second boundary condition is represented by the parameter 0.42 ($H_b/h_b \rightarrow 0.42$) in eq. (4.2) because in this case only the quadratic terms remain in the equation. The two other parameters can be used to determine the exact location of the peak around $\xi_b = 1$. The ξ_b-value at this maximum H_b/h_b-value can be calculated as $\xi_{b,max} = -2 \cdot 1.86/(-3.56) = 1.045$ and the corresponding breaker criterion is obtained by inserting this value in equation (4.2) resulting in: $(H_b/h_b)_{max} = 1.48$. A slight underestimation by eq. (4.2) of the actual maximum value is observable but the deviation is still acceptable.

$$\frac{H_b}{h_b} = \frac{\xi_b^2}{\frac{\xi_b^2}{0.42} - 3.56 \cdot \xi_b + 1.86} \tag{4.2}$$

Overall, the values of the breaking criterion H_b/h_b are similar to those of former studies. Especially, the maximum of $(H_b/h_b)_{max} \approx 1.6$ fits very well with that from former studies (e.g. Goda, 2000). However, the surf similarity parameter is often not used. Therefore, a comparison with a generally well accepted formula is performed in the following. Using eq. (2.15) developed by Goda (2000) to calculate the critical wave steepness H_b/L_0, Fig. 4.12 is

obtained. It is clear, that eq. (2.15) overestimates the critical wave steepness for all tested slope steepnesses. For a flat slope (cotα = 6), eq. (2.15) is most accurate and it is expected, that for even flatter slopes a very good agreement would be obtained. This underlines again the need for the present study.

So far, it can be concluded that an improved approach to calculate the wave set-down is still needed. However, an approach together with the data of the wave set-up is provided in the next section. Furthermore, a prediction approach for the location (in this case the breaking criterion) is proposed.

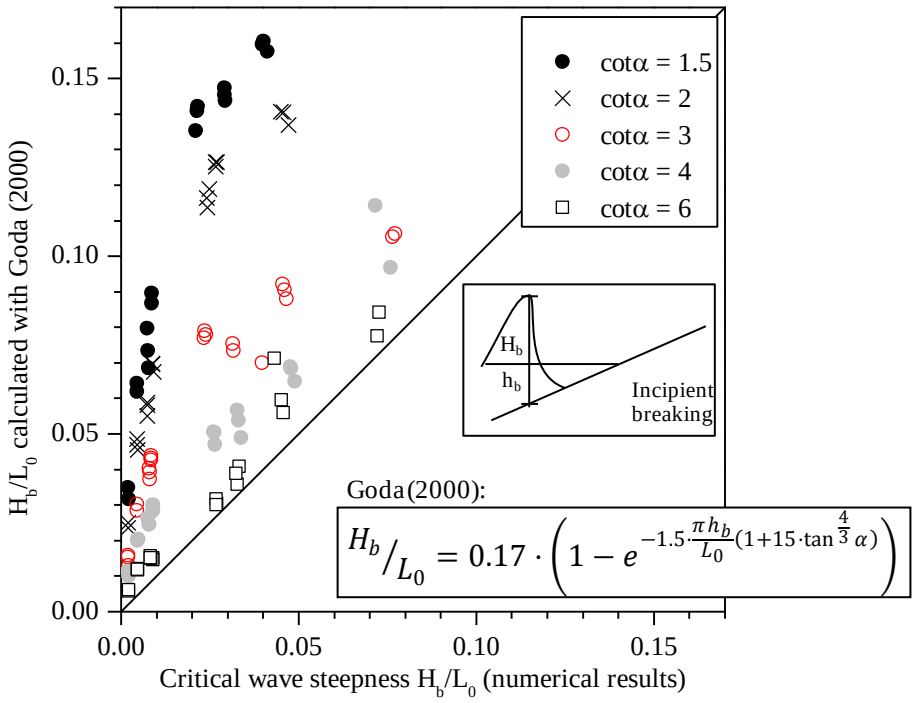

Fig. 4.12 Comparison of the critical wave steepness from numerical data and from the approach by Goda (2000) for cotα = 1.5 - 6

4.2.4 Wave Set-Up

In almost all former studies (e.g. Hanslow & Nielsen, 1993; Stockdon et al., 2006) the relative maximum wave set-up η_{max}/H_m was used which differs from the usage of the relative wave set-down η_{min}/L_0 considered in the previous subsection (4.2.3). In Fig. 4.13, η_{max}/H_m is plotted against ξ_m for comparison with the prediction formulae proposed in Hanslow & Nielsen (1993) (based on eq. (2.12)). The depicted linear relationship only describes an approximate upper limit of η_{max}/H_m for $\xi_m = 0 - 4$. The equation was developed especially for very flat slopes (cotα ≈ 6 - 16). However, even the results for cotα = 6 are located only partly on the line (Fig. 4.13). For surf similarity parameter $\xi_m > 4$, a decrease of the relative wave set-up η_{max}/H_m is depicted which complies with the boundary condition given in Tab. 2.5 but this tendency was not identified in former studies. In comparison, in Fig. 4.14 the relative wave set-up η_{max}/L_0 for all five slope steepnesses is presented. The data sets line up almost perfectly as before the data for the wave set-down (Fig. 4.10). The steepest slope tested in this study

(cotα = 1.5) results in the highest relative wave set-up (for constant ξ_m) on the revetment whereas for the flattest slope (cotα = 6), the smallest relative wave set-up is obtained. The remaining slope steepnesses are all located between those two. These findings correlate with that for the wave set-down (Fig. 4.10). Because of the negligible effect of the revetment thickness on the wave set-up, this parameter is not considered here (see also Foyer & Oumeraci, 2012). In consequence of the comparison of the data presentation in Fig. 4.13 and Fig. 4.14, it was decided to use the relative wave set-up η_{max}/L_0 for a fitting process, because the data sets line up much better.

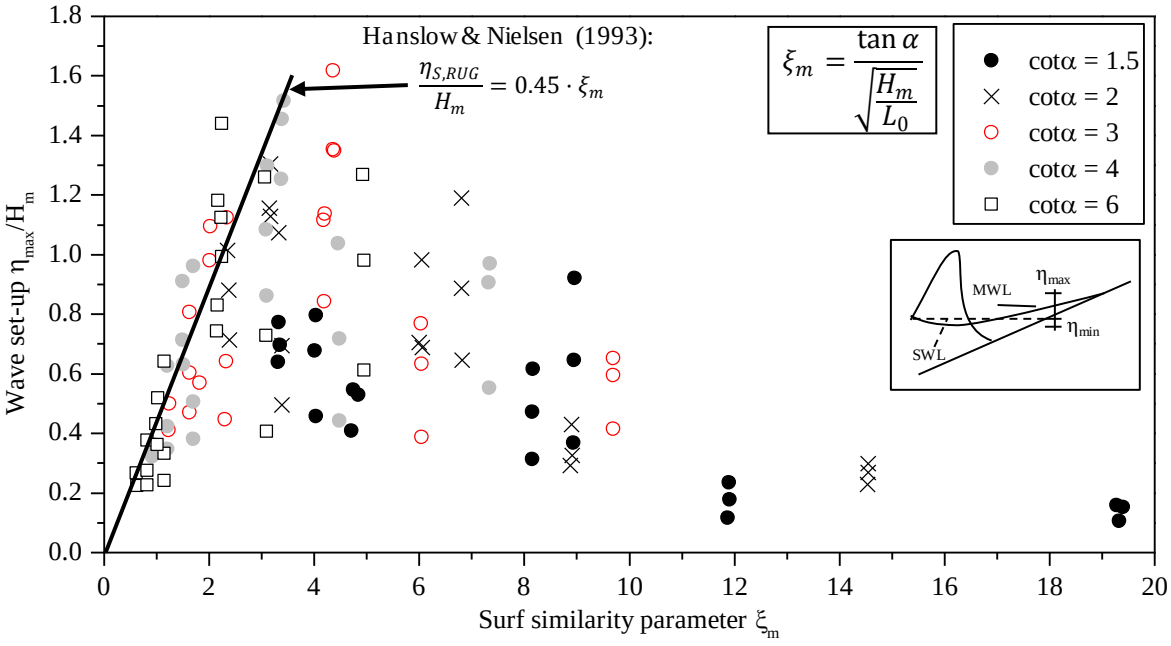

Fig. 4.13 Relative wave set-up η_{max}/H_m for different slope steepnesses (only numerical simulations)

Based on the data presented in Fig. 4.10 and Fig. 4.14, a linear relationship between the wave set-up and set-down was established: $\eta_{max} = -5 \cdot \eta_{min}$ (see also Fig. 4.15). A physical explanation for such a linear relationship is not yet available, but it complies with the theory of Longuet-Higgins & Stewart (1964) for a breaking criterion of $H_b/h_b = 0.8$ (see also Oumeraci, 2007). Based on this relationship, an overall prediction equation for both wave set-up and set-down can be developed. For this purpose, an exponential approach of the same type as eq. (4.1) was first tested, but the results were not satisfying (see Fig. 4.14 and Foyer & Oumeraci, 2013). Therefore, a second approach was adopted using a Multiple Regression Analysis (MRA). The following data sets were used as input:

- Relative wave set-up η_{max}/L_0
- Relative wave set-down $-5\eta_{min}/L_0$
- Surf similarity parameter ξ_m
- Slope steepness cotα

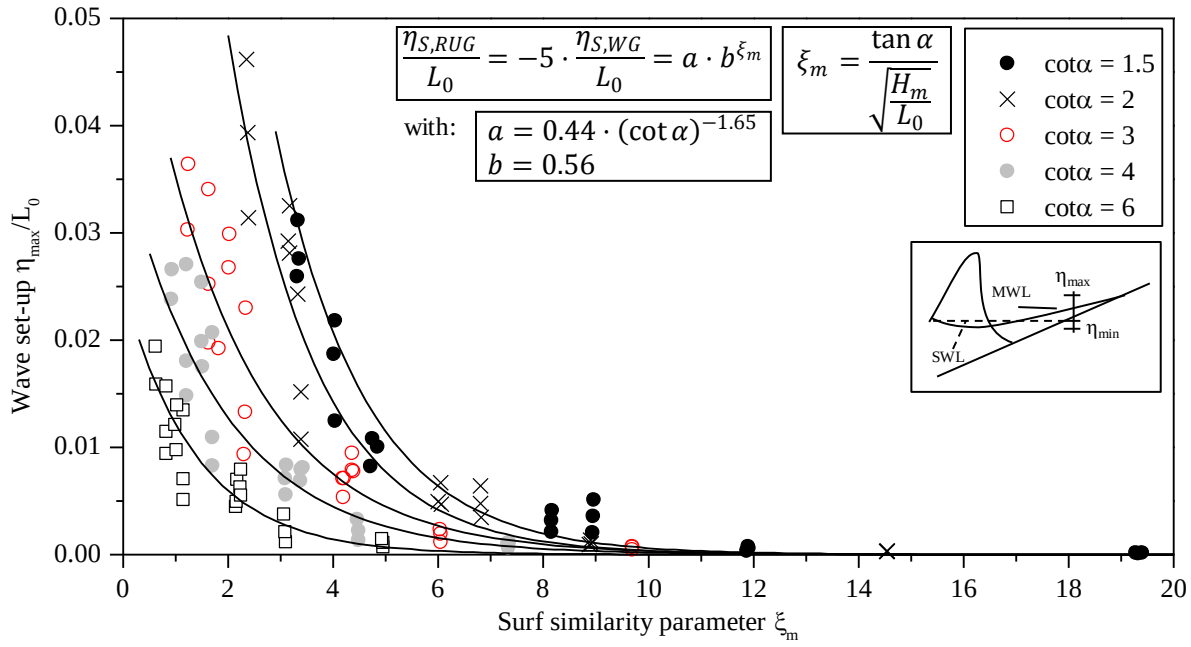

Fig. 4.14 Relative wave set-up η_{max}/L_0 for different slope steepnesses (only numerical simulations)

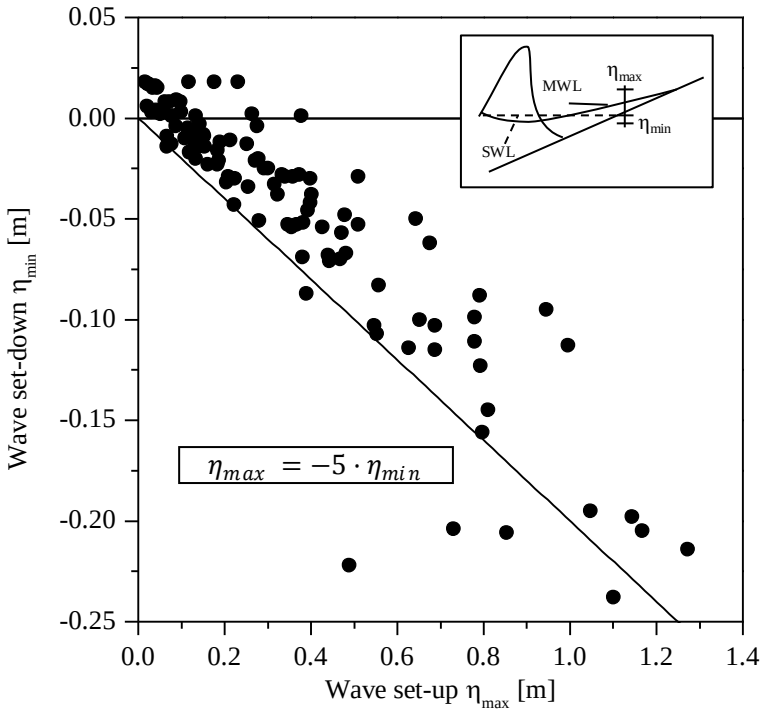

Fig. 4.15 Wave set-up versus wave set-down (only numerical simulations)

As a result of the MRA, eq. (4.3) was obtained. This prediction formula is rather complex, but fulfils the extreme boundary conditions $\eta/L_0 \rightarrow 0$ for $\xi_m \rightarrow \infty$ and $\eta/L_0 \rightarrow \infty$ for $\xi_m \rightarrow 0$. It consists of two terms: the first terms shows that η/L_0 is inverse proportional to the surf

similarity parameter while the second term depends in a much more complex manner on the surf similarity parameter ξ_m and in addition also explicitly on the slope steepness cotα.

$$\frac{\eta_{max}}{L_0} = -5 \cdot \frac{\eta_{min}}{L_0} = \frac{0.0112}{\xi_m} + \frac{\xi_m}{e^{\xi_m + 0.929 \cdot \cot\alpha}} \tag{4.3}$$

The simulated and calculated values are shown in Fig. 4.16 together with the statistical results which are not very good with σ' = 36.2% (wave set-up) and σ' = 36.8% (wave set-down) but still acceptable given the high complexity of the problem. The wave set-up is slightly overpredicted. Generally, the good agreement between the data sets and the prediction equation suggest a very small and negligible effect of the revetment thickness which is not analysed here in detail.

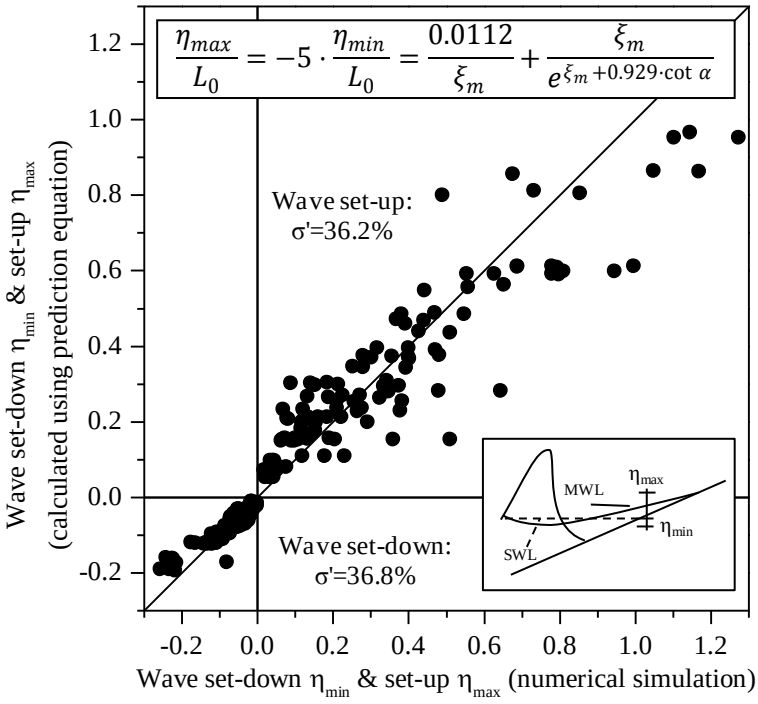

Fig. 4.16 Predicted wave set-up η_{max} and set-down η_{min} using eq. (4.3) versus η_{max} and η_{min} from the numerical simulations

The development of eq. (4.3) can be seen as an important result as it allows for the prediction of the main changes in the mean water level (MWL) from the wave shoaling zone to the shoreline including both wave set-down and set-up for a wide range of wave conditions and slope steepnesses. Above all, the dimension of the wave set-up for relatively steep slopes as they are used for revetments is shown. Possible effects on the processes on and in the structure (e.g. the wave run-up and run-down) are analysed in the following chapters.

A clear definition of wave set-up is given using the wave run-up gauge. An improvement of the spatial resolution compared to laboratory experiments for the analysis of the wave set-down was achieved with the numerical simulations. Prediction equations for the location of incipient breaking and for the calculation of the maximum wave set-down and wave set-up are developed and discussed. A combined approach to the prediction of wave set-up and set-down with $\eta_{max} = -5\ \eta_{min}$ is proposed.

4.3 Wave reflection & dissipation

Several steps are necessary to obtain the reflection coefficient C_r and all wave parameters such as the mean incident wave height H_i and the mean wave period T_m from the data generated by COBRAS-UC:

- Import data of WG01-09 (see Fig. 3.8) into L~Davis
- Set time frame for analysis including 5 – 15 similar waves excluding any irregularities
- Perform reflection analysis according to wave length with WG1+2+3; WG2+3+4 and WG2+3+5 (location of WGs in Appendix A.1 Tab. A.5)
- Obtain reflection coefficient C_r, mean wave height at the wave gauge array H_i and mean wave period T_m from L~Davis
- Calculate shoaling coefficient K_S
- Calculate deep water mean wave height H_m using the shoaling coefficient K_S
- Calculate surf similarity parameter ξ_m with mean wave period T_m and mean deep water wave height H_m

The mean wave parameters in deep water are not only used in this section but in the complete thesis. The energy dissipation can directly be calculated from the wave reflection coefficient using eq. (4.4) (based on eq. (2.4)).

$$C_d = \sqrt{1 - C_r^2} \tag{4.4}$$

For the GWK-experiments the reflection coefficient C_r has already been determined in Oumeraci et al. (2010) and for the numerical simulations it is obtained essentially in the same way. The GWK-results are used as a comparative but neither for the energy dissipation nor for the development of any equations. This is caused by the fact that only one reflection coefficient for two simultaneously tested revetment alternatives in the GWK was obtained (cf. description in Section 3.1 and results in Fig. 2.2).

4.3.1 Wave reflection

Before beginning the detailed analysis of wave reflection for all model configurations, a comparison of the overall results of the numerical simulations with the results from the GWK-experiments is given in Fig. 4.17. The data sets agree fairly well. The larger scatter in the numerical results is mostly due to the different revetment configurations and wave parameters

which are analysed in the following. The analysis of the data from the numerical simulations will also include the steepness of the revetment cotα and the breaker type as well as the different revetment thicknesses d_{rev}.

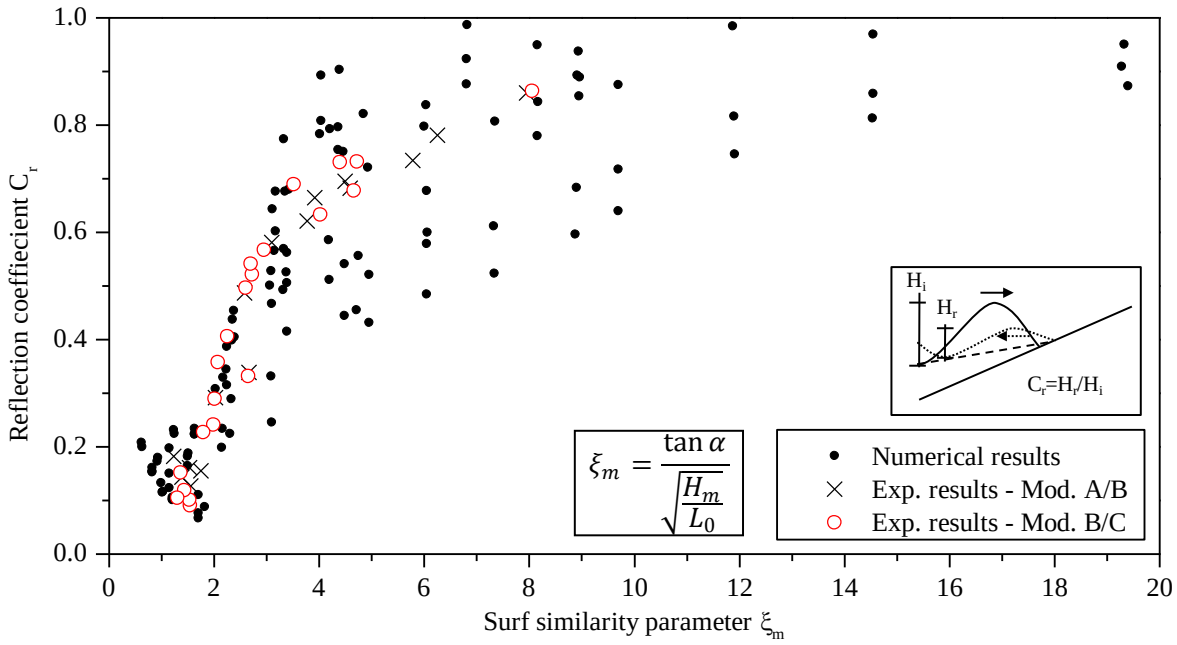

Fig. 4.17 Comparison between numerical results (cotα = 1.5 – 6) and results of the GWK experiments (cotα = 3) for the reflection analysis

The GWK-results are found in the upper range of the numerically obtained reflection coefficients for $\xi_m = 2 – 4$. This is rather unexpected and indicates a slight disagreement between the laboratory tests and the numerical simulations which might be due to characteristics of the revetment surface that could not be reproduced accurately in the numerical simulations.

The most important effects on the reflection performance of a revetment are essentially induced by the surface characteristics of the revetment. Since the revetment is basically the same for all model configurations, the distinguishing parameter between the different configurations is first of all the revetment thickness d_{rev}. Three configurations are, thus, available: (i) a smooth and impermeable slope surface (without revetment $d_{rev} = 0$ m); (ii) a revetment with a thickness $d_{rev} = 0.25$ m, a mean grain size $d_{50} = 0.03$ m and a porosity $n = 0.4$ and (iii) a revetment with a thickness of $d_{rev} = 0.5$ m and with further characteristics identical to those in (ii). The reflection coefficient is plotted against the surf similarity parameter ξ_m in Fig. 4.18 for all three configurations (i) to (iii). The results are in agreement with those of previous studies (e.g. Seelig & Ahrens, 1981) especially with respect to the following effects on the reflection performance:

- Higher reflection coefficient C_r for smooth surfaces especially for $\xi_m = 2 – 15$
- Thicker revetments lead to less reflection but the roughness of the revetment has an even larger effect

- For very high surf similarity parameters (ξ_m > 15) the reflection coefficient is similar for all revetment configurations and tends asymptotically to $C_r \approx 1.0$
- Large scatter of reflection coefficients for all revetment configurations for very small surf similarity parameter $\xi_m < 2$
- Very large scatter found for d_{rev} = 0.25 & 0.5 m between ξ_m = 4 - 10

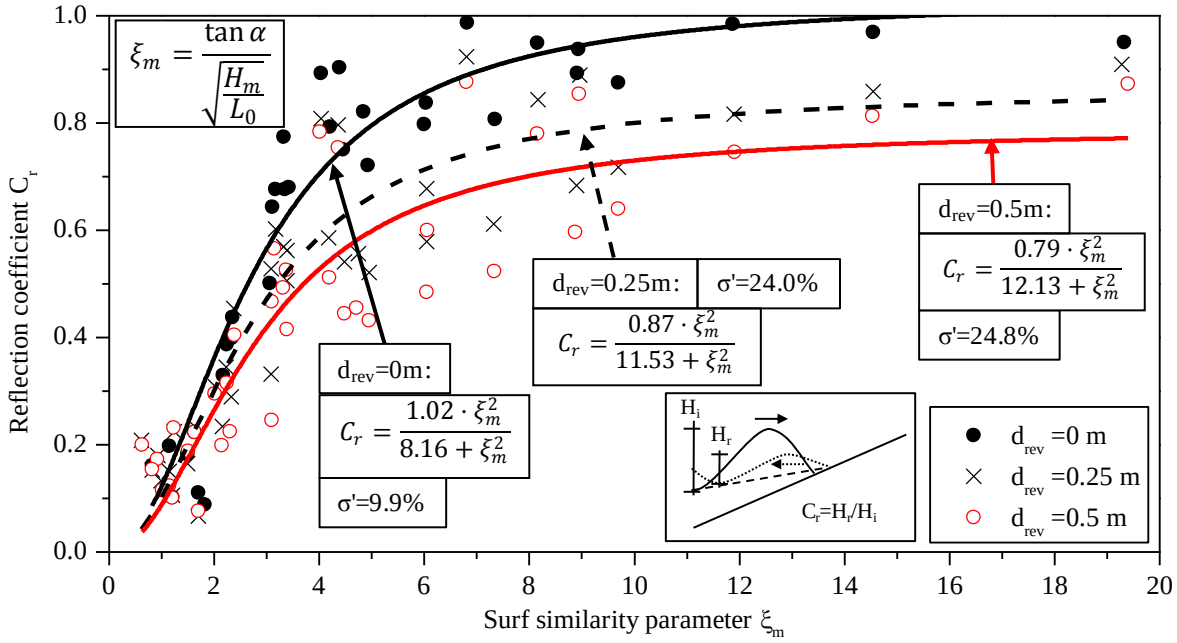

Fig. 4.18 Reflection coefficient vs. surf similarity parameter for different revetment thicknesses (only numerical simulations)

Furthermore, Fig. 4.18 shows the results of a RA using eq. (2.6) of Seelig & Ahrens (1981). The results fit the data sets quite well with an increasing a_1 (as in eq. (2.6)) and a decreasing a_2 (as in eq. (2.6)) for increasing revetment thicknesses d_{rev}. According to the fitted functions, the configurations with d_{rev} = 0.25 m and d_{rev} = 0.5 m lead to a damping of around 15% and 22% compared to the configuration with d_{rev} = 0 m. However, none of the three equations in Fig. 4.18 fulfils the boundary conditions listed in Tab. 2.5. Therefore, a different approach will be presented later in this section.

Concerning the explicit effect of the slope steepness cotα on the reflection coefficient, in addition to that already included in the surf similarity parameter ξ_m, no noticeable influence could be identified (see Foyer & Oumeraci, 2012). Therefore, it can be concluded that the effect of the slope steepness on the wave reflection is adequately accounted for in the surf similarity parameter ξ_m. Besides the slope steepness and the revetment thickness, another reason for the large scatter in the reflection coefficient in Fig. 4.18 might be the breaker type which is not sufficiently described by the surf similarity parameter ξ_m (cf. Section 4.1). Indeed, the classification in Section 4.1 showed several overlaps between the breaker types over the surf similarity parameter ξ_m which might lead to scatter in other data sets over ξ_m. Therefore, the reflection coefficients C_r are presented in Fig. 4.19 for different breaker types for d_{rev} = 0.25 m. The surging breakers are located closely to each other but for the other

breaker types overlaps between the different types are present. In general, two different parts, ① and ②, of the function $C_r = f(\xi_m)$ are found. While the surging, collapsing-surging and collapsing breakers belong to the larger part ①, the spilling and spilling-plunging breakers and most of the plunging breakers belong to the smaller part ②. Due to the very different behaviours of parts ① and ②, it can be assumed that especially the spilling breaker and probably also the plunging breaker may lead to a completely different reflection pattern.

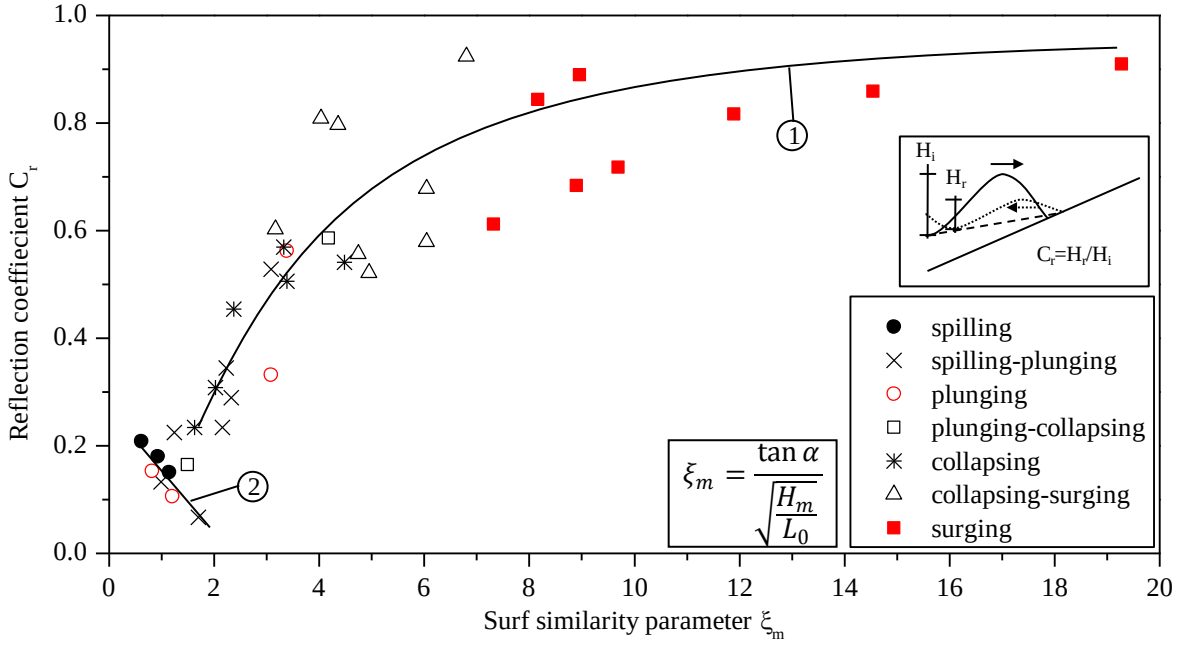

Fig. 4.19 Reflection coefficient for different breaker types on revetments with d_{rev} = 0.25 m (only numerical simulations)

Similar findings can be stated for the other revetment thicknesses d_{rev} = 0.0m & 0.5 m (Foyer & Oumeraci, 2012). A tentative explanation of the development of the two parts ① and ② could be that the deep water wave parameters do not show the best relation to the process of wave reflection which occurs directly at the structure. Further research into this issue is, therefore, required to provide a final explanation.

The shift of breaker types between the three revetment configurations (see Tab. 4.1) and the large scatter in Fig. 4.18 is accounted for by using a modified surf similarity parameter ξ_{mod} which also includes the effect of the revetment thickness:

$$\xi_{mod} = \frac{\tan\alpha}{\sqrt{\frac{H_m}{L_0} \cdot \left(1 + \frac{d_{rev}}{H_m}\right)}} \tag{4.5}$$

This modified surf similarity parameter ξ_{mod} accounts directly for the thickness of the revetment in relation to the wave height. Furthermore, it leads to the original surf similarity parameter ξ_m for d_{rev} = 0.0 m (smooth and impermeable slope). The reflection coefficient C_r is plotted in Fig. 4.20 against the modified surf similarity parameter ξ_{mod}. The most important

consequence of the alteration of the surf similarity parameter ξ_m is the smaller difference between the revetment configurations with d_{rev} = 0 m; 0.25 m and 0.5 m. The results for all three configurations are within the same range. The different behaviour with the reflection coefficients C_r for $\xi_{mod} < 2$, as depicted in Fig. 4.19, is, however, still present. A regression analysis (RA) is applied to the obtained data set using the same approach as for Fig. 4.18 with the exception that parameter a_1 of eq. (2.6) is set to $a_1 = 1$ to obtain $C_r \rightarrow 1$ for $\xi \rightarrow \infty$. This results in the following prediction formula:

$$C_r = \frac{\xi_{mod}^2}{6.74 + \xi_{mod}^2} \tag{4.6}$$

The resulting curve is plotted in Fig. 4.20 showing a relatively good correlation. The largest scatter is found for ξ_{mod} = 3 – 7 and occurs for all three revetment configurations. Therefore, it has to be caused by something else than the revetment thickness d_{rev}, but based on the used data sets no distinct explanation for this scatter can be given.

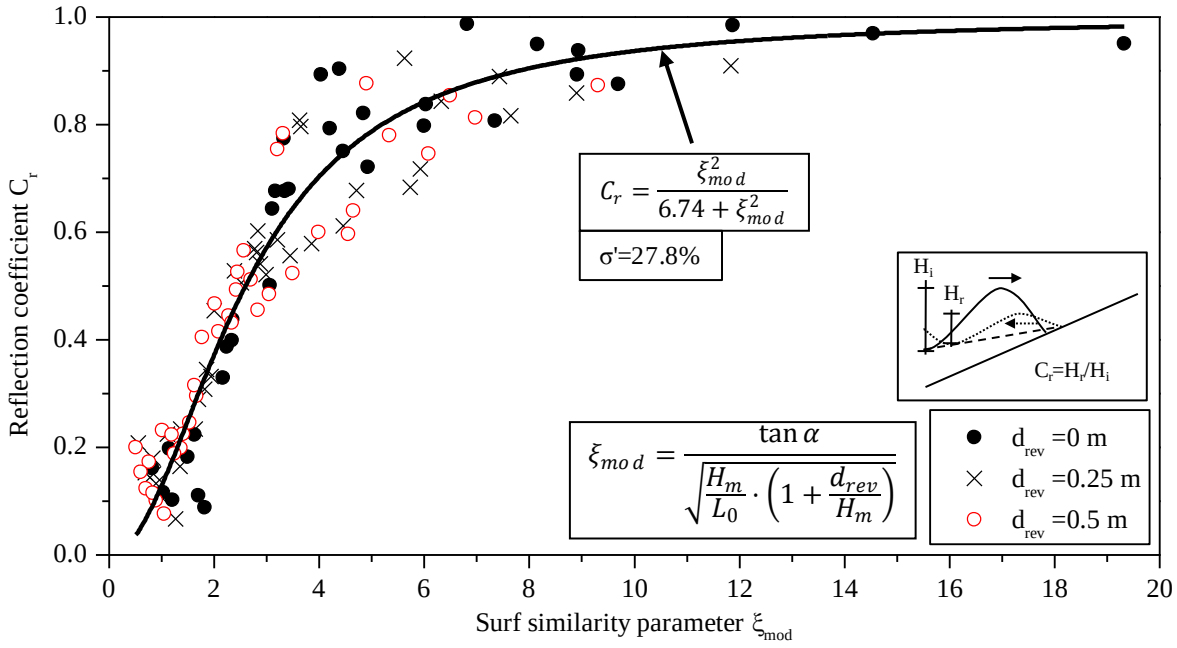

Fig. 4.20 Reflection coefficient over modified surf similarity parameter ξ_{mod} with fitted curve (only numerical simulations)

Finally, the parameters:

- Surf similarity parameter ξ_m
- Relative revetment thickness d_{rev}/H_m
- Slope steepness cotα

were used in a MRA. The best results are presented by eq. (4.7) & (4.8). The two equations show similarities with a quadratic term of the surf similarity parameter in both numerator and denominator. The coefficients of variation σ' for both equations are also provided. For

eq. (4.7), the coefficient of variation σ' is slightly smaller than that for eq. (4.8). This is rather surprising, because the inclusion of the slope steepness cotα in eq. (4.8) was expected to result in a substantial improvement.

$$C_r = \frac{\frac{d_{rev}}{H_m} + \xi_m^2 - \xi_m \cdot \frac{d_{rev}}{H_m}}{7.04 + \xi_m^2} \quad \sigma' = 14.4\% \tag{4.7}$$

$$C_r = \frac{\xi_m^2 + \xi_m \cdot \left(1 - \frac{d_{rev}}{H_m}\right)}{5.52 + \cot\alpha + \xi_m + \xi_m^2} \quad \sigma' = 14.8\% \tag{4.8}$$

Fig. 4.21 shows the results of the two equations (4.7) & (4.8) versus the reflection coefficient obtained from the numerical simulations. No significant difference is found here for both equations. For reflection coefficients $C_r > 0.3$, the scatter around the marked line is very similar for both versions and for reflection coefficients $C_r < 0.3$ the scatter is larger for both versions.

The analysis of the extreme values for equations (4.7) & (4.8) reveals issues for $\xi_m \rightarrow 0$ in equations (4.7), because it does not result in $C_r = 0$ for $d_{rev} \neq 0$. However, eq. (4.8) fulfils this requirement. Both versions result in $C_r = 1$ for $\xi_m \rightarrow \infty$. Due to its slightly better fit and because it is simpler, eq. (4.7) is recommended for calculations.

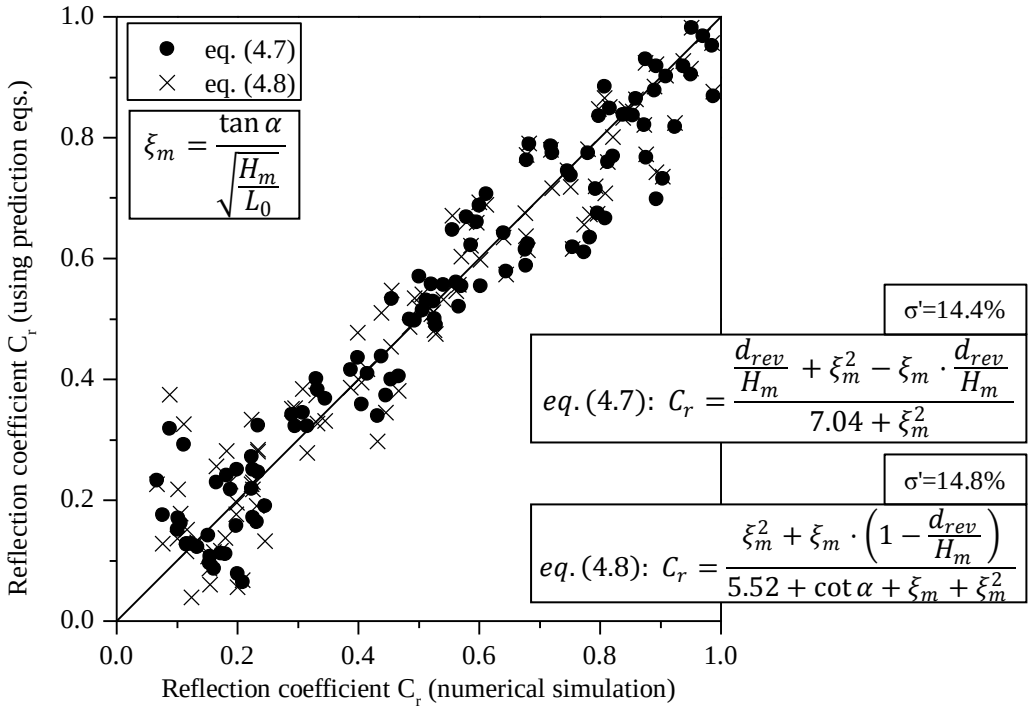

Fig. 4.21 Predicted reflection coefficient C_r using eqs. (4.7) & (4.8) versus C_r from the numerical simulations

4.3.2 Wave energy dissipation

Generally, there are several hydrodynamic parameters indicating the occurrence of energy dissipation. The most important is the reflection coefficient C_r. In this study, where only reflected and dissipated energy are present, the energy dissipation coefficient C_d can be directly calculated from C_r by applying eq. (4.4). The objective of this section is to find relations between energy dissipation and other hydrodynamic parameters than wave reflection in order to develop an approach to calculate energy dissipation independently from the reflection coefficient C_r. The surf similarity parameter ξ_m is, however, not used, because it is the main parameter in the previous section in the analysis of the wave reflection. Any result from that analysis can, thus, also be applied to the dissipation by simply using eq. (4.4).

The most important parameters are therefore:

- Dimensionless parameter $(\eta_{max} - \eta_{min})/L_0$ where η_{max} is the wave set-up, η_{min} the wave set-down and L_0 the deep water wave length and
- Dimensionless parameter $H_b/(R_u - R_d)$ where H_b is the breaker height, R_u the wave run-up and R_d the wave run-down

because both dimensionless parameters strongly depend on the energy dissipation.

The parameters $(\eta_{max} - \eta_{min})/L_0$ and $H_b/(R_u - R_d)$ as well as the slope steepness $\cot\alpha$ are considered in a MRA. Generally, the first dimensionless parameter $(\eta_{max} - \eta_{min})/L_0$ seemed to have only small effects on the dissipation and a focus on the second parameter $H_b/(R_u - R_d)$ was, therefore, chosen. The results from the MRA were analysed for the extreme values (see Tab. 2.5) and the best fit was then chosen. This resulted in eq. (4.9).

$$C_d = 1 - \frac{0.6}{0.6 + \frac{H_b}{R_u - R_d} \cdot \cot\alpha} \tag{4.9}$$

The direct comparison between the final prediction formula for the energy dissipation and the dissipation calculated using the reflection coefficient is shown in Fig. 4.22. The results depict a large scatter. The statistical results are slightly worse than those for the reflection coefficient using eq. (4.7) (σ' = 15.8% > 14.4%). Therefore, a calculation of the dissipated energy should be performed based on eq. (4.4) using the reflection coefficient C_r according to eq. (4.7).

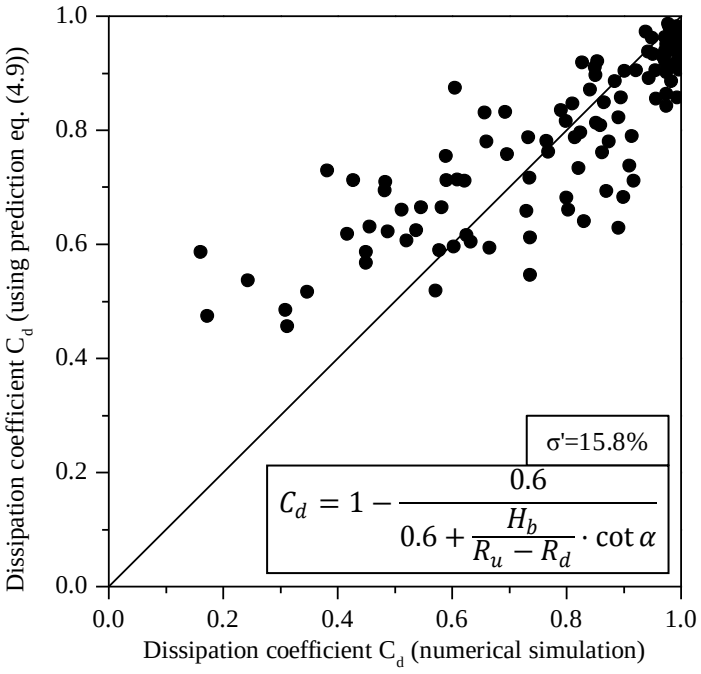

Fig. 4.22 Predicted dissipation coefficient C_d using eq. (4.9) versus C_d from the numerical simulations

The reflection coefficient C_r is mostly affected by the presence of a rough, porous revetment and not by its thickness. A modification of the surf similarity parameter might enable a better approach to also account for the revetment characteristics as e.g. revetment thickness d_{rev} directly and not through empirical parameters. Furthermore, deviations of the trend of the reflection coefficients for very small surf similarity parameter were found for which further research is needed. The dissipation coefficient shows a strong relation to the wave run-up and run-down height, but a calculation using the reflection coefficient (eq. (4.8)) is still to be recommended.

4.4 Summary of key results

1) A distinct classification of the breaker types based on the surf similarity parameter is still very difficult. An effect of the revetment thickness is found especially for the limits between plunging and collapsing and between collapsing and surging breakers.
2) A good correlation between the results of the GWK-tests and the numerical simulations was found for all parameters investigated in this chapter.
3) A distinct improvement of the spatial resolution for the analysis of the wave set-down was achieved by the numerical simulations.
4) The maximum wave set-down is found to be around one fifth of the maximum wave set-up. This is in the same range as predicted by theoretical studies (Longuet-Higgins & Stewart, 1964; see also Oumeraci, 2007). However, a distinct physical explanation for this relation cannot be provided. Using this finding an overall prediction approach for wave set-up and set-down was developed (see eq. (4.3)).

5) A new formula for the prediction of the critical wave height H_b/h_b at incipient breaking (breaking criterion) was developed which only depends on the surf similarity parameter ξ_b (eq. (4.2)).
6) The effect of the surface roughness on C_r is higher than that of the revetment thickness and no further significant effect of the slope steepness on the reflection coefficient C_r in addition to that accounted for in the surf similarity parameter was found.
7) A modified surf similarity parameter is introduced to directly account for the effect of the rough porous revetment (eq. (4.6)).
8) Additionally, a more complex approach to the effect of the revetment thickness on the reflection coefficient is proposed in eq. (4.7).
9) A different reflection behaviour for very small surf similarity parameter $\xi_m < 2$ is identified (Fig. 4.19)
10) An additional prediction equation for the energy dissipation is found using the relation between the wave height at breaking H_b and the total swash height $R_u - R_d$ together with the slope steepness $\cot\alpha$ as non-dimensionless parameter $(H_b)/(R_u - R_d)\cot\alpha$ (see eq. (4.9)).

Consequently, the findings of this chapter are used for further investigations in Chapters 5 - 7. More particularly, the determined wave set-up values are needed for the analysis of the wave run-up in relation to the MWL on and in the revetment, because the wave set-up was found to be much more important than initially expected.

5 Processes on the Revetment

Generally, swash heights, the associated velocities and pressures are used to describe the most important processes on the revetment. The analysis of the pressures had to be dropped due to two reasons: (i) an extensive analysis has already been performed in Ludwigs (2009) and Oumeraci et al. (2010) and (ii) it was not possible to simulate the pressures with COBRAS-UC to full satisfaction mainly due to the limitation of the model to only one fluid (Foyer & Oumeraci, 2012). For all other results from the numerical simulations, no serious problems were expected and the analysis of the swash processes was, therefore, performed as planned.

For the analysis of the processes on the revetment and the development of prediction equations, only the results from the numerical simulations are used. The reason for this decision is the problem with the measurements of the wave run-down height in the GWK-tests (see Fig. 3.6). The wave run-up gauge was not able to reliably resolve very thin water layers on the revetment (cf. Section 3.2.2) leading to an underestimation of the water level elevation at the revetment surface. However, for some comparisons, the GWK-data is used as reference.

Generally, similar approaches are used for all parameters. The most important one is based on the formula for the reflection coefficient of Seelig & Ahrens (1981) (eq. (2.6)):

$$f(\xi_m) = \frac{\xi_m^2 + a \cdot \xi_m}{\xi_m^2 + b} \tag{5.1}$$

Equation (5.1) has an additional linear term compared to eq. (2.6). Furthermore, for surf similarity parameter $\xi_m \rightarrow \infty$ a value of $f(\xi_m) \rightarrow 1$ is ensured.

5.1 Wave run-up & run-down heights

In Section 4.2.1.2 the approach to deploy several measuring devices in the numerical simulations is described. The time series of the RUGs (external and internal) is used for the determination of the wave run-up as well as the wave run-down on and in the revetment. An event analysis is performed using the LWI-Software "L~Davis" to determine all wave run-up and run-down events within a time frame. Generally, all wave run-up and run-down heights from the numerical simulations are related to MWL (see Fig. 5.1 and Fig. 2.3). At the same time the notation with wave run-up height R_u and wave run-down heights R_d remains.

The time frame for the determination of the external wave run-up height included between three and 15 waves and the maximum, minimum and mean wave run-up and run-down heights were saved to a file. For the analysis the extreme values in the time frame are used: the maximum for the wave run-up height and the minimum for the wave run-down height.

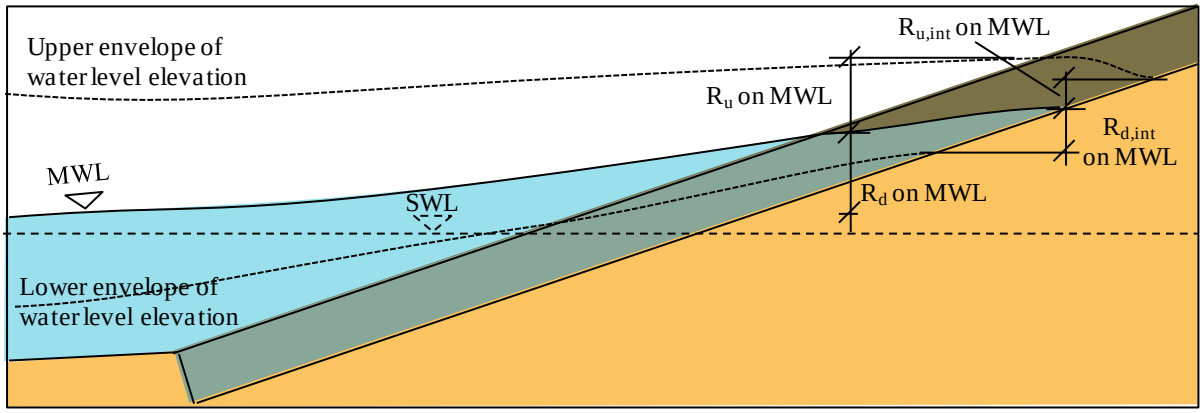

Fig. 5.1 Definition of the wave run-up and run-down heights

Before starting the detailed analysis of the wave run-up and run-down heights, a comparison between the data from the GWK and that from the numerical simulations is performed and shown in Fig. 5.2. The figure shows a similar relation between the GWK-data and the numerical simulations as Fig. 4.17 for the reflection coefficient. The GWK-data is always located around the upper/lower limit of the range of the numerical results. The deviation of the wave run-down height might be caused by the small difference in the location of the measuring devices (Section 3.2.2). Overall, the agreement is acceptable.

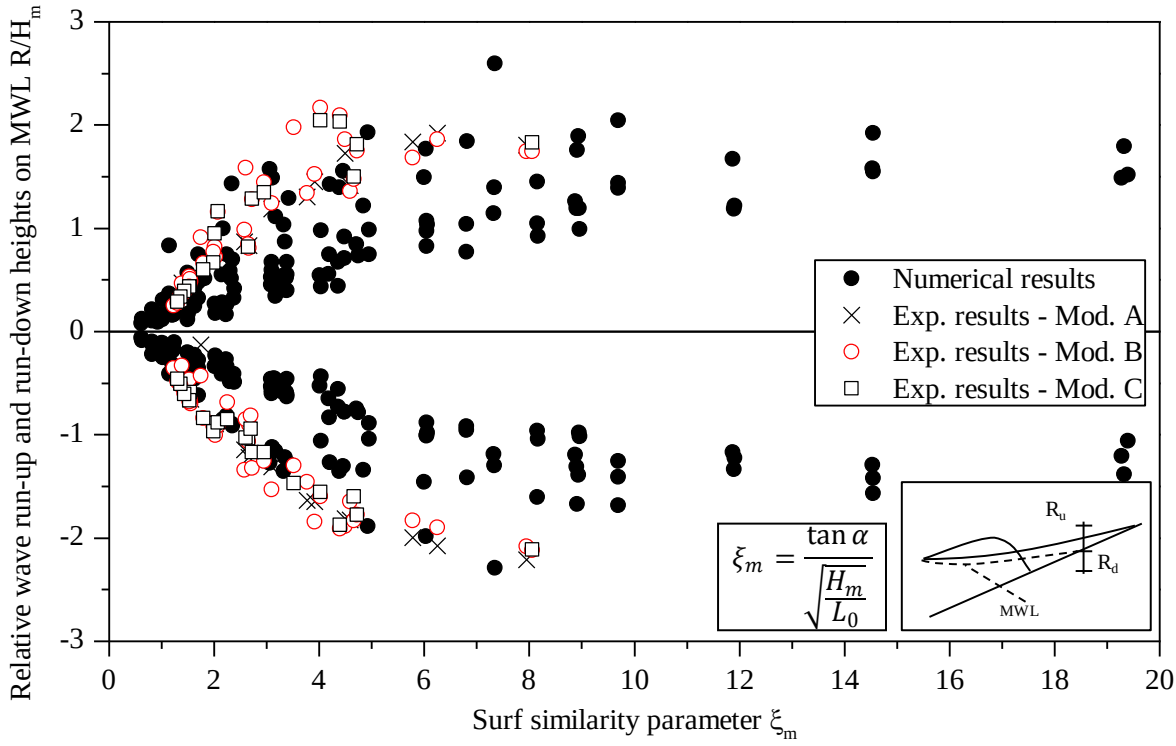

Fig. 5.2 Comparison of wave run-up and run-down heights in GWK-experiments and numerical simulations (cotα = 1.5 – 6)

In Fig. 5.3 the wave run-up and run-down heights of the numerical simulations are plotted according to the revetment thickness that was used in the numerical test (d_{rev} = 0.0 m; 0.25 m;

0.5 m as shown in Fig. 3.7). A clear damping of the swash is present for the tests with porous revetments while higher absolute values are obtained for the smooth and impermeable slope without revetment (d_{rev} = 0 m). However, no clear difference between the results for the revetment thicknesses d_{rev} = 0.25 m and d_{rev} = 0.5 m is found. Surprisingly, the results of d_{rev} = 0.5 m are often even larger than those of d_{rev} = 0.25 m. From this finding, it can be tentatively concluded that the swash heights (wave run-up and run-down height) are mostly affected by a rough and permeable revetment surface but not by the thickness of the revetment. Therefore, the analysis of the revetments with d_{rev} = 0.25 m & 0.5 m is performed without distinguishing between the two revetments.

The swash zone as the primary impact zone of waves on coastal structures is normally considered to move around MWL with the same positive (wave run-up height) and negative (wave run-down height) amplitudes at least for a frictionless (ideal) surface as indicated in Fig. 5.1. This was verified for the numerical simulations (Fig. 5.4b) as well as for the experimental results from the GWK (Fig. 5.4a). Except for some outliers, the data sets of the wave run-up and run-down heights are almost similar. Therefore, the data of both wave run-up and run-down height are merged into one data set and analysed together.

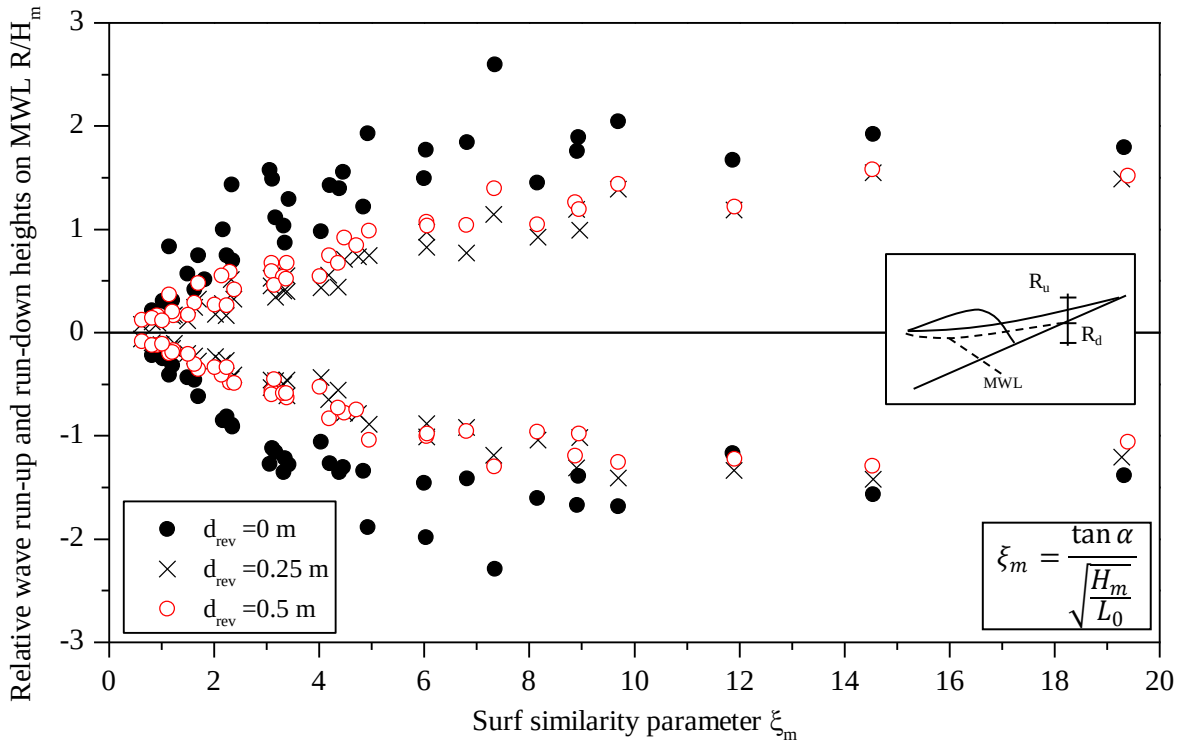

Fig. 5.3 Relative wave run-up and run-down heights R/H_m for different revetment thicknesses (only numerical simulations)

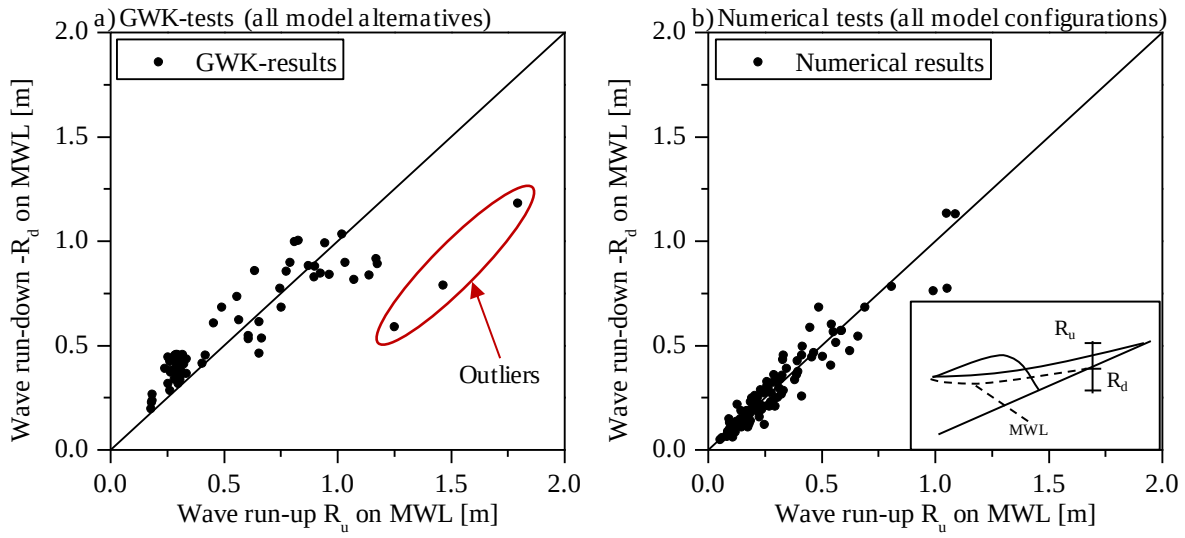

Fig. 5.4 Wave run-up and run-down heights related to MWL for the GWK-tests and the numerical simulations

There are two main issues with existing prediction formulae for the wave run-up and run-down height: (i) they normally relate wave run-up and run-down heights to SWL thus including wave set-up and (ii) they do not consider the physical plausible extreme case $\xi \rightarrow \infty$ where $R_u = -R_d = H_{loc}$ (H_{loc} = local wave height) if an ideal system is assumed (see Tab. 2.5). For the second issue, several values can be found in literature mostly in the form of R_u/H resp. R_d/H but none predicts $R_u/H = -R_d/H = 1$ (cf. Tab. 5.1).

Tab. 5.1 Wave run-up and run-down heights for $\xi \rightarrow \infty$ as found in literature

References	R_u/H	R_d/H
Schüttrumpf (2001)	3	-1.4
USACE (2002)	∞	-1.5
EurOtop (2007)	4	-

The difference between the different local and deep water wave heights can be neglected, because for $\xi \rightarrow \infty$ ($\cot\alpha \rightarrow 0$) no shoaling occurs. Only the difference between wave spectra (as used in literature) and regular waves (as used here) has to be considered. Because this difference does not change the extreme cases, the results in Tab. 5.1 may be considered physically unsound. It has to be noted that none of the given formulae are proposed for a very wide range of surf similarity parameter and $\xi \rightarrow \infty$ was, thus, not included in their development.

During the investigations of the wave run-up and run-down heights, a relation to the reflection coefficient was found. The standard prediction equation for the reflection coefficient as shown in eq. (5.2) is very similar to that found for the wave run-up and run-down height (see eq. (5.3)). Parameter a is the same for equations (5.2) and (5.3). Furthermore, it was found that for both, the reflection coefficient (see Section 4.3.1) and the wave run-up and run-down (Fig. 5.3), the effect of the revetment mostly depends on the roughness of the surface and not on the thickness of the revetment. In both cases, no large differences between the alternatives with $d_{rev} = 0.25$ m and $d_{rev} = 0.5$ m were found even though for the reflection coefficient it

was large enough to be accounted for. Therefore, a combined analysis was performed on the reflection coefficient C_r and the wave run-up and run-down heights using a combined RA. The resulting parameters a and b from equations (5.2) and (5.3) are presented in Tab. 5.2 and the data sets with the corresponding fitted graphs are shown in Fig. 5.5 and Fig. 5.6. These figures also show the coefficients of variation for all data sets.

$$C_r = \frac{\xi_m^2}{\xi_m^2 + a} \tag{5.2}$$

$$\frac{R_u}{H_m} = -\frac{R_d}{H_m} = \frac{\xi_m^2 + b \cdot \xi_m}{\xi_m^2 + a^2} \tag{5.3}$$

The combined RA shows a good performance especially for the wave run-up and run-down heights. For the reflection coefficient, the statistical results are acceptable with σ' = 22.9% but not as good as for the proposed equations in Section 4.3.1 (eqs. (4.6) - (4.8)). However, considering the quality of the fits for all analysed parameters together, the results are relatively satisfying.

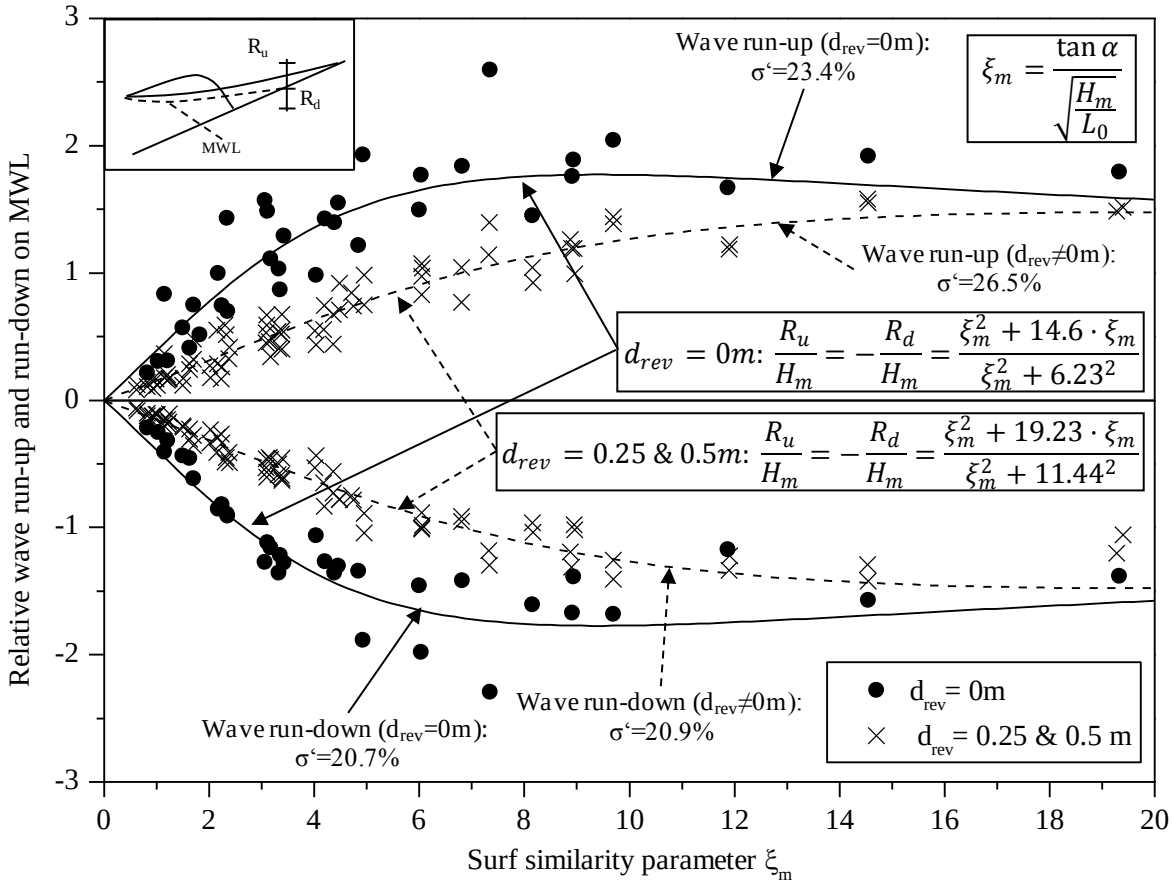

Fig. 5.5 Fitted curves for the wave run-up and run-down height related to MWL with and without revetment (only numerical simulations)

Tab. 5.2 Parameters a and b for the combined RA of wave run-up and run-down and the reflection coefficient

	d_{rev} = 0 m	d_{rev} = 0.25 m & d_{rev} = 0.5 m
a	6.23	11.44
b	14.58	19.23

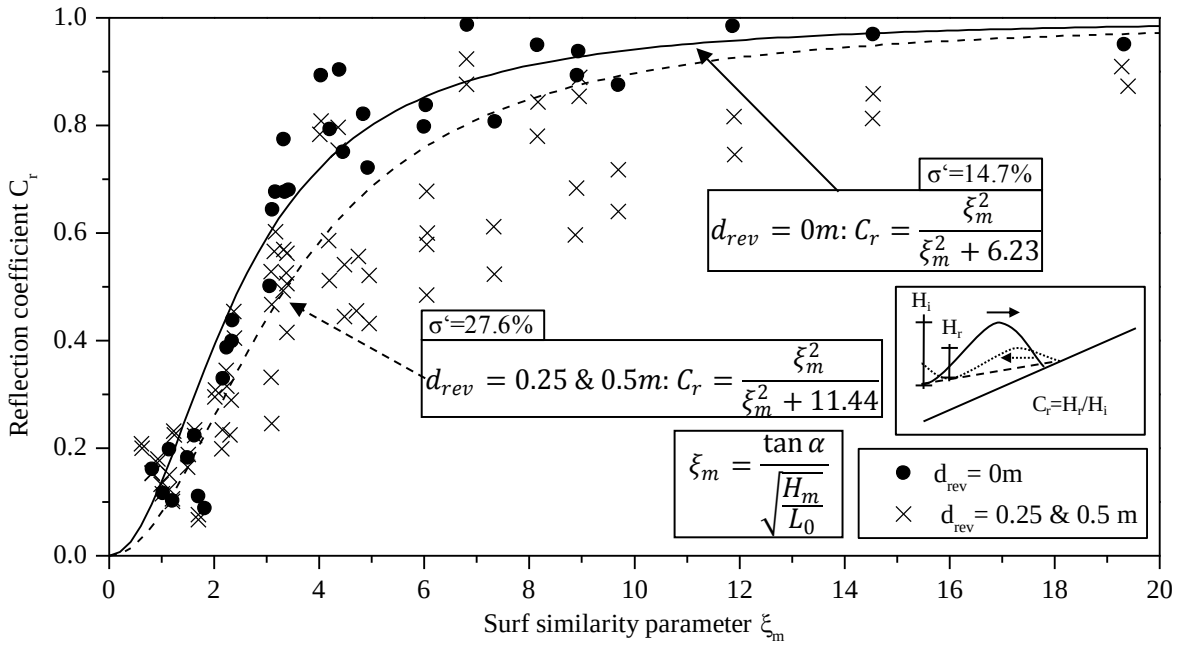

Fig. 5.6 Corresponding fitted curves of the reflection coefficient (only numerical simulations) for the combined RA with the wave run-up and run-down height (see Fig. 5.5)

As for the other parameters, a MRA was performed. A choice of input parameters had, therefore, to be inserted into the tool:

- Reflection coefficient C_r
- Slope steepness cotα
- Breaker criterion H_b/h_b

The last parameter H_b/h_b was chosen because it describes the situation directly in front of the structure and the other two parameter are included due to general dependencies.

The result of the MRA is shown in eq. (5.4). For both, the wave run-up and the wave run-down height, the statistical values show a worse fit than for eq. (5.3). The coefficients of variation result in the following: (i) for the wave run-up height σ’ = 49.4% and (ii) for the wave run-down height σ’ = 42.9%.

$$\frac{R_u}{H_m} = -\frac{R_d}{H_m} = \frac{0.28 + 0.284 \cdot \cot\alpha \cdot C_r^2}{H_b/h_b} \tag{5.4}$$

Overall, the approach described in eq. (5.3) and in Tab. 5.2 proves to be better than the one obtained in the MRA (eq. (5.4)). The parameter a used in eq. (5.3) seems to be linked to the

roughness, permeability or porosity of the revetment because it does not change with the revetment thickness. A more precise analysis is needed to conclude which structural parameter exactly affect parameters a and b (see eq. (5.3)). For this, tests with an even wider range of the revetment thickness and also with revetments with different roughnesses, permeabilities and porosities are needed.

The wave run-up and run-down heights R_u and R_d are found to oscillate symmetrically around MWL (just considering the maximum heights and not the temporal development). The wave set-up should, therefore, always be taken into account separately for the determination of the highest wave run-up and the lowest wave run-down. A significant effect of the revetment surface properties (roughness, permeability and porosity) rather than the revetment thickness is found, as well as a close link to the reflection coefficient C_r. A prediction equation similar to that of the reflection coefficient was, therefore, developed (see eq. (5.3)).

5.2 Wave run-up and run-down velocities

The wave run-up and run-down velocities were obtained from the recording of the wave run-up gauge (RUG) and are defined as the velocity of the water layer on and in the revetment as shown in Fig. 5.7. The maximum and minimum derivates of the RUG are determined for every wave and the mean value per test is taken for the analyses. Furthermore, the values had to be corrected, because the RUG measures the vertical water level elevation and the velocities are directed along the slope. Therefore, the wave run-up and run-down velocities are multiplied by $\sqrt{(\cot^2\alpha+1)}$ to calculate the velocity along the slope from the vertically directed velocities (see Fig. 5.8). Both, vertical velocities and velocities along the slope are used for the analyses to also determine an effect of the slope steepness.

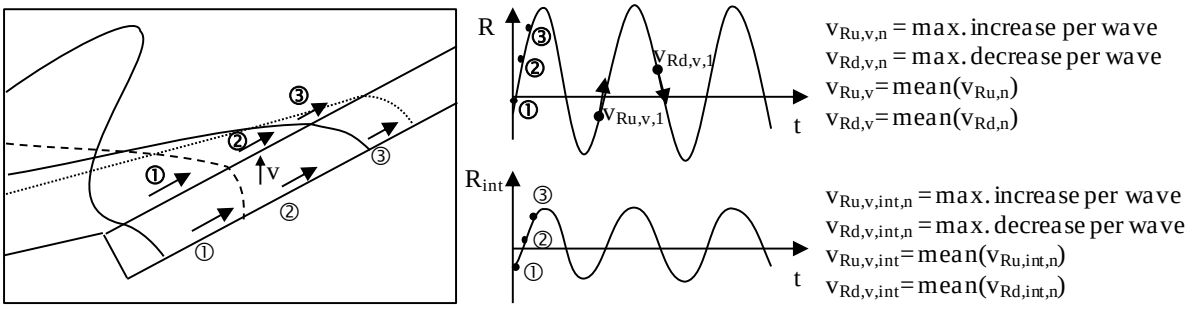

Fig. 5.7 Definition of wave run-up and run-down velocities as derivates of the wave run-up and run-down (all velocities are in vertical direction)

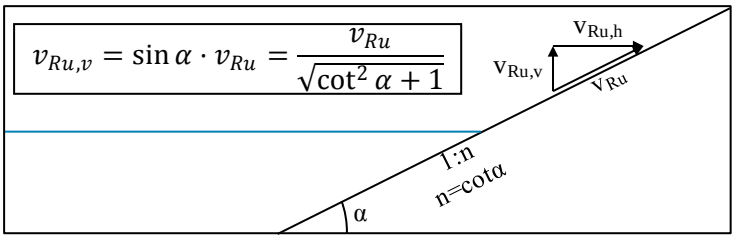

Fig. 5.8 Definition of vertical velocities and velocities along the slope surface

In Fig. 5.9 the relative wave run-up and run-down velocities $v_R T_m/H_m$ of the numerical simulations for all slope steepnesses and of the GWK-tests are plotted versus the surf similarity parameter ξ_m. The relation $v_r T_m/H_m$ is chosen to enable a better comparison with Schüttrumpf (2001). Generally, the scatter in the numerical data is very high compared to the GWK-results while the GWK-points line up almost perfectly which might indicate an effect of the slope steepness. Furthermore, the absolute GWK-data for both, wave run-up and the run-down velocities, is in the range of the large values of the numerical results as it was already found for the reflection coefficient (Fig. 4.17). But overall the trend is the same for all data sets; the relative wave run-up velocities increase with increasing surf similarity parameter ξ_m until $\xi_m \approx 5$ (GWK-data) respectively $\xi_m \approx 7$ (numerical results). For the wave run-down velocity this applies, too, but inversely (decreasing values for increasing ξ_m). For surf similarity parameter $\xi_m > 5$ the GWK-results reach a maximum (respectively minimum) and the numerical results turn towards zero for $\xi_m > 7$. This implies small changes in the relative velocity for very high surf similarity parameters which were not captured by the GWK-experiments.

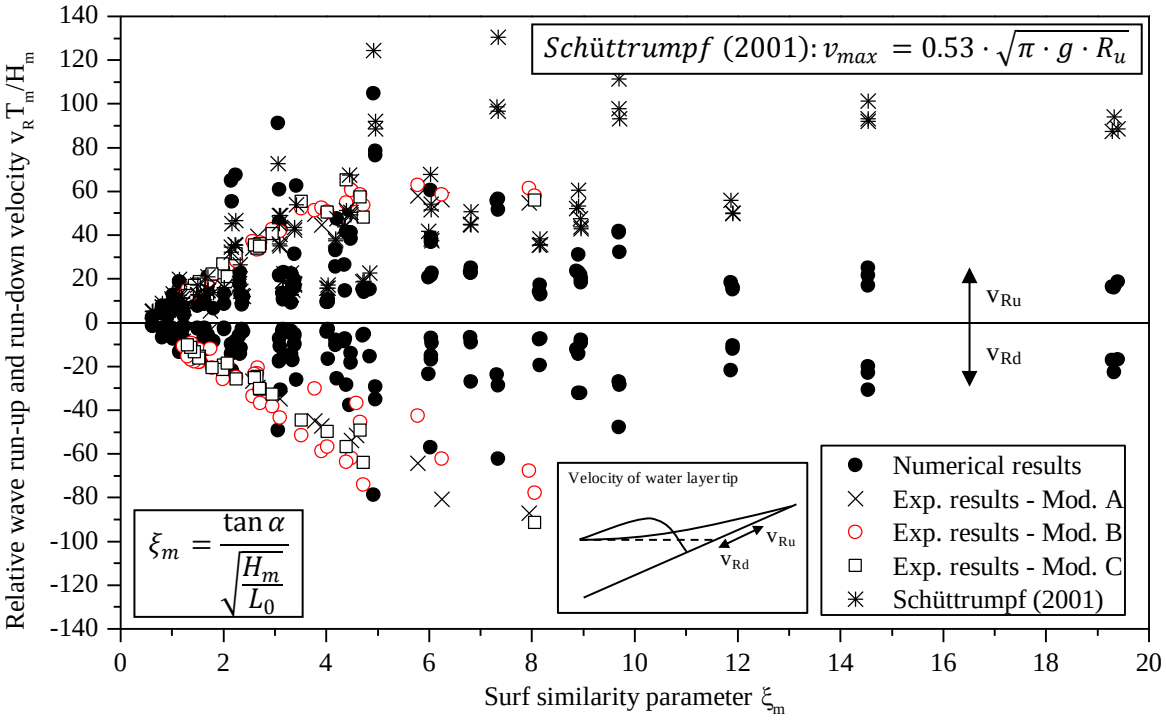

Fig. 5.9 Comparison of wave run-up and run-down velocities on the revetment in GWK experiments and numerical simulations (cotα = 1.5; 2; 3;4 6)

In addition to the comparison between the GWK-results and the results of the numerical simulation, Fig. 5.9 shows also the upwards directed velocities as calculated using the approach of Schüttrumpf (2001) at SWL (eq. (2.28)). The obtained relative velocities are larger than those obtained in the GWK-tests and the numerical simulations especially for surf similarity parameter $\xi_m > 5$. This could partly be caused by the damping of the revetment. In Schüttrumpf (2001) a smooth, impermeable slope was investigated and furthermore, eq.

(2.28) was not validated for surf similarity parameter $\xi_m > 10$. It can definitely be concluded that a better prediction equation is needed especially for that range of surf similarity parameters.

As for the wave run-up and run-down heights, the relation between the wave run-up and run-down velocities is tested for a possible merging of the data sets. Fig. 5.10 presents the wave run-up and run-down velocities for the GWK-tests (Fig. 5.10a) and for the numerical simulations (Fig. 5.10b). First of all, the figure shows differences between the GWK and the numerical results. For the GWK-tests, the wave run-up and run-down velocities are very similar except for some outliers and for the numerical results, the wave run-down velocities tend to be smaller than the wave run-up velocities. Consequently, the wave run-up and run-down velocities are investigated separately in the following. However, the parameters are still presented together for a better comparability.

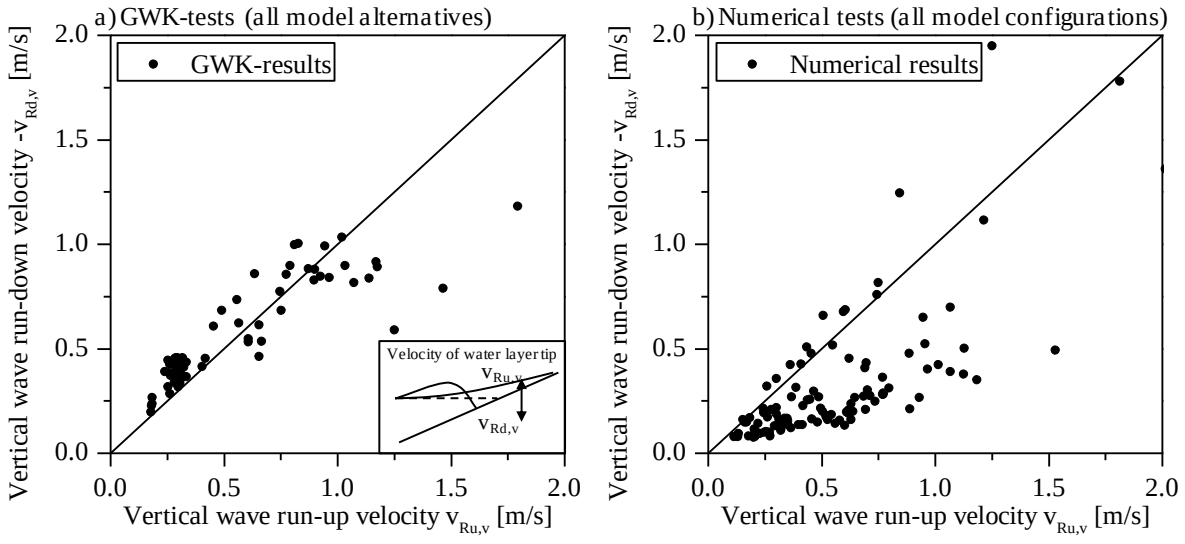

Fig. 5.10 Wave run-up and run-down velocities for the GWK-tests and the numerical simulations

In Fig. 5.9 a large scatter was found in the data from the numerical simulations. Therefore, it was decided to use the vertical velocity for all further analyses (see also Fig. 5.8). Moreover, the relation was changes from $v_r T_m/H_m$ to $v_R T_m/(2\pi H_m)$ to ensure a better comparability with the assumption made in Tab. 2.5 for $\xi \rightarrow \infty$. Using this new relation, the effect of the revetment thickness is presented in Fig. 5.11. It shows the relative wave run-up and run-down velocities for all three revetment configurations with d_{rev} = 0, 0.25 and 0.5 m. First of all, the scatter in Fig. 5.11 is much smaller than in Fig. 5.9. Furthermore, the difference between the tests with porous revetments and the tests without a revetment (d_{rev} = 0 m) is visible. The smooth and impermeable slope leads to slightly higher wave run-up velocities and especially to very small wave run-down velocities. Second, no difference between the two porous alternatives is observable and it can, therefore, be concluded that only roughness or permeability of the revetment are affecting the velocities.

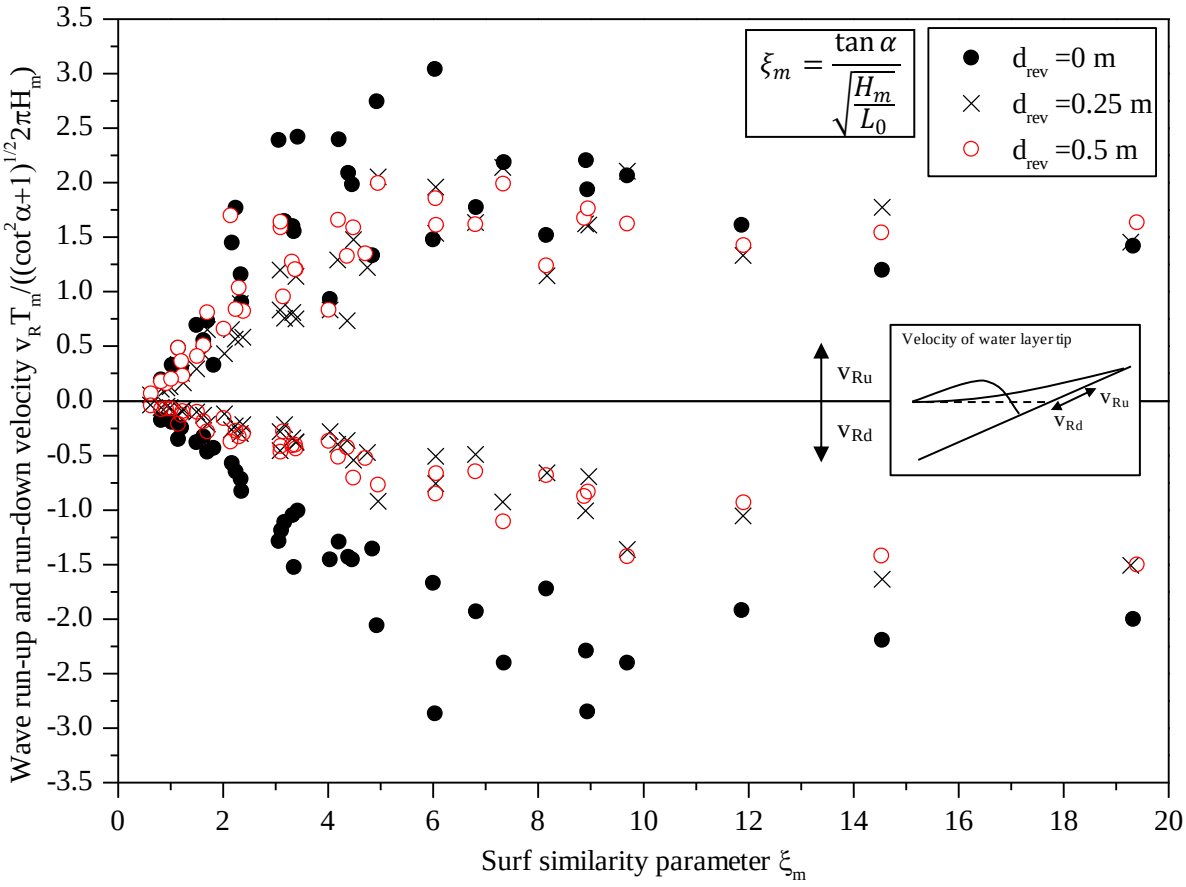

Fig. 5.11 Relative wave run-up and run-down velocity on the revetment for different revetment thicknesses (only numerical simulations)

The vertical component ($v_v = v/\sqrt{(\cot^2\alpha+1)}$) of the wave run-up velocity divided by $2\pi H_m/T_m$ (limit for $\xi_m \rightarrow \infty$; see Tab. 2.5) is plotted against the surf similarity parameter ξ_m for the revetment thicknesses $d_{rev} = 0.25$ & 0.5 m and $d_{rev} = 0$ m separately in Fig. 5.12. For small surf similarity parameters ($\xi_m < 3$) the relative vertical wave run-up velocity for $d_{rev} = 0.25$ m & 0.5 m is smaller than 1 with a steep rise for increasing ξ_m. This rise is continued until a maximum value of around 2 is obtained for $\xi_m \approx 6$. For larger surf similarity parameters, a slight decrease in the velocity can be observed which coincides with the extreme case for the relative value being $v_{Ru,v}T_m/(2\pi H_m) = 1$ for $\xi_m \rightarrow \infty$. A similar tendency is found for the data set with $d_{rev} = 0$ m but the maximum value of $v_{Ru,v}T_m/(2\pi H_m) \approx 2.5$ is found around $\xi_m = 5$.

The two data sets of the wave run-up velocity shown in Fig. 5.12 were used for a nonlinear RA. Due to the similarity of the extreme values and the trend of the data sets (Fig. 5.5), a similar function as for the wave run-up and run-down height data was used (eq. (5.3)). This procedure resulted in eq. (5.5). The empirical parameters for $d_{rev} = 0.25$ & 0.5 m are similar to that of the wave run-up and run-down (see Tab. 5.2 on p. 78) considering the quadratic parameter a in the wave run-up and run-down approach. Thus, the graph for the wave run-up data on the smooth slope is almost the same as for the wave run-up velocity on a porous

revetment (parameter sets: 14.6 & 6.23² and 14 & 40). Both graphs of eq. (5.5) are also plotted in Fig. 5.12 and show a good agreement with the data points.

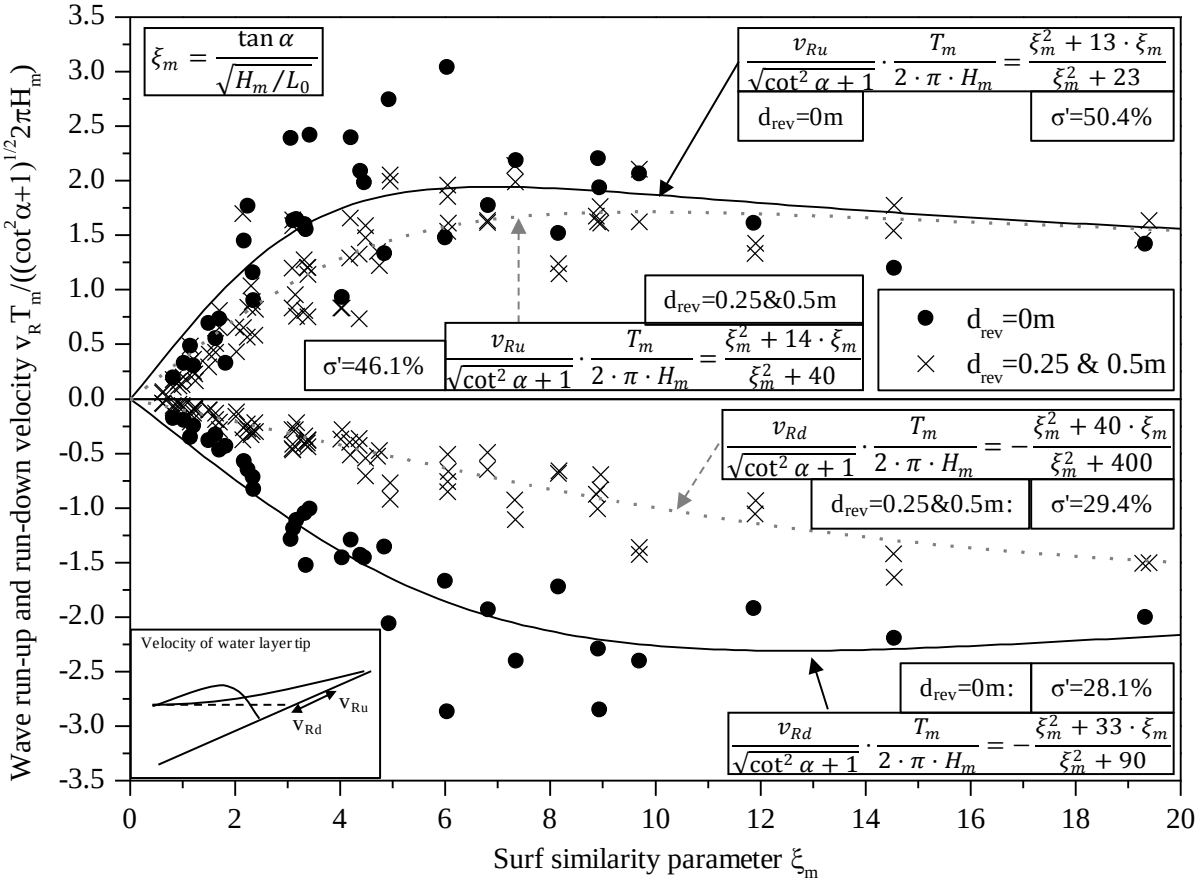

Fig. 5.12 Relative vertical wave run-up and run-down velocity for tests with and without porous revetments (only numerical simulations)

$$\frac{v_{Ru}}{\sqrt{cot^2\,\alpha+1}} \cdot \frac{T_m}{2\pi H_m} = \frac{\xi_m^2 + a\cdot\xi_m}{\xi_m^2 + b} \quad \begin{matrix} for\ d_{rev} = 0m: & a = 13;\ b = 23 \\ for\ d_{rev} = 0.25\&0.5m & a = 14;\ b = 40 \end{matrix} \tag{5.5}$$

At the beginning of Section 5.2, it was found that the wave run-up and run-down velocities deviate too much from each other to be analysed together. However, the same approach as for the wave run-up velocities is used to analyse the wave run-down velocities. This also includes the separation into vertical and horizontal components as for the wave run-up velocity. Fig. 5.12 shows the relative vertical wave run-down velocity $v_{Rd,v}T_m/(2\pi H_m)$ for the tests with and without porous revetments versus the surf similarity parameter ξ_m. On the one hand similarities to the wave run-up velocity can be found: e.g. there is no difference in wave run-down velocity due to different slope steepnesses. On the other hand, the shape of the data pattern is quite different for the larger part of the surf similarity parameter range. Unlike the wave run-up velocity, the wave run-down velocity does not reach a distinct local extreme for d_{rev} = 0.25 & 0.5 m (here a minimum would be expected where a maximum was found for the

wave run-up velocity). For the smooth surface with d_{rev} = 0 m, a minimum of $v_{Rd,v}T_m/(2\pi H_m)$ = -3 is found around ξ_m = 7 which is similar to the wave run-up velocity.

The differences between the wave run-up and run-down velocities also affect the results of the RA. The smoother increase of the absolute velocity for surf similarity parameter ξ_m = 0 – 6 and the absence of a distinct minimum for d_{rev} = 0.25 & 0.5 m lead to larger empirical parameters as shown in eq. (5.6). Considering this result, it is advisable to look for a different approach to develop a prediction equation for the relative vertical wave run-down velocity.

$$\frac{v_{Rd}}{\sqrt{cot^2\,\alpha+1}}\cdot\frac{T_m}{2\pi H_m}=-\frac{\xi_m^2+a\cdot\xi_m}{\xi_m^2+b}\quad\begin{matrix}for\ d_{rev}=0m: & a=36;\ b=70\\ for\ d_{rev}=0.25\&0.5m & a=40;\ b=400\end{matrix} \tag{5.6}$$

To get a better overview of all parameters obtained with the approach presented in eqs. (5.5) & (5.6), they are summarised in Tab. 5.3. The results show that parameter a is similar for both surface types (smooth impermeable slope and rough porous revetment) but different for the wave run-up and run-down velocities (a = 13 & 14 vs. a = 36 & 40). The variance in parameter b is, however, much larger (b = 23 – 400).

To evaluate the quality of each result of the regression analyses, the coefficients of variation are given in Fig. 5.12. The results are overall better for the wave run-down velocities, which is most likely caused by the smaller scatter in the data set.

Tab. 5.3 Parameters a and b for the RA of the wave run-up and run-down velocities

a and b according to eq. (5.1)	v_{Ru}		v_{Rd}	
	d_{rev} = 0 m	d_{rev} = 0.25 m & 0.5 m	d_{rev} = 0 m	d_{rev} = 0.25 m & 0.5 m
a	13	14	36	40
b	23	40	70	400

In addition to the RA a MRA was performed for the wave run-up velocity. The relative vertical wave run-up velocity $v_{Ru}T_m/(2\pi H_m\sqrt{(\cot^2\alpha+1)})$ is targeted using the following parameter:

- Surf similarity parameter ξ_m
- Slope steepness $\cot\alpha$
- Relative revetment thickness d_{rev}/H_m

The results of the MRA were checked for plausibility. This included the right range of velocities (e.g. no negative wave run-up velocity) and the tendency for $\xi_m \rightarrow \infty$ which should be $v_{Ru}T_m/(2\pi H_m\sqrt{(\cot^2\alpha+1)}) \rightarrow 1$ (see Tab. 2.5). The best fit of the remaining results is the following:

$$\frac{v_{Ru}}{\sqrt{\cot^2\,\alpha+1}}\cdot\frac{T_m}{2\cdot\pi\cdot H_m}=\frac{\xi_m+0.561\cdot\cot\alpha\cdot\xi_m-2.67}{\xi_m+\cot\alpha-1.48} \tag{5.7}$$

Because the data set used for the MRA is the complete one with all data points at once (d_{rev} = 0; 0.25 & 0.5 m) it was expected that the fit is worse than the separated RAs. This

assumption is, however, not verified by the statistical results: σ' = 35.1% is better than the RA-results indicating a higher effect of the revetment thickness than expected after analysing Fig. 5.11. A different approach is, therefore, suggested but this cannot be achieved based on the data at hand.

The MRA with the wave run-down velocities was performed identically to the one for the wave run-up velocities but did not lead to satisfying results (Foyer & Oumeraci, 2013).

The wave run-up and run-down velocity v_{Ru} & v_{Rd} are analysed separately, because they are found to be different especially if a porous revetment is present. Furthermore, no distinct effect of the revetment thickness on both swash velocities could be observed. A similar prediction approach as for the wave run-up and run-down heights was used because a close relation between the parameter was found.

5.3 Local flow velocities

The local flow velocities could easily be read from the data saved from the numerical simulations. For this purpose, a MATLAB-routine (Appendix B.4) was used. Next to the velocities in several locations (see Tab. A.5), the cell with the maximum amplitude of velocities was saved. All velocities were defined as positive when directed upwards and negative when directed downwards irrespective from any revetment angle. The precise direction was not analysed and all velocities were assumed to be parallel to the revetment. From the six recordings on the revetment surface, the maximum (upwards directed) and the minimum (downwards directed) velocities were determined as exemplarily shown for two locations in Fig. 5.13. The mean values of each recording and each parameter (v_{max} and v_{min}) is considered for the determination of the overall maximum and minimum for each test. The name "local flow velocities" was chosen because of the local fixation of the measurements in comparison to the wave run-up and run-down velocities presented in Section 5.2. This location is, however, differing from test to test and only the largest/smallest velocities irrespective of their location of occurrence are analysed.

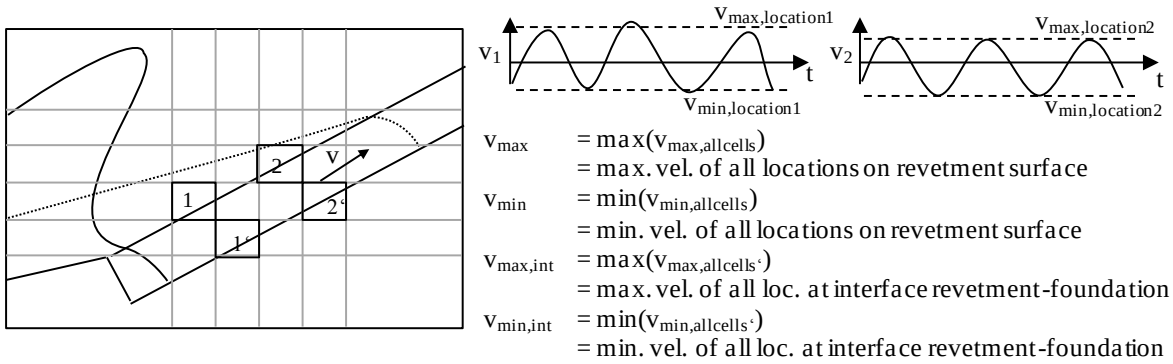

Fig. 5.13 Definition of local flow velocities

Only with the help of the numerical simulations in COBRAS-UC it was possible to analyse the local swash velocities and not only the velocity of the moving tip of the water layer.

Therefore, only the data from the numerical simulations can be used in the following. For a good comparison, the same relative velocities are used for the swash velocities as for the wave run-up and run-down data meaning only the vertical component is used (Fig. 5.8). Furthermore, similar effects of the revetment thickness and the slope steepness are found for the local swash velocities as for the wave run-up and run-down velocities (Fig. 5.11) and the same approaches are, therefore, used in the following.

Before starting the analysis, it has to be decided, whether the data sets of the maximum and minimum flow velocity can be merged. The two parameters are presented in Fig. 5.14 and it is obvious that the analysis of the local swash velocities has to be performed separately because the maximum local velocities are much larger than the minimum local velocities. This finding is agreement with the comparison between wave run-up and run-down velocity (Fig. 5.9).

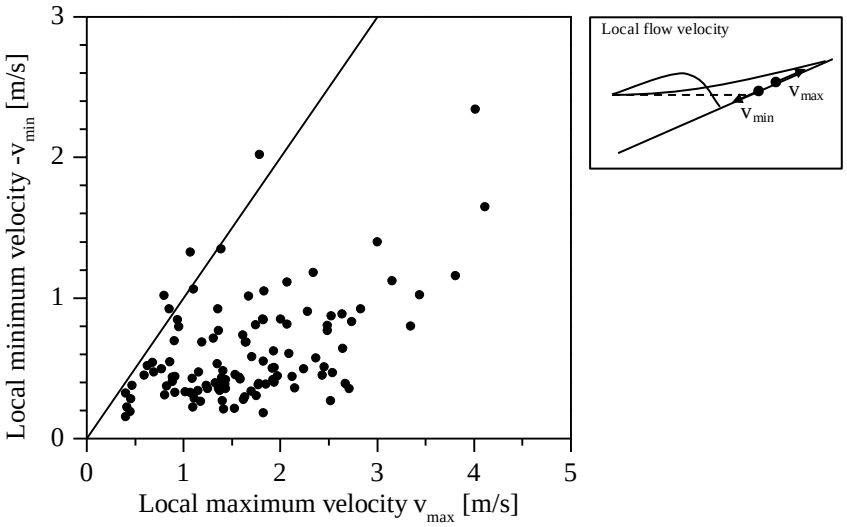

Fig. 5.14 Local maximum and minimum (inverse algebraic sign) flow velocities on the revetment

The relative vertical component of the maximum local flow velocity $v_{max}T_m/(2\pi H_m\sqrt{(\cot^2\alpha+1)})$ is plotted versus the surf similarity parameter ξ_m together with the corresponding data set of the wave run-up velocities in the upper part of Fig. 5.15. In general the two data sets are very similar. For surf similarity parameter $\xi_m < 2$, the results are almost identical. For $\xi_m = 2 – 10$, a high scatter in the same range is found for both sets and for $\xi_m > 10$, the local flow velocity is larger than the wave run-up velocity. It can be concluded from these results, that the highest velocities are normally found at the tip of the water layer. Only for very high surf similarity parameter $\xi_m > 10$, the local velocities are higher than the velocity of the tip of the water layer meaning the water further down is rushing over the tip and thus overtaking it.

Fig. 5.15 also shows the minimum local flow velocity and the wave run-down velocity. Overall, both data sets are very similar. Some deviations are found especially for surf similarity parameter $\xi_m = 1 – 5$ where the minimum flow velocity is larger (smaller considering the absolute values) than the wave run-down velocity. For all other ranges of surf similarity parameter the results for both kinds of velocities are almost identical.

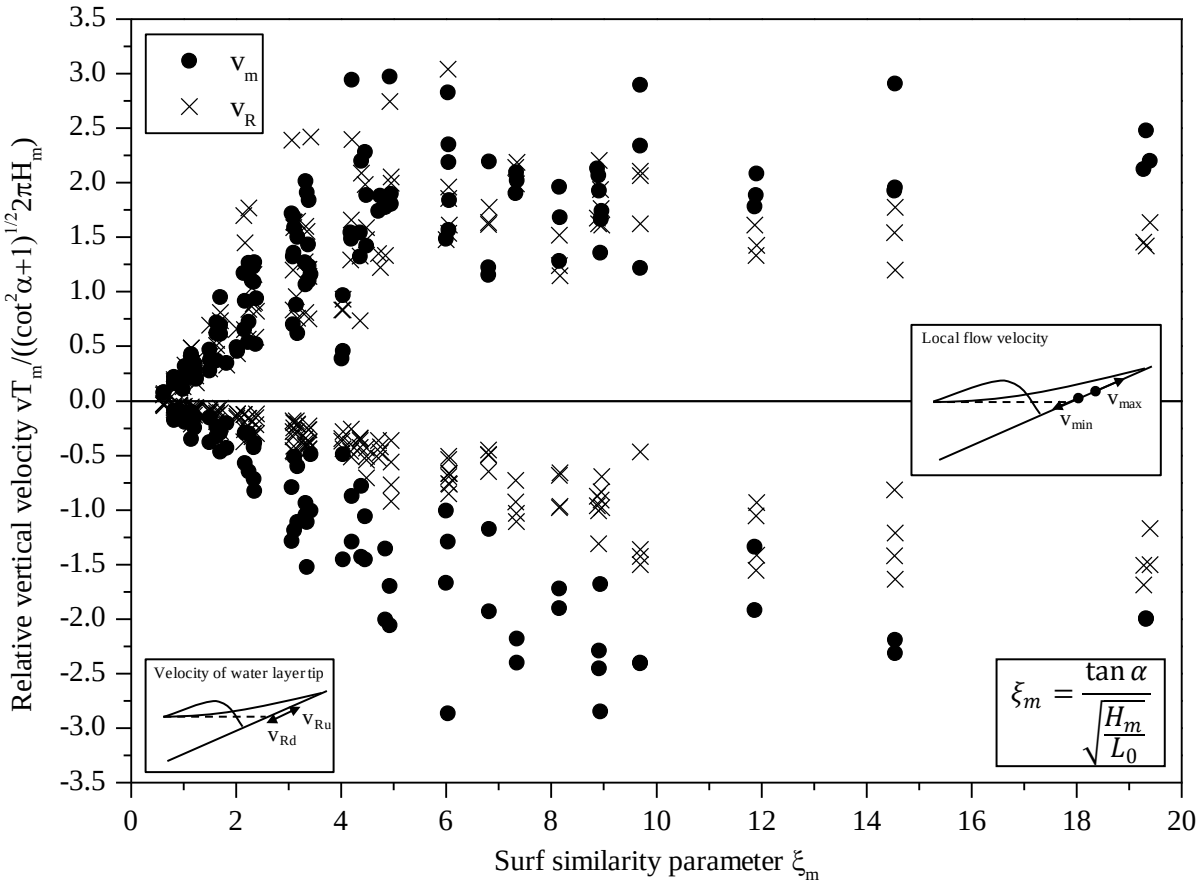

Fig. 5.15 Wave run-up & run-down velocity and maximum & minimum local swash velocity for porous and smooth revetments

The deviation between the data sets of the downwards directed velocities in Fig. 5.15 might be caused by the slightly different directions of the velocities. For the analyses it has been assumed, that the minimum and maximum flow velocities are in the same direction as the revetment surface. A small deviation from this assumption makes the analysis of the vertical component vulnerable to errors. However, these errors are most likely very small and therefore the approach was not modified.

In the upper part of Fig. 5.16, the vertical component of the local maximum flow velocity is given separately for the tests with a smooth slope (d_{rev} = 0 m) and with a porous revetment (d_{rev} = 0.25 & 0.5 m). As expected, the velocities on the smooth revetment are higher than those on the porous revetment. Furthermore, a small local maximum is present in the data set of the smooth revetment as before for the wave run-up velocity (Fig. 5.12).

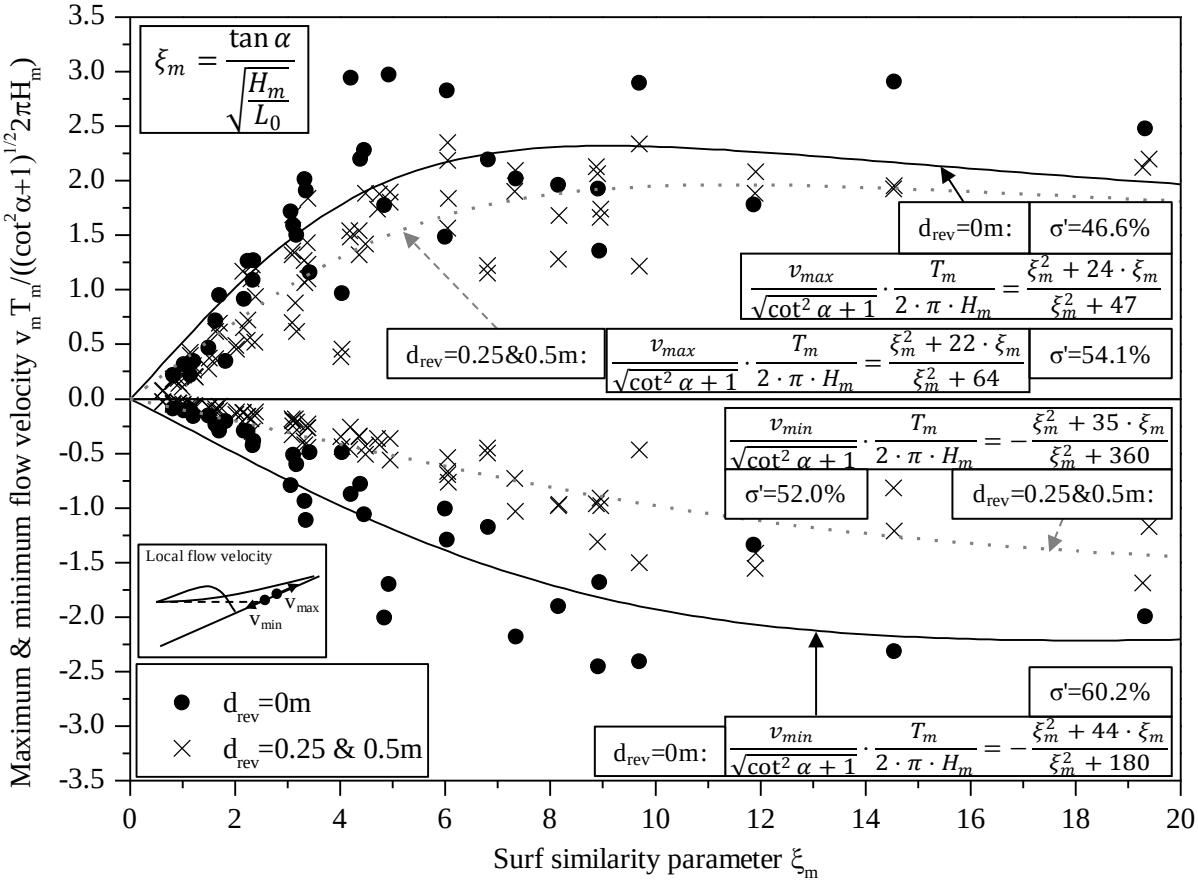

Fig. 5.16 Relative vertical local maximum and minimum flow velocity for porous revetments

The scatter for both data sets for the maximum local flow velocity in Fig. 5.16 is quite large but because no other parameter was found to have a noticeable effect on the maximum flow velocity, the same approach as before (see eq. (5.1)) is applied here to the data set in Fig. 5.16 resulting in eq. (5.8). The resulting empirical parameters are all larger than for the wave run-up velocity (eq. (5.5)) thus making the curve for $\xi_m > 12$ less steep compared to that of the wave run-up velocity. Some similarities with the results from the wave run-up velocity are, however, present. The values for the a-parameter are for instance similar for the two model alternatives (smooth impermeable slope and rough porous revetment) with a = 22 and 24 and the b-parameter is larger for the rough porous alternative.

$$\frac{v_{max}}{\sqrt{cot^2\,\alpha+1}} \cdot \frac{T_m}{2\pi H_m} = \frac{\xi_m^2 + a\cdot\xi_m}{\xi_m^2 + b} \quad \begin{matrix} for\ d_{rev} = 0m: & a = 24;\ b = 47 \\ for\ d_{rev} = 0.25\&0.5m & a = 22;\ b = 64 \end{matrix} \tag{5.8}$$

Fig. 5.16 also presents the vertical component of the relative local minimum flow velocity for the tests with a smooth impermeable slope $d_{rev} = 0$ m and with a porous revetment $d_{rev} = 0.25$ & 0.5 m. The local minimum flow velocity is even more reduced by the rough porous revetment than the local maximum flow velocity, thus indicating a stronger influence of the porous revetment on the downwards directed flow velocity than for the wave run-down velocity (Section 5.2).

The two data sets for the local minimum flow velocity depicted in Fig. 5.16 are also used for a nonlinear RA. The result of this analysis is shown in eq. (5.9). The absence of any distinct minimum in the data set leads to rather large values for parameter a and b (cf. eq. (5.1)).

$$\frac{v_{min}}{\sqrt{cot^2\,\alpha + 1}} \cdot \frac{T_m}{2\pi H_m} = -\frac{\xi_m^2 + a \cdot \xi_m}{\xi_m^2 + b} \quad \begin{matrix} for\ d_{rev} = 0m: & a = 44;\ b = 180 \\ for\ d_{rev} = 0.25\&0.5m & a = 35;\ b = 360 \end{matrix} \tag{5.9}$$

For a good comparison of all resulting equations, Tab. 5.4 shows the parameters a and b for all RAs in the present section. Moreover, the respective results of the wave run-up and run-down velocities are given in brackets. For three of the four considered cases, the parameters obtained for the local flow velocities are larger than those for the wave run-up and run-down velocities. This difference indicates a smoother gradient in the resulting graphs for the flow velocities. As can be seen in e.g. Fig. 5.16, this behavior can lead to two different results: (i) larger absolute values for the flow velocities for large surf similarity parameters (Fig. 5.16) or (ii) smaller absolute values for the flow velocities for small surf similarity parameters (Fig. 5.16).

Tab. 5.4 Parameters a and b for the RA of the local flow velocities (in brackets: wave run-up & run-down velocities)

a and b according to eq. (5.1)	v_{max}		v_{min}	
	d_{rev} = 0 m	d_{rev} = 0.25 m & 0.5 m	d_{rev} = 0 m	d_{rev} = 0.25 m & 0.5 m
a	24 (13)	22 (14)	44 (36)	35 (40)
b	47 (23)	64 (40)	180 (70)	360 (400)

For a further analysis, a MRA was performed for the local flow velocities using the same parameters as before for the wave run-up and run-down velocities. Regretfully, no satisfying results were obtained. A second prediction equation could therefore not be developed.

It was found that the local maximum flow velocities v_{max} are larger than the wave run-up velocities v_{Ru} for large values of the surf similarity parameter indicating that the friction is highest at the tip of the water layer. For the local minimum flow velocities v_{min}, a larger reduction due to the rough porous revetment is present than for the local maximum flow velocities. Therefore, it can be assumed that the effect of the porous revetment adds up over one wave cycle thus having more effect during down-rush than during up-rush.

5.4 Summary of key results

The most important findings on the processes associated with the wave run-up and wave run-down on the slope surface may be summarised as follows:

1) The wave run-up and run-down heights R_u and R_d are found to be symmetrically around MWL. Therefore, a combined analysis to enlarge the investigated data set was possible.
2) The wave run-up and run-down velocities v_{Ru} and v_{Rd} are only affected by the type of surface (smooth, impermeable or rough, porous revetment) but not by the thickness of

the revetment. This indicates a significant effect of the permeability rather than the porosity of the revetment for all swash processes.

3) For a smooth revetment, the wave run-up and run-down velocities are very similar while for a porous revetment the absolute wave run-down velocities are smaller than the corresponding wave run-up velocities. Therefore, it can be assumed that the wave run-down is automatically affected by the precedent wave run-up and if this is already dampened, the wave run-down is even more dampened by the porous revetment.
4) The wave run-up and run-down velocities are highly linked to the wave run-up and run-down heights. This is mostly shown by the similarity in the regression analyses. Therefore, it can be assumed that even though the temporal development of the wave run-up and run-down is affected by possible asymmetries of the wave, these processes do not affect the maximum gradient of the temporal development.
5) The flow velocities v_{max} and v_{min} are very similar to the wave run-up and run-down velocities. Small differences might be caused by differences in direction (local flow velocities are only assumed to be along the slope surface).
6) For the upwards directed velocities, higher flow velocities than wave run-up velocities were observed for large surf similarity parameter and for the downwards directed velocities, smaller absolute flow velocities were observed than wave run-down velocities for small surf similarity parameter. This issue is most likely linked to the effect of breaking on the velocities. Breaking has naturally a higher effect on the uprush velocities, especially for plunging breakers for which these very high upwards directed flow velocities are found. The downwards directed velocities are less affected than the upwards directed velocities and the largest absolute values are therefore found for the largest surf similarity parameters.

6 Processes in the Revetment

The processes within the revetment are particularly interesting but it was not possible to directly observe these processes in the GWK-tests. However, the numerical simulations made this investigation possible. This chapter therefore only uses the data obtained from the numerical simulations. The analysis includes the internal wave set-up, the internal swash heights and the velocities in the revetment (swash velocities and local flow velocities). No pressure analysis is presented here due to the unsatisfactory numerical results (see beginning of Chapter 5 and Foyer & Oumeraci, 2012). Furthermore, for all parameters, a close relation to the processes on the revetment is assumed.

6.1 Internal wave set-up

The internal wave set-up η_{int} was obtained in the same manner as the wave set-up η_{max} on the slope (see Section 4.2.1.2) using an internal wave run-up gauge placed directly at the bottom of the revetment in the numerical set-up. Thus, the numerical simulations make it possible to investigate also the wave set-up at the interface between revetment and foundation (Fig. 6.1).

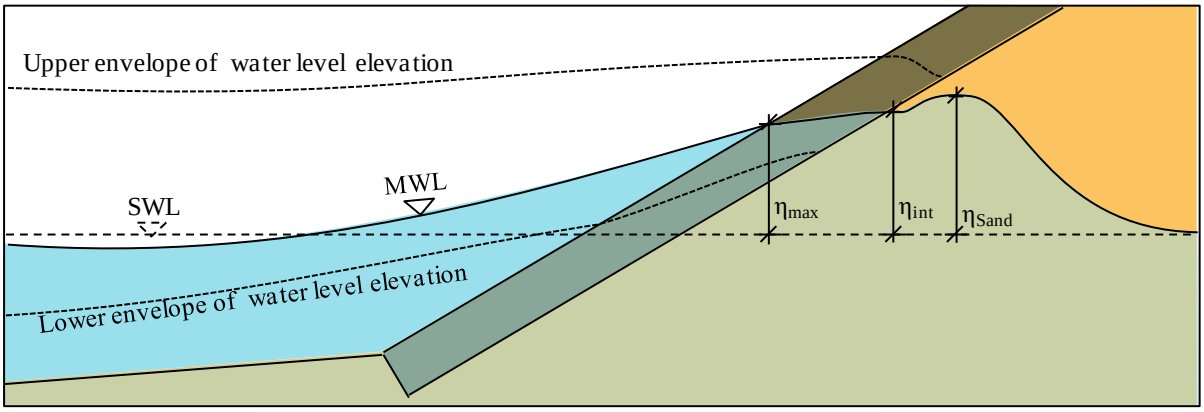

Fig. 6.1 Definition of internal wave set-up at the interface between revetment and foundation and set-up in the sand foundation

The relative internal wave set-up η_{int} is plotted together with the numerical results of the wave set-up obtained from the wave run-up gauge on the surface of the revetment η_{max} (see also Fig. 2.3) in Fig. 6.2. For the wave set-up, only the revetment configurations with d_{rev} = 0.25 and 0.5 m were considered, because for the configuration with d_{rev} = 0 m the internal set-up does not exist due to the absence of the revetment. The relative external and internal wave set-ups are very similar. A few deviations are found only for very small surf similarity parameter ξ_m < 2. This result is expected, because no significant changes of the MWL through the revetment can be induced due to the high porosity and relatively small thickness of the layer.

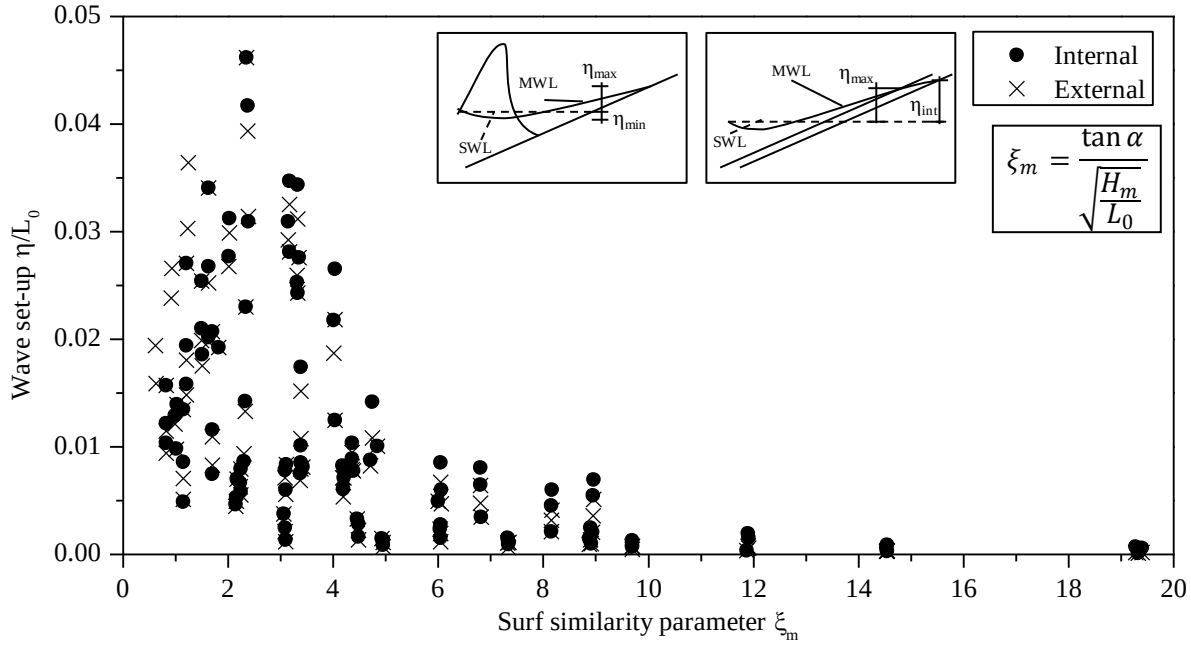

Fig. 6.2 Relative wave set-up in the revetment and on the revetment vs. surf similarity parameter

Because of the strong effect of the slope steepness on the wave set-up on the revetment, it has to be expected, that it is similar for the wave set-up in the revetment. This assumption is supported by Fig. 6.3 where the relative internal wave set-up η_{int}/L_0 is plotted versus the surf similarity parameter ξ_m for d_{rev} = 0.25 & 0.5 m. As for the wave set-down (Fig. 4.10) and the wave set-up on the slope surface (Fig. 4.14), a distinct grouping of the data sets can be observed.

The effect of the revetment thickness d_{rev} on η_{int} was also analysed. A relation between the results from tests with d_{rev} = 0.25 m and those with d_{rev} = 0.5 m was considered. Because these two values were not measured in one test simultaneously (only one d_{rev} is present during the complete test duration), tests with similar input parameters (H, T and cotα) are considered (cf. also Tab. A.6). A constant factor between the two data sets was found. In this case, the wave set-up in a revetment with d_{rev} = 0.5 m is only 78% of that in a revetment with d_{rev} = 0.25 m (eq. (6.1) and Fig. 6.3). This finding indicates a strong relation between the revetment thickness and the resulting internal wave set-up as expected. A more detailed prediction approach is still needed, but additional tests with more revetment thicknesses are needed for such a task.

$$\eta_{int,(d_{rev}=0.5m)} = 0.78 \cdot \eta_{int,(d_{rev}=0.25m)} \tag{6.1}$$

Based on eq. (6.1) and Fig. 6.3, a regression analysis (RA) with an exponential approach was also applied for the internal wave set-up in the same way as for the wave set-up and wave set-

down in Section 4.2. The results were, again, not very good and they are, therefore, not presented in detail (for more information see Foyer & Oumeraci, 2013).

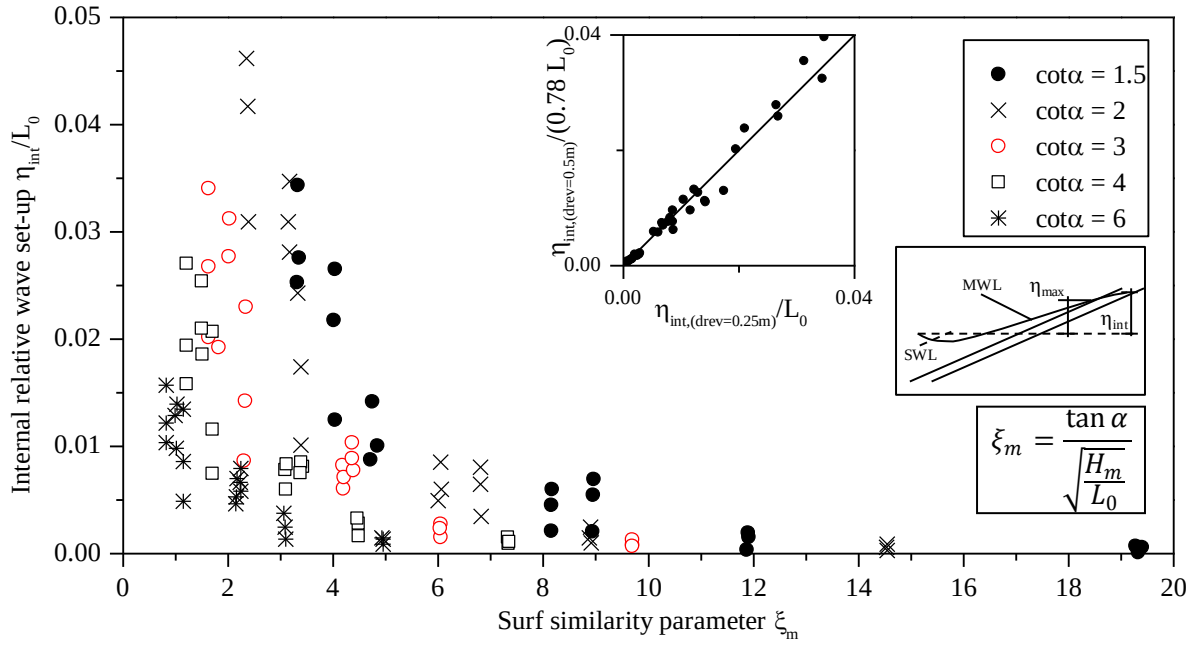

Fig. 6.3 Internal relative wave set-up for all slope steepnesses

In addition to the RA, a multiple regression analysis (MRA) was performed using the following parameters as input:

- Relative internal wave set-up η_{int}/L_0
- Relative wave set-up η_{max}/L_0
- Relative revetment thickness d_{rev}/H_m
- Surf similarity parameter ξ_m

The best result is shown in eq. (6.2). Furthermore, the result is also shown in Fig. 6.4. The agreement between the simulated and calculated values is relatively good which is also underlined by the coefficient of variation σ' = 10.9%.

$$\eta_{int} = \eta_{max} \cdot \frac{d_{rev}/H_m}{d_{rev}/H_m - 0.0102 \cdot \xi_m} \tag{6.2}$$

Eq. (6.2) results in $\eta_{int} = \eta_{max}$ for $\xi_m = 0$ which complies with the boundary conditions in Tab. 2.5. For $\xi_m \rightarrow \infty$ a value of $\eta_{int} = 0$ is obtained, this finding also agrees with the assumption made in Tab. 2.5. Furthermore, for the processes in the revetment it is always interesting, how the prediction equation deals with the case of $d_{rev} = 0$ m. In this case, for $d_{rev} = 0$ m an internal wave set-up of $\eta_{int} = 0$ m is obtained which is satisfactory because no internal set-up exists for this impermeable surface layout. Finally, based on eq. (6.2) it can be stated that the internal wave set-up η_{int} is generally larger than the wave set-up on the revetment surface η_{max}. This is most likely caused by internal breaking in the revetment causing the MWL to rise further.

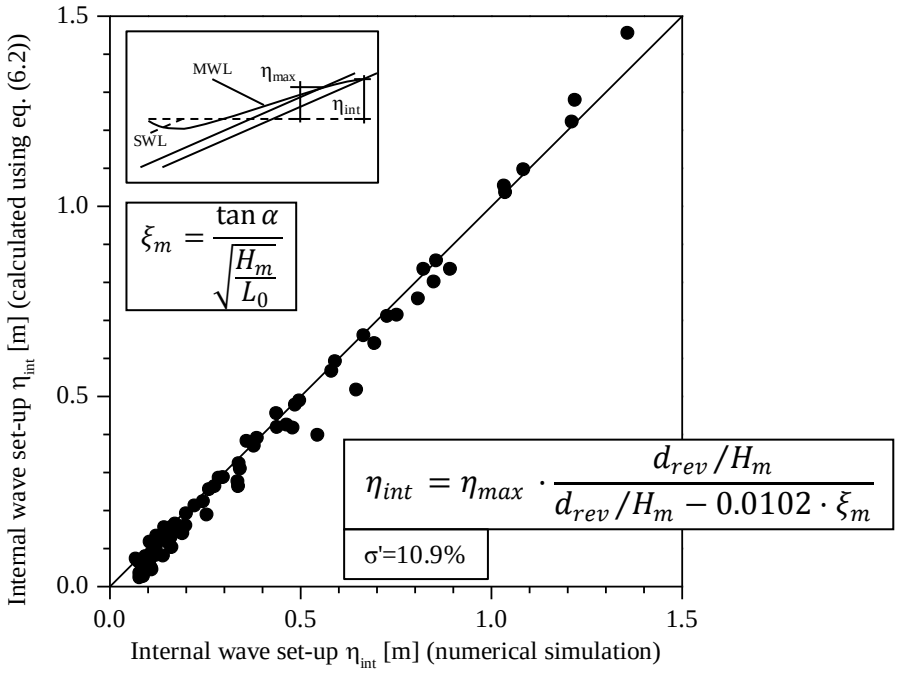

Fig. 6.4 Predicted internal wave set-up η_{int} using eq. (6.2) versus η_{int} from the numerical simulations

The internal wave set-up η_{int} is found to be in the same range and equally dependent on the slope steepness as the wave set-up η_{max} on the slope surface. The internal wave set-up η_{int} is mostly larger than the wave set-up η_{max} which is caused by internal breaking in the revetment. Based on a multiple regression analysis a prediction formula for the internal wave set-up η_{int} (eq. 6.2) with a coefficient of variation in the range of 10% is obtained, showing a dependency of η_{int} on the wave set-up η_{max} as well as on the relative revetment thickness d_{rev}/H_m and the surf similarity parameter ξ_m

6.2 Internal wave run-up & run-down

In the GWK-tests, it was not possible to determine the swash zone within the revetment. For this purpose, numerical simulations were used. As a result, the internal wave run-up and run-down heights are obtained by using the internal wave run-up gauge that was also used for the determination of the internal wave set-up (Section 6.1). In the same way as for the wave run-up and run-down heights on the slope surface (see Section 5.1), only values in relation to the MWL are considered for the analyses. A definition sketch is given together with the wave run-up and run-down height on the revetment surface in Fig. 5.1.

First of all, the internal and external wave run-up and run-down heights are plotted in Fig. 6.5 versus the surf similarity parameter ξ_m for revetment configuration d_{rev} = 0.25 m, showing the damping effect induced by the porous revetment on both wave run-up and run-down. The damping is slightly larger for the wave run-up. The relation to the surf similarity parameter ξ_m is similar for all four depicted data sets with an increase of the absolute values of the relative wave run-down and run-up heights. The increase rate becomes smaller with higher values of

the surf similarity parameter resulting in constant values of the wave run-up and run-down heights for $\xi_m = 19$. Due to the boundary conditions defined in Tab. 2.5, especially the absolute values of the wave run-up and run-down heights on the revetment surface must decrease after the highest measured surf similarity parameter of $\xi_m \approx 19$ in this study.

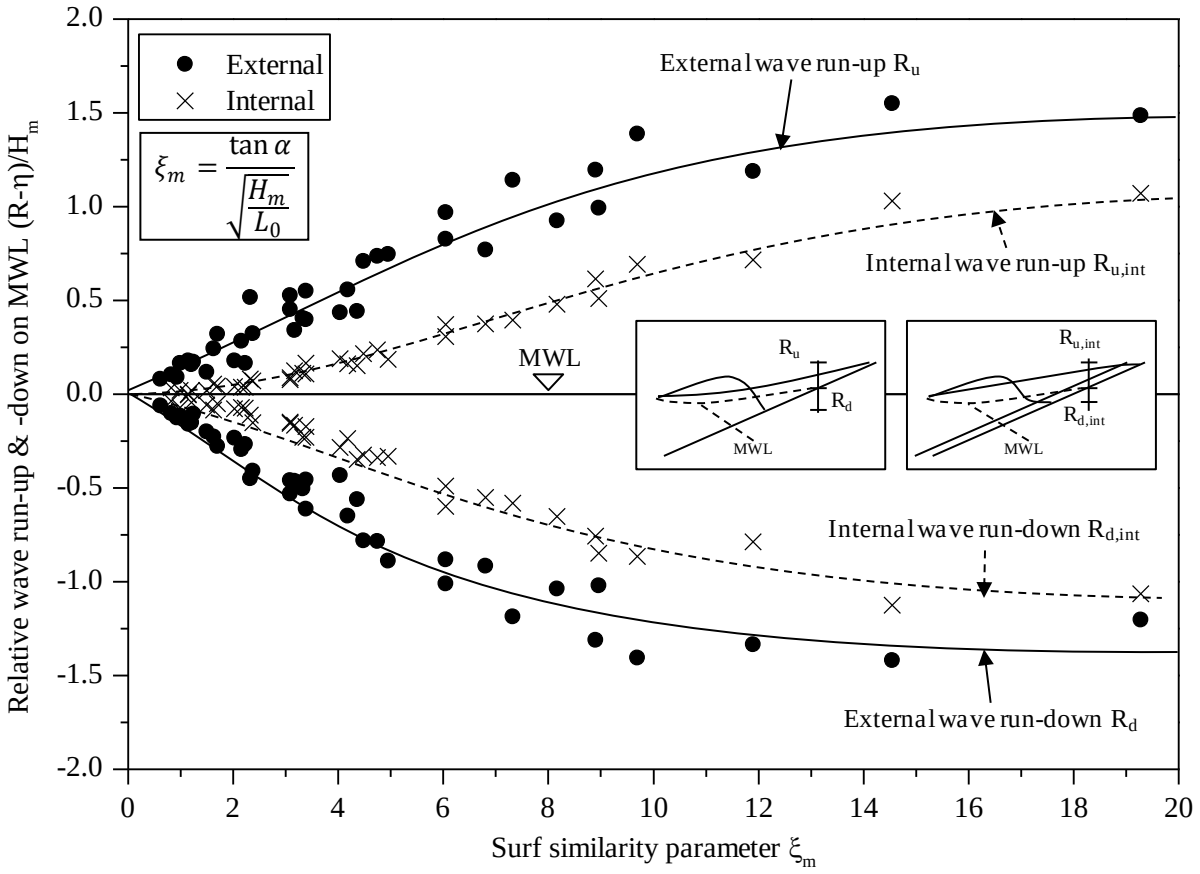

Fig. 6.5 Relative internal and external wave run-up and wave run-down heights vs. surf similarity parameter ξ_m for $d_{rev} = 0.25$ m

In Fig. 6.5, the absolute values of the wave run-up and wave run-down heights are very similar for the internal and external swash. But before starting the analysis of the internal wave run-up and run-down heights, it has to be determined whether a combined analysis as for the wave run-up and run-down on the slope surface (see Section 5.1) is possible. For this purpose, the internal wave run-up and run-down heights (related to MWL) are directly compared in Fig. 6.6, showing that the internal wave run-down height is larger than the internal wave run-up height. Because of this large deviation between the two parameters, the analysis of the internal wave run-up and run-down heights is performed with separated data sets but for a better comparability, most of the results will be presented together in the following. The much larger internal wave run-down height than internal wave run-up height also indicates a larger effect of the porous revetment on the internal swash than on the wave run-up and run-down heights on the revetment surface (Fig. 5.2).

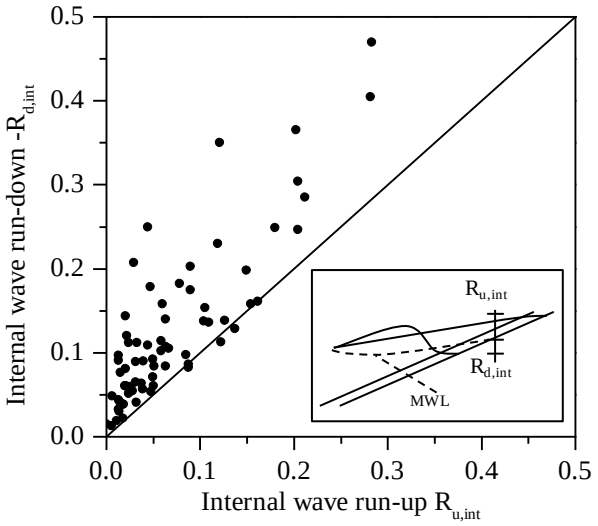

Fig. 6.6 Internal wave run-up and run-down heights

Because the slope steepness did not affect the wave run-up and run-down heights on the slope surface more than is accounted for in the surf similarity parameter, it is assumed that this is also valid for the internal swash. Therefore, the analysis is started with the investigation of the effect of the revetment thickness. In Fig. 6.7 the relative internal wave run-up and run-down heights are plotted according to the revetment thickness in the test (either d_{rev} = 0.25 m or 0.5 m). The differences between the two data sets are surprisingly small. For the internal wave run-up height, almost no additional damping for the revetment with d_{rev} = 0.5 m as compared to that with d_{rev} = 0.25 m is found. For the internal wave run-down height, the damping is slightly more distinct but still rather small.

A similar RA as for the wave run-up and run-down height on the slope surface was used (see eq. (5.1)). This approach resulted in eqs. (6.3) and (6.4). The corresponding graphs are plotted in Fig. 6.7. The four depicted curves in Fig. 6.7 describe the trend of the data sets satisfactorily for surf similarity parameter $\xi_m < 10$. For larger surf similarity parameter, the agreement is, however, less pronounced. Especially for the internal wave run-up height, both curves (for d_{rev} = 0.25 m and 0.5 m) do not fully reach the maximum of the data points at $\xi_m \approx 19.5$. Due to the slightly different trends of the data sets of the internal wave run-up height and the internal wave run-down height, the obtained empirical parameters differ greatly. Furthermore, it can be seen that especially for surf similarity parameter $\xi_m < 4$ the obtained curves do not fully catch the trend of the internal wave run-down height data points.

$$\frac{R_{u,int}}{H_m} = \frac{{\xi_m}^2 + a \cdot \xi_m}{{\xi_m}^2 + b} \quad \begin{matrix} for\ d_{rev} = 0.25m\text{:}\ \ a = -0.17; b = 62 \\ for\ d_{rev} = 0.5m\text{:}\quad a = -0.36; b = 81 \end{matrix} \tag{6.3}$$

$$\frac{R_{d,int}}{H_m} = -\frac{\xi_m^2 + a \cdot \xi_m}{\xi_m^2 + b} \quad \begin{matrix} for\ d_{rev} = 0.25m\text{:}\ \ a = 12; b = 190 \\ for\ d_{rev} = 0.5m\text{:}\quad a = 0.38; b = 71 \end{matrix} \tag{6.4}$$

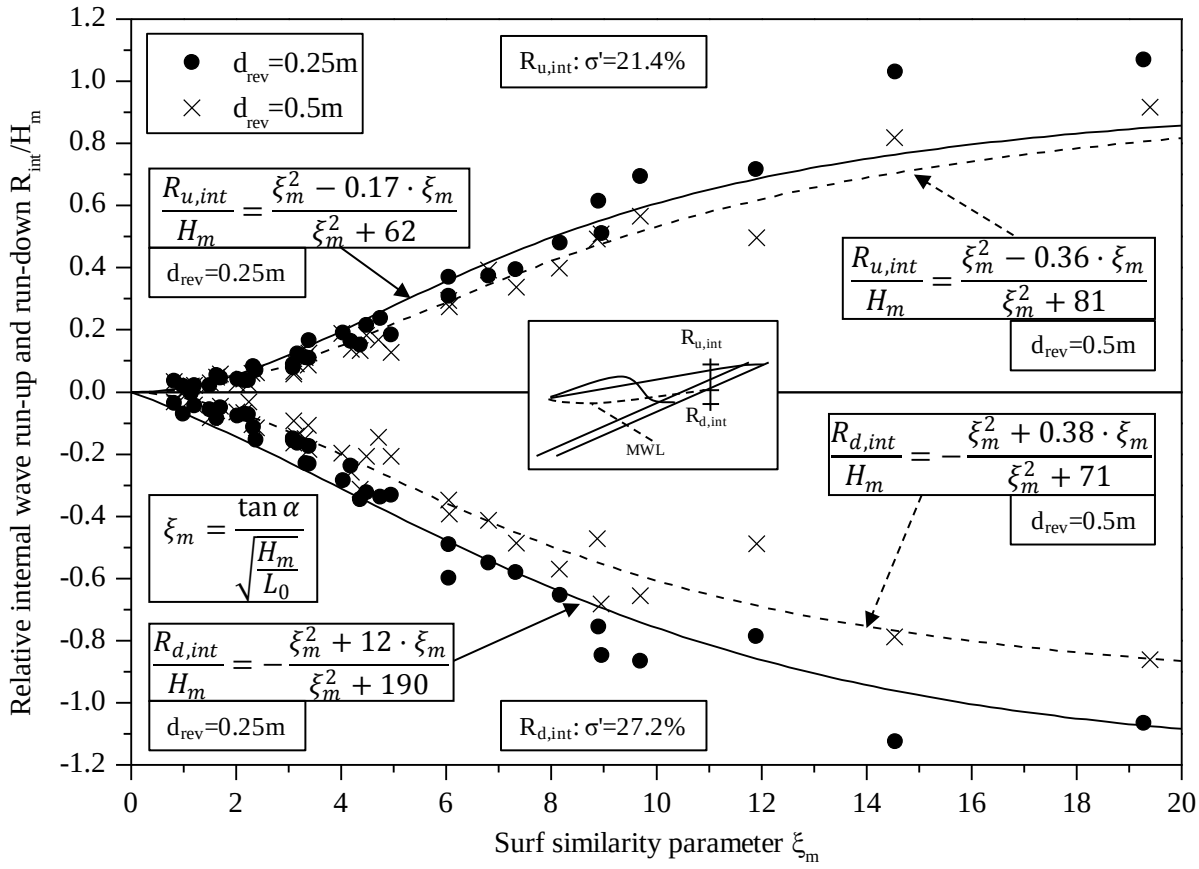

Fig. 6.7 Relative internal wave run-up and run-down heights related to MWL vs. surf similarity parameter

As a second step of the development of a prediction equation for the internal wave run-up height $R_{u,int}$, a MRA was performed. The following input parameters were used:

- Relative internal wave run-up height $R_{u,int}/H_m$
- Relative wave run-up height on the slope surface R_u/H_m
- Relative revetment thickness d_{rev}/H_m
- Surf similarity parameter ξ_m.

The result (eq. (6.5)) is shown in Fig. 6.8 together with eq. (6.3) and the better fit is obtained by eq. (6.5). Equation (6.5) fulfils all boundary conditions as defined in Tab. 2.5: (i) for $\xi_m \rightarrow 0 \hookrightarrow R_{u,int}/H_m \rightarrow 0$; (ii) for $\xi_m \rightarrow \infty \hookrightarrow R_{u,int}/H_m \rightarrow R_u/H_m$ and (iii) for $d_{rev}/H_m = 0 \hookrightarrow R_{u,int}/H_m = R_u/H_m$. The good fit of the data for $d_{rev} = 0$ m is caused by the inclusion of the respective data set for the RA. Furthermore, as compared to eq. (6.3), in eq. (6.5) only one empirical parameter needs to be determined.

$$\frac{R_{u,int}}{H_m} = \frac{R_u}{H_m} \cdot \frac{\xi_m^2}{66.1 \cdot \frac{d_{rev}}{H_m} + \xi_m^2} \tag{6.5}$$

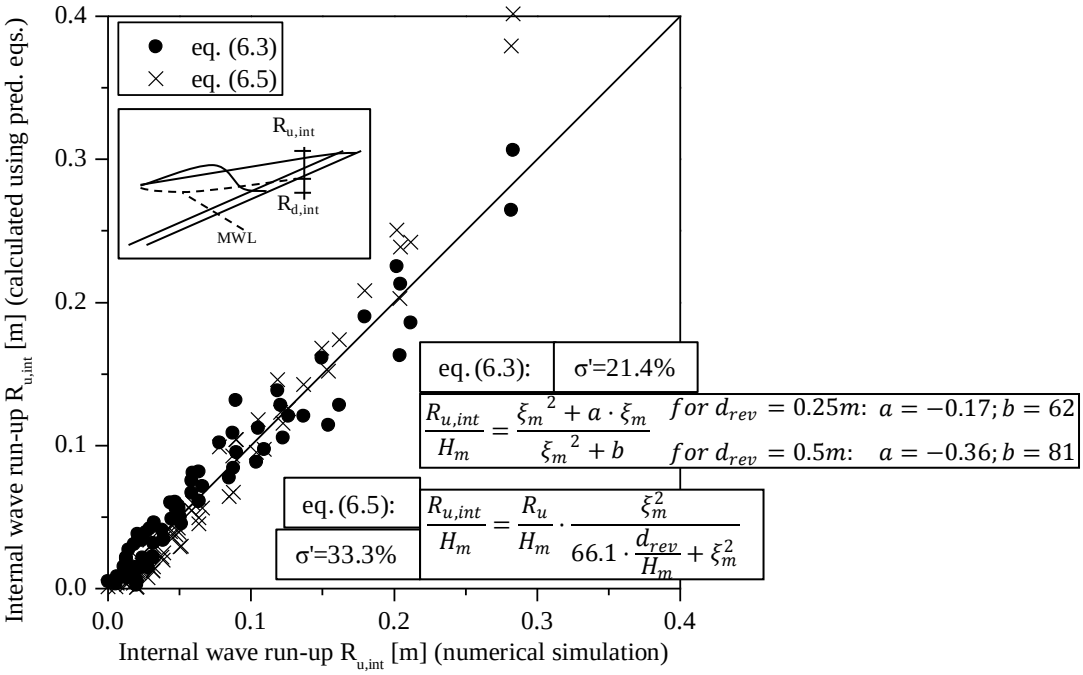

Fig. 6.8 Predicted internal wave run-up height $R_{u,int}$ using eqs. (6.3) & (6.5) versus $R_{u,int}$ from the numerical simulations

With a coefficient of variation of σ' = 33.3%, eq. (6.5) is statistically worse than eq. (6.3). These statistics of eq. (6.5) are due to the underestimation of the internal wave run-up height for small values and the overestimation for larger values as shown in Fig. 6.8. Furthermore, the results of the data set with d_{rev} = 0 m were not included into the statistics. The other prediction equation (eq. (6.3)) shows the opposite behaviour with an overestimation for small wave run-up heights and a slight underestimation for large wave run-up heights. Generally, the approach described in eq. (6.3) should be favoured, because it gives the best results.

As a second step of the development of a prediction equation for the internal wave run-down height $R_{d,int}$, a MRA was also performed. Similarly to the wave run-up height $R_{u,int}$ above, the following input parameters were considered:

- Relative internal wave run-down height $R_{d,int}/H_m$
- Relative wave run-down height on the slope surface R_d/H_m
- Relative revetment thickness d_{rev}/H_m
- Surf similarity parameter ξ_m

The resulting equation (6.6) is somehow similar to that obtained for the internal wave run-up height $R_{u,int}$ (eq. (6.5)) but much more complex. Like eq. (6.5), it also includes only one empirical parameter. A comparison of equations (6.5) and (6.6) shows that the coefficient of variation is smaller for the internal wave run-down height $R_{d,int}$ (σ' = 23.1%) than for the internal wave run-up height $R_{u,int}$ (σ' = 33.3%). This tendency is also underlined by the direct comparison of the simulated and calculated wave run-down heights $R_{d,int}$ in Fig. 6.9 where eq. (6.6) shows the better fit for the numerical data compared to eq. (6.4). However, the scatter for small absolute internal wave run-down values is quite high for both approaches

and, therefore, it is suggested to use eq. (6.4). This way all wave run-up and run-down heights, in and on the revetment, can be described using the same basic approach.

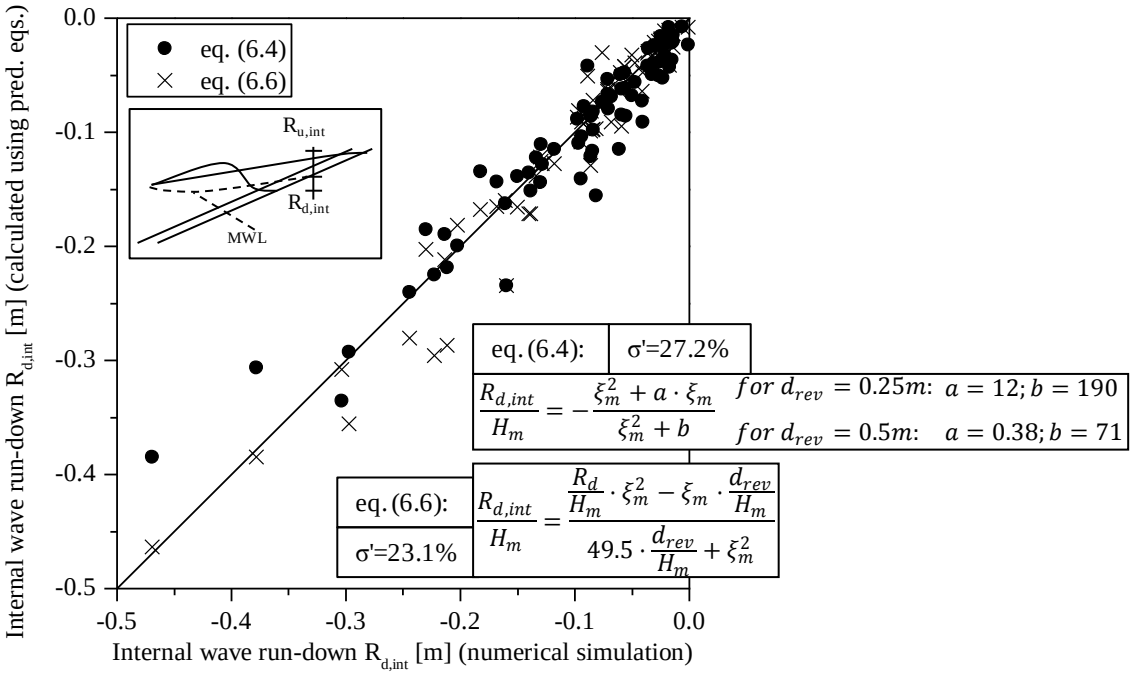

Fig. 6.9 Predicted internal wave run-down height $R_{d,int}$ using eqs. (6.4) & (6.6) versus $R_{d,int}$ from the numerical simulations

$$\frac{R_{d,int}}{H_m} = \frac{\frac{R_d}{H_m} \cdot \xi_m^2 - \xi_m \cdot \frac{d_{rev}}{H_m}}{49.5 \cdot \frac{d_{rev}}{H_m} + \xi_m^2} \tag{6.6}$$

Several approaches to develop prediction formulae for the internal wave run-up height $R_{u,int}$ and wave run-down height $R_{d,int}$ were proposed and comparatively analysed in this section. A high dependency of $R_{u,int}$ and $R_{d,int}$ on the wave run-up and run-down heights can be observed which, however, cannot be described by a simple linear relationship by applying a single damping factor, because the processes associated with the damping are non-linear and highly complex. Furthermore, the effect of the porous revetment thickness is larger for the internal wave run-down than for the internal wave run-up.

6.3 Internal velocities

As for the velocities on the slope surface, two different types of velocities were measured on the bottom of the revetment: the internal wave run-up and run-down velocities and the associated local flow velocities (see also Fig. 5.7). Both will be analysed in the following. Similarly to the other processes in the revetment, the analyses of the velocities in the revetment are also based on the respective processes on the revetment (see Sections 5.2 and 5.3). Therefore, a comparison with the respective velocities on the revetment is made at the

beginning of each analysis. For the regression analyses, the vertical components of the velocities are used while for the first overview the velocities parallel to the revetment surface are used (definition in Fig. 5.8).

6.3.1 Internal wave run-up and run-down velocities

The internal wave run-up and run-down velocities are obtained in the same way as the wave run-up and run-down velocities on the slope surface (Section 5.2). A high scatter is expected in all results, caused by the relatively coarse resolution of the numerical simulations which led to issues with the temporal development of the internal wave run-up. These disturbances are mostly caused by the relatively small changes in the internal swash of only few centimetres, which cannot fully be captured by the coarse grid used in COBRAS-UC (see Section 3.2.2).

A comparison between the results of the relative wave run-up and run-down velocities on and beneath the revetment is shown in Fig. 6.10 for the revetment configuration with d_{rev} = 0.25 m. The internal velocities are much smaller than the velocities on the revetment especially for the wave run-up. Comparatively, the internal wave run-down velocities are less dampened.

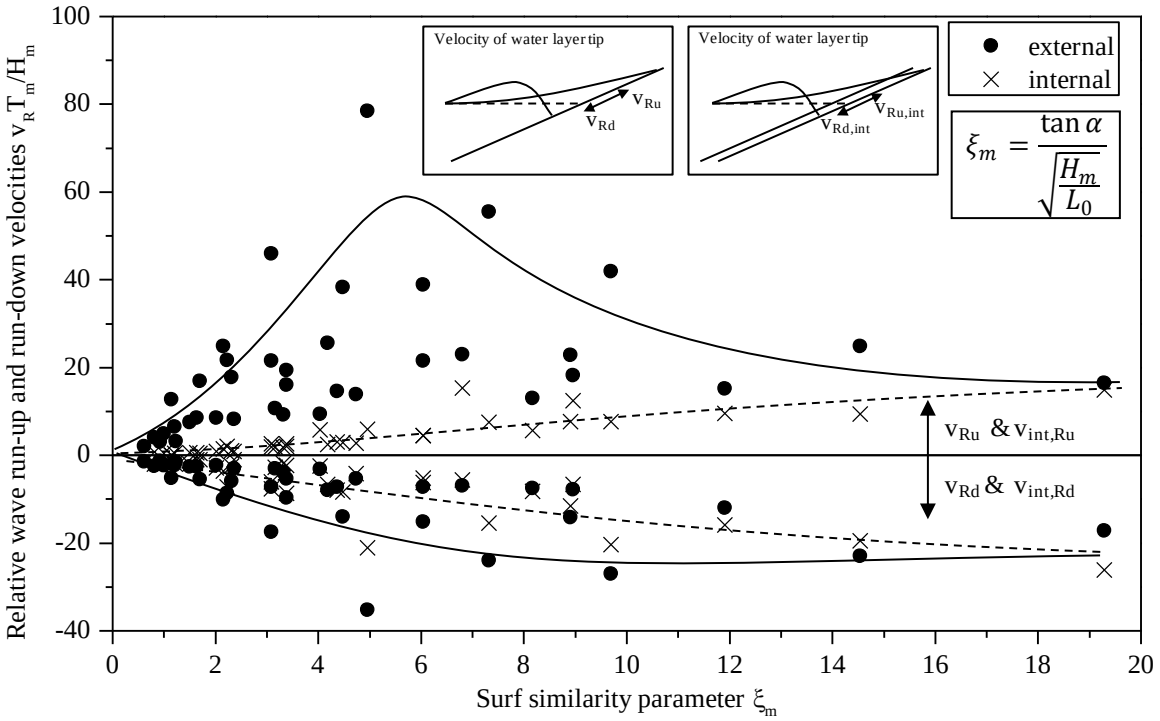

Fig. 6.10 Internal and external wave run-up and run-down velocities for d_{rev} = 0.25 m

Before starting a detailed analysis of the internal wave run-up and run-down velocities, it has to be decided whether a combined analysis of both is feasible. In Fig. 6.11 the vertical component ($v_v = v/\sqrt{(\cot^2\alpha+1)}$) of the internal wave run-up velocities are plotted against the vertical component of the internal wave run-down velocities. For small velocities, the

difference is very small but it increases dramatically with increasing values of the velocities. For large velocities, the internal wave run-up velocity becomes much larger than the internal wave run-down velocity. These results show that the analysis of the internal wave run-up and run-down velocities have to be performed separately. However, for a good comparison the parameters will be plotted together.

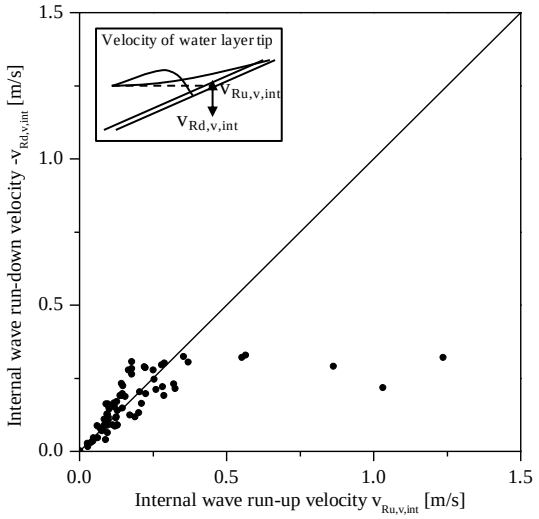

Fig. 6.11 Comparison of vertical components of internal wave run-up and run-down velocities

In Fig. 6.12 the vertical component of the relative internal wave run-up and run-down velocities is plotted versus the surf similarity parameter ξ_m for the revetment thicknesses d_{rev} = 0.25 m & 0.5 m. In contrast to the velocities on the revetment (Fig. 5.12), these absolute values of the velocities do not reach an upper limit for the range of surf similarity parameter considered in the numerical simulations. Moreover, the scatter in the data sets is quite large.

Even though the layouts of the data sets for the internal wave run-up and run-down velocities differ substantially from the corresponding velocities on the slope surface the same approach as in Chapter 5 is used for a RA (cf. eq. (5.1)). The results are shown in Fig. 6.12 and eqs. (6.7) & (6.8) for d_{rev} = 0.25 & 0.5 m. The trends of the depicted data sets are almost linear. These trends lead to very high values for the parameters a and b of eq. (5.1), especially for the internal wave run-down velocity. Even though parameters a and b are very high for the relative internal wave run-down velocity, the statistical results are still slightly better than for the relative internal wave run-up velocity. However, the overall statistical results are not satisfying. Therefore, a better approach has to be developed.

$$\frac{v_{Ru,int}}{\sqrt{\cot^2\alpha+1}}\cdot\frac{T_m}{2\cdot\pi\cdot H_m}=\frac{\xi_m^2+a\cdot\xi_m}{\xi_m^2+b}\qquad \begin{array}{l} for\ d_{rev}=0.25m:\ a=110;\ b=750 \\ for\ d_{rev}=0.5m:\quad a=2\cdot10^{16};b=2\cdot10^{17}\end{array} \tag{6.7}$$

$$\frac{v_{Rd,int}}{\sqrt{\cot^2\alpha+1}}\cdot\frac{T_m}{2\pi H_m}=-\frac{\xi_m^2+a\cdot\xi_m}{\xi_m^2+b}\qquad \begin{array}{l} for\ d_{rev}=0.25m:a=2.2\cdot10^{15};\ b=1.8\cdot10^{16} \\ for\ d_{rev}=0.5m:\ a=9.8\cdot10^{6};\ b=1.1\cdot10^{8}\end{array} \tag{6.8}$$

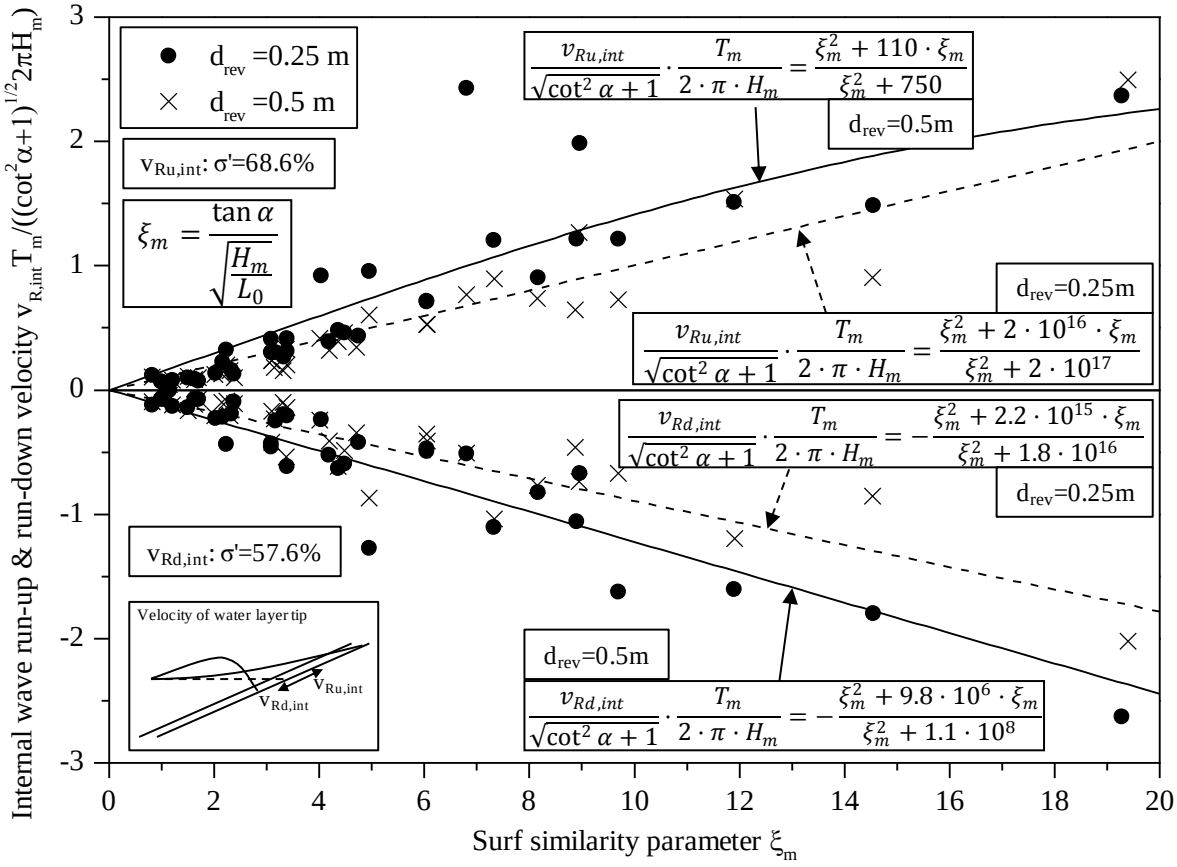

Fig. 6.12 Vertical component of the relative internal wave run-up and run-down velocities and results from the RA

In addition to the RA, MRAs were performed for the internal wave run-up and run-down velocities. For the two analyses the following parameters were used:

- Relative vertical component of the internal wave run-up and run-down velocity $v_{R,int}T_m/(2\pi H_m\sqrt{(\cot^2\alpha+1)})$ as defined in Fig. 5.7 and Fig. 5.8
- Relative vertical component of the wave run-up and run-down velocity on the slope surface $v_R T_m/(2\pi H_m\sqrt{(\cot^2\alpha+1)})$ as defined in Fig. 5.7 and Fig. 5.8
- Surf similarity parameter ξ_m
- Relative revetment thickness d_{rev}/H_m

The results are presented in eq. (6.9) (internal wave run-up velocity) and eq. (6.10) (internal wave run-down velocity).

For the relative internal wave run-up velocity a linear relation to the relative wave run-up velocity on the slope surface is obtained (eq. (6.9)). The linear factor only depends on the surf similarity parameter ξ_m and the relative revetment thickness d_{rev}/H_m. Thus, only one empirical parameter is required and at the same time the equation fulfills the boundary conditions as defined in Tab. 2.5.

$$\frac{v_{Ru,int}}{\sqrt{\cot^2\alpha+1}}\cdot\frac{T_m}{2\cdot\pi\cdot H_m}=\frac{v_{Ru}}{\sqrt{\cot^2\alpha+1}}\cdot\frac{T_m}{2\cdot\pi\cdot H_m}\cdot\frac{\xi_m^2}{28.3\cdot\frac{d_{rev}}{H_m}+\xi_m^2} \tag{6.9}$$

The simulated and calculated values of the internal wave run-up velocity are shown in Fig. 6.13 for the results of eqs. (6.7) and (6.9). The results are similar for both approaches and both are not satisfying. For small values $v_{Ru,int}/\sqrt{(\cot^2\alpha+1)} < 0.4$, both approaches overestimate the internal wave run-up velocity and for larger values $v_{Ru,int}/\sqrt{(\cot^2\alpha+1)} > 0.4$, both approaches result in an underestimation of the values. The statistical result is slightly better for the results of the MRA (σ' = 57.2%) but both results are not satisfying.

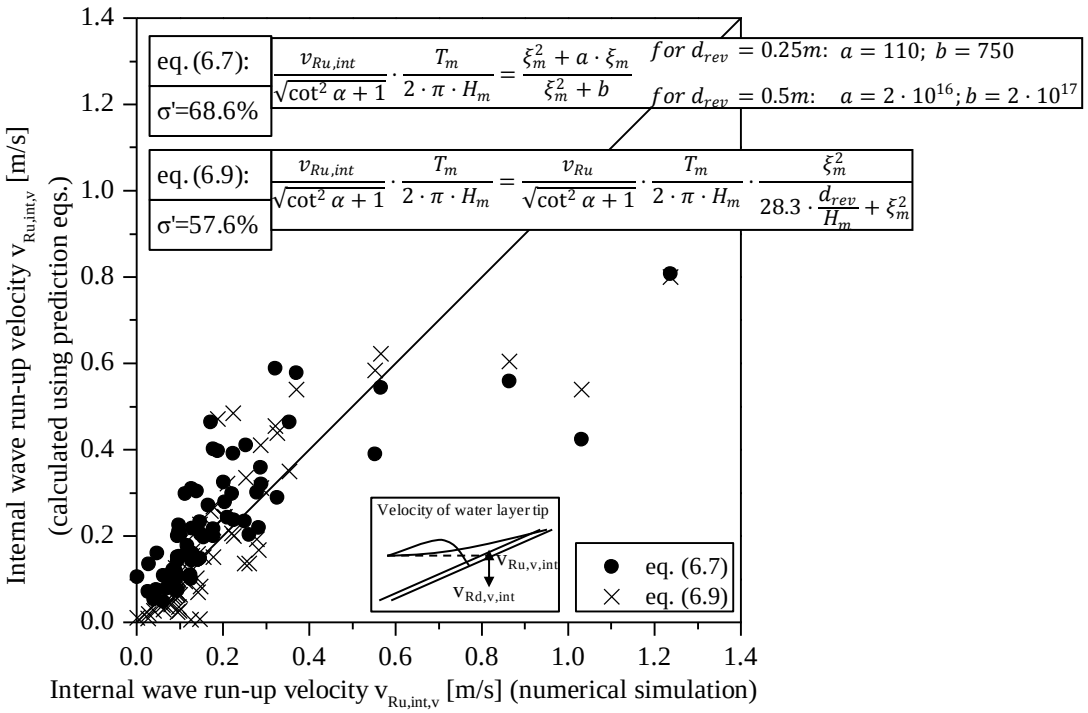

Fig. 6.13 Predicted vertical component of the internal wave run-up velocity $v_{Ru,int,v}$ using eqs. (6.7) & (6.9) versus $v_{Ru,int,v}$ from the numerical simulations

For the MRA of the internal wave run-down velocity, the result is presented in eq. (6.10) which is more complex than eq. (6.9) for the internal wave run-up velocity. However, the surf similarity parameter ξ_m seems to have no effect on the relation between external and internal wave run-down velocities. The higher complexity of eq. (6.10) does not necessarily lead to a better statistical result. Even though the coefficient of variation of σ' = 55.4% for eq. (6.10) is smaller than for eq. (6.9) (see also Fig. 6.13), the difference is not substantial. This is also shown in Fig. 6.14 where the simulated internal wave run-down velocities are compared to the calculated values by applying eqs. (6.8) and (6.10). As for the internal wave run-up velocity, the two approaches for the internal wave run-down velocity give no satisfying output.

$$\frac{v_{Rd,int}}{\sqrt{\cot^2\alpha+1}}\cdot\frac{T_m}{2\cdot\pi\cdot H_m} = \frac{v_{Rd}}{\sqrt{\cot^2\alpha+1}}\cdot\frac{T_m}{2\cdot\pi\cdot H_m} + \frac{d_{rev}/H_m}{216+\frac{140\cdot v_{Rd}}{\sqrt{\cot^2\alpha+1}}\cdot\frac{T_m}{2\cdot\pi\cdot H_m}-3.46\cdot\frac{d_{rev}}{H_m}} \tag{6.10}$$

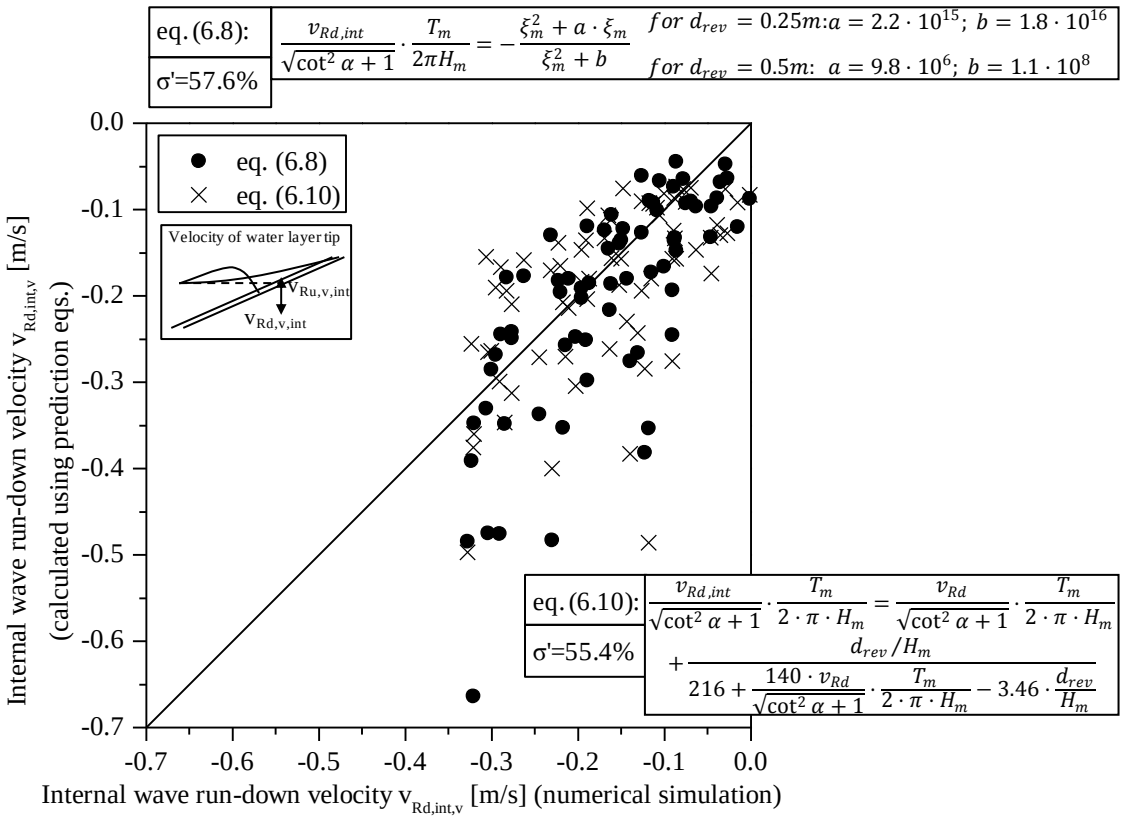

Fig. 6.14 Predicted vertical component of the internal wave run-down velocity $v_{Rd,int,v}$ using eqs. (6.8) & (6.10) versus $v_{Rd,int,v}$ from the numerical simulations

6.3.2 Internal local flow velocities

The internal local flow velocities are obtained from the COBRAS-UC simulations at distinct positions along the bottom of the porous revetment (see Tab. A.5 and Fig. 5.13) similarly to the procedure used to obtain the local flow velocities on the slope surface (see Section 5.3) with the difference that here only tests with $d_{rev} = 0.25$ m and $d_{rev} = 0.5$ m need to be considered. The velocities that are obtained from COBRAS-UC are spatial mean velocities in the porous media and not the actual internal flow velocity within the pores. This is also the case for the internal wave run-up and run-down velocities and, therefore, a good comparison is not endangered.

First of all, a comparison of the internal maximum (upwards directed) and minimum (downwards directed) local flow velocities with the maximum and minimum flow velocities

v_{max} and v_{min} (Fig. 6.15) shows similar results as the same comparison for the wave run-up and run-down velocities (Fig. 6.10). The velocities in the revetment are strongly dampened. Especially the minimum internal flow velocity shows a more pronounced reduction than it was obtained for the internal wave run-down velocity in Section 6.3.1 and Fig. 6.10. This difference might be caused by the slight difference in the direction between the wave run-up and run-down velocity and the flow velocities: the wave run-up and run-down velocities are always directed parallel to the slope surface while the local flow velocities are the maximum and minimum velocities in one cell of the numerical simulations disregarding the precise direction (described in Section 5.3). The latter one is assumed to be directed parallel to the slope surface, but it seems that for the internal down-rush the water leaves the revetment through the surface of the revetment rather than rushing down within it which changes the direction of the velocity.

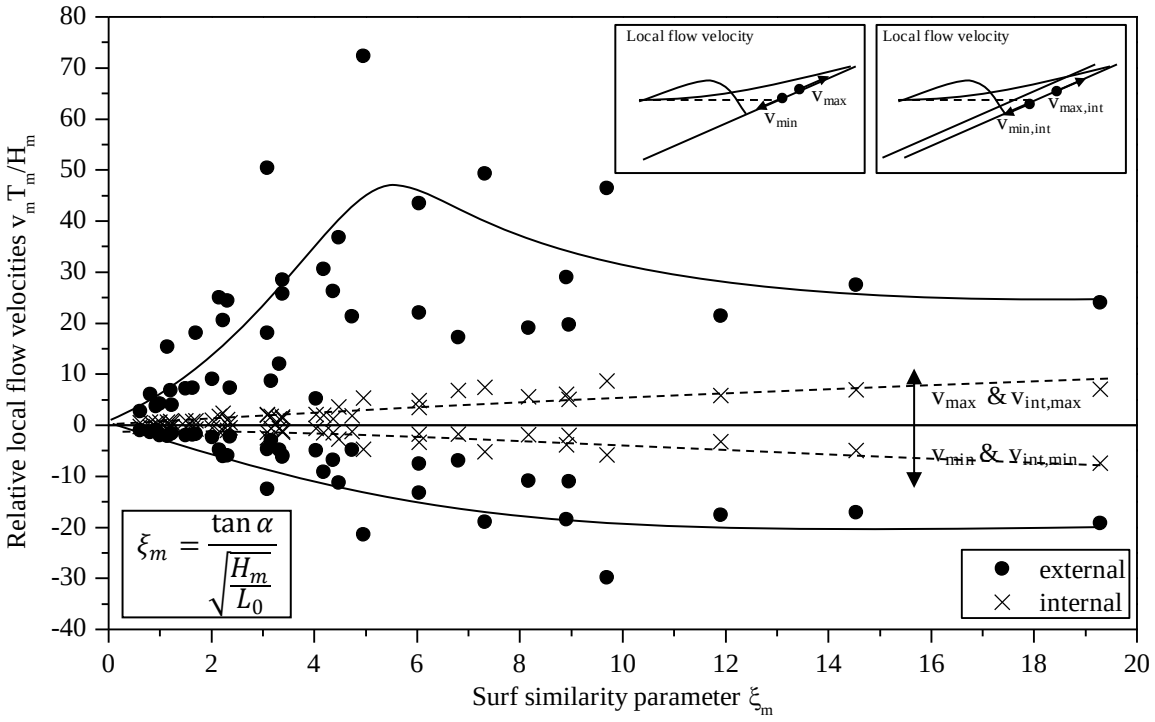

Fig. 6.15 Internal and external minimum and maximum local flow velocities for d_{rev} = 0.25 m

Furthermore, a comparison of the maximum and minimum internal flow velocity is presented in Fig. 6.16. It can be seen that the internal local maximum velocity is larger than the internal local minimum velocity (absolute values) except for some tests where the values are quite similar. Therefore, the development of prediction equations for the internal flow velocities has to be performed separately.

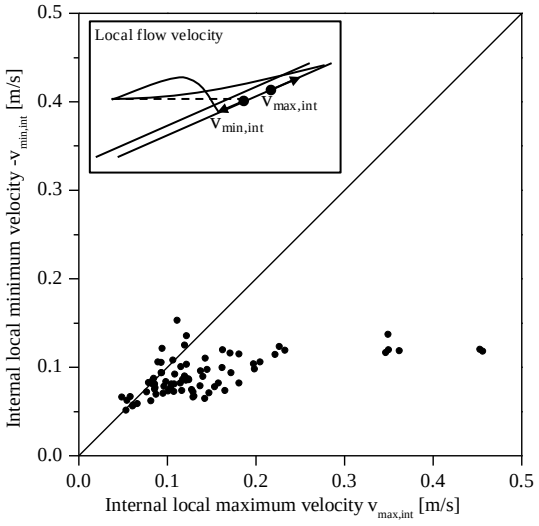

Fig. 6.16 Internal maximum and minimum local flow velocities

As for the previously shown parameters in Chapters 5 & 6, the vertical component of the internal flow velocities (see Fig. 5.8) are plotted together in Fig. 6.17 showing the maximum and minimum internal flow velocity for the revetment thicknesses d_{rev} = 0.25 m and 0.5 m. A similar relation between the four data sets as for the internal wave run-up and run-down velocities (Fig. 6.12) is found. For all four data sets, the absolute values of the relative flow velocities increase continuously over the entire range of surf similarity parameters ξ_m considered in the numerical simulations. However, the absolute values for the internal flow velocities are smaller than for the wave run-up and run-down with absolute values of the relative vertical velocity component of up to $|v_{m,v}T_m/(2\pi H_m)| = 0.9$ while values of up to $|v_{R,v}T_m/(2\pi H_m)| = 2.8$ were reached for the internal run-up and run down velocities. This indicates that the internal wave run-up and run-down is mainly affected by the in- and outflow of water in and from the revetment and not so much by water running up and down in the revetment, thus leading to smaller internal flow velocities than internal wave run-up and run-down velocities. Moreover, the velocities measured in the thinner revetment are, as expected, slightly larger than for the thicker revetment especially for surf similarity parameter $\xi_m > 4$.

The first RA presented below for the internal local flow velocities is based on the analysis of the velocities on the slope surface (see Section 5.3). The results are shown in Fig. 6.17 and in eqs. (6.11) and (6.12) separately for the two cases d_{rev} = 0.25 m and 0.5 m and for the maximum (upwards directed) and minimum (downwards directed) value. The trends of the data sets are represented quite well by the graphs of eqs. (6.11) and (6.12) except for some outliers around $\xi_m = 15 – 20$.

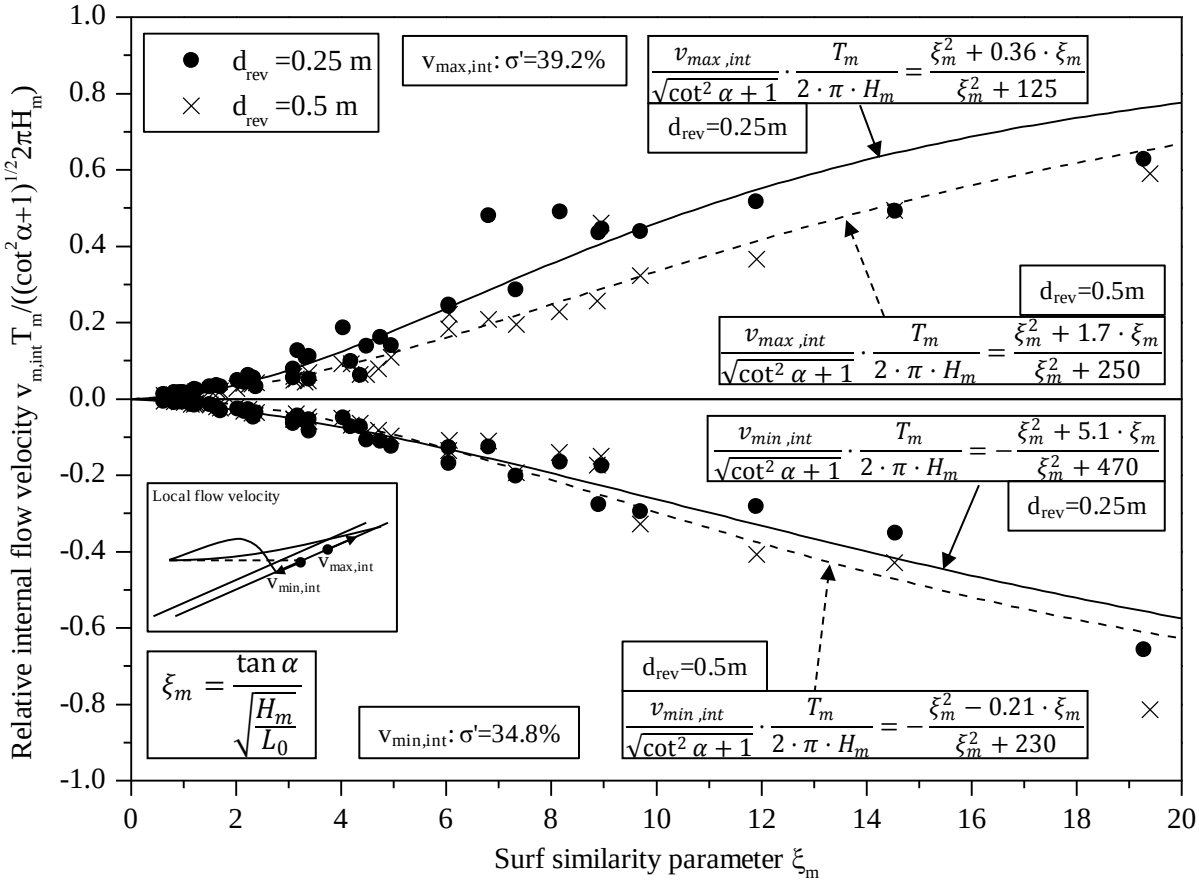

Fig. 6.17 Vertical component of the relative internal maximum and minimum flow velocity and results from the RA

The empirical parameters in the two equations are more practical and the statistical results are also better than those obtained for the internal wave run-up and run-down velocities (see Section 6.3.1). For the revetment with d_{rev} = 0.5 m, however, a negative a-value was obtained for the minimum internal flow velocity.

$$\frac{v_{max,int}}{\sqrt{\cot^2\alpha+1}}\cdot\frac{T_m}{2\cdot\pi\cdot H_m}=\frac{\xi_m^2+a\cdot\xi_m}{\xi_m^2+b}\quad \begin{matrix} for\ d_{rev}=0.25m:\ a=0.36;\ b=125 \\ for\ d_{rev}=0.5m:\quad a=1.70;\ b=250 \end{matrix} \tag{6.11}$$

$$\frac{v_{min,int}}{\sqrt{\cot^2\alpha+1}}\cdot\frac{T_m}{2\pi H_m}=-\frac{\xi_m^2+a\cdot\xi_m}{\xi_m^2+b}\quad \begin{matrix} for\ d_{rev}=0.25m:\ a=5.1;\quad b=470 \\ for\ d_{rev}=0.5m:\quad a=-0.21;\ b=230 \end{matrix} \tag{6.12}$$

MRAs were also performed for the internal maximum and minimum flow velocities in the same way as for the internal wave run-up and run-down velocity. The following input parameters were considered:

- Relative vertical component of the internal local maximum and minimum flow velocity $v_{m,int}T_m/(2\pi H_m\sqrt{(\cot^2\alpha+1)})$

- Relative vertical component of the local maximum and minimum flow velocities on the slope surface $v_m T_m/(2\pi H_m \sqrt{(\cot^2\alpha+1)})$
- Surf similarity parameter ξ_m
- Relative revetment thickness d_{rev}/H_m

The results for the internal maximum (eq. (6.13)) and minimum (eq. (6.14)) flow velocities are similar to those of the internal wave run-up velocity (eq. (6.9)) showing a linear relationship between the internal ($v_{Ru,int}$) and external (v_{Ru}) values. Furthermore, they only depend on one empirical parameter.

$$\frac{v_{max,int}}{\sqrt{\cot^2\alpha+1}} \cdot \frac{T_m}{2\cdot\pi\cdot H_m} = \frac{v_{max}}{\sqrt{\cot^2\alpha+1}} \cdot \frac{T_m}{2\cdot\pi\cdot H_m} \cdot \frac{\xi_m}{33.2\cdot\frac{d_{rev}}{H_m}+\xi_m} \tag{6.13}$$

$$\frac{v_{min,int}}{\sqrt{\cot^2\alpha+1}} \cdot \frac{T_m}{2\cdot\pi\cdot H_m} = \frac{v_{min}}{\sqrt{\cot^2\alpha+1}} \cdot \frac{T_m}{2\cdot\pi\cdot H_m} \cdot \frac{\xi_m}{21.9\cdot\frac{d_{rev}}{H_m}+\xi_m} \tag{6.14}$$

The results of the MRA are, however, for both cases, $v_{max,int}$ and $v_{min,int}$, worse than the results of the first RA (cf. Fig. 6.18 and Fig. 6.19). Eq. (6.13) overestimates the flow velocity $v_{max,int}$ for many cases (Fig. 6.18). Therefore, the statistical results are less good for eq. (6.13) than for eq. (6.11). The coefficient of variation is almost double as high as for the first approach: σ' = 68.8% for eq. (6.13) compared to σ' = 39.2% for eq. (6.11).

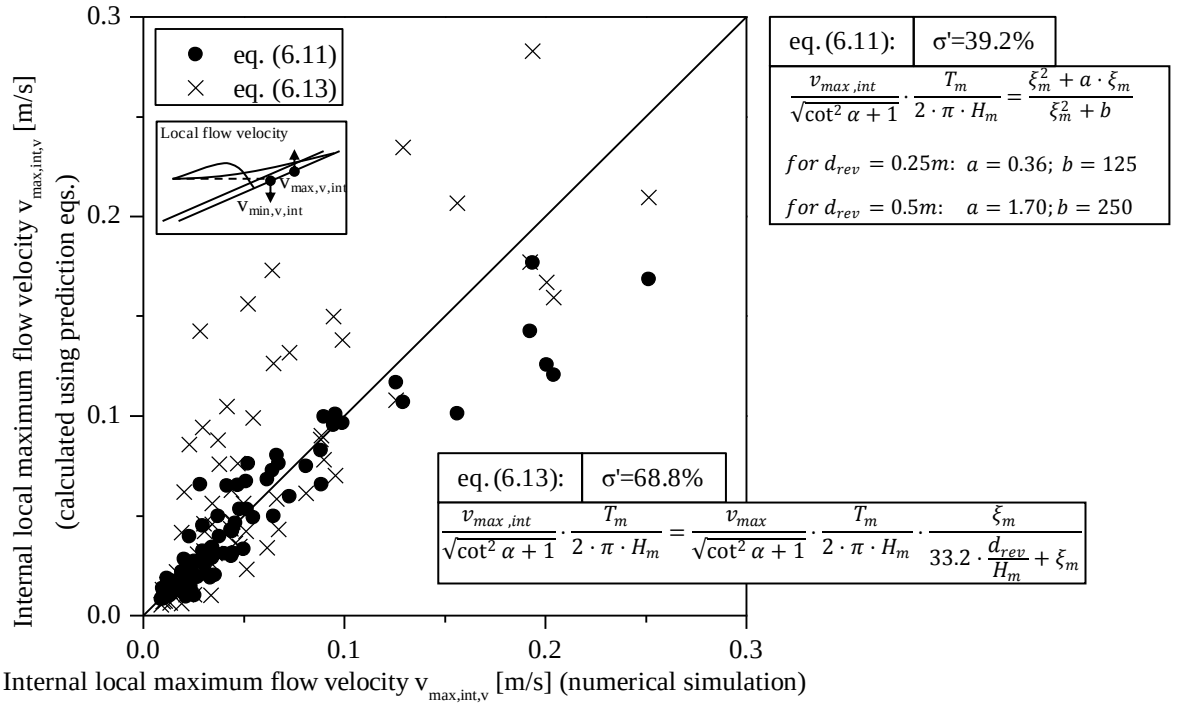

Fig. 6.18 Predicted vertical component of the internal local maximum flow velocity $v_{max,int,v}$ using eqs. (6.11) & (6.13) $v_{max,int,v}$ from the numerical simulations

On first sight, the results of the MRA for the internal flow velocity $v_{min,int}$ are better than that for the corresponding internal flow velocity $v_{max,int}$ (cf. Fig. 6.18 and Fig. 6.19). Only for large absolute values a large deviation from the simulated values can be noticed (Fig. 6.19). The coefficient of variation is extremely high: σ' = 103%. This issue can only be explained either by inaccuracies in the numerical simulations or by the inapplicability of the prediction approach shown in eq. (6.14) to the data set. In this case both reasons may apply. Due to the very coarse resolution of the velocity measurements, many inaccuracies are expected. Therefore, a better approach has to be found in future studies.

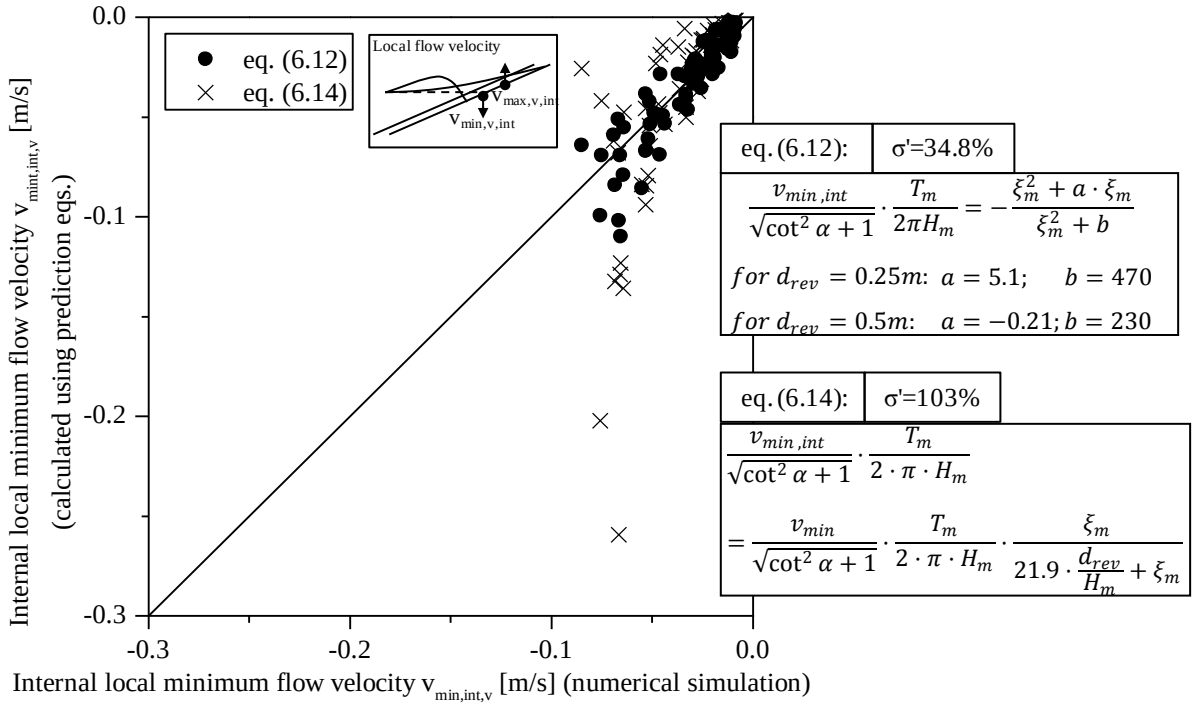

Fig. 6.19 Predicted vertical component of the internal local minimum flow velocity $v_{min,int,v}$ using eqs. (6.11) & (6.13) $v_{min,int,v}$ from the numerical simulations

The internal flow velocities $v_{max,int}$ and $v_{min,int}$ show a similar dependency on the surf similarity parameter ξ_m as the internal wave run-up and run-down velocities $v_{Ru,int}$ and $v_{Rd,int}$. However, the absolute values of the flow velocities are only about half as large as the wave run-up and run-down velocity. The damping of the downwards directed internal flow velocity within the porous revetment is more pronounced than that of the internal wave run-down velocity. Differences between the internal wave run-up and run-down velocities and the internal local flow velocities might be caused by the difference in the definition of the velocities. From the results, it can be concluded that the swash within the revetment is dominated by in- and exfiltration and less by an up-/downrush of water inside the revetment.

6.4 Summary of key results

The processes inside the revetment are much more complex than those on the revetment, implying that more parameters need to be considered in the analysis than in Chapter 5. Therefore, it was difficult to come up with final generic results. Nevertheless the following tentative findings can be listed which show the effect of the different parameters separately as well as the encountered difficulties:

1) A linear relation between internal wave set-up η_{int} for $d_{rev} = 0.25$ m and $d_{rev} = 0.5$ m was found resulting in an internal set-up η_{int} for $d_{rev} = 0.5$ m being 78% of that for $d_{rev} = 0.25$ m. For more generic relations, tests with additional revetment thicknesses are required.
2) Internal wave run-up and run-down and the corresponding velocities are analysed separately due to different layouts of all data sets. This difference in the data pairs suggests either a larger influence of the breaking effect on the upwards directed processes or a larger influence of the porous medium on the downwards directed processes or a combination of both.
3) The approaches from the revetment surface (see eq. (5.1)) were applied to all uprush and backwash parameters (internal wave run-up and run-down height $R_{u,int}$ and $R_{d,int}$ and the corresponding wave run-up and run-down velocities $v_{Ru,int}$ and $v_{Rd,int}$ as well as the local flow velocities $v_{max,int}$ and $v_{min,int}$). Tab. 6.1 gives an overview of the resulting parameters a and b for the tests with $d_{rev} = 0.25$ m, implying that the wave run-down height is least affected by the porous revetment. This explains why no large differences between the parameters for the internal and external wave run-down heights are found while the corresponding velocities are significantly affected by the revetment.

Tab. 6.1 Parameters a and b according to eq. (5.1) for the dimensionless values (all for drev = 0.25 m)

	R_u	$R_{u,int}$	R_d	$R_{d,int}$	v_{Ru}	$v_{Ru,int}$	v_{Rd}	$v_{Rd,int}$	v_{max}	$v_{max,int}$	v_{min}	$v_{min,int}$
a	19.23	-0.17	19.23	12	14	110	40	$2.2 \cdot 10^{15}$	22	0.36	35	5.1
b	130.87	62	130.87	190	40	750	400	$1.8 \cdot 10^{6}$	64	125	360	470

4) The internal wave run-up and run-down are also highly affected by the flow through the revetment (infiltration and exfiltration) thus leading to larger internal wave run-up and run-down velocities $v_{Ru,int}$ and $v_{Rd,int}$ than internal local flow velocities $v_{max,int}$ and $v_{min,int}$.

7 Processes in the Sand Foundation

The processes in a foundation are very important for any analysis of the stability of an entire structure. The analysis of all processes in the sand foundation of the structure in focus of this thesis can only be based on the results of the GWK-experiments. In fact, the sand foundation was assumed to be impermeable in the numerical simulations (see Section 3.2.3).

As found in previous studies, the pore pressure is characterised by a transient part and a residual part (cf. Section 2.4.2). Moreover, the pore pressure is also affected by changes in the water table (cf. Section 2.4.1). Because a considerable wave set-up on the revetment surface was found (Section 4.2), an effect on the internal water table is also expected. Therefore, Section 7.1 deals with the analysis of the internal water table and with the difference between the pressure build-up due to both, residual pressures and changes in water table. Section 7.2 of this chapter presents a tentative stability analysis based on the findings of Section 7.1.

7.1 Internal water table

The main objective of this chapter is to analyse the internal mean water level (IMWL) and its relation to the external mean water level (EMWL). For this purpose, the wave gauges (WG11 – 13) in front of the structure as well as the wave run-up gauge (RUG1+2) were used. Additionally, times series from pore pressure transducers PT22 - 25 were analysed to determine the internal water level (Fig. 7.1).

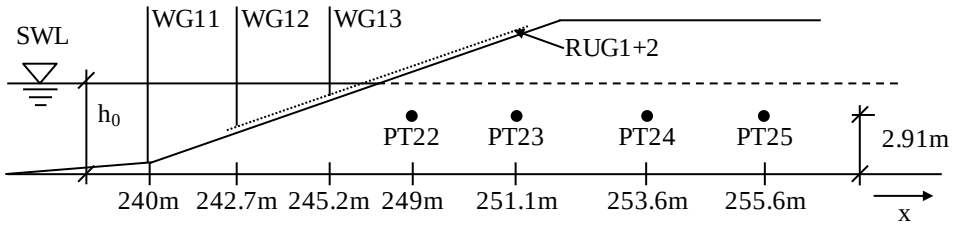

Fig. 7.1 Experimental set-up for the determination of the internal water level (GWK-experiments)

The determination of wave set-up/set-down is described in Section 4.2. However, the changes in the internal mean water level (IMWL) in the sand core beneath the revetment differ from those in the external MWL induced by the wave set-up on the slope (compare Fig. 4.6 and Fig. 7.2). The deviation of the IMWL from SWL in the sand η_{Sand} is defined in Fig. 7.2 for pore pressure transducer PT22 (location shown in Fig. 7.1). In this case, $\eta_{Sand,PT22}$ represents the hydraulic head corresponding to the measured pore pressure $u_{r,PT22}$ ($\eta_{Sand,PT22} = u_{r,PT22}/(\rho_w g)$). The set-up in the sand foundation for the tests with wave spectra is determined accordingly despite the difficulties associated with an objective determination of the exact time where the build-up process is completed.

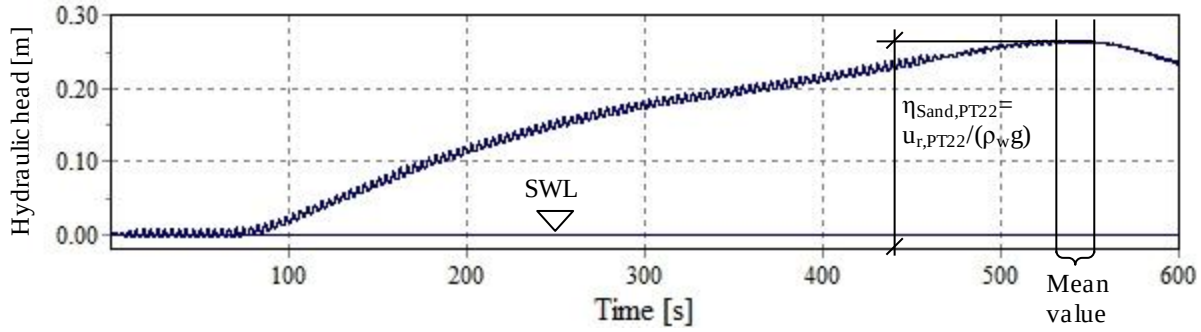

Fig. 7.2 Definition of the water level set-up in sand foundation at PT22 (see also Fig. 7.1)

The following four subsections will describe (i) the internal water level changes for tests with regular waves (Section 7.1.1); (ii) the internal water level changes for tests with wave spectra (Section 7.1.2); (iii) the difference between residual pore pressures and water level changes (Section 7.1.3) and (iv) the spatial layout of the entire water table for tests with wave spectra (Section 7.1.4).

7.1.1 Internal water level for regular waves

For a good overview of the processes involved in the change of the water table, four representative tests, each test corresponding to one of the four breaker types observed (see Section 4.1.1), were selected from the GWK-tests. The selected tests are referred to using the associated breaker type. The wave parameters of the tests are listed in Tab. 7.1.

Tab. 7.1 Overview of selected representative tests from all GWK-experiments with regular waves

Breaker type	H_m [m]	T_m [s]	ξ_m [-]	h_0 [m]
Plunging	0.918	3.005	1.31	3.5
Plunging-collapsing	0.220	2.986	2.65	3.4
Collapsing	0.442	7.004	4.39	3.8
Surging	0.171	7.998	8.05	3.4

Fig. 7.3 shows the resulting internal (PT22 – 25 as depicted in Fig. 7.1) and external (WG11 – 13 & RUG as shown in Fig. 7.1 and described in Tab. A.1) water levels for the four representative tests. A tendency of a relatively higher IMWL compared to EMWL for higher surf similarity parameters can be observed. The infiltration depth is, however, similar for all four representative tests. Without wave action IMWL and EMWL would have the same level (SWL) at the revetment, so the results imply several physical interpretations:

(i) For relatively short and high waves (plunging and plunging-collapsing breakers) the exfiltration of water during wave run-down dominates over the infiltration during wave run-up;
(ii) For waves with moderate wave periods (collapsing breakers) exfiltration and infiltration are balanced;
(iii) For relatively long waves (surging breakers) infiltration dominates over exfiltration.

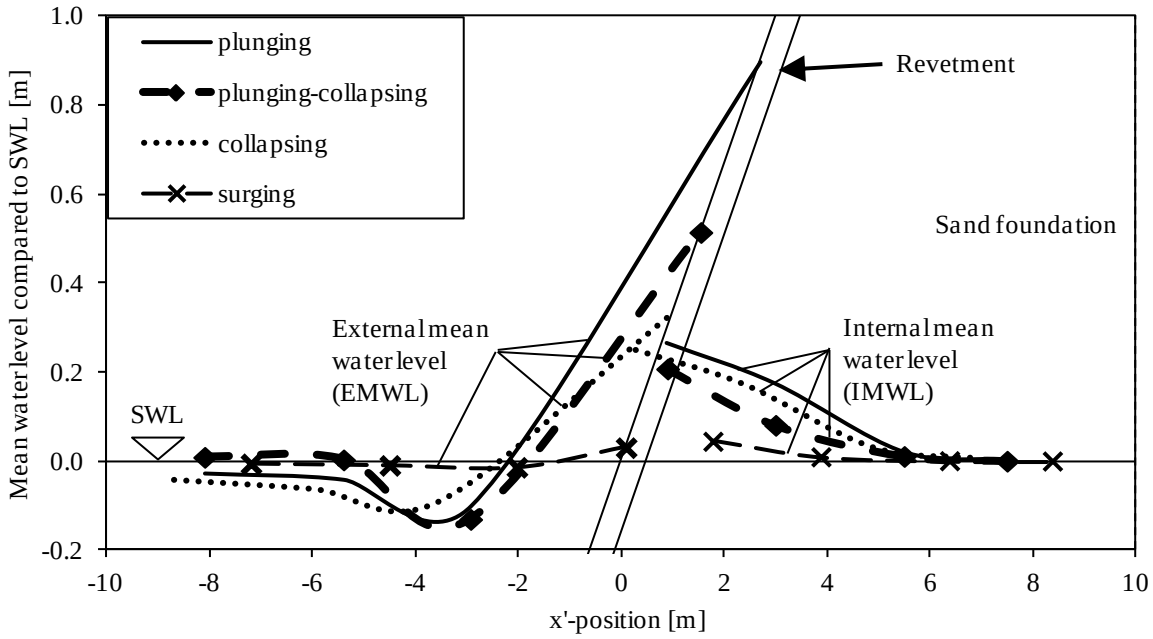

Fig. 7.3 Effect of the breaker types on the external and internal mean water levels for regular waves

However, especially for the surging breaker case, the changes in the MWL are so small that no definite conclusions can be drawn. Furthermore, the temporal build-up of the IMWL is expected to depend on the wave length and thus be different for each test. Consequently, tests with only about 100 waves as they were performed for the representative tests are not ideal for a process analysis. Therefore, in Subsection 7.1.2, a similar analysis is then performed for the GWK-tests with wave spectra.

For a better overall analysis e.g. to include the surf similarity parameter ξ_m into the analysis, the relation between IMWL and EMWL near the revetment is analysed for all available tests with regular waves. The maximum rise of the wave set-up in the sand foundation η_{Sand} for all tests was divided by the wave length L_0 and plotted against the surf similarity parameter ξ_m (Fig. 7.4). Additionally, the wave set-up on the slope η_{max} (model alternative B – RUG3+4) is plotted for comparison. The first findings from the representative tests in Fig. 7.3 can, thus, be verified: the difference between the outer and inner water level generally decreases with higher surf similarity parameters ξ_m and almost no difference is noticeable for $\xi_m > 4$.

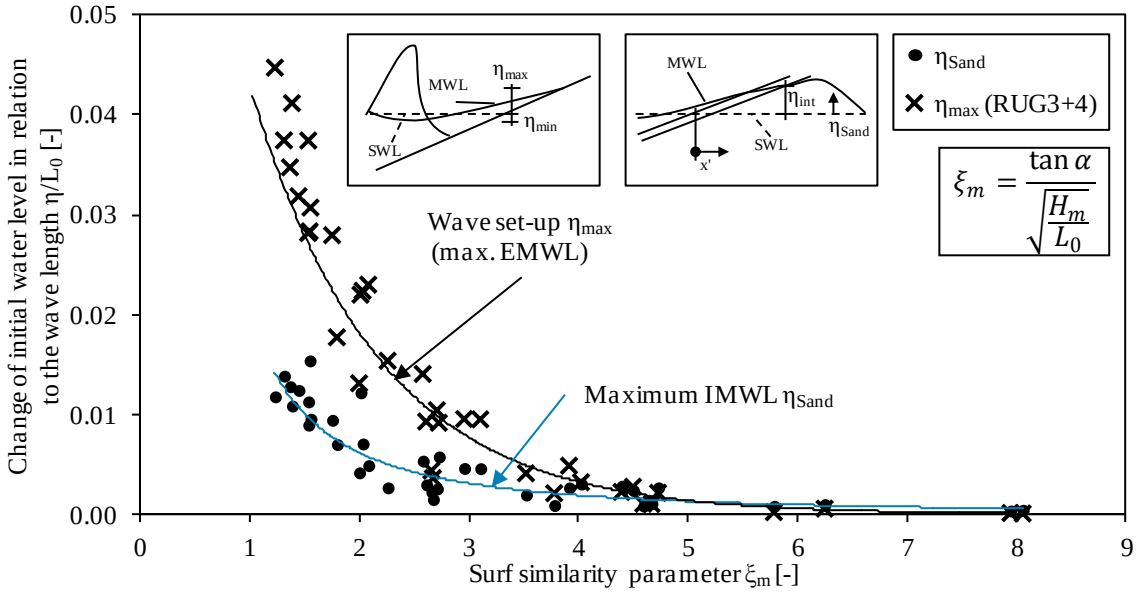

Fig. 7.4 Internal water level and wave set-up on the slope versus surf similarity parameter for GWK-tests with regular waves

7.1.2 Internal water level for wave spectra

One of the most obvious difficulties in the analysis of the pore pressure development during a test with regular waves arose from the too short test duration. For many tests, the development of the IMWL was not completed at the end of the test (similarly to what can be seen in Fig. 7.2). Therefore, the development of the IMWL is analysed in this subsection for selected wave spectra tests (Tab. 7.2). These normally include about 1000 waves while the tests with regular waves only lasted for 100 waves. The results are shown for four different breaker types (Tab. 7.2 and Fig. 7.5) in the same way as for the regular wave tests (Fig. 7.3).The classification into different breaker types is more difficult for wave spectra than for regular waves. Therefore, tests with similar surf similarity parameters (based on deep water wave height H_{m0} and wave period $T_{m-1,0}$) as for the regular tests are chosen for comparison.

Tab. 7.2 Overview of selected representative tests from all GWK-experiments with wave spectra

Test	H_{m0} [m]	$T_{m-1,0}$ [s]	$\xi_{m-1,0}$ [-]	h_0 [m]
Plunging	0.948	4.626	1.98	3.9
Plunging-collapsing	0.583	4.601	2.51	3.8
Collapsing	0.546	6.963	3.92	3.8
Surging	0.204	7.043	6.50	3.4

The results for the wave spectra (Fig. 7.5) show several differences compared to the results of the regular waves (Fig. 7.3):

(i) Absolute values of IMWL for wave spectra are generally higher for comparable wave heights
(ii) Absolute values of EMWL are generally smaller for wave spectra for comparable wave heights
(iii) The absolute values from (i) and (ii) then result in a ratio of IMWL to EMWL, which is higher for all breaker types for wave spectra with a generally higher IMWL than EMWL.

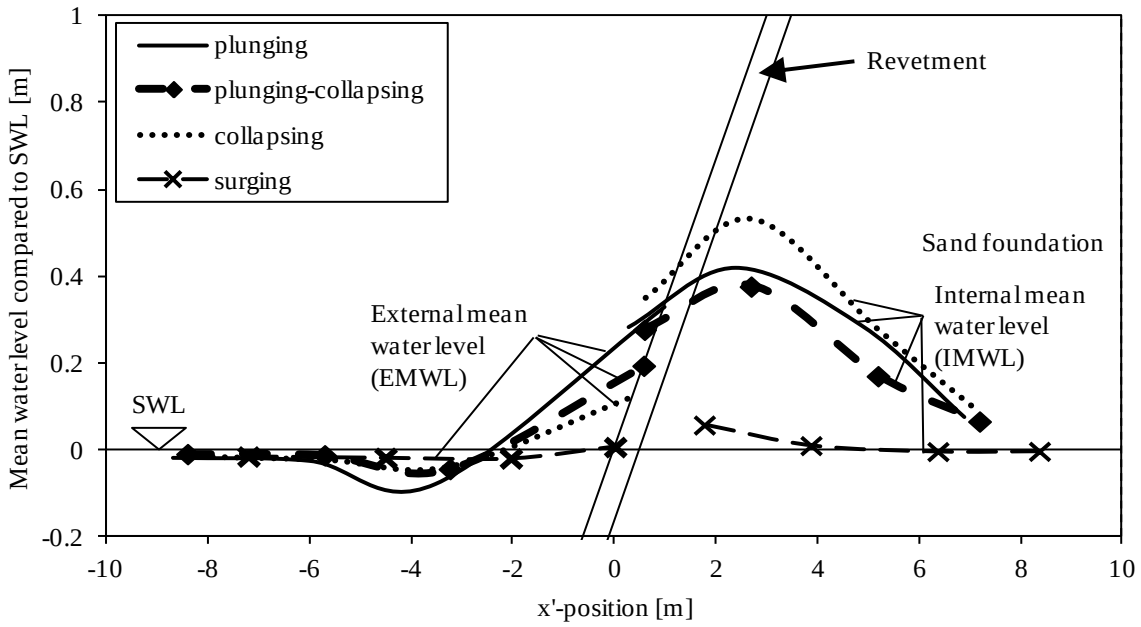

Fig. 7.5 Effect of the breaker types on the external and internal mean water levels for wave spectra

These results are also found for other tests with wave spectra as shown in Fig. 7.6 where the relative maximum wave set-up on the slope η_{max} and the maximum set-up in the sand foundation η_{Sand} are plotted for all tests with wave spectra as a function of the surf similarity parameter $\xi_{m-1,0}$. Fig. 7.6 shows a similar wave set-up on the revetment surface and in the sand for all surf similarity parameters $\xi_{m-1,0}$. Moreover, the resulting set-up in the sand foundation of the tests with wave spectra is in the same range as the set-up in the sand foundation for the tests with regular waves (Fig. 7.4).

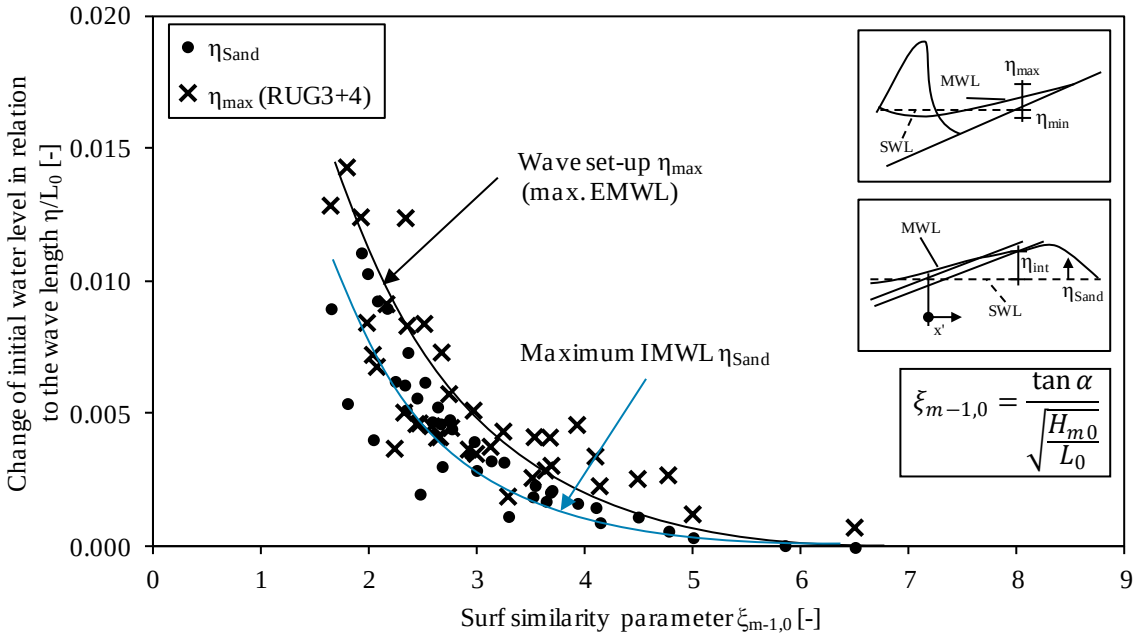

Fig. 7.6 External and internal (at PT22) water level set-up vs. surf similarity parameter for GWK-tests with wave spectra

7.1.3 Residual pore pressures versus change in water table

To determine whether a residual pore pressure build-up occurred, the change of the mean pressure values are analysed for all pressure transducers PT01 - 25 (see Fig. 3.1 and Fig. 3.2) in the impact area for the representative wave spectra tests (Tab. 7.2). The locations of these pressure transducers are listed in Tab. A.2 (Appendix A.1). In the following only those transducers located below the minimum wave run-down are shown, as they could record the full swash. Furthermore, the transducers (all in model alternative C) are grouped into layers as in Oumeraci et al. (2010). The first example is shown in Fig. 7.7. The solid markers represent the IMWL and EMWL recorded by WG11 – 13 and PT22 – 25 (Fig. 7.1).

For the plunging breaker test as shown in Tab. 7.2, a quite good correlation between the results from the wave gauges and the pressure transducers beneath the revetment is found (Fig. 7.7). The results from all four layers are in agreement with the results for the EMWL as shown above. This implies that no pore pressure build-up is present in the lower areas beneath the impact zone and that only the change in MWL affects the mean pressures at those pressure transducers. Thus, the pressure transducers in the impact area can also be used to determine the EMWL in more detail. Especially, the point of lowest wave set-down can be determined more precisely. Some deviations between the results of the wave gauges and the pressure transducers are only found for the lowest layer (layer 5), at which the mean values are slightly larger than for the other pressure transducers. This could either be caused by a slight pore pressure build-up or simply by the distance to the slope surface which leads to a delayed response of the PTs in this layer to the change in MWL.

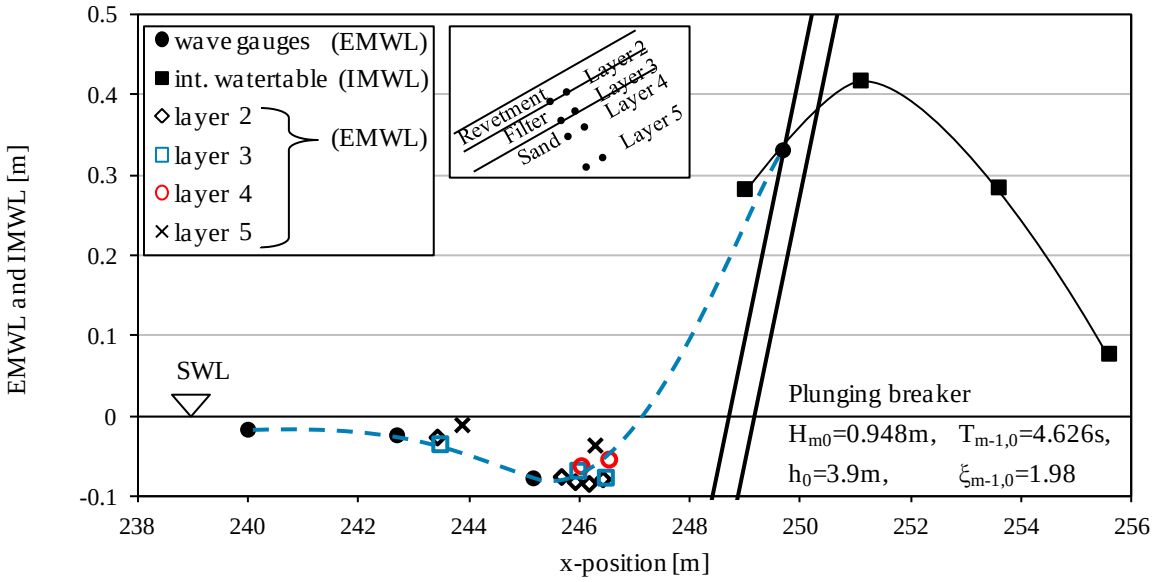

Fig. 7.7 MWL including results from pressure transducers (plunging breaker case, wave spectrum)

For the plunging-collapsing breaker test as shown in Tab. 7.2, the surf similarity parameter is slightly larger than in Fig. 7.7 (Fig. 7.8). However, the results are very similar: the mean values recorded by all instruments align quite well with a small deviation for the lower layers (especially layer 5). Additionally, a small divergence of the results of layer 2 from the other layers is perceptible for x ≈ 246 m.

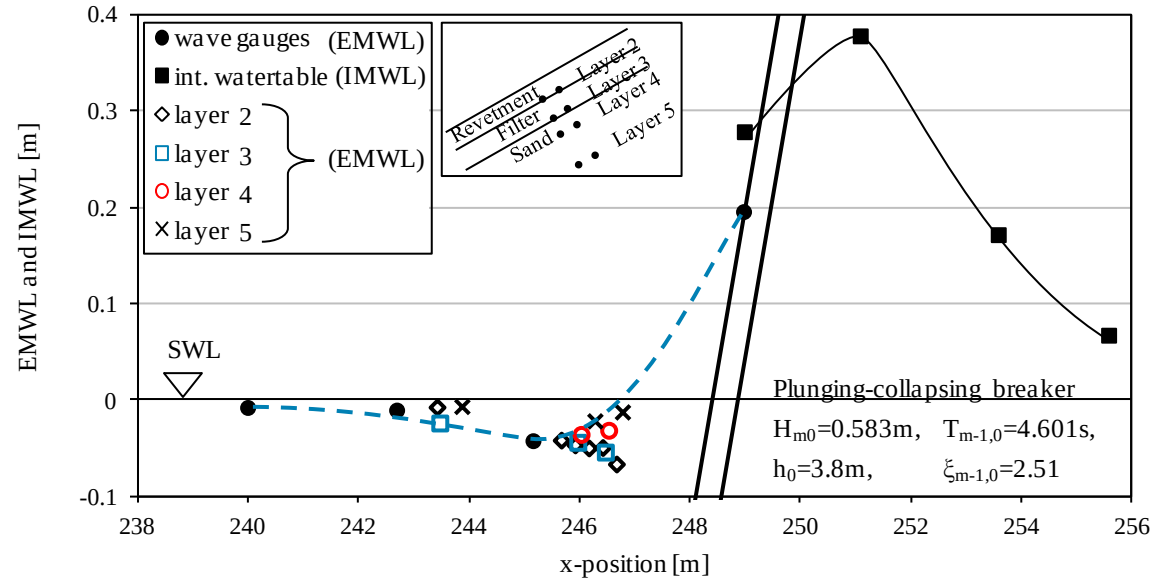

Fig. 7.8 MWL including results from pressure transducers (plunging-collapsing breaker case, wave spectrum)

Because the results for the collapsing and surging breaker cases are quite similar to the two here presented cases, they are not presented here. An overview of all four representative tests and a more detailed analysis can be found in Ludwigs & Oumeraci (2011b). Overall, it can be

concluded that no residual pore pressure development is present and that all not transient pressures result from changes in the MWL.

7.1.4 Spatial water table layout for tests with wave spectra

One unexpected result of this overall section has to be pointed out: the maximum set-up in the sand foundation is found at or near the revetment surface (see Subsections 7.1.1 and 7.1.2) which stands in contradiction to former studies (Losada et al., 1998; Barends & van Hoven, 2007), indicating maximum set-up values farther inside in the structure or even at the rear end of a closed dam. These deviations may be due to the different porous media considered: sand core in this study and rubble material in the former studies. The grain size of the porous medium is expected to affect the internal wave breaking process which represents the main source of a rising set-up in the foundation (Losada et al., 1998). For sand material the maximum set-up is observed near the revetment and might, therefore, be caused by the smaller grain diameter and a faster internal breaking. This would lead to two possibilities after the maximum internal set-up is reached near the revetment: (i) the water table decreases to the original SWL or (ii) the water table remains at the maximum throughout the structure. Both options are depicted in Fig. 7.9.

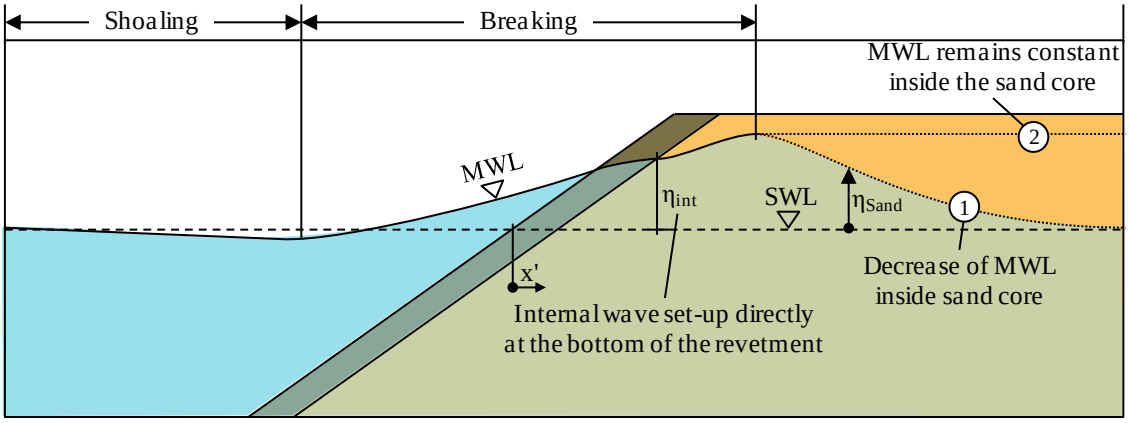

Fig. 7.9 Spatial layout of the mean water level (MWL) outside and inside the porous structure

To analyse the location of the maximum internal wave set-up further, the data from the GWK-experiments with wave spectra are plotted in a non-dimensionless form in Fig. 7.10. For this purpose, the internal wave set-up in the sand core η_{Sand} is related to the internal wave set-up η_{int} directly at the bottom of the revetment. Because η_{int} was not measured in the GWK-tests, the approach formulated for the numerical results (eq. (6.2)) is applied to the data set using a mean revetment thickness of $d_{rev} = 0.3$ m to obtain the wave set-up η_{int} from the wave set-up on the slope surface η_{max}. On the x-axis, the dimensionless distance x'/H_{m0} uses the distance of the measured set-up in the sand from the crossing point between SWL and the surface of the revetment x' (see Fig. 7.9). Furthermore, the results are split into five equally sized groups (all groups have a similar number of data points) according to their respective surf similarity parameter $\xi_{m-1,0}$. Generally, four data points are obtained for each test (one result for each pressure transducer).

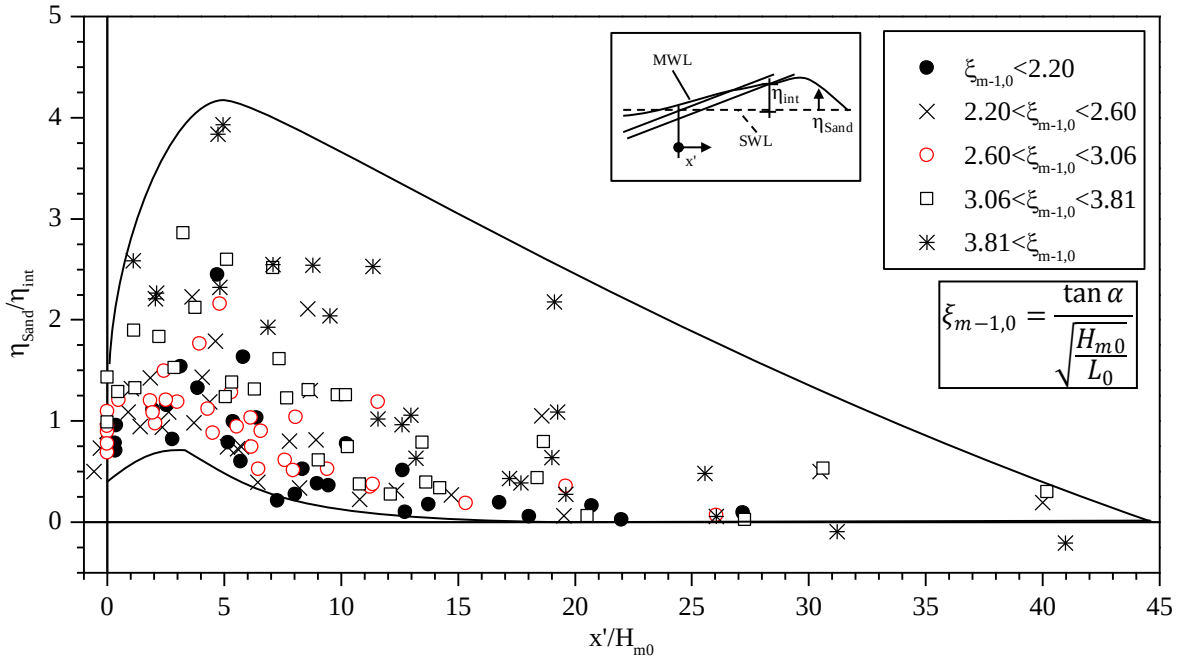

Fig. 7.10 Relative internal mean water level for the tests with wave spectra in the GWK (7 outliers removed)

Fig. 7.10 underlines particularly the previous findings of Sections 7.1.1 and 7.1.2: the maximum wave set-up in the sand core is found near the revetment for all surf similarity parameters and the mean water level is decreasing further into the sand core from the maximum near the revetment. Based on the data groups and the related surf similarity parameter, a second trend is visible: the highest relative set-up in the sand occurs for the group with the highest surf similarity parameter ($\xi_{m-1,0} > 3.81$). Moreover, the location of the maximum set-up is found to depend primarily on the wave height. For almost all tests the maximum is located around $x'/H_{m0} = 4$, indicating a direct relation between the wave height and the location of the breaking inside the sand.

A MRA was performed to describe the trends shown in Fig. 7.10. The best result is shown in eq. (7.1) which takes into account the effect of the surf similarity parameter $\xi_{m-1,0}$, the distance from SWL x'/H_{m0} and the wave set-up in the revetment η_{int}. The statistical results show still room for improvement with $\sigma' = 38.0\%$. One main reason for this problem might be the inapplicability of eq. (6.2) to irregular waves which was used to obtain η_{int}.

$$\frac{\eta_{Sand}}{\eta_{int}} = \frac{29.4 + e^{\xi_{m-1,0}}}{50.3 + \left(\frac{x'}{H_{m0}}\right)^2 - 7.27 \cdot \frac{x'}{H_{m0}}} \tag{7.1}$$

Furthermore, eq. (7.1) underlines the findings of the previous subsections where it is suggested that the internal water table decreases after reaching a maximum near the revetment instead of remaining constant (cf. Fig. 7.9). This can also be seen in Fig. 7.11 which presents eq. (7.1) for five different surf similarity parameter $\xi_{m-1,0} = 1; 2; 3; 4; 5$. The result fits with the experimental results shown in Fig. 7.10. However, the exponential effect of the surf

similarity parameter leads to a drastic increase of the maximum η_{Sand}/η_{int}. Therefore, the approach should only be used for surf similarity parameter $\xi_{m-1,0} < 5$. Fig. 7.11 also shows that for eq. (7.1) the maximum internal set-up is found at $x'/H_{m0} = 3.6$ which is backed up by the experimental data in Fig. 7.10.

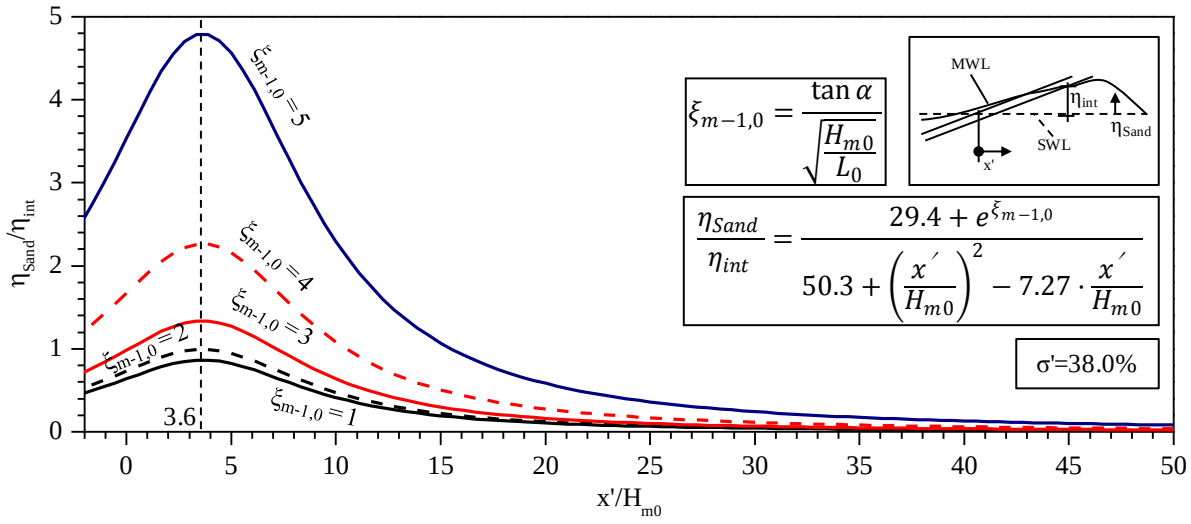

Fig. 7.11 Relative internal mean water level for different surf similarity parameters according to eq. (7.1)

Overall, the available data is not sufficient to fully understand the processes underlying the development of the internal mean water level in the sand core, thus making the development of a final generic formula difficult. However, it important to stress that:

(i) The breaking processes is generally difficult to describe and the breaking in a fine porous medium such as sand makes the problem even more difficult;
(ii) A finer spatial resolution is needed to precisely follow the development of the MWL inside the entire sand core, but also outside the structure;
(iii) Longer test durations are needed – also with regular waves.

The analysis of the pore pressures showed that the tests with regular waves were too short to fully reach the maximum internal mean water level (IMWL) in the sand core. Furthermore, it was found that no residual pore pressure build-up occurs. In fact, all mid to long-term variations of the pore pressure signals are caused by the change in the internal mean water level. Finally, the maximum set-up in the sand foundation was found to be near the revetment surface rather than at the rear end of the test set-up. The location of this maximum set-up most likely indicates the point where the internal wave breaking processes is completed. This needs, however, to be verified in future research studies.

7.2 Tentative stability analysis of the sand foundation

When considering the processes which have been analysed in this study, bonded porous revetments are similar to most other porous revetments. However, when it comes to their stability, the behaviour of a bonded revetment is completely different from that of for

example a rubble revetment. In this section, a few stability issues are investigated especially focussing on the failure of model alternative A in the GWK-tests. In Oumeraci et al. (2010) it is suggested that transient soil liquefaction during the test caused the failure. Soil liquefaction can be induced by different processes but due to the high porosity of the revetment, upwards directed pore pressure gradients represent the most likely trigger for soil liquefaction as described by Oumeraci et al. (2010).

The main loads leading to the effective soil stresses are summarised in Fig. 7.12 sorted according to their effect on the total stress σ and the pore pressure u. The case related to the loss of shear resistance is particularly important for the analysis of the structural stability of the sand foundation. The same approach to the particular case of soil liquefaction as proposed by Oumeraci et al. (2010) is adopted but a different physical interpretation is proposed. For the point of loss of shear resistance the following equation applies (see also Fig. 7.12 & Fig. 7.13):

$$\text{loss of shear resistance: } \sigma' = \sigma_{mass} + u_0 - u_t \leq 0 \tag{7.2}$$

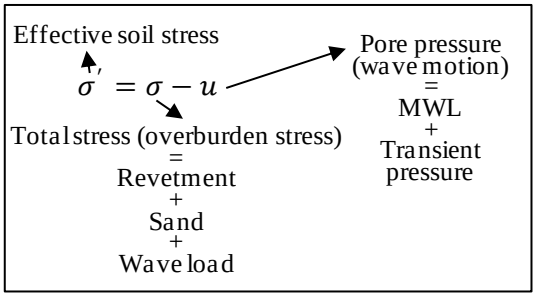

Fig. 7.12 Effective & total stress and pore pressure

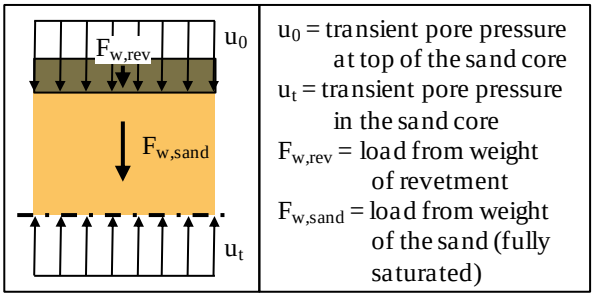

Fig. 7.13 Loads considered in the stability analysis

σ_{mass} is the stress resulting from the resisting weight of the revetment and the sand foundation (overburden pressure) at the respective location. u_0 is the water pressure on top of the sand foundation, which is considered here as a load and not as a pore pressure. u_t is the transient pore pressure at the respective location (definition of locations B, C and D in Fig. 7.16). All components are also schematically shown in Fig. 7.13.

As shown in Section 7.1, no residual pressures are found beneath the highly porous revetment. A separation into transient and residual pore pressure is, therefore unnecessary. The parameter of interest for the stability analysis is the difference of the pore pressure at the surface of the upper sand layer and at any other lower location within the sand core beneath the revetment. The following analysis only considers the data of model alternatives A and C because in model alternative B (see Fig. 3.1) the third layer of pressure transducers (on top of the sand foundation) is only represented by a single pressure transducer.

In contrast to Oumeraci et al. (2010), a slightly different approach for the calculation of the maximum upwards transient pressure difference is used for the stability analysis. The approach used by Oumeraci et al. (2010) can be summarised as follows:

- Filtering of time series of the pressure transducers in the impact area to separate the transient from the residual pressures,
- Determination of the minimum for all time series separately (not necessarily from the same event for all locations),
- Calculating the pore pressure gradient from the determined minima for each location (B, C, D) and layer combination (layer 3 - layer 4, layer 3 - layer 5).

This procedure was adapted to make it feasible for all tests but also to account for the findings of the present chapter. This entails the following changes:

- No separation of transient and residual part of the pore pressure is necessary as shown in Section 7.1
- The difference between u_0 and u_t is calculated for the entire time series
- The maximum upwards directed pressure gradient is determined on the resulting time series after applying a 12 HZ low pass filter to the calculated time series ($u_0 - u_t$)

A further alteration made in the present study compared to Oumeraci et al. (2010) is that the pore pressure u_0 is only assumed to be a load on the sand core. This does not lead to a change in the calculation approach. Furthermore, the buoyancy of the revetment is included, for the cases where layer 3 of the pressure transducers at the respective location B, C & D is below the point of lowest wave run-down (Fig. 7.14). This is decided for every test and every location separately.

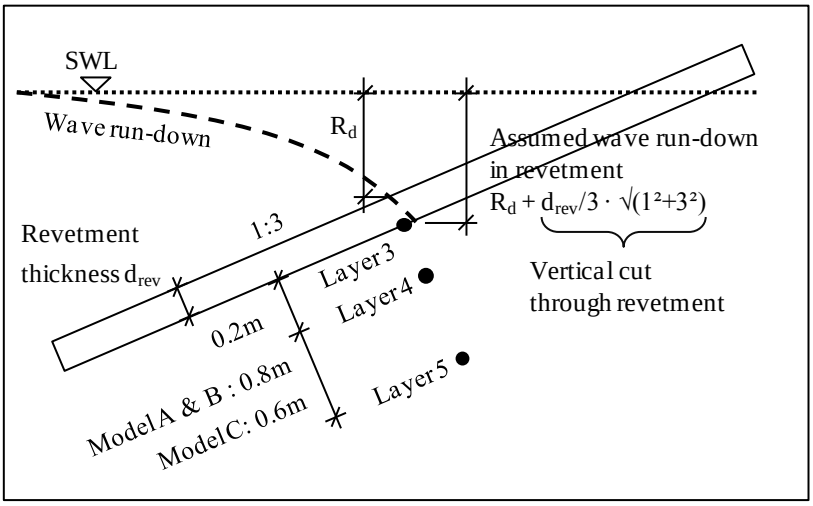

Fig. 7.14 Definition sketch for buoyancy of revetment and layers 3-4

Based on the aforementioned data analysis procedure, the pore pressure difference ($u_0 - u_t$) is calculated for all events in tests with model alternatives A and C (model alternative B cannot be analysed due to already described reasons). The minimum pressure difference ($u_0 - u_t$) is then determined by an event analysis. The ($u_0 - u_t$) values divided by $\rho g H_m$ are plotted in Fig. 7.15 for layers 4 and 5 versus the surf similarity parameter ξ_m. An almost linear relation is found between the two parameters. As expected, the pressure differences in model alternative

A are larger for both layers and the pressure difference from the top of the sand foundation to layer 5 is generally larger than those to layer 4.

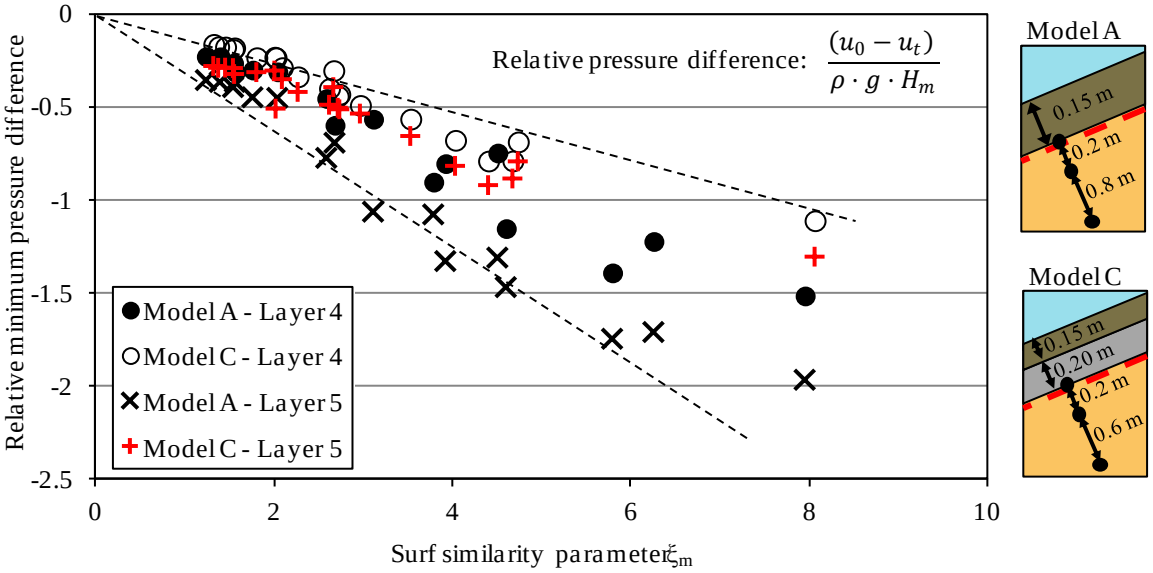

Fig. 7.15 Minimum pressure differences of all pressure transducers in the layer versus surf similarity parameter for model alternatives A and C

The primary objective of the analysis is, however, the determination of the effect of the pressure difference ($u_0 - u_t$) on the stability of the soil beneath the revetment. For this purpose, the load from the weight of the revetment and the soil at layer 3 is calculated using the approach schematically shown in Fig. 7.13. This parameter and the determined pressure difference ($u_0 - u_t$) (Fig. 7.15) are then inserted in equation (7.3), which is directly derived from eq. (7.2) and gives a relative loading parameter and the condition to ensure shear stability of the soil beneath the revetment (stability criterion).

$$\text{stability criterion: } -\frac{u_0 - u_t}{\sigma_{mass}} \leq 1 \tag{7.3}$$

Using this stability criterion, Fig. 7.16a and Fig. 7.17 are generated. For all tests the less stable layer is always layer 4 and in layer 5 no failures are recorded. Therefore, only the results for layer 4 are presented here.

In Fig. 7.16, the tests performed on model alternative A are shown chronologically versus the relative loading $-(u_0 - u_t)/\sigma_{mass}$. Moreover, Fig. 7.16b depicts the permanent displacement of the revetment after each of the tests. A loss of stability is observable for the last 4 tests (13 – 16) of the test series (see list in Tab. A.3, cf. also Oumeraci et al., 2010). For test number 14 (H_m = 0.54 m; T_m = 6.95 s; h_0 = 3.9 m, ξ_m = 3.91), a loss of shear stability of the soil beneath the revetment for all three locations is first documented. This is also shown in the number of shear losses (also Fig. 7.16a) which describes the number of wave cycles per test that have led to a loss of shear stability (all tests were performed with 100 waves). At the same time neither a distinct relocation of the revetment nor a failure of the revetment is recorded (Fig. 7.16b).

This disagreement is mostly caused by the effect of the bonding of the revetment which is not taken into account by this approach. However, in test 16 (H_m = 1.37 m; T_m = 4.9 s; h_0 =3.9 m; ξ_m = 1.75) a failure occurred. This could, therefore, be a consequence of the numerous partial failures of the sand foundation. This conclusion is also underlined by Fig. 7.15 where the tests for which failures occurred do not show any particular differences to the other tests that did not lead to partial failures.

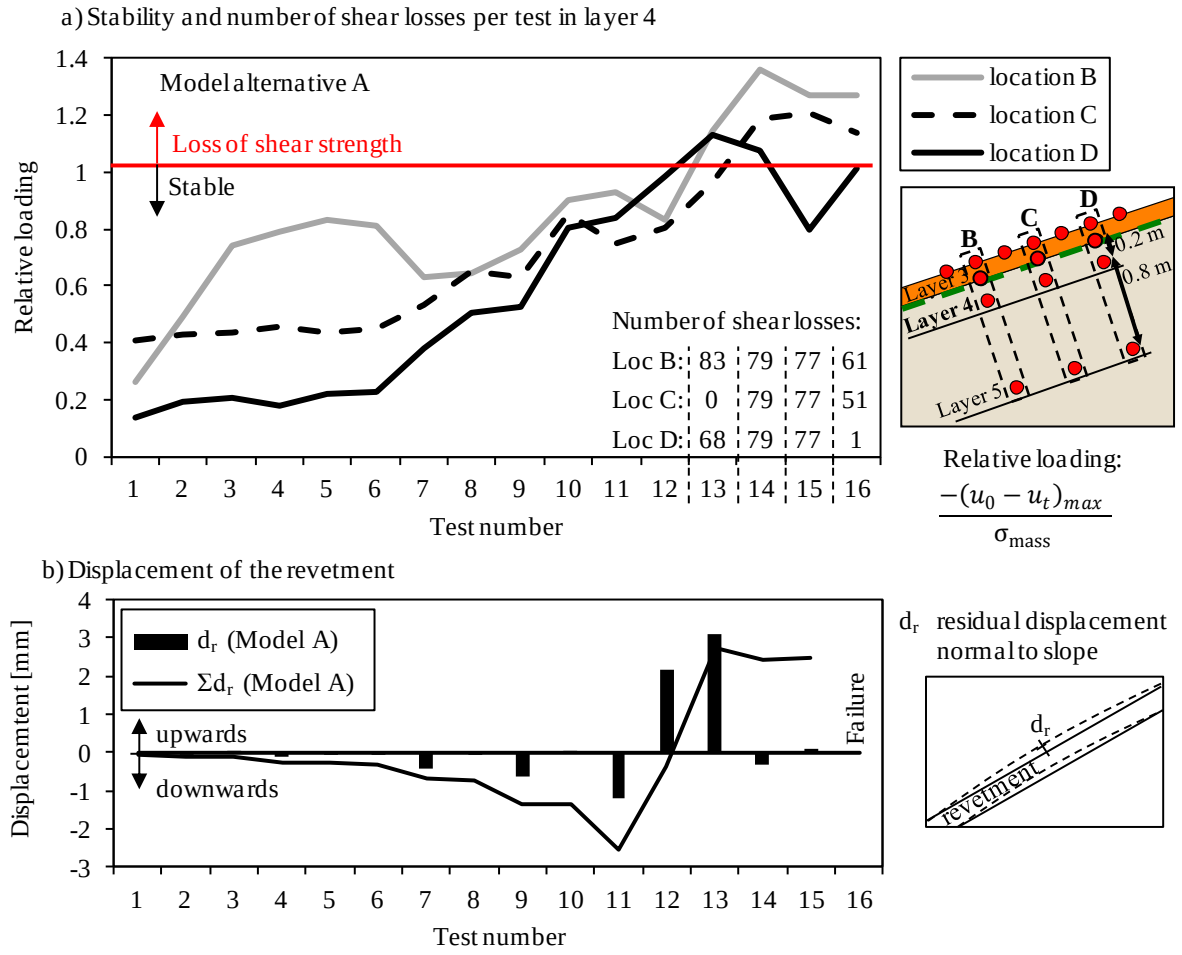

Fig. 7.16 Stability analysis and number of shear losses per test for model alternative A in layer 4 (regular wave tests, list in Tab. A.3)

Model alternative C was tested in the second test phase with regular and irregular (wave spectra) waves and Fig. 7.17 presents the results of the stability analysis of the regular wave tests in chronological order. Times when wave spectra tests were performed are marked as disruptions. In contrast to the results of model alternative A with several tests exceeding the calculated threshold for shear stability, no stability losses occurred for any of the regular wave tests performed on model alternative C (Fig. 7.17). Although the relative loading increases during the test series and is especially near the threshold for failure at location C for test numbers 20 (H_m = 1.17 m; T_m = 7.02 s; h_0 = 3.4 m; ξ_m = 2.7) and 21 (H_m = 0.91 m; T_m = 8.05 s; h_0 = 3.6 m; ξ_m = 3.52), a complete loss of stability is never reached. Furthermore, the disruptions by sets of tests with irregular waves seem to have no effect on the results from

the regular tests: after the disruption between tests 5 and 6, an increase in the relative loading is documented and after the disruption between tests 8 and 9, a decrease is found. Only after the last disruption between tests 16 and 17, a quite distinct rise in the relative loading is observed. This is most likely caused by the incident wave parameters (see Appendix A.1 Tab. A.4).

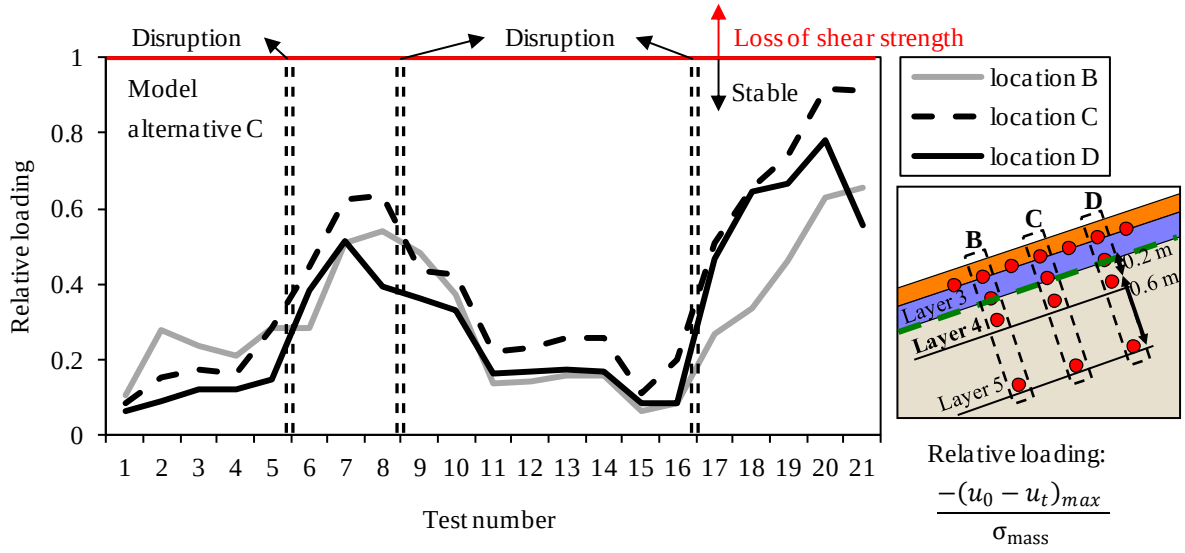

Fig. 7.17 Stability analysis for tests on model alternative C in layer 4 (regular wave tests, list in Tab. A.4)

Generally, partial failures could have occurred for all tests but these were not recorded by the installed pressure transducers. The effect of the bonding of the revetment is neglected for the calculation (only the weight of the revetment is taken into account) and further investigations are, therefore, advisable. These should focus on both the hydrodynamic and the geotechnical processes. A coupled numerical model would, therefore, be appropriate.

A simplified approach to tentatively evaluate the stability of the sand foundation in the GWK-tests is implemented for the tested conditions for model revetment alternatives A and C. It predicts a failure of model alternative A earlier than it actually occurred. Furthermore, no failure was predicted for model alternative C. Therefore, the approach could be applied for a first estimate. Generally, it can be assumed that the sand relocation below the revetment caused by the predicted failures caused the final revetment failure due to the changes in the bearing area by the formation of "holes" and "bumps" in the sand foundation.

7.3 Summary of key results

In this chapter the effect of the wave set-up on the pore pressure development within the sand core beneath bonded porous revetments was analysed solely based on GWK-tests performed by Oumeraci et al. (2010) with regular waves and wave spectra (no numerical simulations). Furthermore, the residual pore pressures in the sand beneath the impact area are checked for a possible pore pressure build-up. Finally, a tentative simplified analysis of the stability of the sand foundation was performed.

Among the difficulties encountered in this chapter, the following are noteworthy: (i) the high degree of complexity of the processes involved at the interface revetment/sand and in the sand core including the diversity of the influencing factors; (ii) the very coarse spatial resolution of the measuring locations in the GWK-tests particularly in the sand core and (iii) the absence of a numerical model capable of reliably reproducing the most important processes at the interface revetment/sand and at deeper locations in the sand core. These reasons may explain why, at this stage, only tentative results can be obtained and why it is difficult to come up with more generic results. Nevertheless, the main outcomes may be summarised as follows:

1) The internal mean water level (IMWL) depends highly on the external mean water level (EMWL) which is induced by the wave set-up at the revetment.
2) The relation between IMWL and EMWL at the revetment depends on the breaker type.
3) A prediction equation for the spatial distribution of the set-up in the sand foundation considering the external wave set-up and also the revetment thickness was developed. This equation, though tentative and not fully physically based, suggests a decrease of the internal water table further into the sand foundation. For the development of a more generic and final prediction formula, further research is needed in order to substantially improve the understanding of the wave induced processes in the entire sand core of the porous revetment. Since the available GWK-tests did not prove sufficient and no appropriate numerical model was available for this purpose further research is recommended.
4) Residual pore pressure build-up beneath the porous revetment does not occur. Any recorded changes only depend on the change in MWL and not on insufficient drainage.
5) The tentative approach proposed for the analysis of the stability shows more (partial) failures below model alternative A in the GWK-tests than expected. This finding indicates a stepwise relocation of the sand below the revetment before the revetment actually failed. Furthermore, the bonding of the revetment seems to enhance the stability of the structure.

For a better analysis of the processes in the sand foundation, more detailed tests are needed. This includes the wider range of materials as also a higher resolution of the measurements.

8 Summary, Discussion and Outlook

This study deals with the processes involved in the interaction between waves, a porous bonded revetment and its sand foundation. Data from large-scale model tests and additionally performed numerical simulations form the data base for the investigations which focussed on the analysis of the processes and on the development of formulae for their prediction. The numerical model COBRAS-UC was validated using the experimental data from the Large Wave Flume (GWK) and then used to extend the range of the tested conditions in the GWK. The processes in the sand foundation could, however, not be simulated with the numerical model COBRAS-UC, so that the analysis of these processes was solely based on the GWK-tests. Overall the agreement between the laboratory tests and the numerical simulations is surprisingly good except for the wave pressure values which are, therefore, not considered.

8.1 Summary of findings

The most important processes in the interaction between waves and porous bonded revetments were analysed in four groups according to their location of occurrence (Fig. 1.3). Before starting the development of prediction equations, the corresponding values for the boundary conditions were determined (Tab. 2.5) in order to ensure physically based equations. The most important prediction equations are listed in Tab. 8.2 and the key results are briefly summarised in the following subsections. A more detailed summary is provided at the end of each chapter.

8.1.1 Processes in front of the structure

(i) The breaker type affects most of the processes on and beneath the porous revetment, but a distinct classification into breaker types is quite difficult to achieve. Nevertheless, the proposed ranges of the surf similarity parameter for the four main breaker types are listed in Tab. 8.1.

Tab. 8.1 Surf similarity parameter range for the four main breaker types (Fig. 4.1) and three different revetment thicknesses

Breaker type	d_{rev} = 0 m	d_{rev} = 0.25 m	d_{rev} = 0.5 m
Spilling	$\xi_m < 1.5$	$\xi_m < 1.5$	$\xi_m < 1.5$
Plunging	$1.5 \leq \xi_m = < 2.0$	$1.5 \leq \xi_m = < 2.4$	$1.5 \leq \xi_m < 2.8$
Collapsing	$2.0 \leq \xi_m < 4.0$	$2.4 \leq \xi_m < 5.5$	$2.8 \leq \xi_m < 5.5$
Surging	$4.0 \leq \xi_m$	$5.5 \leq \xi_m$	$5.5 \leq \xi_m$

(ii) For the mean water level (MWL) in front of the structure, a much better spatial resolution was obtained with the numerical simulations than in the GWK-tests.

(iii) The maximum wave set-down η_{min} is about one fifth of the maximum wave set-up η_{max} on the slope surface. Former studies suggest relations in a similar range (USACE, 2002; Oumeraci, 2007), but a final physical interpretation of this result is still lacking.

(iv) A new prediction equation for the location of incipient breaking was developed in the form of the breaking criterion H_b/h_b (see eq. (4.2) in Tab. 8.2). This is only based on the surf similarity parameter ξ_b for which the wave height at the breaking point H_b is used.
(v) A prediction approach for the reflection coefficient including a modified surf similarity ξ_{mod} parameter which takes into account the revetment thickness is provided (see eq. (4.7) Tab. 8.2).

8.1.2 Processes on the revetment

(i) The wave run-up and run-down heights R_u and R_d show similar values around the MWL which underlines the importance of the consideration of the wave set-up.
(ii) The velocities on the slope surface (wave run-up (v_{Ru}) and run-down (v_{Rd}) velocity as well as the upwards (v_{max}) and downwards (v_{min}) directed flow velocity) and the wave run-up and run-down heights (R_u and R_d) are affected mostly by the presence of the surface roughness rather than by the thickness of the revetment.
(iii) The downwards directed velocities (v_{Rd}, v_{min}) are more affected by the porous revetment than the upwards directed velocities (v_{Ru}, v_{max}). This might also be caused by the larger influence of the breaking on the upwards velocities directed.

8.1.3 Processes in the revetment

(i) The prediction equations for the processes inside the revetment could mostly be based on the respective equations for the processes on the revetment. However, the derived relationships between the processes on and inside the revetment are generally neither linear nor simple.
(ii) The wave set-up in the revetment (η_{int}) and the wave set-up on the slope surface (η_{max}) are similar suggesting that only a small amount of energy is dissipated due to internal wave breaking in the revetment.
(iii) The internal downwards directed velocities ($v_{Rd,int}$ and $v_{min,int}$) are more affected by the porous revetment than the upwards directed velocities ($v_{Ru,int}$ and $v_{max,int}$).
(iv) The local internal flow velocities ($v_{max,int}$, $v_{min,int}$) are more strongly dampened than the internal wave run-up/ run-down velocities ($v_{Ru,int}$, $v_{Rd,int}$). This could be caused by the slightly different direction of the velocities but a more likely reason is that the internal swash is mostly influenced by flow processes associated with infiltration and exfiltration.

8.1.4 Processes in the sand foundation

(i) In contrast to former studies, the maximum set-up in the sand foundation was found directly beneath the bottom of the porous revetment or in very close vicinity. This is most likely caused by the internal wave breaking which proceeds faster in a sand core (this study) than in a gravel/rubble core (former studies).
(ii) No residual pore pressure build-up is found. All pore pressures that developed in a mid- to long-term are caused by changes in the water table.

(iii) A stability analysis of the sand foundation of the GWK-tests showed several partial failures that led to sand relocations which finally would result in an overall failure like the observed one. Apparently, the bonding of the revetment enhances the stability of the foundation, thus explaining why an overall failure was observed only once in the GWK-tests.

Tab. 8.2 Overview of proposed prediction formulae

Parameter	Equation	No.	σ'
Breaking criterion 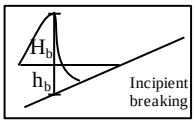	$\frac{H_b}{h_b} = \frac{\xi_b^2}{\frac{\xi_b^2}{0.42} - 3.56 \cdot \xi_b + 1.86}$	(4.2)	27.7 %
Wave set-down and wave set-up 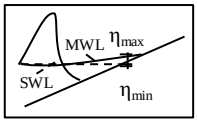	$\frac{\eta_{max}}{L_0} = -5 \cdot \frac{\eta_{min}}{L_0} = \frac{0.0112}{\xi_m} + \frac{\xi_m}{e^{\xi_m + 0.929 \cdot \cot\alpha}}$	(4.3)	36.2 % (η_{max}) 36.8 % (η_{min})
Reflection coefficient 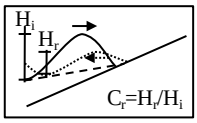	$C_r = \frac{\frac{d_{rev}}{H_m} + \xi_m^2 - \xi_m \cdot \frac{d_{rev}}{H_m}}{7.04 + \xi_m^2}$	(4.7)	14.4 %
Wave run-up and run-down height 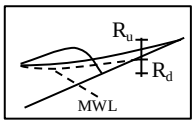	$\frac{R_u}{H_m} = -\frac{R_d}{H_m} = \frac{\xi_m^2 + a \cdot \xi_m}{\xi_m^2 + b}$ $for\ d_{rev} = 0m$: $a = 14.58;\ b = 38.81$ $for\ d_{rev} = 0.25\&0.5m$ $a = 19.23;\ b = 130.87$	(5.3)	25.9 % (R_u) 21.7% (R_d)
Wave run-up & run-down velocity 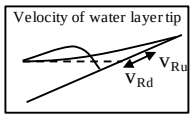	$\frac{v_{Ru}}{\sqrt{cot^2\alpha + 1}} \cdot \frac{T_m}{2\pi H_m} = \frac{\xi_m^2 + a \cdot \xi_m}{\xi_m^2 + b}$ $for\ d_{rev} = 0m$: $a = 13;\ b = 23$ $for\ d_{rev} = 0.25\&0.5m$ $a = 14;\ b = 40$	(5.5)	48.5 %
	$\frac{v_{Rd}}{\sqrt{cot^2\alpha + 1}} \cdot \frac{T_m}{2\pi H_m} = -\frac{\xi_m^2 + a \cdot \xi_m}{\xi_m^2 + b}$ $for\ d_{rev} = 0m$: $a = 36;\ b = 70$ $for\ d_{rev} = 0.25\&0.5m$ $a = 40;\ b = 400$	(5.6)	32.4 %
Upwards and downwards directed flow velocity 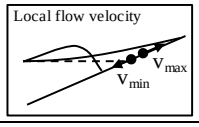	$\frac{v_{max}}{\sqrt{cot^2\alpha + 1}} \cdot \frac{T_m}{2\pi H_m} = \frac{\xi_m^2 + a \cdot \xi_m}{\xi_m^2 + b}$ $for\ d_{rev} = 0m$: $a = 24;\ b = 47$ $for\ d_{rev} = 0.25\&0.5m$ $a = 22;\ b = 64$	(5.8)	51.1 %
	$\frac{v_{min}}{\sqrt{cot^2\alpha + 1}} \cdot \frac{T_m}{2\pi H_m} = -\frac{\xi_m^2 + a \cdot \xi_m}{\xi_m^2 + b}$ $for\ d_{rev} = 0m$: $a = 44;\ b = 180$ $for\ d_{rev} = 0.25\&0.5m$ $a = 35;\ b = 360$	(5.9)	62.1 %
Internal wave set-up 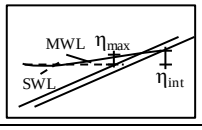	$\eta_{int} = \eta_{max} \cdot \frac{d_{rev}/H_m}{d_{rev}/H_m - 0.0102 \cdot \xi_m}$	(6.2)	10.9 %

Parameter	Equation	No.	σ'
Internal wave run-up & run-down 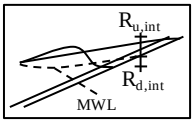	$\frac{R_{u,int}}{H_m} = -\frac{\xi_m^2 + a \cdot \xi_m}{\xi_m^2 + b}$ $for\ d_{rev} = 0.25m$: $a = -0.17;\ b = 62$ $for\ d_{rev} = 0.5m$ $a = -0.36;\ b = 81$	(6.3)	21.4 %
	$\frac{R_{d,int}}{H_m} = \frac{\xi_m^2 + a \cdot \xi_m}{\xi_m^2 + b}$ $for\ d_{rev} = 0.25m$: $a = 12;\ b = 190$ $for\ d_{rev} = 0.5m$ $a = 0.38;\ b = 71$	(6.4)	27.2 %
Internal wave run-up & run-down velocity 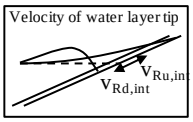	$\frac{v_{Ru,int}}{\sqrt{cot^2\alpha + 1}} \cdot \frac{T_m}{2\pi H_m} = \frac{\xi_m^2 + a \cdot \xi_m}{\xi_m^2 + b}$ $for\ d_{rev} = 0.25m$: $a = 110;\ b = 750$ $for\ d_{rev} = 0.5m$ $a = 2 \cdot 10^{16};\ b = 2 \cdot 10^{17}$	(6.7)	68.6 %
	$\frac{v_{Rd,int}}{\sqrt{cot^2\alpha + 1}} \cdot \frac{T_m}{2\pi H_m} = -\frac{\xi_m^2 + a \cdot \xi_m}{\xi_m^2 + b}$ $for\ d_{rev} = 0.25m$: $a = 2.2 \cdot 10^{15};\ b = 1.8 \cdot 10^{16}$ $for\ d_{rev} = 0.5m$ $a = 9.8 \cdot 10^{6};\ b = 1.1 \cdot 10^{8}$	(6.8)	57.6 %
Internal upwards and downwards directed flow velocity 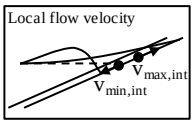	$\frac{v_{max,int}}{\sqrt{cot^2\alpha + 1}} \cdot \frac{T_m}{2\pi H_m} = \frac{\xi_m^2 + a \cdot \xi_m}{\xi_m^2 + b}$ $for\ d_{rev} = 0.25m$: $a = 0.36;\ b = 125$ $for\ d_{rev} = 0.5m$ $a = 1.7;\ b = 250$	(6.11)	39.2 %
	$\frac{v_{min,int}}{\sqrt{cot^2\alpha + 1}} \cdot \frac{T_m}{2\pi H_m} = -\frac{\xi_m^2 + a \cdot \xi_m}{\xi_m^2 + b}$ $for\ d_{rev} = 0.25m$: $a = 5.1;\ b = 470$ $for\ d_{rev} = 0.5m$ $a = -0.21;\ b = 230$	(6.12)	34.8 %
Wave set-up in sand core 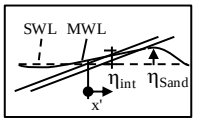	$\frac{\eta_{Sand}}{\eta_{int}} = \frac{29.4 \cdot e^{\xi_{m-1,0}}}{50.3 + \left(\frac{x'}{H_{m0}}\right)^2 - 7.27 \cdot \frac{x'}{H_{m0}}}$ $(wave\ spectra)$	(7.1)	38.0 %

C_d	-	Dissipation coefficient
C_r	-	Reflection coefficient
d_{rev}	m	Revetment thickness
H_b	m	Wave height at breaking point
h_b	m	Water depth at breaking point
H_m	m	Mean deep water wave height
H_{m0}	m	Significant deep water wave height
L_0	m	Deep water wave length
R_d	m	Wave run-down height (from MWL)
$R_{d,int}$	m	Internal wave run-down height (from MWL)
R_u	m	Wave run-up height (from MWL)
$R_{u,int}$	m	Internal wave run-up height (from MWL)
T_m	s	Mean wave period
$v_{int,max}$	m/s	Max. upwards directed internal local flow velocity
$v_{int,min}$	m/s	Max. downwards directed internal local flow velocity
$v_{int,Rd}$	m/s	Max. internal wave run-down velocity
$v_{int,Ru}$	m/s	Max. internal wave run-up velocity

v_{max}	m/s	Max. upwards directed external local flow
v_{min}	m/s	Max. downwards directed external local flow velocity
v_{Rd}	m/s	Max. external wave run-down velocity
v_{Ru}	m/s	Max. external wave run-up velocity
x'	m	Distance from the crossing SWL-slope surface
α	°	Slope angle
η_{int}	m	Wave set-up on core surface within revetment
η_{max}	m	Wave set-up on slope surface
η_{min}	m	Wave set-down at wave gauge
η_{Sand}	m	Internal set-up in the sand foundation
ξ_b	-	Surf similarity parameter (SSP) based on mean wave height at breaking point H_b and L_0: $\xi_b = \frac{\tan\alpha}{\sqrt{H_b/L_b}}$
ξ_m	-	SSP based on mean values in deep water: $\xi_m = \frac{\tan\alpha}{\sqrt{H_m/L_0}}$
$\xi_{m-1,0}$	-	SSP based on H_{m0} and L_0: $\xi_{m-1,0} = \frac{\tan\alpha}{\sqrt{H_{m0}/L_0}}$
σ'	-	Coefficient of variation: $\sigma' = \frac{\sqrt{\frac{1}{n}\cdot\Sigma\left(y - f(x)\right)^2}}{\bar{y}}$

8.2 Discussion

The numerical study using a RANS-VOF model was successful in the sense that the range of the tested conditions in the GWK was substantially extended. The model was applied for this purpose after successful validation by selected large-scale test data. All hydrodynamic parameters except for the pressure measurements showed a good agreement between the

laboratory tests and the numerical simulations. Thus, the numerical simulations enabled to perform an analysis of the processes in the revetment. Moreover, they also made a much higher spatial resolution of the water surface elevation possible than in the GWK-tests.

The most novel and equally relevant finding of this thesis was to show the importance of the wave set-up on the slope and inside the revetment and the sand foundation as it affects all other processes on and beneath the revetment. It is rather surprising that this was not or not sufficiently recognised in former studies. The wave set-up on a structure with a slope between 1:6 and 1:1.5 is found to be larger than often proposed in previous studies. This finding is important as the wave set-up also affects the determination of the structure height. Furthermore, the consideration of the wave set-up on the slope (as part of the MWL) enables to distinguish between the wave run-up and the wave set-up which are associated with totally different time scales, thus also allowing to assess wave up/run-down heights more reliably. Therefore, the wave set-up on the slope surface has always to be taken into account accordingly and separately from the wave run-up for the design of structures.

The analysis of the internal mean water level (IMWL) showed some differences to former studies in respect to the location of the maximum set-up in the sand foundation. This is most likely caused by the different types of core materials of the structure used in the different studies. However, the analysis has also clearly shown that the drainage of a porous bonded revetment is sufficient to prevent the build-up of residual pore pressure. All mid- to long-term changes in the pore pressure development were shown to be induced by changes in IMWL. This finding also underlines the importance of a precise knowledge of the IMWL for the assessment of the pore pressure development in the sand core.

Empirical based prediction equations were developed which are generally based on a good understanding of the underlying processes and which aim to reproduce physically sound values for the extreme boundary conditions for $\xi = 0$ and $\xi = \infty$. The fulfilment of these boundary conditions also ensured a good physical interpretation of most of the results. Though the prediction equations in Tab. 8.2 can be considered as generic, their application far outside the range of the tested conditions without further validation is not advisable.

Among the advantages of the bonded porous revetment which could be identified, the following are noteworthy: (i) the stability of the foundation is enhanced by the bonding of the revetment (ii) the loading on the revetment surface is reduced by the roughness and the porosity of the revetment and (iii) no residual pore pressure build-up is possible as a result of the good drainage through the highly porous revetment.

Among the limitations of the bonded porous revetment the following have been found (i) the very slippery surface of the revetment used in the GWK-tests and (ii) the failure due to sand relocations. The first issue is already solved by spreading sand over the revetment when the bonding agent is still wet. Thus, a slightly rougher surface is obtained also making it easier to walk on it. The second issue might be handled by either not using uniform slopes but more natural profiles such as S-profiles or by inserting moving joints, so that the stresses in the revetment due to the deformation of the soil foundation are not as high as those on a uniform slope like in the GWK-tests.

8.3 Outlook

Several difficulties were encountered and several problems were identified which could not be solved in the frame of this thesis. Therefore, further research is needed for example to determine the separate effect of the roughness and the porosity of the revetment. Systematic wave flume tests to solve this issue are being performed in the frame of the DFG-Project BoPoRe at the Leichtweiß-Institute for Hydraulic Engineering and Water Resources (LWI) (Liebisch & Oumeraci, 2013).

Moreover, a more appropriate numerical model is needed to improve the simulation of the wave induced pressures on and beneath the revetment as well as in the sand foundation. The limitations of COBRAS-UC which were more precisely identified in this thesis have enabled to develop and successfully validate a new CFD-CSD model system based on the OpenFOAM modelling framework (see Alcérreca Huerta, 2014). The new model is being used for a very systematic parametric study in order to improve the understanding of the hydro-geotechnical processes in the sand foundation beneath sloped revetments subjected to sea waves.

For a better understanding of the internal wave breaking a higher spatial resolution of the surface elevation over the slope as well as inside the revetment and the sand core would be required, including tests with different types of material for the embankment.

References

Alcérreca Huerta, J.C (2014): Interaction of waves with a porous bonded revetment and its soil foundation: Process-based modelling. TU Braunschweig, Leichtweiß-Institut für Wasserbau (in progress).

Allsop, N.W.H.A; McConnell, K. J. (1999): Revetment protection for coastal and shoreline structures exposed to wave attack. In: McGraw-Hill (Hg.): Handbook of Coastal Engineering, S. 2.1-2.24.

Arcadis (2008): Early colonization of littoral communities on polyurethane coated substrates. A field and laboratory study.

Barends, F.B.J (1993): Hydromechanics of Porous Media in the Maritime Environment. In: Coastal, Estuarial and Harbour Engineer's Reference Book. chapter 30: Chapman & Hall, London, S. 425–438.

Barends, F.B.J; van Hoven, A. (2007): Internal setup in porous dams and dikes. In: Proceedings of the 14th European Conference on Soil Mechanics and Geotechnical Engineering, S. 821–826.

Battjes, J. A.; Janssen, J.; others (1978): Energy loss and set-up due to breaking of random waves. In: Proc. 16th Int. Conf. Coastal Eng., Bd. 1, S. 649–660.

Battjes, J.A (1974): Computation of set-up, longshore currents, run-up and overtopping due to wind-generated waves. Ph.D. thesis. Delft University of Technology.

Burcharth, H. F.; Andersen, O. H. (1995): On the one-dimensional steady and unsteady porous flow equations. In: *Coastal Engineering* 24, S. 233–257.

Carman, P. C. (1937): Fluid flow through granular beds. In: *Transactions-Institution of Chemical Engineeres* 15, S. 150–166.

COBRAS (2005): Manual. Version 1.01. Cornell University.

Davidson, M. A.; Bird, P. A. D.; Bullock, G. N.; Huntley, D. A. (1996): A new non-dimensional number for the analysis of wave reflection from rubble mound breakwaters. In: *Coastal Engineering* 28 (1–4), S. 93–120.

Engelund, F. (1953): On the laminar and turbulent flows of ground water through homogeneous sand: Transactions of the Danish Academy of Technical Sciences (3).

Ergun, S. (1952): Fluid flow through packed columns. In: *Chem. Eng. Prog.* 48, S. 89–94.

EurOtop (2007): European Overtopping Manual (Pullen, T.; Allsop, N.W.H; Bruce, T.; Kortenhaus, A.; Schüttrumpf, H.; van der Meer, J.W: Kuratorium für Forschung im Küsteningenieurwesen: Die Küste, Heft 73).

Fenton, J.D (1985): A fifth-order Stokes theory for steady waves. In: *Journal of Waterway, Port, Coastal, and Ocean Engineering* (Vol. 111, No. 2), S. 216–234.

Foyer, G.; Oumeraci, H. (Advisor) (2012): Process analysis and model development for wave loading of porous bonded revetments - Progress report 3 - Analysis of the numerical simulations. TU Braunschweig, Leichtweiß-Institut für Wasserbau.

Foyer, G.; Oumeraci, H. (Advisor) (2013): Process analysis and model development for wave loading of porous bonded revetments - Progress report 4 - Model development. TU Braunschweig, Leichtweiß-Institut für Wasserbau.

Franzius, L. (1965): Wirkung und Wirtschaftlichkeit von Rauhdeckwerken im Hinblick auf den Wellenauflauf. Hannover (Mitteilungen des Franzius-Institut für Grund- und Wasserbau der Technischen Hochschule Hannover, Band 25).

Goda, Y. (1975): Irregular wave deformation in the surf zone. In: *Coastal Engineering in Japan* vol. 18, S. 13–26.

Goda, Yoshimi (2000): Random Seas and Design of Maritime Structures: World Scientific (Advanced series on ocean engineering, v. 15).

Gourlay, M.R (1992): Wave set-up, wave run-up and beach water table: interaction between surf zone hydraulics and groundwater hydraulics. In: *Coastal Engineering* vol. 17, S. 93–144.

Groot, M.B de; Bolton, M.D; Foray, P.; Meijers, P.; Palmer, A.C; Sandven, R. et al. (2006): Physics of liquefaction phenomena around marine structures. In: *Journal of Waterway, Port, Coastal and Ocean Engineering* vol. 132 (4), S. 227–243.

Gu, Zhihao; Wang, Hsiang (1991): Gravity waves over porous bottoms. In: *Coastal Engineering* 15 (5-6), S. 497–524.

Hall, Kevin R.; Foster, D. N. (1990): Internal and external pressure measurements in reshaped breakwaters. In: *Coastal Engineering* 14 (3), S. 215–232.

Hanslow, David; Nielsen, Peter (1993): Shoreline set-up on natural beaches. In: *Journal of Coastal Research*, S. 1–10.

Hughes, A.S (2004): Estimation of wave run-up on smooth, impermeable slopes using the wave momentum flux parameter. In: *Coastal Engineering* vol. 51, S. 1085–1104.

Kirkgöz, M. S. (1981): A theoretical study of plunging breakers and their run-up. In: *Coastal Engineering* 5, S. 353–370.

Kortenhaus, A. (2003): Probabilistische Methoden für Nordseedeiche. Dissertation. TU Braunschweig, Leichtweiß-Institut für Wasserbau.

Kozeny, J. (1927): Ueber kapillare leitung des wassers im boden. In: *Wien, Akad. Wiss* 136 (2a), S. 271.

Kudella, M.; Oumeraci, H. (2004): Wave-induced pore pressure in the sandy seabed underneath a caisson breakwater. Leichtweiss Institut for Hydromechanics and Coastal Engineering. Braunschweig, Germany (Berichte Leichtweiß-Institut für Wasserbau, Technische Universität Braunschweig, 900).

Lara, J. L.; Losada, I. J.; Guanche, R. (2008): Wave interaction with low-mound breakwaters using a RANS model. In: *Ocean Engineering* 35 (13), S. 1388–1400.

Liebisch, S.; Oumeraci, H. (Advisor) (2013): BoPoRe – Bonded Porous Revetments - Preliminary model tests to investigate the effect of porosity on wave-induced loads and hydraulic performance-. Progress Report. TU Braunschweig, LWI.

Longuet-Higgins, M. S.; Stewart, R. w. (1964): Radiation stresses in water waves; a physical discussion, with applications. In: *Deep Sea Research and Oceanographic Abstracts* 11 (4), S. 529–562.

Losada, Iñigo J.; Dalrymple, Robert A.; Losada, Miguel A. (1998): Wave-induced mean flows in vertical rubble mound structures. In: *Coastal Engineering* 35 (4), S. 251–281.

Losada, Inigo J.; Lara, Javier L.; Guanche, Raul; Gonzalez-Ondina, Jose M. (2008): Numerical analysis of wave overtopping of rubble mound breakwaters. In: *Coastal Engineering* 55 (1), S. 47–62.

Losada, M.A; Giménez-Curto, L.A (1981): Flow characteristics on rough, permeable slopes under wave action. In: *Coastal Engineering* vol. 4, S. 187–206.

Ludwigs, G. (2009): Wave loads on Elastocoast revetment in the large wave flume. Diplomarbeit. TU Braunschweig, Leichtweiß-Institut für Wasserbau.

Ludwigs, G.; Oumeraci, H. (Advisor) (2011a): Process analysis and model development for wave loading of porous bonded revetments - Progress report 1 - State of the art. TU Braunschweig, Leichtweiß-Institut für Wasserbau.

Ludwigs, G.; Oumeraci, H. (Advisor) (2011b): Process analysis and model development for wave loading on porous bonded revetments - Progress report 2 - Analysis of large-scale experiments. TU Braunschweig, Leichtweiß-Institut für Wasserbau.

Madsen, P.A; Fuhrman, D.R (2007): Run-up of tsunamis and long waves in terms of surf-similarity. In: *Coastal Engineering* vol. 55, S. 209–223.

Nielsen, Peter (1989): Wave setup and runup: An integrated approach. In: *Coastal Engineering* 13 (1), S. 1–9.

NLWKN (2012): Niedersachsen Küstendeiche werden ab sofort höher gebaut als bisher.

Oertel, H.; Laurien, E. (2003): Numerische Strömungsmechanik. 2. Auflage. Braunschweig/Wiesbaden: Vieweg.

Oumeraci, H. (2007): Vertiefervorlesung Küsteningenieurwesen I - Küstennahe Strömungen. TU Braunschweig, 2007.

Oumeraci, H.; Staal, T.; Pfoertner, S.; Ludwigs, G.; Kudella, M. (2010): Hydraulic performance, wave loading and response of Elastocoast revetments and their foundation - A large scale model study -. Braunschweig, Germany (Berichte Leichtweiß-Institut für Wasserbau, Technische Universität Braunschweig, 988).

Pilarczyk, K. W.; Klein Breteler, M.; Bezuijen, A. (1995): Wave Forces and Structural Response of Placed Block Revetments on Inclined Structures. In: Z. Demirbiles und N. Kobayashi (Hg.): Wave forces on inclined and vertical structures. New York, S. 52–87.

Schüttrumpf, Holger (2001): Hydrodynamische Belastung der Binnenböschung von Seedeichen durch Wellenüberlauf, Dissertation, Fachbereich Bauingenieurwesen, Leichtweiß-Institut für Wasserbau, Abt. Hydromechanik und Küsteningenieurwesen, Technische Universität Braunschweig.

Seelig, W.N (1983): Wave reflection from coastal structures. In: American Society of Civil Engineers (ASCE) (Hg.): Proceedings of Coastal Structures. Coastal Structures, S. 961–973.

Seelig, W.N; Ahrens, J.P (1981): Estimation of wave reflection and energy dissipation coefficients for beaches, revetments, and breakwaters. Fort Belvoir, Va., USA (Technical Paper. Coastal Engineering Research Center, 81-1).

Shih, R.W.K (1990): Permeability characteristics of rubble material-new formulae. In: Proc. 22nd Int. Conf. Coastal Eng., Bd. 1, S. 1499.

Sigloch, H. (2009): Technische Fluidmechanik. 7. Auflage. Berlin, Heidelberg: Springer.

Sollitt, C.K; Cross, R.H (1972): Wave Transmission Through Permeable Breakwaters. In: Proc. 13th Int. Conf. Coastal Eng.

Stockdon, Hilary F.; Holman, Rob A.; Howd, Peter A.; Sallenger, Asbury H., JR. (2006): Empirical parameterization of setup, swash, and runup. In: *Coastal Engineering* 53 (7), S. 573–588.

USACE (2002): Coastal Engineering Manual. 6 volumes; Engineer Manual 1110-2-1100, U. Army Corps of Engineers Washington D.C USA (Ed.), 2002.

van der Meer, J.W (1993): Conceptual design of rubble mound breakwaters (Publications Delft Hydraulics, No. 483).

van der Meer, J.W; Stam, C. -J M. (1991): Wave runup on smooth and rock slopes (Publications Delft Hydraulics, No. 454).

van Dorn, W.G (1976): Set-up and run-up in shoaling breakers. In: Proc. 15th Int. Conf. Coastal Eng., S. 738–751.

van Gent, M.R.A (1993): Stationary and oscillatory flow through coarse porous media. In: *Communications on Hydraulic and Geotechnical Engineering*, S. 62; 4 Appendices.

Ward, J. C. (1964): Turbulent flow in porous media. In: *J. Hydraul. Div.* (90), S. 1–12.

Software

Eureqa Formulize for Multiple Regression Analyses (MRA): Nutonian Inc. (2012): Eureqa. Online available at http://www.nutonian.com/eureqa-ii/

L~Davis for reflection and event analyses: lwi, mk (2012): L~Davis: Leichtweiß-Institute

MATLAB for importing into L~Davis from the numerical simulations and partly for analyses: The MathWorks (2010): MATLAB

OriginPro for the graphical display and Regression Analyses (RA): OriginLab Corporation (2012): OriginPro. Online available at http://www.originlab.com/

Appendices

A Test Set-Up and –Programme

A.1 GWK-tests

Tab. A.1 Measuring devices in the GWK (initial test set-up)

Description		X [m]	Y [m]	Z [m] (separation wall=0)
PT 01	Mod. A, EC top, toe	243.45	2.15	1.10
PT 02	Mod. A, EC top, impact area	245.70	2.90	1.10
PT 03		245.95	2.98	1.10
PT 04		246.20	3.07	1.10
PT 05		246.45	3.15	1.10
PT 06		246.70	3.23	1.10
PT 07		246.95	3.32	1.10
PT 08		247.20	3.40	1.10
PT 09	Mod. A, EC top, SWL	249.00	4.00	1.10
PT 10	Mod. A, EC bottom, toe	243.50	2.01	1.10
PT 11	Mod. A, EC bottom, impact area	246.00	2.84	1.10
PT 12		246.50	3.01	1.10
PT 13		247.00	3.17	1.10
PT 14	Mod. A, EC bottom, SWL	249.05	3.86	1.10
PT 15	Mod. A, Sand top, impact area	246.06	2.65	1.10
PT 16		246.56	2.82	1.10
PT 17		247.06	2.99	1.10
PT 18	Mod. A, Sand bottom, toe	243.90	1.06	1.10
PT 19	Mod. A, Sand bottom, impact area	246.31	1.89	1.10
PT 20		246.81	2.06	1.10
PT 21		247.31	2.23	1.10
PT 22	Mod. A, Sand bottom, SWL	249.00	2.91	1.10
PT 23	Mod. A, water table	251.10	2.91	1.10
PT 24		253.60	2.91	1.10
PT 25		255.60	2.91	1.10
RUG 1	Mod. A, toe	244.75	2.50	0.80
RUG 2	Mod. A, crest	250.14	4.38	0.80
RUG 3	Mod. B, toe	246.45	2.50	0.80
RUG 4	Mod. B, crest	250.14	4.38	0.80
WG 09	underwater slope low	220.00	0.00	0.60
WG 10	underwater slope high	230.00	0.50	0.60
WG 11	EC low	240.00	1.00	0.60
WG 12	EC middle	242.70	1.90	0.60
WG 13	EC high	245.17	2.72	0.60

Tab. A.2 Measuring devices in the GWK (changes for model alternative C)

Description		X [m]	Y [m]	Z [m] (separation wall=0)
PT 01	Mod. C, EC bottom, toe	243.497	2.008	1.10
PT 02	Mod. C, EC bottom, impact area	245.747	2.758	1.10
PT 03		245.997	2.838	1.10
PT 04		246.247	3.928	1.10
PT 05		246.497	3.08	1.10
PT 06		246.747	3.088	1.10
PT 07		246.997	3.178	1.10
PT 08		247.247	3.258	1.10
PT 09	Mod. C, EC bottom, SWL	249.047	3.858	1.10
PT 10	Mod. C, filter bottom, toe	243.563	1.82	1.10
PT 11	Mod. C, filter bottom, impact area	246.063	2.65	1.10
PT 12		246.563	2.82	1.10
PT 13		247.063	2.984	1.10
PT 14	Mod. C, filter bottom, SWL	249.113	3.67	1.10
PT 15	Mod. C, Sand , impact area	246.123	2.46	1.10
PT 16		246.623	2.63	1.10
PT 17		247.123	2.795	1.10
PT 18	Mod. C, Sand bottom, toe	243.90	1.06	1.10
PT 19	Mod. C, Sand bottom, impact area	246.31	1.89	1.10
PT 20		246.81	2.06	1.10
PT 21		247.31	2.23	1.10
PT 22	Mod. C, Sand bottom, SWL	249.00	2.91	1.10
PT 23	Mod. C, water table	251.10	2.91	1.10
PT 24		253.60	2.91	1.10
PT 25		255.60	2.91	1.10

Tab. A.3 Regular wave tests of the first test phase in the GWK (before failure, model alternatives A and B)

Test number	H_m [m]	T_m [s]	h_0 [m]	ξ_m [-]
1	0.22	3.00	3.4	2.67
2	0.19	4.00	3.4	3.77
3	0.21	5.00	3.4	4.59
4	0.18	5.93	3.4	5.78
5	0.22	7.00	3.4	6.24
6	0.17	7.90	3.4	7.94
7	0.65	3.00	3.4	1.55
8	0.68	4.01	3.6	2.02
9	1.04	3.00	3.6	1.22
10	0.64	4.95	3.7	2.57
11	1.14	3.92	3.7	1.53
12	1.40	3.92	3.7	1.38
13	0.65	6.00	3.9	3.1
14	0.54	6.93	3.9	3.91
15	0.55	7.98	3.9	4.49
16	1.37	4.90	3.9	1.75

Tab. A.4 Regular wave tests of the second test phase in the GWK (after failure, model alternatives B and C)

Test number	H_m [m]	T_m [s]	h_0 [m]	ξ_m [-]
1	0.22	2.99	3.4	2.65
2	0.20	5.00	3.4	4.66
3	0.17	8.00	3.4	8.05
4	0.66	3.00	3.4	1.54
5	0.69	4.00	3.6	2
6	0.58	4.99	3.8	2.72
7	0.72	6.00	3.9	2.95
8	0.52	6.99	3.9	4.02
9	0.44	7.00	3.8	4.39
10	0.50	7.99	3.7	4.72
11	0.67	3.00	3.5	1.53
12	0.75	3.00	3.5	1.44
13	0.84	3.00	3.5	1.36
14	0.92	3.01	3.5	1.31
15	0.39	3.00	3.4	1.99
16	0.49	3.00	3.4	1.79
17	1.01	5.01	3.9	2.08
18	0.92	6.02	4.1	2.61
19	1.24	6.03	4.2	2.25
20	1.17	7.02	4.2	2.7
21	0.91	8.05	4.2	3.52

A.2 Numerical simulations

Tab. A.5 Measuring devices in the numerical simulations

	Measuring device	x-position	y-position
		[m]	[m]
WG01	Wave gauge	0.02	0.00
WG02	Wave gauge	1.40	0.00
WG03	Wave gauge	5.0	0.00
WG04	Wave gauge	13.0	0.00
WG05	Wave gauge	20.0	0.00
WG06	Wave gauge	24.0	0.20
WG07	Wave gauge	28.0	0.40
WG08	Wave gauge	32.0	0.60
WG09	Wave gauge	36.0	0.80
WG10	Wave gauge	40.0	1.00
WG11	Wave gauge	40.0+cot α	2.00
WG12	Wave gauge	40.0+2cot α	3.00
WG13	Wave gauge	40.0+3cot α	4.00
RUG	Run-up gauge	-	-
RUG-int	Run-up gauge	-	-
RD	Run-down indicator	-	-
p1_top	Pressure transducer	-	-
p2_top	Pressure transducer	40.0+3cot α	4.00
p3_top	Pressure transducer	40.0+2.5cot α	3.50
p4_top	Pressure transducer	40.0+2cot α	3.00

	Measuring device	x-position	y-position
		[m]	[m]
p5_top	Pressure transducer	$40.0+1.5\cot\alpha$	2.50
p6_top	Pressure transducer	$40.0+\cot\alpha$	2.00
pI_top	Pressure transducer	-	-
p1_bottom	Pressure transducer	-	-
p2_bottom	Pressure transducer	$40.0+3\cot\alpha+d_{rev}/\sqrt{(1+(\cot\alpha)^2)}$	$4.00+\cot\alpha\ d_{rev}/\sqrt{(1+(\cot\alpha)^2)}$
p3_bottom	Pressure transducer	$40.0+2.5\cot\alpha+d_{rev}/\sqrt{(1+(\cot\alpha)^2)}$	$3.50+\cot\alpha\ d_{rev}/\sqrt{(1+(\cot\alpha)^2)}$
p4_bottom	Pressure transducer	$40.0+2\cot\alpha+d_{rev}/\sqrt{(1+(\cot\alpha)^2)}$	$3.00+\cot\alpha\ d_{rev}/\sqrt{(1+(\cot\alpha)^2)}$
p5_bottom	Pressure transducer	$40.0+1.5\cot\alpha+d_{rev}/\sqrt{(1+(\cot\alpha)^2)}$	$2.50+\cot\alpha\ d_{rev}/\sqrt{(1+(\cot\alpha)^2)}$
p6_bottom	Pressure transducer	$40.0+\cot\alpha+d_{rev}/\sqrt{(1+(\cot\alpha)^2)}$	$2.00+\cot\alpha\ d_{rev}/\sqrt{(1+(\cot\alpha)^2)}$
pI_bottom	Pressure transducer	-	-
v1_top	Velocity meter	-	-
v2_top	Velocity meter	$40.0+3\cot\alpha$	4.00
v3_top	Velocity meter	$40.0+2.5\cot\alpha$	3.50
v4_top	Velocity meter	$40.0+2\cot\alpha$	3.00
v5_top	Velocity meter	$40.0+1.5\cot\alpha$	2.50
v6_top	Velocity meter	$40.0+\cot\alpha$	2.00
vI_top	Velocity meter	-	-
v1_bottom	Velocity meter	-	-
v2_bottom	Velocity meter	$40.0+3\cot\alpha+d_{rev}/\sqrt{(1+(\cot\alpha)^2)}$	$4.00+\cot\alpha\ d_{rev}/\sqrt{(1+(\cot\alpha)^2)}$
v3_bottom	Velocity meter	$40.0+2.5\cot\alpha+d_{rev}/\sqrt{(1+(\cot\alpha)^2)}$	$3.50+\cot\alpha\ d_{rev}/\sqrt{(1+(\cot\alpha)^2)}$
v4_bottom	Velocity meter	$40.0+2\cot\alpha+d_{rev}/\sqrt{(1+(\cot\alpha)^2)}$	$3.00+\cot\alpha\ d_{rev}/\sqrt{(1+(\cot\alpha)^2)}$
v5_bottom	Velocity meter	$40.0+1.5\cot\alpha+d_{rev}/\sqrt{(1+(\cot\alpha)^2)}$	$2.50+\cot\alpha\ d_{rev}/\sqrt{(1+(\cot\alpha)^2)}$
v6_bottom	Velocity meter	$40.0+\cot\alpha+d_{rev}/\sqrt{(1+(\cot\alpha)^2)}$	$2.00+\cot\alpha\ d_{rev}/\sqrt{(1+(\cot\alpha)^2)}$
vI_bottom	Velocity meter	-	-
v_Ru	Velocity meter	-	-
v_Ru,int	Velocity meter	-	-

Tab. A.6 Test protocol (input values for the numerical simulation)

Test number	H_{nom} [m]	T_{nom} [s]	cotα [-]	d_{rev} [m]
2011122301	0.3	3	6.0	0.50
2011122302			4.0	
2011122303			3.0	
2011122304			6.0	0.25
2011122305			4.0	
2011122306			3.0	
2011122307	1.0		6.0	0.50
2011122308			4.0	
2011122309			3.0	
2011122310			6.0	0.25
2011122311			4.0	
2011122312			3.0	
2011122701	0.6		6.0	0.50
2011122702			4.0	
2011122703			3.0	

Test number	H_{nom} [m]	T_{nom} [s]	cotα [-]	d_{rev} [m]
2011122704	0.3	6	6.0	0.25
2011122705			4.0	
2011122706			3.0	
2011122801			6.0	0.50
2011122802			4.0	
2011122803			3.0	
2011122804			6.0	0.25
2011122805			4.0	
2011122806			3.0	
2011123001	0.6		6.0	0.50
2011123002			4.0	
2011123003			3.0	
2011123004			6.0	0.25
2011123005			4.0	
2011123006			3.0	

Test number	H_{nom} [m]	T_{nom} [s]	cotα [-]	d_{rev} [m]
2011123101	0.3	3	6.0	0.00
2011123102			4.0	
2011123103			3.0	
2012010201		9	6.0	0.50
2012010202			4.0	
2012010203			3.0	
2012010204			6.0	0.25
2012010205			4.0	
2012010206			3.0	
2012010601	0.3	3	2.0	0.25
2012010602		6	2.0	
2012010603		9	2.0	
2012010604		3	1.5	
2012010605		6	1.5	
2012010606		9	1.5	
2012011301		3	2.0	0.50
2012011302		6	2.0	
2012011303		9	2.0	
2012011304		3	1.5	
2012011305		6	1.5	
2012011306		9	1.5	
2012011307		3	2.0	0.00
2012011308		6	2.0	
2012011309		9	2.0	
2012011310		3	1.5	
2012011311		6	1.5	
2012011312		9	1.5	
2012011901			6.0	
2012011902			4.0	
2012011903			3.0	
2012011904		6	6.0	
2012011905			4.0	
2012011906			3.0	
2012011907	0.6		6.0	
2012011908			4.0	
2012011909			3.0	
2012011910		3	6.0	
2012011911			4.0	
2012011912			3.0	
2012012601			2.0	
2012012602			2.0	0.25
2012012603			2.0	0.50

Test number	H_{nom} [m]	T_{nom} [s]	cotα [-]	d_{rev} [m]
2012012604	0.6	6	1.5	0.00
2012012605			1.5	0.25
2012012606			1.5	0.50
2012012607			2.0	0.00
2012012608			2.0	0.25
2012012609			2.0	0.50
2012012610			1.5	0.00
2012012611			1.5	0.25
2012012612			1.5	0.50
2012021301	1.0	5	3.0	0.00
2012021302			4.0	
2012021303			6.0	
2012021304			2.0	
2012021305			1.5	
2012021306			3.0	0.25
2012021307			4.0	
2012021308			6.0	
2012021309			2.0	
2012021310			1.5	
2012021311			3.0	0.50
2012021312			4.0	
2012021313			6.0	
2012021314			2.0	
2012021315			1.5	
2012021316	0.6	8	3.0	0.00
2012021317			4.0	
2012021318			6.0	
2012021319			2.0	
2012021320			1.5	
2012021321			3.0	0.25
2012021322			4.0	
2012021323			6.0	
2012021324			2.0	
2012021325			1.5	
2012021326			3.0	0.50
2012021327			4.0	
2012021328			6.0	
2012021329			2.0	
2012021330			1.5	

B MATLAB Routines

All routines are only presented partially so the concept becomes clear.

B.1 Merging of RUGs

Routine for the merging of the wave run-up gauges of the GWK-tests with different calibrations for RUG1+2 and RUG3+4 as well as for different test phases.

```
% Routine to calculate resulting data from two wave gauges for a lower
% location of the upper wave gauge at z=4.38m
% All batches have to be performed separately.
test=['09061803';...
 h=[3.8;...

 frequency=500;         % for test batch 1+2 = 100 and for 3 500
 loc='C:\...

 %% Model A/C

 % entering of calibration data - see also below (row 69-72)!
 % cal1=0.09031516000;   % before connecting lower and upper gauge (batch 1)
 % cal2=0.09254925000;
 cal1=0.09120946000;     % after connecting lower and upper gauge (batch 2+3)
 cal2=0.49119820000;

 channel='53';       % channel of lower gauge
 channel2='54';      % channel of upper gauge
 channel_new='104';  % new channel

 for i=1:size(test,1)    % loop over all tests selected
    % reading of data from lower gauge
    fid=fopen([loc,'Data\',test(i,1:6),'\',test(i,7:8),'\',test(i,1:end),'.G',channel]);
    a=fread(fid,'int16')*cal1*0.001;
    fclose(fid);
    a=a-mean(a(1:5*frequency)); % determination of zero value

    % reading of data from upper gauge
    fid2=fopen([loc,'Data\',test(i,1:6),'\',test(i,7:8),'\',test(i,1:end),'.G',channel2]);
    if test(i,4)=='6'&&
           not(strcmp(test(i,5:end),'2913')||strcmp(test(i,5:end),'2914')||strcmp(test(i,5:end),'2915')||strcmp(test(i,5:e
       % quadratic calibration for tests 09062913-16
       a2=fread(fid2,'int16');
       a2=a2.^2*(-2E-07)-0.0003*a2+5.8331;
    else
       a2=fread(fid2,'int16')*cal2*0.001;
    end
    fclose(fid2);

    % calculation of new data
    a2=a2-mean(a2((a>(4.38-h(i)))&(a<(4.381-h(i)))))+4.38-h(i); % mean zero of upper gauge
    a2(a<=(4.38-h(i)))=0;   % delete unnecessary data from upper gauge
    a(a>(4.38-h(i)))=0;     % delete unnecessary data from lower gauge
    a_new=(a+a2)*1000/cal1; % adding up to new channel
```

```
    % writing of data
    fid=fopen([loc,'NewData\',test(i,1:6),'\',test(i,7:8),'\',test(i,1:end),'.',channel_new],'w');
    fwrite(fid,a_new,'int16');
    fclose(fid);
    close all
    clear a a2
end

clear a a2 cal1 cal2 channel channel2 channel_new

similar routine for model B
```

B.2 RUG & RUG-int

Calculation of the wave run-up gauges on the revetment and directly on the bottom of the revetment in the numerical simulations.

```
path='C:\...
test=...
n=...
drev=...
h0=4;
dx=0.02;    % cell width [m]
dy=load('C:\Users\new_Gisa\Dissertation\Numerische Arbeit\Durchführung-Planung
          COBRAS\Input\delta_y.txt'); % cell height [m]
%dy_cor=dy(18:end);
path_save='C:\Users\new_Gisa\Dissertation\Numerische Arbeit\L~Davis\NewData';
for test_num=1:length(test)
if n(test_num)~=6
   x=6/dx*n(test_num);     % number of cells in x-direction
else
   x=1790;
end
y=151;      % number of cells in y-direction
h_flume=7;  % flume height [m]
x_rev=1; % cell number in x-direction at the start of the revetment
y_rev=1; % cell number in y-direction at the start of the revetment
% number of saved time steps per file is 600!!!
ind_break=1;
ind2_break=1;
indR_break=1;
%% Calculation of wave run-up

% determine number of cells
D=dir([path,'\',char(test(test_num,1:8)),'\',char(test(test_num,9:end)),'\t']);
l=length(D(not([D.isdir])));
clear D

for i=1:l   % loop over files
   fid=fopen([path,'\',char(test(test_num,1:8)),'\',char(test(test_num,9:end)),'\t\t',num2str(i,'%03.0f'),'.dat']);
   for ii=1:600
      % read data set
      time(ii+(i-1)*600)=fread(fid,1,'float64');
      vof=fread(fid,[x y],'float32');
      eta=[];
```

```
        % test from left to right for end of water layer
        for iii=1:x
           ind=find(vof(iii,:)>0.3);   % find filled cells
           ind2=ind;
           ind(ind<(find(dy<(iii)*dx/n(test_num)+1,1,'last')-16))=[];
          % ind(find(ind<(find(dy<(iii-1)*dx/n+1,1,'last')-17)))=[];  % ignore cells below revetment
           if (~isempty(ind))&&(ind_break<3)
              eta(iii)=dy(max(ind)+16)+(vof(iii,max(ind)))*(dy(max(ind)+17)-dy(max(ind)+16));
           else ind_break=ind_break+1;
           end
           ind2(ind2<(find(dy<(iii)*dx/n(test_num)+1-drev(test_num)/n(test_num)*sqrt(n(test_num)^2+1),1,'last')-
             16))=[];
           if (~isempty(ind2))&&(ind2_break<3)
              eta2(iii)=dy(max(ind2)+16)+(vof(iii,max(ind2)))*(dy(max(ind2)+17)-dy(max(ind2)+16));
           else ind2_break=ind2_break+1;
           end
           clear ind ind2
           indR=find(vof(iii,:)<0.3);
           indR(indR<(find(dy<(iii)*dx/n(test_num)+1,1,'last')-16))=[];
           if (~isempty(indR))&&(indR_break<3)
              R(iii)=dy(min(indR)+15)+(vof(iii,min(indR)-1))*(dy(min(indR)+16)-dy(min(indR)+15));
           else indR_break=indR_break+1;
           end
           clear indR
        end
        ind_break=0;
        ind2_break=0;
        indR_break=0;
        h(ii+(i-1)*600)=eta(end);   % run-up ext
        clear eta
        h2(ii+(i-1)*600)=eta2(end);   % run-up int
        Rd(ii+(i-1)*600)=min(R);  % run-down
        clear R
save data for wave gauges...
        clear eta2
        % Test for end of file marker
        a=ftell(fid);
        fread(fid,1,'float32');
        if feof(fid)
           break
        else
           fseek(fid,a,'bof');
        end
        clear a
     end
     fclose(fid);
end

clear i ii iii cell vof l ind ind2 indR
%% Smooth frequency to equally distanced time steps
...
%% Saving run-up and run-down into test folder
fid=fopen([path_save,'\',char(test(test_num,1:8)),'\',char(test(test_num,9:end)),'\',char(test(test_num,1:end)),'.014'
          ],'w');
fwrite(fid,h*1000,'int16');
fclose(fid);
...(all other channels)
```

```
fid=fopen([path_save,'\',char(test(test_num,1:8)),'\',char(test(test_num,9:end)),'\',char(test(test_num,1:end)),'.mtx'
        ],'a');
fprintf(fid,'Channel   10\r\n  Range  -32768 N/Min/Max/Mean/Zero      %4.0f   %4.0f   %4.0f    %4.2f
        %4.2f\r\n  WG10\r\n  X-Pos/Y-Pos/Cal/Dim    %2.2f  %2.2f     1.0000   [m]\r\n  Frequency/Delay
        50.000     0.00000000\r\n',[length(WG10) 1000*min(WG10) 1000*max(WG10) 1000*mean(WG10)
        1000*WG10(1) 40 1]);
...(all other channels)
fclose(fid);
```

B.3 Wave set-down

Calculation of the maximum wave set-down in front of the structure (numerical simulations).

```
path_save= 'C:\...
 % Create file for set-down
 fid=fopen([path_save,'\setdown.dat'],'w');
 fprintf(fid,'test number \t setdown \t location \r\n');
 fclose(fid);

 path= 'C:\Users\...
test=['2012021301';...
n=[3.0; ... %  slope steepness
drev=[0.00;...  % thickness of revetment
dx=0.02;     % cell width [m]
dy=load('C:\...\delta_y.txt'); % cell height [m]

 for test_num=1:1:size(test,1)
 if n(test_num)~=6
    x=6/dx*n(test_num);      % number of cells in x-direction
else
    x=1790;
end
y=151;       % number of cells in y-direction
h_flume=7;   % flume height [m]
x_rev=1; % cell number in x-direction at the start of the revetment
y_rev=1; % cell number in y-direction at the start of the revetment
 % number of saved time steps per file is 600!!!

 % Search for time frame
 fid=fopen([path_save,'\',char(test(test_num,1:8)),'\',char(test(test_num,9:end)),'\',char(test
        (test_num,1:end)),'.tfr']);
 i=1;
while i<25
    line=fgetl(fid);
     if strcmp(line, '[TF_001]')==1
        i=18;
     end
    i=i+1;
end
 clear line i
tf_start=fgetl(fid);
tf_start=str2num(tf_start(9:end));
tf_end=fgetl(fid);
tf_end=str2num(tf_end(7:end));

  % determine number of cells
 D=dir([path,'\',char(test(test_num,1:8)),'\',char(test(test_num,9:end)),'\t']);
```

```
l=length(D(not([D.isdir])));
 clear D
number=0;
 for i=1:l   % loop over files
   fid=fopen([path, '\',char(test(test_num,1:8)),'\',char(test(test_num,9:end)),'\t\t',num2str(i,'%03.0
 f'),'.dat']);
    for ii=1:600
       % read data set
       time=fread(fid,1, 'float64');
       vof=fread(fid,[x y], 'float32');
       if time>tf_end
          clear vof
          break
       end
       if time>=tf_start
       eta=[];
       number=number+1;
       % test from left to right for end of water layer
       for iii=1:x
          ind=find(vof(iii,:)>0.3);    % find filled cells
ind2=ind;
          ind(ind<(find(dy<(iii)*dx/n(test_num)+1,1, 'last')-16))=[];
         % ind(find(ind<(find(dy<(iii-1)*dx/n+1,1,'last')-17)))=[];  % ignore cells below revetment
          if (~isempty(ind))
             eta(iii)=dy(max(ind)+16)+(vof(iii,max(ind)))*(dy(max(ind)+17)-dy(max(ind)+16));
          else break
          end
          clear ind
       end
       if number==1
          h=eta;
       else
          h_new(1:min(length(eta),length(h)))=(h(1:min(length(eta),length(h))).*(number-1)+eta(1:min
 (length(eta),length(h))))/number;
          clear h
          h=h_new;
          clear h_new
       end
       clear eta
       end
       clear vof
       % Test for end of file marker
       a=ftell(fid);
       fread(fid,1, 'float32');
       if feof(fid)
          break
       else
          fseek(fid,a, 'bof');
       end
       clear a
    end
   fclose(fid);
    if time>tf_end
          break
    end
end
 setd=min(h)-4;
 loc=3*n(test_num)-(find(h==min(h))*dx-0.01);
```

```
 fid=fopen([path_save,'\setdown.dat'],'a');
 fprintf(fid,'%10.0f \t %1.3f \t %4.3f \r\n',[str2num(test(test_num,1:end));setd;loc]);
 fclose(fid);
 clear tf_start tf_end setd time h loc
end
end
 clear all
```

Due to a problem with the still water level in COBRAS-UC, 0.02 m had to be subtracted from the resulting wave set-down.

B.4 Velocities

Calculation of the flow velocities on the revetment and directly on the bottom of the revetment in the numerical simulations.

```
path_save='C:\...

% Create file for location of maximum pressure
fid=fopen([path_save,'\vmax.dat'],'w');
fprintf(fid,'test number \t z(vmax1) \t z(vmax2) \r\n');
fclose(fid);

path='C:\...
test=
n=    % slope steepness
drev=% thickness of revetment

h0=4;
dx=0.02;    % cell width [m]
dy=load('C:\...\delta_y.txt'); % cell height [m]
%dy_cor=dy(18:end);

for test_num=1:1:size(test,1)
if n(test_num)~=6
   x=6/dx*n(test_num);     % number of cells in x-direction
else
   x=1790;
end
y=151;      % number of cells in y-direction
h_flume=7;  % flume height [m]
x_rev=1; % cell number in x-direction at the start of the revetment
y_rev=1; % cell number in y-direction at the start of the revetment
% number of saved time steps per file is 600!!!

%% Determination of velocities

% determine number of cells/files
D=dir([path,'\',char(test(test_num,1:8)),'\',char(test(test_num,9:end)),'\u']);
l=length(D(not([D.isdir])));
clear D

for i=1:l   % loop over files
   fid1=fopen([path,'\' char(test(test_num,1:8)) '\',char(test(test_num,9:end)),'\u\u',num2str(i,'%03.0f'),'.dat']);
   fid2=fopen([path,'\' char(test(test_num,1:8)) '\',char(test(test_num,9:end)),'\w\w',num2str(i,'%03.0f'),'.dat']);
```

```
   for ii=1:600
      % read data set
      time(ii+(i-1)*600)=fread(fid1,1,'float64');
      fread(fid2,1,'float64');
      u=fread(fid1,[x y],'float32');
      w=fread(fid2,[x y],'float32');
      v=sqrt(u.^2+w.^2).*sign(w);
      gamma=radtodeg(sin(w./abs(v)));
      gamma(isnan(gamma))=0;
      clear u w
      for iii=1:x
         ind=find(dy<(iii)*dx/n(test_num)+1,1,'last')-16;
         if ~isempty(ind)&&ind<y
            v_rev(iii,ii+(i-1)*600)=v(iii,ind+1);
            gamma_rev(iii,ii+(i-1)*600)=gamma(iii,ind+1);
         else v_rev(iii,ii+(i-1)*600)=0;
            gamma_rev(iii,ii+(i-1)*600)=0;
         end
         ind=find(dy<(iii)*dx/n(test_num)+1-drev(test_num)/n(test_num)*sqrt(n(test_num)^2+1),1,'last')-16;
         if ~isempty(ind)&&ind>=0&&ind<y
            v_bottom(iii,ii+(i-1)*600)=v(iii,min(ind+2,151));
         else v_bottom(iii,ii+(i-1)*600)=0;
         end
      end
      clear v ind gamma

      % Test for end of file marker
      a=ftell(fid);
      fread(fid,1,'float32');
      if feof(fid)
         break
      else
         fseek(fid,a,'bof');
      end
      clear a
   end
   fclose(fid1);
   fclose(fid2);
end

% Search for time frame
fid=fopen([path_save,'\',char(test(test_num,1:8)),'\',char(test(test_num,9:end)),'\',char(test(test_num,1:end)),'.tfr'])
          ;
i=1;
while i<25
   line=fgetl(fid);
   if strcmp(line,'[TF_001]')==1
      i=18;
   end
   i=i+1;
end
clear line i
tf_start=fgetl(fid);
tf_start=str2num(tf_start(9:end));
tf_end=fgetl(fid);
tf_end=str2num(tf_end(7:end));

% Determine maximum velocity on revetment and corresponding velocity in
```

```
% the revetment
v_start=find(time>tf_start,1,'first');
v_end=find(time<tf_end,1,'last');
v_tf=v_rev(1:end,v_start:v_end);
delta=max(v_tf,[],2)-min(v_tf,[],2);
[~,ind]=sort(delta,'descend');
v1_top=v_rev(ind(1),1:end);
ang=gamma_rev(ind(1),1:end);
v1_bottom=v_bottom(round(ind(1)+drev(test_num)/sqrt(1+n(test_num)^2)/dx),1:end);
% Location of maximum velocity on revetment and corresponding velocity in
% the revetment
loc(1,1)=ind(1)*dx;
loc(1,2)=ind(1)*dx/n(test_num);
loc(8,1)=ind(1)*dx+drev(test_num)/sqrt(1+n(test_num)^2);
loc(8,2)=ind(1)*dx/n(test_num)-n(test_num)*drev(test_num)/sqrt(1+n(test_num)^2);
clear delta ind v_start v_end v_tf
% Determine maximum velocity in revetment and corresponding velocity on
% the revetment
As above
% Location of maximum velocity in revetment and corresponding velocity on
% the revetment
As above
% Fixed velocity values on and in revetment
v2_top=v_rev(round(3*n(test_num)/dx),1:end);
...
% Location of velocity measurements
loc(2:6,1)=(3:-0.5:1)*n(test_num);
loc(2:6,2)=(3:-0.5:1);
loc(9:13,1)=(3:-0.5:1)*n(test_num)+drev(test_num)/sqrt(1+n(test_num)^2);
loc(9:13,2)=(3:-0.5:1)-n(test_num)*drev(test_num)/sqrt(1+n(test_num)^2);
clear i ii iii cell l v_rev v_bottom gamma_rev delta ind v_start v_end v_tf tf_start tf_end
fid=fopen([path_save,'\vmax.dat'],'a');
fprintf(fid,'%10.0f \t %1.3f \t %1.3f \r\n',[str2num(test(test_num,1:end));loc(1,2);loc(7,2)]);
fclose(fid);

%% Smooth frequency to equally distanced time steps

%% Saving parameters into test folder
fid=fopen([path_save,'\',char(test(test_num,1:8)),'\',char(test(test_num,9:end)),'\',char(test(test_num,1:end)),'.031'
        ],'w');
fwrite(fid,v1_top*1000,'int16');
fclose(fid);
...all other channels
fid=fopen([path_save,'\',char(test(test_num,1:8)),'\',char(test(test_num,9:end)),'\',char(test(test_num,1:end)),'.mtx'
        ],'a');
fprintf(fid,'Channel   31\r\n Range -32768 N/Min/Max/Mean/Zero      %4.0f   %4.0f   %4.0f    %4.2f
        %4.2f\r\n v1_top\r\n X-Pos/Y-Pos/Cal/Dim    %2.2f  %2.2f     1.0000  [m/s]\r\n Frequency/Delay
        50.000     0.00000000\r\n',[length(v1_top) 1000*min(v1_top) 1000*max(v1_top) 1000*mean(v1_top)
        1000*v1_top(1) loc(1,1) loc(1,2)]);
...all other channels
fclose(fid);
```